# VOLUMETRIC ANALYSIS AND TISSUE CHARACTERISATION OF CARDIAC DISEASE BY MAGNETIC RESONANCE IMAGING

LINDSAY W TURNBULL

BSC (Hons), MB ChB, DMRD, FRCR

Thesis submitted to the University of Edinburgh

for the degree of Doctor of Medicine

June 1991

I declare that this thesis was composed by myself and relates to work carried out by myself during my clinical appointment as New Blood Lecturer in Medical Radiology in the University of Edinburgh from September 1986. Contributions by other individuals are clearly indicated in the Acknowledgements.

TABLE OF CONTENTS


| | | Page |
|---|---|---|
| Abstract | | 7 |
| Acknowledgments | | 9 |
| Declaration of Published Work | | 11 |
| List of Tables | | 12 |
| List of Figures | | 18 |
| Chapter 1A | Basic Principles of Nuclear Magnetic Resonance | 27 |
| 1A.1 | Introduction | 27 |
| 1A.2 | Bulk Magnetisation | 30 |
| 1A.3 | Resonance and Precession | 32 |
| 1A.4 | Radiofrequency Pulses, Slice Width and Slice Selection | 35 |
| 1A.5 | Production of the NMR Signal | 35 |
| 1A.6 | Spatial Encoding of the NMR Signal | 36 |
| 1A.7 | Decay Characteristics of the NMR Signal | 38 |
| 1A.8 | Measurement Pulse Sequences | 41 |
| 1A.9 | Magnetic Field Strength, Type of Magnet and Field Homogeneity | 47 |
| 1A.10 | Spatial Resolution | 48 |
| 1A.11 | Slice Thickness | 49 |
| 1A.12 | Signal Averaging | 49 |
| 1A.13 | Scan Time | 49 |

| | | | |
|---|---|---|---|
| | 1A.14 | Chemical Shift | 50 |
| | 1A.15 | Magnetic Susceptibility | 51 |
| | 1A.16 | Blood Flow | 51 |
| | 1A.17 | Other Factors Affecting Pixel Intensity | 51 |
| Chapter 1B | | Development of Magnetic Resonance Imaging | 52 |
| Chapter 1C | | Uses of Magnetic Resonance Imaging in Cardiovascular Disease | 60 |
| | 1C.1 | Assessment of Anatomy | 60 |
| | 1C.2 | Myocardial Tissue Characterisation | 63 |
| | 1C.3 | Dimensional Accuracy | 64 |
| Chapter 2 | | Safety Considerations in Magnetic Resonance Imaging | 67 |
| | 2A | Physical Effects of a Static Magnetic Field | 67 |
| | 2B | Biological Effects of a Static Magnetic Field | 69 |
| | 2C | Effects of a Rapidly Varying Magnetic Field | 70 |
| | 2D | Effects of Radiofrequency Time-Varying Magnetic Fields | 71 |
| | 2E | Psychological Effects | 72 |
| Chapter 3 | | Technological Developments | 73 |

| | | | |
|---|---|---|---|
| | 3A | Patient Positioning | 73 |
| | 3B | Cardiac Gating | 77 |
| | 3B.1 | Development of Cardiac Gating | 77 |
| | 3B.2 | Position and Type of Electrodes | 80 |
| | 3B.3 | Influence of Electrocardiographic Wave Form | 81 |
| | 3B.4 | Influence of Cardiac Arrythmias | 82 |
| | 3B.5 | Influence of Coughing | 82 |
| | 3C | Accuracy of Measurement of the Relaxation Times, T1 and T2 | 83 |
| | 3D | Effects of Changes in Heart Rate on T1 and T2 Relaxation Times | 89 |
| | 3E | Effect of Slice Angulation on T1 Measurement | 101 |
| | 3F | Measurement of Partial Volume Effects | 104 |
| Chapter 4 | | Radionuclide Cardiac Imaging | 107 |
| | 4A | First Pass Bolus Technique | 107 |
| | 4B | Equilibrium Ventriculography | 109 |
| Chapter 5 | | Chronic Bronchitis and Emphysema | 112 |
| | 5A | Incidence | 113 |
| | 5B | Right Ventricular Anatomy | 114 |

| | | |
|---|---|---|
| 5C | Pathological Changes in Chronic Obstructive Pulmonary Disease | 115 |
| 5D | Techniques Used to Assess Right Ventricular Hypertrophy | 119 |
| 5D.1 | Chest Roentgenology | 120 |
| 5D.2 | Electrocardiography | 121 |
| 5D.3 | Thallium-201 Myocardial Perfusion Scanning | 123 |
| 5D.4 | Echocardiography | 125 |
| 5D.5 | Magnetic Resonance Imaging | 128 |
| 5E | Techniques used to Assess Right Ventricular Chamber Volume | 131 |
| 5E.1 | Contrast Angiography | 131 |
| 5E.2 | Radionuclide Angiocardiography | 133 |
| 5E.3 | Echocardiography | 136 |
| 5E.4 | Magnetic Resonance Imaging | 138 |
| 5F | Aims | 140 |
| 5G | Patients | 143 |
| 5H | Methods | 145 |
| 5H.1 | Magnetic Resonance Imaging | 145 |
| 5H.2 | Right Heart Catheterisation | 152 |
| 5H.3 | Right Ventricular Ejection Fraction | 152 |
| 5I | Results | 155 |

| | | | |
|---|---|---|---|
| | 5I.1 | T1 Values | 155 |
| | 5I.2 | Heart Rate | 161 |
| | 5I.3 | Right Ventricular Chamber Volume | 161 |
| | 5I.4 | Left Ventricular Chamber Volume | 165 |
| | 5I.5 | Ejection Fraction and Stroke Volume | 165 |
| | 5I.6 | Right Ventricular Free Wall Volume | 168 |
| | 5I.7 | Left Ventricular Wall Volume | 170 |
| | 5I.8 | Comparative Results | 172 |
| | 5I.9 | Reproducibilities | 182 |
| | 5J | Effects of Long Term Oxygen Therapy | 184 |
| | 5K | Discussion | 193 |
| Chapter 6 | | Volumetric Analysis and Tissue Characterisation after Myocardial Infarction | 211 |
| | 6A | Methods of Reducing Myocardial Infarct Size | 211 |
| | 6B | Techniques Used to Quantify Myocardial Infarct Size | 221 |
| | 6B.1 | Electrocardiography | 221 |
| | 6B.2 | Enzymatic Estimation | 222 |
| | 6B.3 | Echocardiography | 223 |
| | 6B.4 | Radionuclide Imaging | 224 |
| | 6B.5 | X-ray Computed Tomography | 226 |
| | 6B.6 | Magnetic Resonance Imaging | 226 |

| | | | |
|---|---|---|---|
| | 6C | Aims | 231 |
| | 6D | Estimation of Myocardial Infarct Size from T1 images | 233 |
| | 6D.1 | Patients | 233 |
| | 6D.2 | Methods | 233 |
| | 6D.3 | Results | 243 |
| | 6E | Comparison of T1 and T2 Images in the Estimation of Myocardial Infarct Size | 256 |
| | 6F | Changes in Myocardial Infarct Size with Time | 267 |
| | 6G | Effect of Oral Captopril and Isosorbide Dinitrate on Myocardial Infarct Size and Left Ventricular Volume | 272 |
| | 6H | Discussion | 279 |
| References | | | 297 |
| Appendices | | 1 (Tables 5 - 10) | 355 |
| | | 2 (Tables 13 - 20) | 362 |

**ABSTRACT**

Magnetic resonance imaging (MRI) offers the unique ability to examine the heart in three dimensions and to provide tissue characterisation. This thesis aims to investigate two areas of particular interest, namely the quantification of cor pulmonale and acute myocardial infarction.

The methods currently available for assessing right ventricular hypertrophy and dilatation are discussed, with particular reference to patients with chronic obstructive pulmonary disease. The results of pulmonary haemodynamic and blood gas data are compared with the results from cardiac gated MRI. A good correlation is obtained between the mean and systolic pulmonary artery pressures, the pulmonary vascular resistance and the right ventricular wall volume measured by MRI. This technique is subsequently used in a small group of patients to determine the response to long term oxygen therapy.

The various techniques employed to assess the size of myocardial infarcts are discussed, and the previous literature on the ability of MRI to detect infarction is reviewed. A new technique, which is supported by phantom experiments, is described to measure the volume of infarcted myocardium using saturation recovery - inversion recovery and spin-echo images. The T1 images are compared with radionuclide pyrophosphate scanning and serum creatine kinase-MB release and a satisfactory agreement obtained. Myocardial infarct size measured by both pulse sequences is

compared directly. The spin-echo technique is used to assess alterations in myocardial infarct size with time and the response to various therapeutic options is compared.

In conclusion the limitations of both techniques are discussed and future developments proposed.

**ACKNOWLEDGEMENTS**

I wish to express my sincere thanks to the following:

Professor J J K Best, Professor of Medical Radiology for encouraging me to pursue my research in magnetic resonance imaging and for helping me to develop my career in Academic Radiology.

Dr A L Muir, Post-Graduate Dean and Honorary Consultant in the Royal Infirmary of Edinburgh, for making available patients who presented with acute myocardial infarction, and for his constant advice, valuable criticism and help throughout my career both as a Radiologist and in General Medicine. It has been much appreciated.

Dr W MacNee, Consultant Physician in Respiratory Medicine at the City Hospital for his assistance in data collection and allowing me to study a cohort of patients with chronic obstructive pulmonary disease.

Dr J P Ridgway from the Medical Physics Department, without whose help in the development of cardiac gating and various software programmes, this thesis would not have been possible. His support and friendship throughout the years have been greatly valued.

Dr D M Kean, Senior Lecturer in Medical Radiology for his continuing advice, friendship and never ending good humour.

Miss Felice Taddei and Dr Jeremy Nicoll from the Departments of Medicine and Medical Physics for their help in performing radionuclide ventriculography.

Mrs Colette Rowan for the many hours of hard work spent typing the thesis and attempting to decipher my writing, and to Mr Ian Lennox, Department of Medical Illustration for his help in preparing diagrams.

My sister, Dr Lesley Turnbull for her invaluable encouragement and help at all times.

And mostly to my mother, Mrs Morag Turnbull for her great tolerance, for all her support during my career and for painstakingly correcting the manuscript.

## DECLARATION OF PUBLISHED WORK

1. Turnbull LW, Ridgway JP, Biernacki W, McRitchie HA, Muir AL, Best JJK and McNee W. Assessment of the right ventricle by magnetic resonance imaging in chronic obstructive lung disease. Thorax 1990;45:597-601.

2. Turnbull LW, Bell D, Nicoll JJ, Ridgway JP, Muir AL and Best JJK. Myocardial infarct sizing by magnetic resonance imaging and 99m-Tc pyrophosphate. (Submitted to British Heart Journal)

## LIST OF TABLES


| Table Number | | Page |
|---|---|---|
| 1. | Comparison of measured against calibrated T1 and T2 values for 12 phantom objects, using a field strength of 0.08 Tesla and a standard region of interest | 87 |
| 2. | Variation in measured T1 value with heart rate for a series of calibrated T1 phantoms | 91 |
| 3. | Variation in signal intensity of the first-echo (TE = 42ms) of a double spin-echo pulse sequence with heart rate for a series of calibrated T2 phantoms | 96 |
| 4. | Variation in signal intensity of the second-echo (TE = 120ms) of a double spin-echo pulse sequence with heart rate for a series of calibrated T2 phantoms | 97 |
| 5. | Variation in measured T1 value with heart rate and slice angulation for a calibrated T1 value of 118ms | 355 |
| 6. | Variation in measured T1 value with heart rate and slice angulation for a calibrated T1 value of | 356 |

240ms

7. Variation in measured T1 value with heart rate and slice angulation for a calibrated T1 value of 333ms 357

8. Variation in measured T1 value with heart rate and slice angulation for a calibrated T1 value of 444ms 358

9. Variation in measured T1 value with heart rate and slice angulation for a calibrated T1 value of 500ms 359

10. Variation in measured T1 value with heart rate and slice angulation for a calibrated T1 value of 991ms 360

11. Mean, standard deviation and range of T1 values for the right and left ventricular walls and heart rates for the four patient groups studied 154

12. Mean, standard deviation and range of T1 values for the right and left ventricular chamber contents for the four patient groups studied 156

13. Individual T1 values for right and left ventricular wall and chamber contents for patients with chronic 362

obstructive pulmonary disease

14. Individual T1 values for right and left ventricular wall and chamber contents for patients with ischaemic heart disease 363

15. Individual T1 values for right and left ventricular wall and chamber contents for age-matched control group 364

16. Individual T1 values for right and left ventricular wall and chamber contents for normal young volunteer group 365

17. Right and left ventricular "free" wall and chamber volumes obtained at end-systole in patients with chronic obstructive pulmonary disease 366

18. Right and left ventricular "free" wall and chamber volumes obtained at end-systole in patients with ischaemic heart disease 367

19. Right and left ventricular "free" wall and chamber volumes obtained at end-systole in the age-matched control group 368

20. Right and left ventricular "free" wall and chamber volumes obtained at end-systole in the normal young 369

volunteer group

21. Mean, standard deviation and range of right ventricular end-systolic chamber volumes in the four patient groups studied 164

22. Comparison of right ventricular chamber volumes in the four patient groups using an independent student's t-test 164

23. Right and left ventricular chamber volumes obtained at end-systole (ESV) and end-diastole (EDV), the stroke volumes (SV) and calculated ejection fractions (EF) in patients with chronic obstructive pulmonary disease 166

24. Mean, standard deviation and range of right ventricular "free" wall volumes obtained at end-systole in the four patient groups studied 169

25. Comparison of right ventricular "free" wall volumes obtained at end-systole in the four patient groups using an independent student's t-test 169

26. Mean, standard deviation and range of left ventricular wall volumes in the four patient groups studied 171

27. Comparison of left ventricular wall volumes (cm3) between the four patient groups using an independent student's t-test 171

28. Correlations with right ventricular end-systolic chamber volume in 16 patients with chronic bronchitis and emphysema 173

29. Correlations with right ventricular "free" wall volume in 16 patients with chronic bronchitis and emphysema 176

30. Correlations with radionuclide right ventricular ejection fraction in 15 of the 16 patients with chronic bronchitis and emphysema 181

31. Variations in right ventricular "free" wall volume obtained at end-systole in 4 normal volunteers on 3 separate occasions 183

32. Alterations in right and left ventricular wall volume in 8 patients with chronic obstructive pulmonary disease after long-term oxygen therapy 186

33. Alterations in right and left ventricular chamber volume in 8 patients with chronic obstructive pulmonary disease after long-term oxygen therapy 191

34. Location of myocardial infarct, T1 values for normal and infarcted myocardium and heart rate for 19 patients after first untreated infarct 244

35. Myocardial infarct size measured by magnetic resonance imaging (MRI), pyrophosphate scanning (PYP) and creatine kinase-MB release in 19 patients after first uncomplicated infarct 247

36. Correlations obtained between measurements of infarct size, left ventricular ejection fraction (%) and creatine kinase-MB release (units/l) 253

37. Comparison between measurements of myocardial infarct size (cm3) for 4 patients obtained on 3 occasions by 2 observers and the inter-observer variability 255

38. Comparison of myocardial infarct size measurement using saturation recovery-inversion recovery and double spin-echo pulse sequences 264

## LIST OF FIGURES


| Figure Number | | Page |
|---|---|---|
| 1. | Schematic representation of a resistive magnetic resonance imager. | 28 |
| 2. | Four components of the NMR signal. In practice T2 is represented by T2* due to inhomogeneities in the external magnetic field. | 31 |
| 3. | a) After $90^{o}$ pulse there is a net magnetic moment in the horizontal plane.<br>b) As the nuclei precess back towards equilibrium they gradually lose phase coherence and the component of net magnetisation in the horizontal plane is reduced.<br>c) Further reduction in the horizontal component of magnetisation with time.<br>d) All nuclei are precessing out of phase, so there is no component of net magnetisation in the horizontal plane.<br>e) Nuclei precess until equilibrium is reached. | 34 |
| 4. | Variations in the net component of magnetic moment in the horizontal (My) and vertical (Mz) directions with time, after a radio-frequency pulse. The envelope of the NMR signal is only T2 in a | 37 |

hypothetical situation of a perfectly uniform magnetic field.

5. Interleaved saturation recovery-inversion recovery pulse sequence used to produce two images from which T1 map images can be calculated. 42

6. Double spin-echo pulse sequence. 45

7. Schematic representation of the cardiac gating facility. 79

8. Comparison of the measured and calibrated T1 values for the 12 phantoms. 84

9. Comparison of the measured and calibrated T2 values of the 12 phantoms. 86

10. Alteration in signal intensity with heart rate for a series of calibrated phantoms (T1 values of 118, 240, 333, 444 and 500ms) using a saturation recovery-inversion recovery pulse sequence (TR1 = 1000ms; TR2 = 1000ms and TI = 200ms.) 93

11. Alteration in theoretical signal intensity with heart rate for three phantoms with calibrated T1 values of 240, 444 and 991ms. 94

12. Alteration in signal intensity of phantom objects 1, 3 and 4 using a double spin-echo pulse sequence a) first echo = 42ms b) second echo = 120ms, and a variable heart rate (bpm). 98

13. Alteration in theoretical signal intensity for spin-echo images with a TE of 42 and 120ms for a calibrated phantom (TI = 333ms and T2 = 150ms). 99

14. a) Coronal and b) $30^{o}$ angled transverse T1 map images showing pixel lose at the water /copper sulphate boundary (TR = 1000ms; TI = 200ms). 105

15. Using a saturation recovery-inversion recovery pulse sequence, four images are obtained: a) saturation recovery b) inversion recovery c) difference and d) T1 map image. 148

16. a) T1 map image showing good delineation between normal myocardium and intra-ventricular blood, in a patient with marked right ventricular hypertrophy. b) The right ventricular "free" wall is outlined in white. Small pleural effusions are seen posteriorly as areas of increased signal intensity. 150

17. Comparison between T1 values for a) the right and left ventricular walls and b) chamber contents using coefficient of correlation. 158

18. Plot of the difference between T1 values for a) the left and right ventricular walls and b) the chamber contents against their mean values. 160

19. Comparison of T1 values for the right a) and left b) ventricular walls with heart rate for the four patient groups studied. Measured T1 values for calibrated phantom (333ms) are superimposed (----). 162

20. Comparison of right and left ventricular stroke volumes using a) coefficient of correlation and b) difference between right and left ventricular stroke volumes against the mean of the two measurements. 167

21. Relationship between right ventricular "free" wall volume and right ventricular chamber volume in patients with chronic obstructive pulmonary disease. 174

22. Relationship between right ventricular "free" wall volume and a) the systolic pulmonary arterial pressure and b) the pulmonary vascular resistance in patients with chronic obstructive pulmonary disease. 177

23. Relationship between right ventricular "free" wall volume and a) arterial carbon dioxide tension and 179

b) arterial oxygen tension in patients with chronic obstructive pulmonary disease.

24. Typical example of a transverse T1 map image obtained at the level of the right ventricle, showing significant increase in the right ventricular "free" wall volume after long term oxygen therapy (b), compared to pre-treatment examination (a). 185

25. Comparison of right and left ventricular wall volumes before and after domiciliary oxygen therapy. 189

26. Comparison of right and left ventricular chamber volumes before and after domiciliary oxygen therapy. 192

27a. Angled transverse T1 map image at the level of the ventricles showing good contrast between myocardium, pericardial soft tissues and chamber contents. The increased signal intensity (light blue/green areas) seen in the interventricular septum, anterior wall of the right ventricle and anterolaterally in the left ventricle represents extensive infarction. 235

27b&c. Extensive anterolateral myocardial infarction, 237

showing as a large semi-circular area of increased signal intensity.
b) The left ventricular endo- and epicardial borders are outlined in white.
c) Areas within the left ventricle with a T1 value two standard deviations or more above the mean T1 value for normal myocardium are shown in white.

28. Single photon emission tomographic images of 99m-Tc pyrophosphate uptake in the myocardium of the same patient seen in Figure 27 a-c, with an extensive anterolateral infarct. The four images are: a) coronal section, b) sagittal section, c) transverse and d) scout image roughly equating to a planar view. 239

29. Angled transverse T1 map image showing an area of increased signal posteroinferiorly (represented by blue/green area), secondary to myocardial infarction. 242

30. Comparison of T1 values (ms) of normal left ventricular myocardium against heart rate (bpm). Theoretical signal intensity is superimposed on graph (x----x). 245

31. Comparison of myocardial infarct size measured by magnetic resonance imaging and pyrophosphate 248

scanning using a coefficient of correlation.

32. Comparison of myocardial infarct size measured by magnetic resonance imaging and pyrophosphate scanning using a plot of the difference between the two values against the mean of the two values. 251

33. Typical example of a series of first-echo spin echo images (TE = 42ms; TR dependent on heart rate) encompassing part of the left ventricle. 258

34. First-echo image demonstrating an area of increased signal intensity anteriorly due to acute infarction. An incidental finding of a pericardial effusion is noted posterolaterally. 259

35. Two sections from a double spin-echo pulse sequence showing the first (a and c) and second-echo (b and d) images. The anterior myocardial infarct, represented by an area of increased signal intensity is more clearly demonstrated on the second echo images, although the resolution of these images is degraded by motion-induced loss of signal. 261

36. Two sections from a double spin-echo pulse sequence showing the first (a and c) and second-echo images (b and d). The acute anterior 263

myocardial infarct is poorly defined on the second-echo images (particularly image b) due to signal from intracavitary blood.

37. Comparison of T1 and T2 infarct size measurements using a) coefficient of correlation and b) plot of the difference between measurements against the mean of the two measurements. 266

38. Changes in myocardial infarct size with time. Comparison of infarct size before (Scan A) and after treatment (Scan B) for the three groups. 269

39. a) First-echo image showing satisfactory delineation of myocardium and blood pool.
b) Endocardial surface is outlined in white. The irregular region-of-interest is measured to obtain the left ventricular chamber volume. Anterior and posterior papillary muscles are seen on the left lateral ventricular wall. 273

40. Range, mean and standard deviation of myocardial infarct size for the three treatment groups (placebo, captopril and isosorbide dinitrate) at 6-8 weeks post infarction. 275

41. Mean, standard deviation and range of left ventricular volumes (mls) for the three treatment 277

groups (placebo, captopril and isosorbide dinitrate) at 6-8 weeks post infarction.

## 1A BASIC PRINCIPLES OF NUCLEAR MAGNETIC RESONANCE

### 1A.1 Introduction

The phenomenon of nuclear magnetic resonance occurs when nuclei within an object are exposed to an oscillating magnetic field in the radiofrequency region of the electromagnetic spectrum, in the presence of a strong external magnetic field. This causes the nuclei to resonate and after the radiofrequency radiation has been switched off, radiofrequency radiation is then emitted by the resonating nuclei, producing the nuclear magnetic resonance signal. The radiofrequency radiation is both emitted and received by special coils surrounding the object (Figure 1). Absorption of energy will only occur when the radiofrequency radiation is applied at a particular frequency. This resonant frequency, termed the Larmor frequency (W), is related to the external magnetic field strength by the equation

$$W = g\ Ho$$

where g = the gyromagnetic ratio which is constant for a particular nucleus, and Ho = the external magnetic field strength.

Only certain nuclei possess the essential properties for nuclear magnetic resonance to occur, ie only those that possess a non-zero nuclear magnetic moment. The presence of a nuclear magnetic moment is dependent on the number of the protons and neutrons in the nucleus. Both protons and neutrons possess a spin of one half

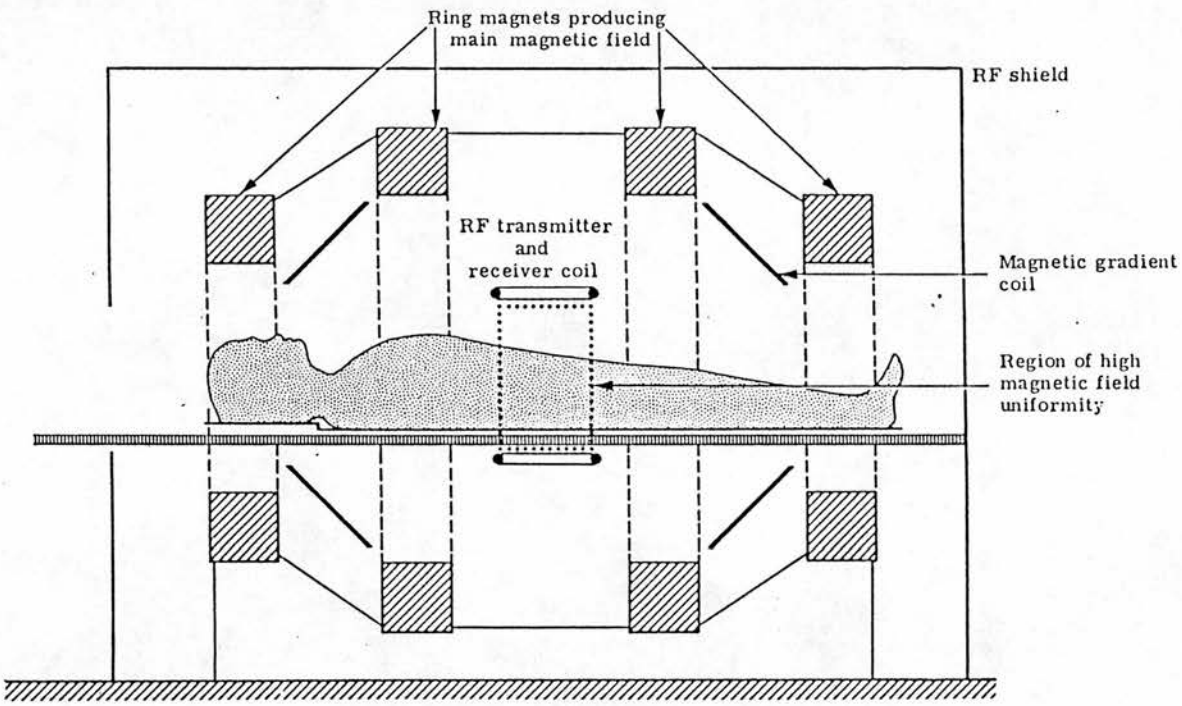


Figure 1. Schematic representation of a resistive magnetic resonance imaging system

and quantum mechanics dictates that pairs of protons or neutrons combine so that their individual spin quantum numbers cancel out. So a nucleus containing even numbers of both protons and neutrons will have a net zero magnetic moment (eg) 12C, 160, 32S, 40Ca. Most of the nuclei studied in biological systems have an odd number of either protons or neutrons and therefore have a magnetic moment of one half. Such nuclei have an intrinsic magnetisation, or magnetic moment that makes each nucleus behave like a magnetic dipole or a small bar magnet. The most commonly studied nuclei are shown below, along with their spin quantum number, the natural abundance (%) and their occurrence in biological systems.

| Nucleus | Spin Quantum Number | Natural Abundance (%) | Natural Occurrence |
|---|---|---|---|
| 1H | 1/2 | 99.9 | All tissues |
| 13C | 1/2 | 1.1 | All tissues |
| 14N | 1 | 99.6 | (Amino acids, Peptides |
| 15N | 1/2 | 0.4 | (Proteins |
| 19F | 1/2 | 100.0 | 'H substitute |
| 23Na | 3/2 | 100.0 | All tissues |
| 31P | 1/2 | 100.0 | Nucleotides, Phospholipids |
| 35Cl | 3/2 | 75.4 | All tissues |
| 39K | 3/2 | 9.1 | All tissues |

The proton clearly has considerable advantages over the other nuclei listed. Not only is it the dominant stable isotope of the

hydrogen nucleus, but it is also present in high concentrations in biological tissues. Although 14N has a spin quantum number of 1, having an odd number of both protons and neutrons, it exhibits the same nuclear magnetic resonance properties as nuclei with a spin quantum number of one half.

### 1A.2 Bulk Magnetisation

When there is no external magnetic field applied, the proton magnetic moments within an object are randomly aligned with respect to one another. In the presence of an external static magnetic field the proton will adopt one of two energy states. These correspond to being aligned either parallel (lower energy) or anti-parallel (higher energy) to the direction of the field. The two energy states are populated by roughly equal numbers of protons with only a slightly greater number occupying the lower energy state thus producing a net magnetisation. The energy difference of the two states is proportional to the strength of the external magnetic field. However a proton can be excited from the lower to the higher energy state by supplying exactly the right amount of energy and thereby increasing the net magnetisation. The population difference between the two energy states is proportional to the magnetic field strength. The greater the field strength the greater is the net magnetisation and therefore the greater the nuclear magnetic resonance signal which is obtainable. It follows from this that systems of higher magnetic field strength produce images of superior quality.

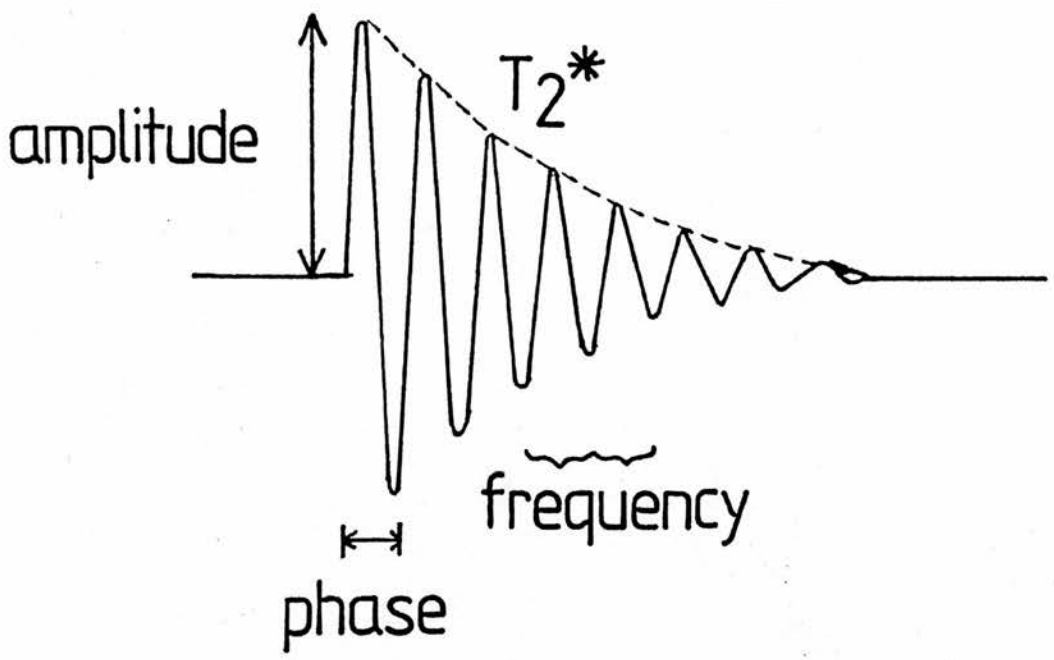


Figure 2. Four components of the NMR signal. In practice T2 is represented by T2* due to inhomogeneities in the external magnetic field.

The net magnetic moment of an object is represented by the bulk magnetisation vector Mo and has components Mx, My and Mz. These are referenced using the Cartesian axes x, y, and z, with the z axis defined in the direction of the external magnetic field.

### 1A.3 Resonance and Precession

In the classical model, resonance of a nucleus is the rotational motion of the bulk magnetisation vector, Mo, about the direction of the external magnetic field. This rotational motion is known as precession and is analogous to the precessional motion of the axis of a spinning top or gyroscope about the earth's gravitational field. At equilibrium the bulk magnetisation vector Mo is aligned with the magnetic field and there is no precession. When an energy source is applied at the resonant frequency the magnetisation vector precesses around the z axis and the bulk magnetisation vector of the nucleus then has three components, Mx, My and Mz. So long as the energy source is applied the angle increases and the bulk magnetisation vector describes a spiral. In the case of a $90^{o}$ pulse, the nucleus is tipped through $90^{o}$ and the component of magnetisation in the x axis, Mx, is equal to Mo, while the component in the z axis, Mz, is equal to zero.

When the nucleus has been tipped through an angle $A^{o}$ and the radiofrequency pulse is switched off, the nucleus precesses back to its original equilibrium position, according to the Larmor equation. The component of the magnetic moment rotating in the horizontal plane perpendicular to the external magnetic field

induces an electric current in a receiver coil around the sample and so a nuclear magnetic resonance signal is detected. Because this occurs in the absence of a driving radiofrequency field it is known as a free induction decay signal (Figure 2). Immediately after the radiofrequency pulse the magnetic moments of the nuclei within the sample are pointing in the same direction and they will all be precessing together (Figure 3a). The nuclei all have the same phase angle $A^{o}$ which is often referred to as being "in phase" or possessing phase coherence. Because all the individual magnetic moments are pointing in the same direction there will be a large net magnetic moment rotating in the horizontal plane which will produce a signal in a radiofrequency receiver coil. Although the sample containing the nuclei is in a hypothetically perfectly uniform external magnetic field each nucleus within the sample will experience an additional minute magnetic field produced by the magnetic moments of other surrounding precessing nuclei. This causes minute variations in the local field throughout the sample resulting in corresponding variations in the Larmor frequency. Thus the nuclei precess at slightly different frequencies and so after a short time all nuclei are not exactly "in phase" and there is loss of phase coherence (Figure 3b & c). This produces a reduction in the net magnetic moment in the horizontal plane and a reduction in the nuclear magnetic resonance signal. Eventually there is complete loss of phase coherence and the horizontal components of the nuclei are randomly arranged and hence no signal is produced (Figure 3d). This occurs before the nuclei have returned to the vertical equilibrium position. The nuclei in the sample continue to precess out of phase until they have all

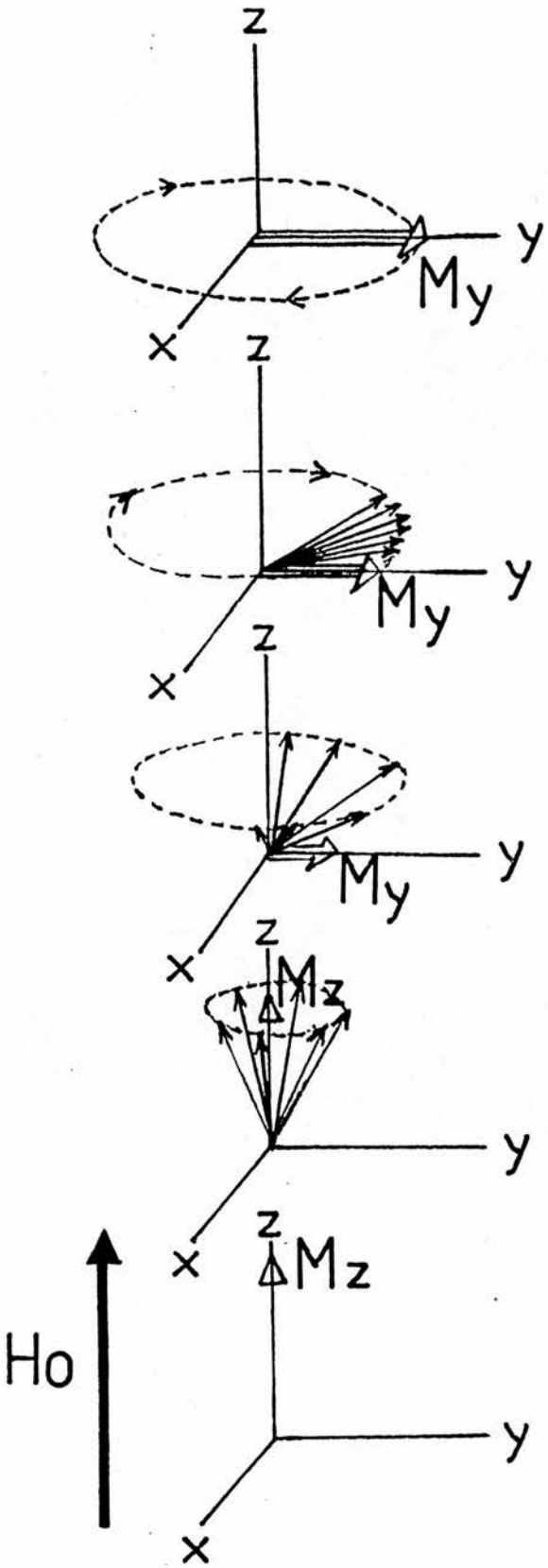


Figure 3.

a) After 90° pulse there is a net magnetic moment in the horizontal plane.

b) As nuclei precess back towards equilibrium they gradually lose phase coherence and the component of net magnetisation in the horizontal plane is reduced.

c) Further reduction in horizontal component of magnetisation with time.

d) All nuclei are precessing out of phase, so there is no component of net magnetisation in the horizontal plane.

e) Nuclei precess until equilibrium is reached.

(Ho: direction of external magnetic field)

returned to the vertical equilibrium position (Figure 3e).

### 1A.4 Radiofrequency Pulses, Slice Width and Slice Selection

The excitation energy used is supplied in pulsed form and has a wide frequency range. Radiofrequency excitation pulses which cause the bulk magnetisation vector to make an angle of $90^{o}$ with the z axis are known as $90^{o}$ pulses whereas excitation pulses which rotate the magnetisation vector through $180^{o}$ are known as $180^{o}$ pulses.

The radiofrequency pulse is composed of a range of frequencies, known as the bandwidth, which is determined by the temporal width of the pulse. The bandwidth determines the slice thickness for a given magnetic field gradient, whilst the central frequency of the pulse determines the slice position along the gradient.

### 1A.5 Production of the NMR Signal

Following the radiofrequency excitation pulse, the slice selection gradient is switched off and a free induction decay signal produced. This signal can be used for image production but is not ideal as it decays very rapidly due to the presence of magnetic field gradients and field inhomogeneity and there is an inevitable time lag between switching on the receiver coil and applying additional field gradients to optimise the signal strength and produce spatial encoding. As a consequence a signal echo rather than a free induction decay signal is commonly used for image production.

## 1A.6 Spatial Encoding of the NMR Signal

The nuclear magnetic resonance signal is produced from a single slice within the imaged sample. In order to reconstruct a two-dimensional image, the signal must be spatially encoded by using magnetic field gradients. The phase and frequency components of the nuclear magnetic resonance signal are used to store information in the x and y directions to produce a two-dimensional image.

### a) Frequency Encoding

In this technique a magnetic field gradient is applied in a direction parallel to the selected plane while the nuclear magnetic resonance signal is being received. This means that although all the nuclei precess at exactly the same frequency immediately after the selective excitation pulse, the addition of the frequency encoding magnetic gradient after the excitation radiofrequency pulse, causes the frequency of resonance of the nuclei to alter throughout the image. A Fourier transformation of this signal produces a plot of the distribution of the frequency components contained with the signal. Since the frequency of the signal is related to the position along the magnetic field gradient, a one-dimensional plot is produced in the direction of the frequency encoding gradient.

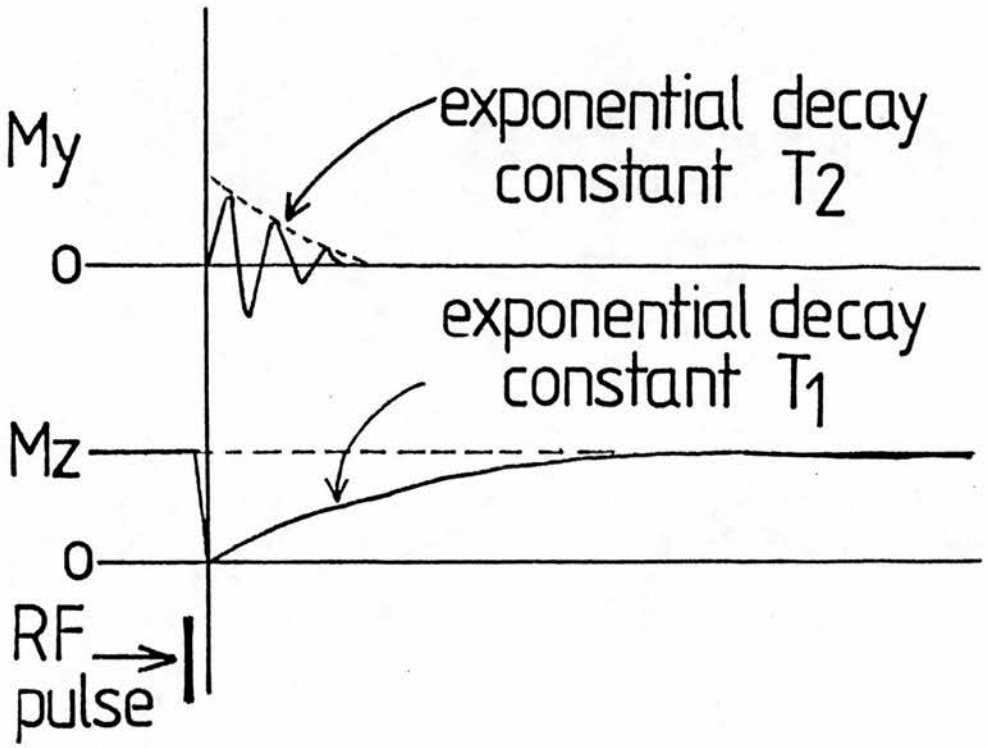


Figure 4. Variations in the net components of magnetic moment in the horizontal (My) and vertical (Mz) directions with time, after a radiofrequency pulse.

The envelope of the NMR signal is only T2 in a hypothetical situation of a perfectly uniform magnetic field.

b) Phase Encoding

In order to produce a two-dimensional image a second gradient is applied perpendicular to the frequency encoding gradient for a short time before the signal echo is produced and detected. This short pulsed gradient, is known as a phase encoding gradient, and it produces a varying phase shift in the nuclear magnetic resonance signal throughout the z direction of the section. This pulsed gradient is repeated on a variable number of occasions usually 64, 128, or 256 depending on the desired matrix size of the final reconstructed image (ie 64 times for a matrix size of 128 x 64). With each repetition the amplitude of the phase encoding gradient is gradually varied through zero to a positive value.

The digitised signal from each repetition of the Gz gradient is stored one above the other to form a two-dimensional array. The final image is obtained from a two-dimensional Fourier transformation of this data. The first Fourier transformation is applied to each signal to obtain the true frequency components of the sample, and the second Fourier transformation is applied to translate the phase encoding into positional information.

## 1A.7 Decay Characteristics of the NMR Signal

As with all excited systems, the population of protons will return to an equilibrium state following excitation via a relaxation process in which energy is emitted. In nuclear magnetic resonance there are two main relaxation processes, namely the longitudinal

relaxation time, T1, and the transverse relaxation time, T2, both of which have characteristic exponential decay times (Figure 4).

a) The Longitudinal Relaxation Time, T1

The return of the bulk magnetisation vector Mo to equilibrium ie parallel with the external magnetic field, following a radiofrequency pulse is described by the exponential decay constant, T1. It is due to the transfer of energy from precessing nuclei to other larger molecules within the surrounding molecular lattice which are not resonating, hence the alternative name of spin-lattice relaxation time.

b) The Transverse Relaxation Time, T2

The exponential decay constant T2, which is also known as the transverse or spin-spin relaxation time is due to the interaction of adjacent protons. During precession the transverse component of the bulk magnetisation Mx, is dependent on the coherence of the precessional motion of the protons within the sample. Whilst individual protons may retain their transverse magnetisation for some time, the bulk magnetisation vector very quickly loses its transverse component as the precessional motion of the population of protons loses its coherence. This incoherence arises from the presence of interactions between adjacent proton spins. This affects the precessional frequency of the individual protons, causing them to move out of phase with one another. Individual magnetic moments cancel-out causing the transverse component of the

magnetisation vector to reduce and the signal magnitude to decay. This decay is exponential with a time constant denoted by T2. The "observed" T2 value is also affected by local inhomogeneities in the external magnetic field, hence the "observed" transverse relaxation time is denoted by T2*.

In general the T1 relaxation time of biological tissues takes longer than the T2 relaxation time. Typical values for normal tissues range from 100 to 1500ms for T1, and 40 to 300ms for T2, although T1 relaxation times are dependent on the field strength. The different T1 and T2 relaxation times are used to discriminate between normal tissues and to demonstrate pathological conditions.

Most of the nuclear magnetic resonance signal comes from water within tissues, and it is thought that the relative percentages of free as opposed to water bound to the surface of proteins determines the values of T1 and T2.

The measurement of the peak value of the free-induction decay signal or the amplitude (Figure 2) represents the magnitude of the magnetisation vector and hence the population density of magnetised protons. This is referred to as the proton density, p. Whilst it is difficult to obtain an absolute measurement of p it is possible to perform quantitative measurements of the relaxation times, T1 and T2 by using particular measurements of the radiofrequency pulse sequences. The most commonly used sequences for measurement are the saturation recovery, inversion recovery, spin-echo, multi spin-echo and field echo sequences.

## 1A.8 Measurement Pulse Sequences

### a) Saturation Recovery

The saturation recovery pulse sequence is used to measure the longitudinal relaxation time T1 and it consists of two $90^{o}$ pulses separated by a time interval, TR, which is the time to repetition

$$90^{o} - TR - 90^{o} - signal$$

ie the time interval between consecutive $90^{o}$ radiofrequency pulses.

Following the first $90^{o}$ pulse the component of magnetisation in the horizontal plane, Mz, returns to the equilibrium position (Mo). The signal obtained following the second $90^{o}$ pulse is dependent on the value of Mz attained after the first $90^{o}$ pulse, and also on the time interval, TR between $90^{o}$ pulses. It is given by the equation

$$Mz = Mo\ [1-exp\ (-TR/T1)]$$

This sequence is repeated for different values of TR to obtain a curve from which T1 can be calculated.

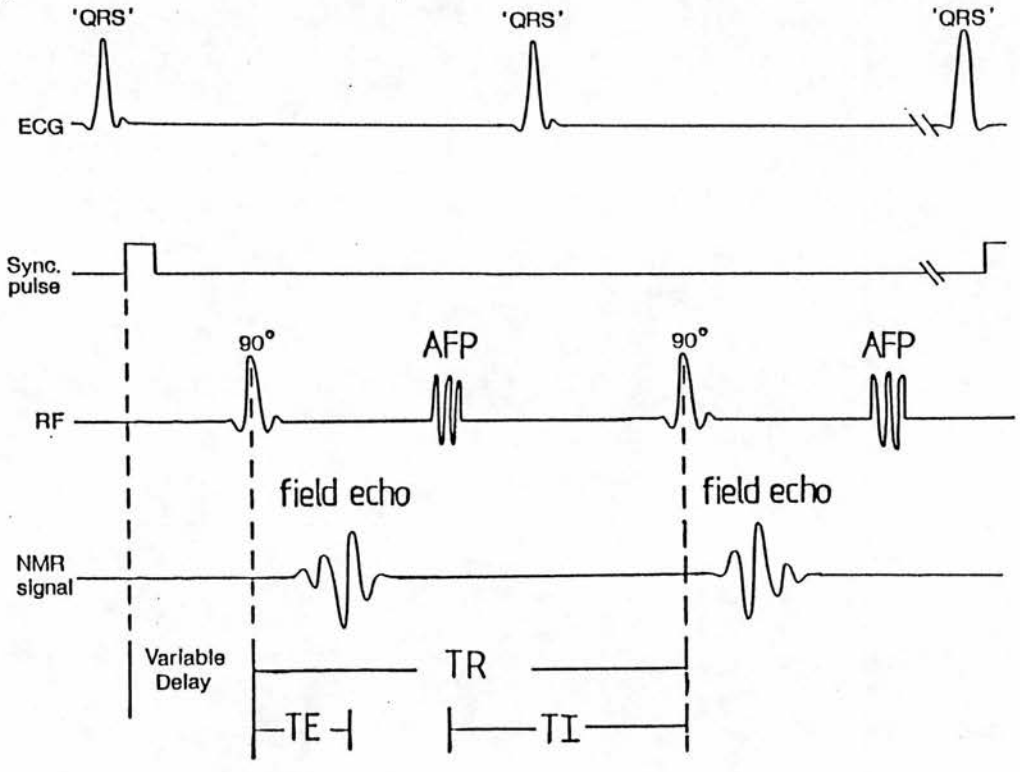


Figure 5. Interleaved saturation recovery and inversion recovery pulse sequence used to produce two images from which T1 map images can be calculated.

b) Inversion Recovery

The inversion recovery sequence is also used to measure T1 and has the form

$$180^{o} - TI - 90^{o} - \text{signal}$$

In this pulse sequence the magnetisation vector is inverted by a $180^{o}$ pulse and then following a time interval TI, the time to inversion, a $90^{o}$ pulse is applied. The signal obtained is a measure of the value Mz, and is given by the equation

$$Mz = Mo\ [1-2\exp\ (-TI/T1)]$$

The sequence is repeated for a number of values of TI to obtain a a value for T1. This technique is more accurate than the saturation recovery sequence as more data points can be obtained. In addition, errors in the value of the $180^{o}$ pulse have less effect on the initial magnetisation vector in the z axis than do errors in the $90^{o}$ pulse. This can be further reduced by using an adiabatic fast passage which is a more efficient method of inverting the magnetisation vector than a $180^{o}$ pulse.

The saturation recovery and inversion recovery pulse sequence can be performed simultaneously using an interleaved saturation recovery-inversion pulse sequence which is shown diagrammatically in Figure 5.

c) Spin-Echo

The spin-echo pulse sequence consists of a $90^{o}$ excitation pulse followed after a time TE/2 which is half the time to echo, by a $180^{o}$ pulse. This pulse sequence has the form

$$90^{o} - TE/2 - 180^{o} - TE/2 - \text{signal (echo)}$$

During the period TE/2, following the $90^{o}$ pulse, the nuclear magnetic moments gradually move out of phase with one another as they experience slight alterations in the local magnetic field values. This results in a loss of coherence and the free induction decay signal decays rapidly. The $180^{o}$ pulse then changes the signal of the phase shift gained by each individual proton by rotating the magnetic moments through $180^{o}$ about the x axis. During a second time period TE/2 following the $180^{o}$ pulse, the nuclear magnetic moments experience the same phase changes as during the first period, again due to the presence of local field inhomogeneities. The net phase changes due to local field inhomogeneities will therefore cancel out and coherence will be re-established for an instant forming a signal echo at a time TE following the $90^{o}$ pulse. As the phase changes continue the nuclei will again lose coherence. The $180^{o}$ pulse does not compensate for loss of coherence due to spin-spin interactions and therefore the magnitude of the signal echo will depend on the T2 of the sample and the value of TE according to the equation.

$$Mxy(TE) = Mo\ [\exp\ (-TE/T2)]$$

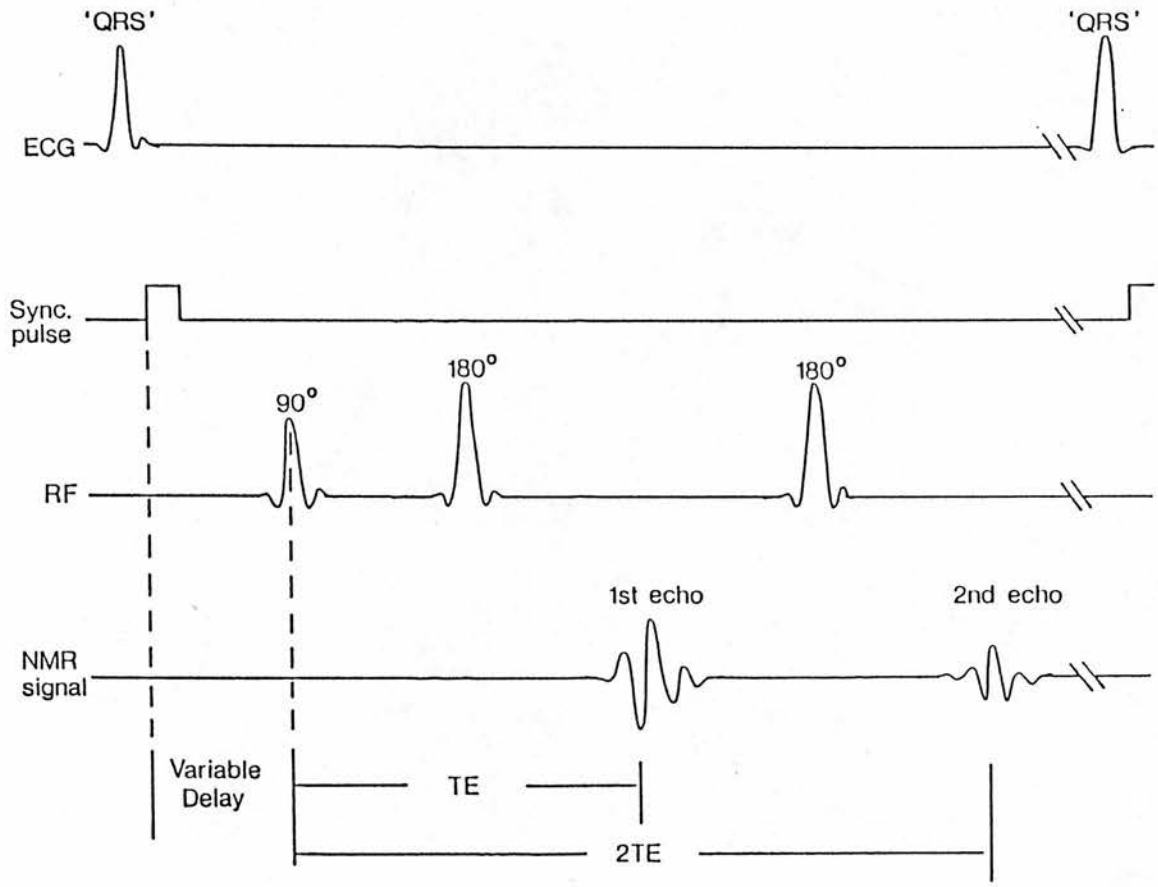


Figure 6. Double spin-echo pulse sequence.

This process of replacing the nuclei using a 180° pulse can be repeated a number of times (1st echo, 2nd echo etc) (Figure 6) and the envelope described by all the echoes is the true T2 relaxation time.

If the TR is short, and the TE is also short, the sequence is effectively the same as a saturation recovery pulse sequence, and the image contrast heavily T1 weighted. As the main application of this sequence is to obtain T2 weighted images, it is important to ensure that the TR is considerably greater than the time to inversion ie between the 90 and 180° excitation pulses, and that the TE is relatively long.

d) Field Echo

In this pulse sequence a signal is produced at a time TE, following the application of an excitation pulse which can be varied from 0-180°. This variable excitation pulse is called the flip angle. In notation form the field echo sequence is given by

$$X^{\circ} - TE - \text{signal},$$

where $X^{\circ}$ is the flip angle. Following the time interval TE, the signal echo is produced by a magnetic field gradient reversal. As with the spin-echo pulse sequence, the T1 weighting increases as the TR and TE are decreased, and the T2 weighting increases as the TR and TE are increased. Increasing the flip angle, increases the T1 weighting for a given TR value, while reducing the flip angle

too close to zero will reduce the signal magnitude to unacceptable levels. However it is possible to optimise the value of the flip angle to maximise the signal-to-noise ratio depending on whether T1 or T2 contrast is required.

There are a number of other parameters which affect the appearance and quality of the magnetic resonance image. These include the operating magnetic field strength and the field homogeneity, the spatial resolution, the field of view and image matrix size, the slice thickness and the scan time.

### 1A.9 Magnetic Field Strength, Type of Magnets and Field Homogeneity

The signal-to-noise ratio obtained is mainly dependent on the magnetic field strength, with systems of stronger magnetic field providing better signal-to-noise ratio and hence improved image resolution. However systems of over 1.5 Tesla field strength also have disadvantages, namely, reduction of T1 contrast and non-linear measurements of T1 values. At very high field strengths ie over 2.0 Tesla, there is absorption of the radiofrequency radiation by surrounding tissues which results in attenuation of the nuclear magnetic resonance signal.

There are three types of magnet used in magnetic resonance imaging. An air cored resistive magnet is used in low field systems operating between 0.02 and 0.15 Tesla, an iron cored resistive magnet between 0.15 and 0.4 Tesla, while power and weight

restrictions necessitate the use of super-conducting electromagnets for field strengths of 0.5 Tesla and above. The electromagnets have a low power consumption, but require liquid helium and nitrogen to cool the magnet to the temperature necessary for super-conduction.

The homogeneity of the magnetic field is usually defined over a sphere at the centre of the system and expressed in parts-per-million. This does not usually alter the appearance of the image, except when scanning outwith the confines of the central sphere.

### 1A.10 Spatial Resolution

The spatial resolution refers to the in-phase resolution of a two-dimensional slice. It is a measure of the minimum distance at which two points can be resolved separately. Provided the signal-to- noise ratio is adequate, the spatial resolution is determined by the pixel size, which is related to the field of view (384mm in this study) and the matrix size (128 x 64mm), by the equation -

$$\text{Resolution} = \text{Field of View/matrix size}$$

The field of view is determined by the magnitude of the frequency encoding and phase encoding gradients and by the imaging bandwidth. The matrix size is directly related to the number of digitised samples acquired and the number of phase encoding steps, ie if 128 samples of the magnetic resonance signal are repeatedly acquired for 64 phase encoding steps, the matrix size of the image is 128 x

64 pixels.

### 1A.11 Slice Thickness

The slice thickness is determined by the bandwidth of the excitation pulse and the magnitude of the magnetic field gradient used for slice selection. Very thin slices will result in a poor signal-to-noise ratio but an increase in slice thickness will lead to partial volume effects, due to the overlap of different structures with a slice. Thus a compromise must be reached between an adequate signal-to-noise ratio and partial volume effects.

### 1A.12 Signal Averaging

In this technique the signal-to-noise ratio is improved not by increasing the slice thickness, which would result in partial volume effects, but by repeating the signal acquisition a number of times for each phase encoding step and then averaging the collected signals. Although the signal-to-noise ratio increases as the square root of the number of acquisitions, the scan time is increased correspondingly. This in turn may lead to image degradation, due to movement artefact.

### 1A.13 Scan Time

The scan time is determined by the repetition time, TR, the number of phase encoding steps employed and the number of signal acquisitions obtained for signal averaging.

## 1A.14 Chemical Shift

Artefacts may be present on images due to the chemical shift phenomenon. The separation of resonant frequencies from an arbitarily chosen reference frequency is termed the chemical shift, and it is expressed in parts per million. Protons within different molecules experience different chemical environments and therefore give rise to separate signals. The only detectable chemical shift in proton signal seen in medical imaging, is between fat (or lipid) and water. At field strengths over 1.0 Tesla this frequency shift can give rise to overlapping of structures at fat-water boundaries in the frequency encoding direction. This effect is less prominent at small receiver bandwidths.

At low field strengths the frequency shift is negligible compared with the imaging bandwidth and no overlapping occurs. Furthermore the use of additional radiofrequency pulses results in a refocusing of magnetisation that eliminates chemical shift as well as the effects of field inhomogenities. However chemical shifts can develop to a significant degree with field echo imaging. With this technique due to the difference in resonant frequencies between fat and water, a phase shift will develop between the signals which increases linearly with time. At its peak the signals from fat and water will be out of phase, so that when they overlap in a voxel there is subtraction of the two signals, with a consequent reduction in image intensity. Dark rims are produced on images where such overlaps occur.

### 1A.15 Magnetic Susceptibility

Magnetic susceptibility may also result in image artefacts. Although the brain has a homogeneous local magnetic field, fluctuations have been demonstrated within the body (Young 1986). Changes in the local magnetic field strength are due to alterations in magnetisation induced in the tissues by the external magnetic field. This effect can either increase or decrease the local field strength, and will give rise to a frequency shift and hence a phase shift in the image. This effect cannot be distinguished on images from the chemical shift effect.

### 1A.16 Blood Flow

It was observed very early that in sequences such as a rapidly repeated free induction decay or partial saturation, that flowing blood gave a high signal intensity. This is because all the blood entering a slice is unsaturated and is available for excitation producing a maximum signal, whereas the tissue remaining in the slice between pulses is already partly excited and hence results in a reduced signal.

### 1A.17 Other Factors Affecting Pixel Intensity

Tissue perfusion and diffusion will not be discussed in this text, but have been well reviewed recently (LeBihan 1990; Chenevert 1990). The effects of cardiac and respiratory motion are discussed in Chapter 3.

## 1B DEVELOPMENT OF MAGNETIC RESONANCE IMAGING

The phenomenon of nuclear magnetic resonance was discovered in the United States of America by two groups working independently - one led by Bloch and the other by Purcell. These results were published almost simultaneously in 1946 and led to the two workers being jointly awarded the Nobel Prize for Physics in 1952.

In 1946 Felix Bloch performed the first biological experiment when he placed his finger in the probe coil of a nuclear magnetic resonance spectrometer and obtained a strong proton signal. This was composed of an integrated signal from the protons in the blood, tissue, fat, bone marrow and the other components of his finger but provided no spatial information concerning the disposition of these structures. Although the first proposal for a magnetic resonance image was provided by Damadian in a patent application filed in 1972, the first practical realisation of a two dimensional image came from Lauterbur in 1973. By applying a field gradient along a number of different directions around an axis through a structured object, a number of different one dimensional projections were obtained and these were combined by computer to give a two dimensional projection image of the object. The method was therefore similar to the projection-reconstruction procedures used in x-ray computed tomography. In this technique a narrow pencil beam of x-rays defines a thin imaging slice. However in magnetic resonance imaging the whole object within the coil is irradiated and an image of a particular slice is obtained by means of either an alternating field gradient or selective irradiation in an

applied gradient.

Magnetic resonance imaging for medical purposes was first reported by Damadian in 1971. Two groups of rats with malignant tumours were studied, one infected with Walker sarcoma and the other with Novikoff hepatoma. The tumours were surgically removed and then measurements of the relaxation parameters, T1 and T2 were made for both tumours and for a range of normal rat tissues. The two malignancies had T1 values that lay entirely outwith the range for normal tissues, in no instances were overlaps encountered. This experiment established that the magnetic resonance signal could detect disease and led to the rapid development of the first body scanning machine. In 1971 results showed that not only could magnetic resonance imaging distinguish between normal and abnormal tissue, but it could also readily distinguish between different normal tissues. This observation led researchers to expand the simple tissue density images of present day radiographic techniques, to obtain high contrast images. The use of T1 values produced pictures with far more contrast discrimination than ever before imagined for non-invasive imaging techniques, the most notable of which was the clear distinction between grey and white matter of brain tissue.

Apparatus to achieve the body scanning objective had to satisfy a new condition not required for measurements on excised tissues and not provided by state of the art magnetic resonance systems. A method was required for "in sample" focusing that could spatially locate a tumour within the body and provide a means for directing

the magnetic resonance beam to specific sites for a locus-by-locus examination of tissue content. A number of different methods have been employed to obtain spatial information regarding the distribution of protons within an object. The most frequently employed is the superimposition over the static magnetic field of another electromagnetic field which varies linearly across the region of interest. In this method, each plane of an object orientated perpendicular to the gradient direction will experience a different magnetic field. Thus, each plane will resonate at a different frequency depending upon its location. In this way the spatial location in the plane of interest is determined by the resonance frequency. The magnetic resonance signal at each frequency thus becomes a one-dimensional projection of the spatial distribution of protons within the object. The imaging methods currently used to obtain images include: sequential point data acquisition, line scanning, planar imaging and three-dimensional imaging.

In sequential point data acquisition at least two different methods have been used that are based upon magnetically localising a small volume of material within a large object. In the steady-state-free-precession method (Hinshaw 1974), the point of interest is isolated by placing the specimen in three orthogonal and nearly linear gradients, all of which are modulated at different frequencies. Using a suitable receiver filter only the signals from the selected "sensitive point" are recorded. Because information is acquired at only one point, the magnetic field gradients can be significantly non-linear compared with other

imaging methods. In the "sensitive point" signal technique, the signal is read out point-by-point by a continuous spin interrogation technique that is usually designated the steady-state-free-precession method. This method uses a continuous stream of high power radiofrequency pulses of short duration (approximately 20ms), to produce images in a single plane. The field focusing nuclear magnetic resonance technique (FONAR) developed by Damadian (1972) exploits the saddle-shaped plot of field intensities which exist in the nuclear magnetic resonance scan. The static magnetic field is degraded everywhere except at the point of the "saddle", by tuning the pick-up coil for resonance at the field value of the "saddle" point. As the signal vanishes when moved off-centre, the object to be imaged is moved repeatedly to align with the centre of the magnetic field. The signal is then read repetitively by a pulse method.

In 1973 Lauterbur suggested line scanning as an alternative to the FONAR method for magnetic resonance scanning which was analagous to the method used in computed x-ray scanning. In line scanning, an entire line or column of material is examined simultaneously. The line of material is defined by multiple magnetic gradient fields (Hinshaw 1976) or by combinations of switched gradients and a selective radiofrequency pulse (Mansfield 1976, Maudsley 1980). The radiofrequency pulses can be altered to excite a specified range of spin magnetisations in the area of a given gradient.

At least three different methods have been developed to study spin magnetisation in a plane of interest within an object. These

planar imaging techniques include project reconstruction, two-dimensional Fourier transformation and echo-planar imaging. In all methods initial slice selection is achieved by selective irradiation. In the project reconstruction technique slice selection utilises gradient modulations as in the point and line scanning methods, but these are coupled with a form of steady-state-free-precession for the signal readout (Lauterbur, 1973). However with this method the received signals are weighted by the sample dependent parameter T2/(T1+T2), which causes loss of signal contrast in the images.

Two-dimensional Fourier transformation has become the standard technique for single slice imaging. In this technique the frequency of the magnetic resonance signal is used to store spatial information in one dimension of a tomographic section and the phase is used to store spatial information in the other dimension. An extension of this technique namely simultaneous slice acquisition has been developed to excite and detect other slices without interfering with the section which is returning to equilibrium.

The last technique is echo planar imaging which was first proposed by Mansfield in 1978. In this technique, which produces images in 40-60ms, a section is selected using a gradient Gy together with a selective radiofrequency pulse. The free induction decay of the section is then subjected to a periodically switched gradient Gx. Further information concerning the spatial distribution within the section is obtained by applying an additional steadily broadening gradient Gz during the signal sampling period.

With these developments in technology a respectable image of a full sized human torso was finally achieved in 1977 by Damadian and his colleagues. This achievement paved the way for successful attempts at body images by other groups. Hinshaw et al produced the first image of the wrist later that year and the FONAR group achieved the first scan of a patient with cancer, namely pulmonary oat cell carcinoma early in 1978. Clough et al (EMI, 1978) at the EMI laboratory produced a reconstruction of the human brain and Mallard et al produced a cross-sectional image of the thorax using a spin-warp technique in 1979.

One of the most striking features seen in early magnetic resonance images of the thorax was the clarity with which the major blood vessels and cardiac chambers were demonstrated even without the use of contrast media. This is due to the intrinsic contrast between the blood pool and the cardiovascular structures. This fact allowed the differentiation of vascular mediastinal masses from tumours by measuring the T1 value of the lesion, thereby avoiding arteriography and bronchoscopy in cases of vascular anomaly and aortic aneurysm. The first proton images of the heart were demonstrated by Damadian et al in 1977. Ungated images were subsequently obtained by several workers using the selective slice excitation technique by which only protons in the slice of interest are excited (Steiner 1983, Hawkes 1981 and Edelstein 1981). Edelstein et al demonstrated the ability to produce sections through the thorax which clearly demonstrated the ventricular chambers and major vessels utilising a saturation recovery - inversion recovery pulse sequence from which a T1 map was produced.

The image reconstruction utilised the phase information contained in the magnetic resonance signal as well as its amplitude to provide information from a tomographic section. In addition to cross sectional images, coronal and sagittal views could also be obtained. Using the saturation recovery - inversion recovery pulse sequence little contrast was obtained between blood and myocardium in the proton density images but a clear distinction was readily seen with inversion recovery studies. Normal and abnormal cardiac images as well as good quality images of the pericardium were reported by many workers (Steiner 1983, Stark 1984).

In magnetic resonance imaging the physiological movements of breathing and cardiac pulsation result in degradation of the images due to general loss of signal. Particularly when imaging the heart this loss is approximately proportional to T1.f, where f is the heart rate. Technical advances including gating of the examination according to the patient's electrocardiogram have led to considerable improvement in image quality over the past few years.

There are however some difficulties, in particular the induction of electrical currents in the electrocardiographic leads produced by the magnetic field pulses as well as the introduction of radiofrequency noise into the system from outside. Filters are available to block outside interference allowing more precise timing of cardiac gating in relation to the R wave, and this will be explained in more detail in Chapter 3B.

Artefacts due to respiration are a major problem in imaging of the

heart, mediastinum and particularly the lungs since they produce considerable image degradation. To overcome this problem, respiratory gating using respiratory ordered phase encoding (ROPE) is feasible but the technique leads to marked delay in imaging time (Lieberman 1984). As respiration is rather slow and only a point at full inspiration can be used as a marker for the radiofrequency pulse, the acquisition time can be three times as long as that required without gating. This method is therefore somewhat impractical.

## 1C USES OF MAGNETIC RESONANCE IMAGING IN CARDIOVASCULAR DISEASE

### 1C.1 Assessment of Anatomy

It is now possible to produce good anatomical information of the heart in the transverse, coronal and sagittal planes by magnetic resonance imaging. Since the introduction of cardiac gating there has been considerable improvement in image quality. The gated images acquired by this method provide sharp definition of internal cardiac morphology and can be temporarily referenced to end-diastole, end-systole or any intermediate point.

There have now been many reports in the literature commenting on the excellent resolution of internal cardiac anatomy (Lanzer 1984, Go 1984, Fletcher 1984). Due to the absence of signal from the blood pool, both sides of the septum as well as the left and right ventricular walls are clearly visualised. With good edge detection the wall thickness and chamber dimensions can easily be measured, and disease processes which result in wall thickening or thinning assessed. Regional myocardial contractility can also be assessed by comparing images obtained at end-diastole and end-systole.

Since magnetic resonance imaging provides sharp delineation of the left ventricular wall, it is an excellent technique for evaluating the presence and severity of cardiomyopathies. It provides accurate definition of the extent, severity and location of left ventricular hypertrophy in hypertrophic cardiomyopathy and has

proved particularly useful in defining the variant forms of this disease, such as the apical and mid-ventricular forms (Higgins 1985, Higgins 1985, Farmer 1985). The patterns of distribution of hypertrophic cardiomyopathy shown by magnetic resonance imaging have correlated well with 2D echocardiography (Been 1985), and have often shown better resolution, particularly in the clearer discrimination of the endocardial and epicardial borders of the left ventricular walls.

Magnetic resonance imaging has also demonstrated the dilatation of the cardiac chambers characteristic of congestive cardiomyopathy. Ischaemic cardiomyopathy can usually be differentiated by the presence of disproportionate wall thinning in one or more regions of the left ventricular wall. This is in contrast to idiopathic cardiomyopathy which is usually characterised by normal wall thickness or mild generalised wall thinning.

Although no consistent changes in magnetic resonance relaxation times have been found in amyloid heart disease (O'Donnell 1984), thickening of the myocardial wall and diminished wall thickening during the cardiac cycle have been demonstrated.

However magnetic resonance imaging is less reliable than 2D echocardiography in depicting the valves and valvular abnormalities. As it scans in fixed imaging planes, the spatial resolution is more than 1mm in thickness and compared to 2D echocardiography the sampling frequency is poor.

Good definition of patho-anatomy in a number of forms of congenital heart disease has been achieved with gated magnetic resonance imaging. Didier and colleagues compared magnetic resonance imaging with angiography and 2D echocardiography in 72 patients with congenital heart disease and showed over a 90 per cent concurrrence rate. It is excellent in complex congenital heart disease where it can define viscero-atrial situs, the type of bulbo-ventricular loop and the relationship of the great vessels. In most patients abnormalities at the level of the great vessels, such as aortic coarctation (von Schulthess 1986) and vascular rings can be identified, and all but small atrial and ventricular septal defects can be located (Didier 1986, Jacobstein 1985). It is useful in defining the intra-atrial anatomy that exists after a Mustard Senning operation to correct transposition of the great vessels. The pulmonary arteries and veins are also clearly shown and magnetic resonance imaging may prove useful for defining pulmonary atresia and anomalous pulmonary venous connections. Precise demonstration of abnormal anatomy has been possible in primary cardiac and mediastinal malignancy (Amparo 1984) and in lesions involving the thoracic cage, although accurate assessment of intra-pulmonary disease requires not only cardiac gating but also respiratory ordered phase encoding.

Gated magnetic resonance imaging provides direct visualisation of the pericardium (Stark 1984). Normal pericardium measures 1.6 $\pm$0.4mm (range 0.8-2.6mm) on magnetic resonance images and has a low signal intensity. Post-mortem data has shown that normal pericardium measures less than 0.5mm suggesting that the low

intensity signal is due not only to the fibrous pericardium but also to adherent pericardial fluid. Constrictive pericarditis due to fibrosis or calcification is seen as a low signal intensity, but in sub-acute forms of constrictive pericarditis caused by irradiation, trauma, or uraemia the thickened pericardium has a moderate to high signal intensity on spin-echo images (Soulen 1985). Small pericardial effusions can be easily seen and unlike echocardiography, pericardial haematoma can be differentiated from other types of effusion.

### 1C.2 Myocardial Tissue Characterisation

Myocardial tissue characterisation at the present time depends on estimation of signal intensity on images with varying TR and TE values, hydrogen density and T1 and T2 relaxation times. Despite these multiple variables, T1 and T2 relaxation times have allowed discrimination between normal and pathological myocardium.

In vitro measurement of relaxation times have revealed that severe myocardial diseases including ischeamic myocardial injury (Williams 1980, Higgins 1983, Johnston 1985), cardiac transplantation and adriamycin cardiomyopathy (Ratner 1983), produce significant alteration in relaxation values. Acute myocardial infarctions have also been characterised in-vivo by increased signal intensity and prolongation of both T1 and T2 relaxation times has been extensively reported. This will be discussed in greater detail in Chapter 6.

Myocardial involvement in patients with active systemic lupus erythematosus has also been demonstrated by an increase in myocardial T1 times (Been 1988). Although this involvement is commonly found at autopsy, it is seldom appreciated by conventional cardiac imaging.

Another model of myocardial disease is provided by cardiac transplant rejection since this mimics acute myocarditis (Ratner 1984, Tscholakoff 1985). Aherne et al in 1986, carried out heterotopic cardiac transplantation in dogs, and as the transplant was placed in parallel with the native heart, relaxation times in the two hearts were compared. In animals not treated with immuno-suppressant therapy, the rejecting allografts showed an increase in the T2 relaxation time of the myocardium compared with the native heart as early as one week post transplantation, but there was no significant difference between the successfully immunosuppressed and the native hearts.

### 1C.3 Dimensional Accuracy

That magnetic resonance can provide high resolution tomographic images of the heart at any part of the cardiac cycle has been demonstrated on both static and dynamic phantoms. These have shown that the technique gives accurate measurements of the ventricular wall thickness, cavity volume and stroke volume. Longmore et al in 1985, compared electrocardiographically gated magnetic resonance images of the left ventricle with x-ray contrast ventriculography. They found a good correlation with the antero-posterior

ventriculograms but a poorer correlation was obtained with the lateral projection due to difficulties in accurately locating the aortic valve. It is known from perspex phantoms that magnetic resonance imaging is accurate in the measurement of linear dimensions, areas and volumes. However it is more difficult to assess the accuracy of this technique for in-vivo measurements. Although there is not an absolute correlation between linear measurements made from ventriculograms with those from magnetic resonance images, this may be explained in several ways. Firstly, it is frequently difficult to ensure that the standardisation marker used in ventriculography is positioned in exactly the same plane as the left ventricle. Secondly, during x-ray contrast ventriculography hypertonic contrast media is injected into the left ventricle thereby potentially increasing the chamber volume. And lastly, the inclusion or exclusion of trabeculae and papillary muscles will alter measurements.

It is now possible to image the heart using a modification of the FLASH technique which was originally described by Frahm and co-workers (1986). In this technique up to forty images can be obtained from an average cardiac cycle and these can be laced together into a cine format for analysis. Good correlations between measurements of left ventricular dimensions by cine magnetic resonance imaging with those from 2D echocardiography and with angiography have recently been reported (Stratemeier 1986, Kaul 1986). Cine magnetic resonance imaging like the standard method is inherently a three dimensional imaging technique so that volume measurements necessary to assess global ventricular function

can be made directly without the need for geometrical assumptions. It also combines good anatomical resolution with high temporal resolution for defining intra-cardiac function. Global and regional ventricular contraction and high velocity flow associated with valvular stenosis or regurgitation and intra-cardiac shunts can also be clearly demonstrated.

## 2 SAFETY CONSIDERATIONS IN MAGNETIC RESONANCE IMAGING

The safety considerations in magnetic resonance imaging for both the patients and hospital staff can be classified into five major areas. For a low field resistive system these include the physical and biological effects of a static magnetic field, the effects of relatively slowly time-varying magnetic fields, the effects of rapidly varying magnetic fields and psychological effects.

### 2A PHYSICAL EFFECTS OF A STATIC MAGNETIC FIELD

There is a potential health hazard from the attractive effect of the static magnetic field on ferromagnetic objects. Depending on the configuration of the magnetic field and the shape and mass of the object and its position within the magnetic field there is either rotation of the object and/or movement towards the magnetic field. The magnitude of this attractive force is dependent on the distance of the object from the centre of the magnet, the geometry of the object, the strength of the magnet and the presence of magnetic shielding. Objects composed of iron, nickel and cobalt are ferromagnetic, as are those types of stainless steel which contain ferritic or martensitic components. When within the body a static magnetic field may potentially exert sufficient torque on ferromagnetic objects that a dangerous situation can exist. For example, foreign bodies including intracranial aneurysm clips, intra-orbital metallic bodies, and shrapnel located near sensitive areas eg spinal cord, could move and create serious clinical problems.

A further hazard is due to the projectile effect, when ferromagnetic objects at a distance from the magnet are attracted towards it, gaining significant speed to act as lethal objects.

The results of numerous studies indicate that patients with non- or minimally ferromagnetic implants or prostheses can safely undergo imaging (Shellock 1988). However patients with ferromagnetic implants, in particular, pacemakers should not undergo scanning, and should be physically restricted from the area surrounding the magnet to at least a point where the field strength of the magnetic field is 5 G or less. It is also known that the reed-switch within the pacemaker which bypasses the normal sensing mechanism and initiates asynchronous function is activated when in proximity to a magnet of sufficient strength (Pavlicek 1983).

Furthermore it is postulated that pacemaker leads may act as antennae and "pace" the heart at the frequency of the imaging pulses. It is also possible that epicardial pacemaker leads which are frequently left in place after cardiac surgery, might also act as antennae during magnetic resonance imaging. Such a scenario has been reported in dogs imaged at 0.15 Tesla (Hayes 1987, Holmes 1986, Fetter 1984), when hypotension was induced during a rapid radiofrequency pulse sequence, following insertion of a pacemaker wire. Similarly, although little documentation is available, two patients with cardiac pacemakers apparently experienced a cardiac arrest during a magnetic resonance scan (Center of Devices & Radiological Health 1989).

Electrocardiographic alterations have also been observed in a static magnetic field (Beischer 1964). Elevation of the T-wave has been reported, which was occasionally so marked that false triggering of radiofrequency pulses occurred. These electrocardiographic manifestations have been reported at field strengths as low as 0.1 Tesla, but disappear as soon as the patient is removed from the magnetic field. This phenomenon has been explained by the induction of current by blood flowing at right angles to the magnetic field. The peak flow potential in man has been calculated at 40 mV in a 2.5 Tesla magnetic field (Saunders 1983). This is the depolarisation threshold for myocardial cells. Although only a fraction of this potential will occur across individual cells, the National Radiation Protection Board has decided the upper limit for field strengths should be 2.5 Tesla until further information is available.

## 2B BIOLOGICAL EFFECTS OF A STATIC MAGNETIC FIELD

This is a controversial area in magnetic resonance imaging. While multiple investigations have failed to reveal any detectable increase in the chromosomal aberration rate or DNA and sister chromatid exchanges (Wolff 1980, 1985; Geard 1984), alteration in spermatogenesis (Withers 1985) or increased tumour cell survival times (Bellossi 1982), one investigator has found a statistically significant increase in the number of chromosomal aberrations in human lymphocyte cultures (Ardito 1984).

Other reports carried out on frogs exposed to high constant

magnetic field gradients during embryogenesis have shown considerable retardation and an increased incidence of malformations (Veno 1984). However no deleterious effects have been recorded due to the static magnetic fields currently used for clinical imaging, although close monitoring continues in this area.

From the cardiac viewpoint there has been no alteration in contractility or function (Knox 1975, Gulch 1986, Doherty 1985, Bellossi 1985) but there was an increase in the length of the cardiac cycle (Jehensen 1988) and increased nerve excitability (Hong 1986).

## 2C EFFECTS OF A RAPIDLY VARYING MAGNETIC FIELD

It is known from Faraday's Law that sudden changes in magnetic field have the potential to induce voltages within the body. The current produced by the induced voltage is dependent on the rate of change of the magnetic field, the cross-sectional area of the conducting tissues and the conductivity of the tissue. The distinction between currents induced by the changing magnetic gradients and those produced by radiofrequency pulses can be explained by the different frequency, wave-form and magnitude of the currents induced in the body. Radiofrequency pulses give rise to oscillating currents of high frequency while gradient switching produces low frequency currents (<1,000Hz). The biological effects of the induced current are either due to the direct effects of the current or thermal effects.

Rapid changes in magnetic field produced only minimal thermal effects which are of no clinical significance. However the direct effects of current induction include an epileptogenic potential, stimulation of visual flash sensation, muscle cell stimulation, ventricular fibrillation and nerve stimulation. The latter two effects only occur at estimated currents higher than those induced under routine clinical conditions (Budinger 1981).

## 2D EFFECTS OF RADIOFREQUENCY TIME-VARYING MAGNETIC FIELDS

These radiofrequency pulses induce currents within the body the majority of which are transformed into heat. This is of major clinical concern. During magnetic resonance imaging tissue heating results primarily from magnetic induction. This occurs mostly at the surface of the body and approaches zero at the centre of the body. Certain organs, such as the testis and eye, are particularly sensitive to heat because of their reduced capability to dissipate heat and their intrinsic biological heat intolerance. Laboratory investigations in dogs carried out at 2.0 Tesla (Berman 1984) have demonstrated elevation of scrotal and testicular tissue temperatures to levels above normal body temperatures, which have resulted in reduced testicular function. However in a preliminary study (Shellock 1990) in humans undergoing whole-body scanning the greatest increase in scrotal skin temperature was only 2.1$^{o}$ C, which was below the level known to impair spermatogenesis.

Similarly corneal temperatures have been measured in patients undergoing magnetic resonance imaging and the largest recorded

change was only 1.8°C (Shellock 1987). As cataractogenesis in animal models only occurs between 41-55°C there is no clinical concern from routine imaging.

## 2E PSYCHOLOGICAL EFFECTS

Claustrophobia is the major psychological problem encountered, although depression, anxiety and panic disorders have also been reported (Quirk 1989, Flaherty 1989). In our institute approximately 1 per cent of patients refused the examination due to a combination of claustrophobia, the noise associated with gradient switching and the ambient temperatures within the magnet bore.

# 3 TECHNOLOGICAL DEVELOPMENTS

## 3A PATIENT POSITIONING

In order to ascertain the optimum plane for visualisation of the ventricular chambers, electrocardiographically gated cardiac imaging was carried out in four normal young volunteers (3 male, 1 female) whose ages ranged from 29 to 34 years.

### 3A.1 Methods

Magnetic resonance imaging was carried out using a low field system operating at 0.08 Tesla. The subjects were placed supine on the imaging couch in a comfortable position so that multiple scans, in different imaging planes could be acquired consecutively. Following application of electrodes and demonstration of an adequate electrocardiographic trigger pulse, scout images were obtained in the coronal plane. These were carried out using a non-gated saturation recovery pulse sequence with a fast repetition time (TR = 240ms) and a field echo time of 22ms. Four slices of 16mm slice collimation and separation were acquired to image the mediastinal structures, and to obtain a long axis view of the ventricles. Gated images were then carried out using an interleaved saturation recovery-inversion recovery pulse sequence (TI = 42ms) from which T1 map and inversion recovery images were generated. The repetition time (TR) varied according to the subject's heart rate, but the slice thickness and separation were constant at 16mm.

From the coronal scout images, multiple paraxial images were programmed which extended both to the right and left beyond the visible cardiac contour. Following acquisition of the paraxial images, multiple coronal scans were obtained extending from the anterior aspect of the sternum into the anterior para-vertebral soft tissues. A mid-coronal image was then selected to programme multiple trans-axial images, extending from the epigastrium to the level of the arch of the aorta. Lastly, multiple short axis views through the vertical long axis were programmed from a mid-coronal image.

### 3A.2 Results

#### a) Paraxial

Paraxial images provided excellent contrast between the anterior surface of the heart formed by the right ventricle, part of the right atrium and at the apex by the left ventricle, from the retrosternal soft tissues formed centrally by the pleural reflections and thymic residue and laterally by lung tissue. Inferiorly, fat was frequently identified as an area of short T1 signal separating the cardiac base from the diaphragmatic surface. Posteriorly, the left atrium was clearly identified separate from the aorta and oesophagus.

However volumetric analysis from these images was frequently hindered by two factors. Firstly, it was difficult to determine the line of separation between atria and ventricles as both the

tricuspid and mitral valves lay within the imaging plane, and were invariably not visualised. Only by the relative thickness and degree of trabeculation could the chambers be separated. And secondly, the point of separation between right and left ventricles was difficult to define.

b) Coronal

As the anterior surface of the right ventricle lies immediately deep to the retrosternal soft tissues, partial volume effects frequently prevented visualisation of the anterior aspect of the chamber, precluding accurate assessment of the right ventricular wall volume. In addition respiratory artefact was particularly noticeable anteriorly. However the mitral and tricuspid valves could be located and the alteration in wall thickness and chamber configuration between atria and ventricles easily identified. This imaging plane also provided good assessment of the ventricular outflow tracts, the main pulmonary arteries, the thoracic aorta and allowed localisation of aortic and pulmonary valves.

c) Trans-axial

These images provided accurate visualisation of the entire cardiac contour from the apex to the ventricular outflow tracts, providing clear delineation of the cardiac chambers and assessment of the relative volumes. However measurements of ventricular wall volume were of necessity obtained oblique to the long axis of the ventricles, resulting in incorrect assessment of wall thickness.

d) Short axis views through vertical long axis

Following upgrading of the M&D system it was possible to obtain images angled from 0 to 30$^{o}$ to the chosen imaging plane. In this study, images were obtained perpendicular to the inter-ventricular septum which frequently necessitated an angulation of 30$^{o}$ cephalad to the transverse plane. These images provided excellent detail of both left and right ventricles which were separated from the retrosternal structures by soft tissues and interposed lungs. Partial volume effects frequently occurred at the extreme cardiac apex and such images were excluded from volumetric analysis. The normal trabeculation of the right ventricle and the inferior and superior papillary muscles within the left ventricle were identified in all normal volunteers. Although due to movement artefact, it was frequently difficult to visualise accurately either the tricuspid or mitral valves, the abrupt alteration in configuration of chamber outlines provided an adequate separation between these structures. Furthermore this orientation had the advantage of providing more accurate measurements of ventricular wall thickness perpendicular to the long axis of the ventricles.

## 3A.3 Conclusions

In all four normal volunteers the short axis view provided the best assessment of ventricular dimensions, particularly of the right ventricle and was therefore chosen for routine use.

## 3B CARDIAC GATING

### 3B.1 Development of Cardiac Gating

Magnetic resonance cardiac imaging requires electrocardiographic gating to reduce movement artefact. The gating signal employed as an external trigger was derived from the rapid upstroke of the R wave of the patient's electrocardiogram. Standard sodium chloride gel electrodes with metal press stud connectors were used initially. Unfortunately the metal press studs in some makes of electrode were found to contain stainless steel which caused a large local defect in the magnetic field. Electrodes with aluminium press studs were therefore preferred but more recently carbon fibre electrodes and leads (standard carbon fibre electrodes, Abingdon Instruments, Oxon) have been used, which do not interfere with the local magnetic field.

The normal electrocardiographic leads required to be electrically screened to reduce the pick-up of external signal noise and radiofrequency pulses by the imager. However the screened leads contained steel wire which in turn altered the local magnetic field. Although thin twin core wire (0.1mm diameter) reduced this problem it was not until carbon fibre leads were introduced that this problem was eliminated. Carbon fibre leads do not suffer from pick-up of magnetic field gradients or radiofrequency signals and could be positioned wherever necessary on the chest wall.

The electrocardiographic leads carried the signal to a battery

powered opto-converter unit which amplified and converted the electrocardiographic signal to an optical signal. Positioning of the opto-converter unit within the machine was found to be crucial. If the unit was placed too far inside the magnet, the radiofrequency shielding caused interference from the unit to be picked up by the receiver coil, reducing the signal-to-noise ratio, whereas placing the unit too far outside the magnet radiofrequency shielding caused pick-up of external signal noise by the electrocardiographic leads. The optimum positioning of the unit was found to be on the patient examination couch level with the opening in the magnet radiofrequency shield.

At the receiver end of the optical fibre link, the optical signals were converted back to electrical signals and then demodulated to obtain the original signal. The demodulated electrocardiographic signal was input to a conventional electrocardiographic monitor (Kontron Micromon 7142) to display the trace and perform R-wave detection. The output from this monitor was relayed to an electronic gating logic module designed by Dr J Amoore of the Department of Medical Physics, Edinburgh. This unit contained an operator controlled time delay between R-wave detection and the onset of the radiofrequency pulse sequence. The delay could be set using coarse and fine setting potentiometers and a marker pulse on the electrocardiographic monitor trace showed the position of the radiofrequency pulse relative to the R-wave.

This system allowed accurate timing of data acquisition provided that there was a dominant positive R-wave. Output from the

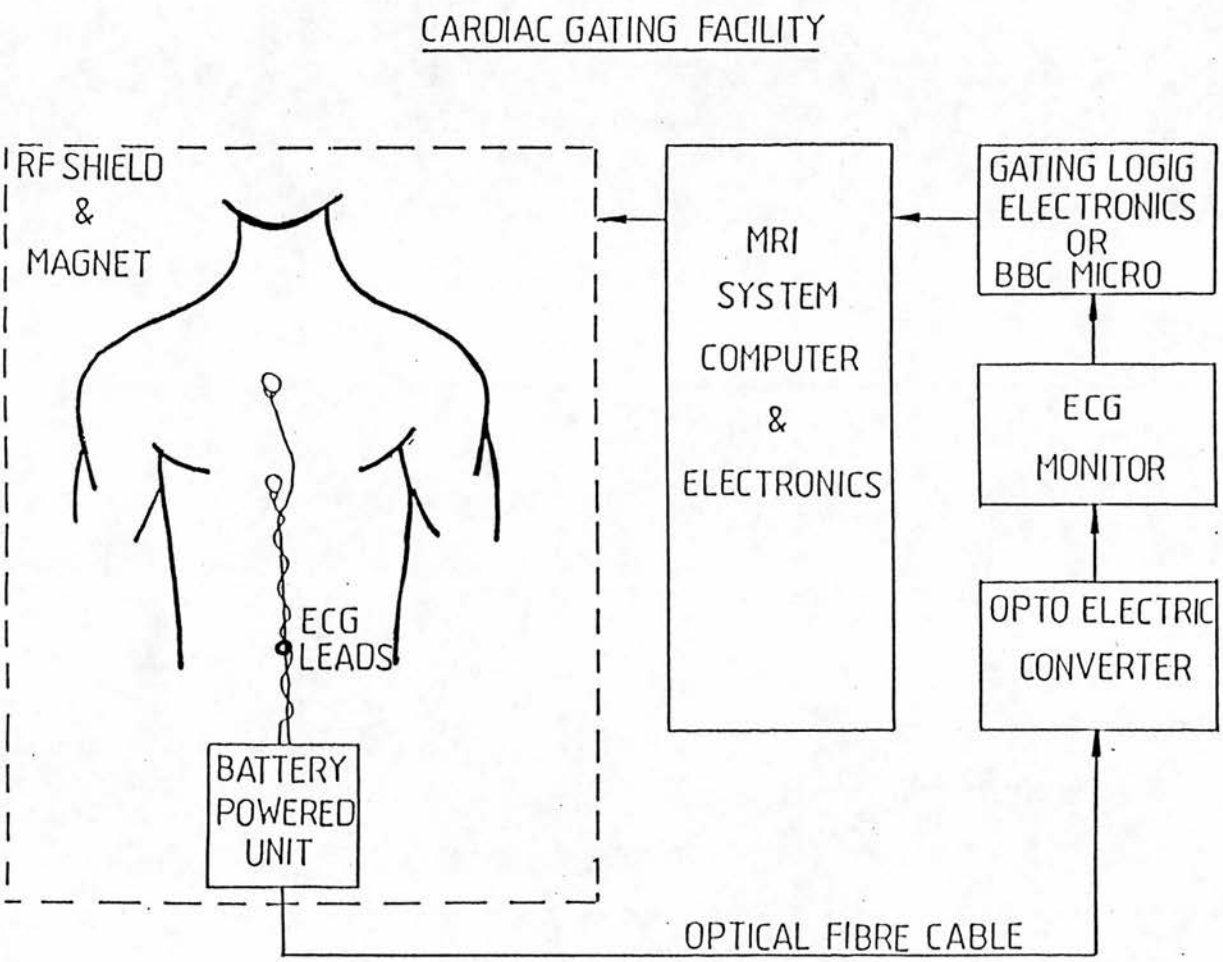


Figure 7. Schematic representation of the cardiac gating facility

dedicated electronic gating logic module was fed to the timer-counter in the system's software which controlled the repetition time of the pulse sequence. The system developed is shown diagrammatically in Figure 7.

### 3B.2 Position and Type of Electrodes

The position of the electrodes on the body was crucial, both to maximise the height of the R-wave and also to minimise gradient and radiofrequency signal pick-up. Two electrode positions have been used. Initially two electrodes were placed on the right lateral chest wall, above and below the heart, in a line parallel to the midline (Smith 1986). This pattern was found to reduce the pick-up from the magnetic field gradients although this varied considerably between patients. Placing the conventional electrodes on the right anterior chest wall ensured that the metal artefact was far from the region of interest. To reduce the magnetic field gradient pick-up further, and to remove metal artefact completely from the chest wall, electrodes were positioned on the left anterior abdominal wall and on the right wrist, with the wrist placed on the left abdominal wall so that the electrodes overlapped. While this position reduced gradient pick-up, excessive abdominal wall movement particularly in patients with respiratory embarrassment resulted in a poor electrocardiographic signal which was generally unacceptable.

With the recent introduction of carbon fibre electrodes and leads (Abingdon Instruments, Oxon), it was possible to position the

electrodes where appropriate to optimise the electrocardiographic signal. These electrodes produced no signal artefact, and although they were not screened, the carbon fibre leads did not suffer from pick-up of external signal noise and the pick-up of magnetic field gradients was less than with conventional leads.

### 3B.3 Influence of Electrocardiographic Wave Form

In all patients it was necessary to adjust the position of the electrodes in order to maximise the height of the upstroke of the QRS complex. In patients with chronic bronchitis and emphysema, accurate positioning of the electrodes was frequently required both to maximise the size of the R-wave and to prevent excessive interference from chest wall movement. In many patients there was a cyclical variation in both the R-R interval and in the height of the QRS complex secondary to exaggerated respiratory effort and alterations in venous return. The R-R interval frequently varied by 50-100ms throughout the study period in such patients, despite allowing time for the patients to relax following any exertion prior to the examination, and supplying oxygen when necessary.

In all patients it was essential that the R-wave was positive and was the dominant deflection in the electrocardiographic trace. Repositioning of electrodes was required if the ST-segment or T-wave were of a similar or greater height than the R-wave, otherwise these acted as an additional or alternative trigger to data acquisition.

### 3B.4 Influence of Cardiac Arrhythmias

Ventricular border definition was adversely affected by marked rhythm irregularities during the relatively long data accumulation period. A regular heart rate with few or no ectopic beats produced the best image quality. Persistent arrhythmias such as frequent ventricular premature beats, bigeminy or atrial fibrillation resulted in significant changes in the ventricular chamber volumes and wall thickness due to marked variations in the R-R interval. This in turn led to significant movement artefact resulting in loss of definition of the endo- and epicardial borders.

From the patient population studied it was apparent that approximately 10 per cent of those individuals recovering from acute myocardial infarction had significant rhythm disturbance, in particular frequent ventricular ectopic beats. Unfortunately using the currently available software package, it was not possible to prevent data accumulation following ectopic beats, so such patients were excluded from this study.

### 3B.5 Influence of Coughing

This occurred primarily in patients with chronic obstructive pulmonary disease, but was reduced to a minimum by allowing the patients to rest whilst on the scanning couch prior to the examination being carried out.

## 3C ACCURACY OF MEASUREMENT OF THE RELAXATION TIMES T1 AND T2

The accuracy of measurement of the relaxation times T1 and T2 was carried out as part of a multi-centre British trial organised by the Medical Research Council and the Department of Health and Social Security, and performed by Dr J P Ridgway of the Department of Medical Physics.

### 3C.1 Methods

The T1 and T2 accuracy tests were carried out using a standard test object. This consisted of a flat perspex cylinder drilled with twelve holes, holding sample tubes of 25mm inner diameter and 60mm total length. The cylinder was filled with a solution with a T1 value typical of biological tissues of about 300ms, measured at low to medium field strength (0.1-0.5 Tesla). The sample tubes contained gadolinium-doped agarose polysaccharide gels of specified T1 and T2 values, which were checked by spectroscopy using a standard measurement protocol (region's of interest of $2cm^2$ or 100 pixels) and the values corrected for temperature at $293^{o}K$ (Lerski 1984). The temperature of the phantom at the time of examination was determined as accurately as possible and the T1 and T2 values obtained were subsequently corrected for temperature. T1 values were measured from the T1 map images obtained from an interleaved saturation recovery-inversion recovery pulse sequence using a TR1 = 1000ms, TR2 = 1000ms and TI = 200ms. The T1 calculations were based on a look-up table which was generated on the assumption that

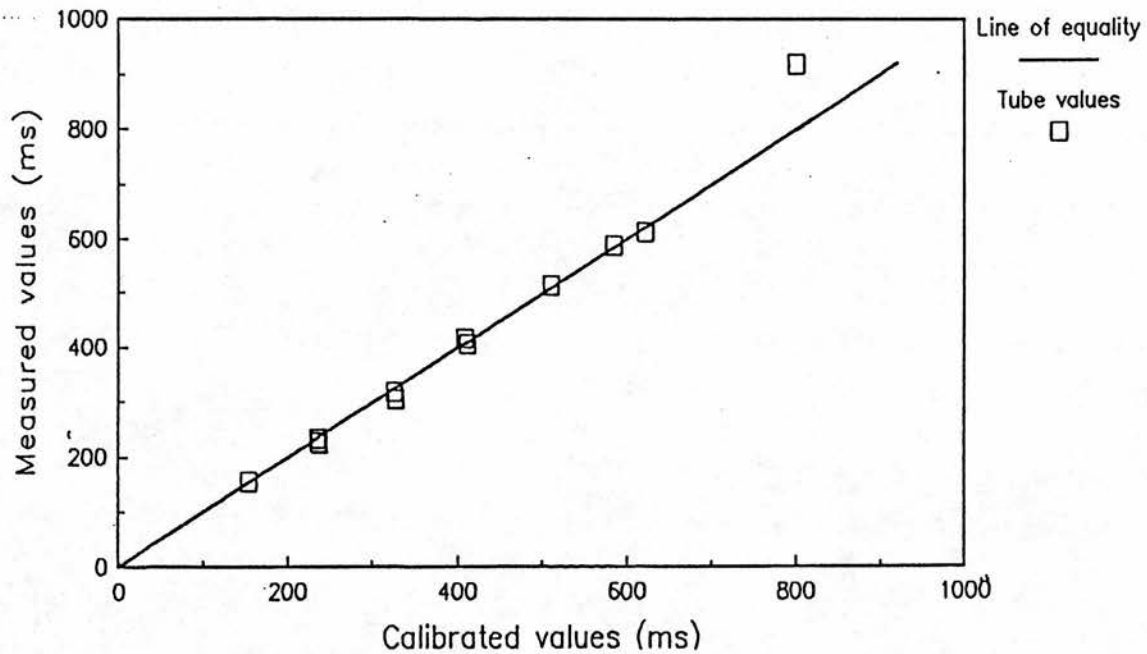


Figure 8. Comparison of measured and calibrated T1 values for the 12 phantoms.

( from the MRC/DHSS Trial of T1 and T2 measurements.)

the signals from the saturation recovery (SR) and 'difference' images (D) are:

$$SR = \exp(-TE/T2)\,[(1 - \exp(-TR/T1)]$$

$$D = \exp(-TE/T2)\,[(\exp(-TI/T1) - \exp(-TR/T1)]$$

The T2 values were measured from the calculated T2 images using a four echo Carr-Purcell-Meiboom-Gill pulse sequence with a TR = 1500ms and a TE = 32ms. The T2 values were calculated from a two point fit of the first and second and the third and fourth echoes.

### 3C.2 Results

The T1 and T2 values of each individual phantom were measured for both sequences using a standard region of interest of $2.28cm^2$ and then compared with the quoted values. The results obtained are shown in Table 1 and represented graphically in Figures 8 and 9.

Figure 8 shows the correlation of the measured T1 values against the line of equality obtained from the values measured spectroscopically. With the exception of the measurement obtained for the 810ms T1 phantom, all other results correlated extremely well with the calibrated values ($r = 0.98$, $p>0.001$). The measured T2 values showed a slightly greater discrepancy. Although the measured values for the 49ms and 62ms T2 phantoms lay on the line of equality, the remainder of the results lay just below the line of equality corresponding with slight under-estimation of the T2 measurements.

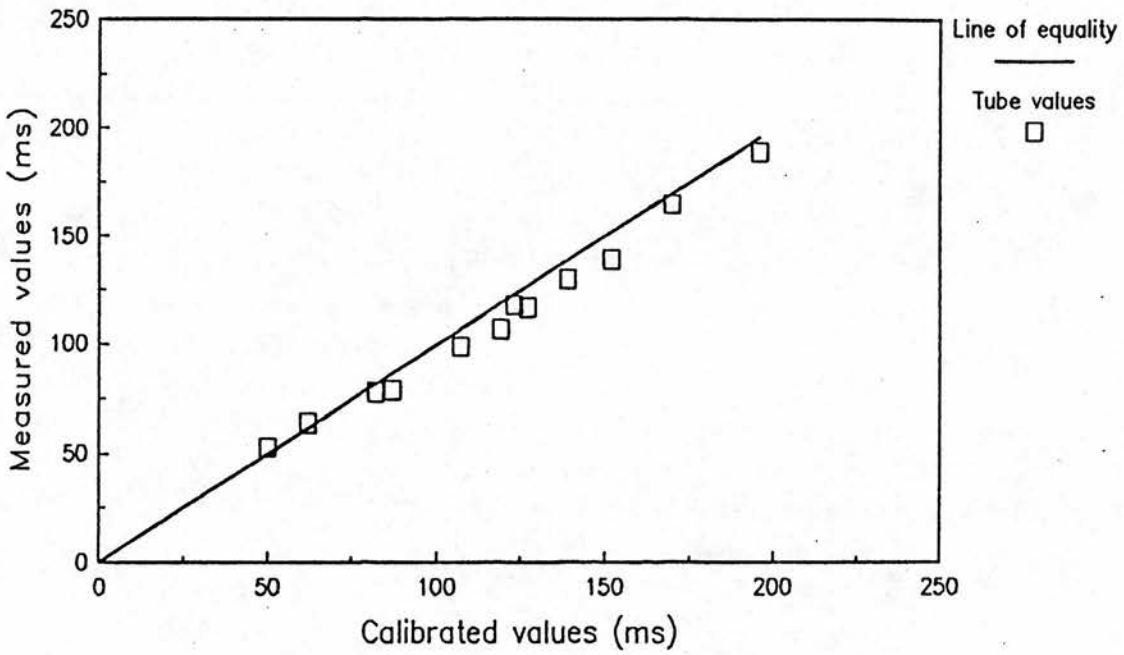


Figure 9. Comparison of measured and calibrated T2 values for the 12 phantoms.

(from MRC/DHSS Trial of T1 and T2 measurements.)

Table 1

Comparison of Measured against Calibrated T1 and T2 Values for 12 Phantoms Objects, Using a Field Strength of 0.08 Tesla and a Standard Region of Interest

(From MRC/DHSS Study of T1 and T2 Measurements)

| Bottle Number | Calibrated Values Quoted at 293°K | | Measured Relaxation Times T1 | T2 |
|---|---|---|---|---|
| | T1 | T2 | Mean ± SD of 3 Measurements at 293°K | Mean ± SD of 6 Measurements at 293°K |
| 2 | 156 | 62 | 155 ±1.4 | 64 ±2.5 |
| 4 | 240 | 49 | 226 ±1.4 | 53 ±1.8 |
| 5 | 239 | 81 | 227 ±2.4 | 78 ±3.0 |
| 6 | 238 | 123 | 234 ±1.7 | 118 ±3.7 |
| 7 | 333 | 86 | 306 ±2.5 | 79 ±5.8 |
| 8 | 331 | 118 | 319 ±1.4 | 107 ±6.9 |
| 9 | 419 | 106 | 408 ±6.6 | 99 ±3.1 |
| 10 | 416 | 138 | 418 ±6.2 | 130 ±3.1 |
| 11 | 519 | 126 | 515 ±8.6 | 117 ±2.8 |
| 13 | 585 | 196 | 588 ±4.6 | 189 ±4.6 |
| 14 | 622 | 152 | 614 ±6.1 | 139 ±5.2 |
| 17 | 801 | 170 | 919 ±15.9 | 165 ±7.0 |

## 3C.3 Conclusions

The look-up tables for T1 and T2 values developed by M&D Technology were generated from an interleaved saturation recovery-inversion recovery pulse sequence using a TR = 1000ms and TI = 200ms, and a four echo Carr-Purcell-Meiboom-Gill pulse sequence employing a TR = 1500ms and a TE = 32ms respectively. When these pulse sequences were used to measure T1 and T2 relaxation times, the values obtained corresponded very well to those obtained spectroscopically. However the same did not pertain to measurements obtained when the TR value was substantially altered and this will be examined in greater detail in the next section.

## 3D EFFECT OF CHANGES IN HEART RATE ON T1 AND T2 RELAXATION TIMES

### 3D.1 Methods

A perspex phantom consisting of six tubes containing varying concentrations of an aqueous manganese chloride solution of known T1 and T2 value was employed. A trigger pulse from a modified electrocardiograph monitor was used to simulate a normal heart beat. This pulse was fed into a BBC model B micro-computer which in turn produced a signal which was relayed into the magnetic resonance system computer to trigger a single data acquisition. By altering the delay between the trigger pulse and signal acquisition, multiple scans were obtained with altering repetition times. Relaxation times were calculated for all six phantoms for twelve different heart rates commencing at 45 bpm and rising by increments of 5 bpm up to 100 bpm.

T1 values were measured from the T1 map images obtained from an interleaved saturation recovery-inversion recovery pulse sequence with a TI = 42ms. This value for TI was chosen as it was used routinely in clinical trials.

The signal intensity of T2-weighted images was calculated for both echoes obtained using a double spin-echo pulse sequence, with echo delay times (TE) of 42ms and 120ms for the first- and second-echo images respectively. Both pulse sequences employed a field-of-view of 384, a matrix size of 128 x 64, a slice thickness of 16mm, and a

single slice technique. The T1 and T2 values were obtained using a standard measurement protocol, employing a circular region of interest of 2.28cm$^3$, and the temperature of the phantom maintained at 20$^{o}$C throughout the examination.

The T1 and T2 values of the six manganese chloride phantoms had previously been calculated using the pulse sequences quoted in Chapter 3C.

The measured T1 values were compared with the predicted signal value, S, for varying heart rates, obtained from the equation -

$$S \propto \frac{[\exp(-TI/T1) - \exp(-TR/T1)]}{1 - \exp(-TR/T1)}$$

where TI, the time to inversion was constant at 42ms, the heart rate (TR) varied from 40 to 100 bpm and three different calibrated T1 values of 240, 444 and 991ms were examined separately.

The theoretical signal intensities for both echoes of a double spin-echo pulse sequence were calculated for phantom object 3 (calibrated T1 = 333ms, calibrated T2 = 150ms) from the expression for signal intensity -

$$S \propto p \exp(-TE/T2) [(1-\exp(-TE/T1) (2\exp(TE/2T1) -1)]$$

where p is the proton density, TR the time to repetition and TE, the time to echo.

TABLE 2

Variation in Measured T1 Value with Heart Rate for a Series of Calibrated T1 Phantoms

| Heart rate (bpm) | Calibrated T1 value (ms) of manganese chloride phantoms (using SR-IR pulse sequence : TR1 = 1,000ms, TR2 = 1,000ms and TI = 200ms) | | | | | |
|---|---|---|---|---|---|---|
| | 118 | 240 | 333 | 444 | 500 | 991 |
| 40 | 83+3 | 162+2 | 215+2 | 270+5 | 305+6 | 511+43 |
| 45 | 85+2 | 165+1 | 223+4 | 289+5 | 333+4 | 546+41 |
| 50 | 94+2 | 186+2 | 257+3 | 336+11 | 402+6 | 672+46 |
| 55 | 92+2 | 198+2 | 279+3 | 357+5 | 398+8 | 912+68 |
| 60 | 94+3 | 193+3 | 263+2 | 322+6 | 333+6 | 695+83 |
| 65 | 93+3 | 196+0 | 269+4 | 341+5 | 362+5 | 897+89 |
| 70 | 87+3 | 171+2 | 222+2 | 264+2 | 281+3 | 470+32 |
| 75 | 88+2 | 166+2 | 215+5 | 258+3 | 278+4 | 343+25 |
| 80 | 87+1 | 164+2 | 210+2 | 252+2 | 273+4 | 415+23 |
| 85 | 86+1 | 160+1 | 207+2 | 254+2 | 273+5 | 405+17 |
| 90 | 87+1 | 160+2 | 207+1 | 252+3 | 276+4 | 413+19 |
| 95 | 88+2 | 167+2 | 220+3 | 277+5 | 303+4 | 476+29 |
| 100 | 89+2 | 162+2 | 215+1 | 266+4 | 296+4 | 455+18 |

## 3D.2 Results

### T1 Values

The variation in measured T1 value with heart rate for the series of calibrated T1 phantoms is tabulated in Table 2 and the results for 5 of the 6 phantoms are shown diagrammatically in Figure 10. The T1 values for the 118ms phantom were relatively constant for heart rates of 50 to 65 bpm with only a slight elevation by 6ms on average, over this range. A similar trend was observed for the 240, 333, 444 and 500ms phantoms with mean increases of approximately 30, 45, 45 and 45ms respectively during the 50-65 bpm time interval. This increase was followed by a slight reduction in values over the 75-90 bpm time interval for the 333, 444, and 500ms phantoms. This fall became more pronounced as the calibrated T1 value increased, with reduction in measured values by 10, 25 & 30ms respectively for the 333, 444 and 500ms phantoms. Measurement of T1 values for the 991ms phantom showed enormous changes with heart rate, particularly over the 50-65 bpm interval with values rising to a maximum of 912ms at 55 bpm compared to a value of 511ms at 40 bpm. This was followed by a fall in measured T1 values between 70-90 bpm with a mimimum value of 343ms recorded at 75 bpm.

Figure 11 shows the alteration in the predicted signal intensity obtained theoretically for the 240, 444 and 991ms calibrated phantoms. The signal intensity obtained for the 240ms phantom was virtually constant with heart rate. There was however, a gradual

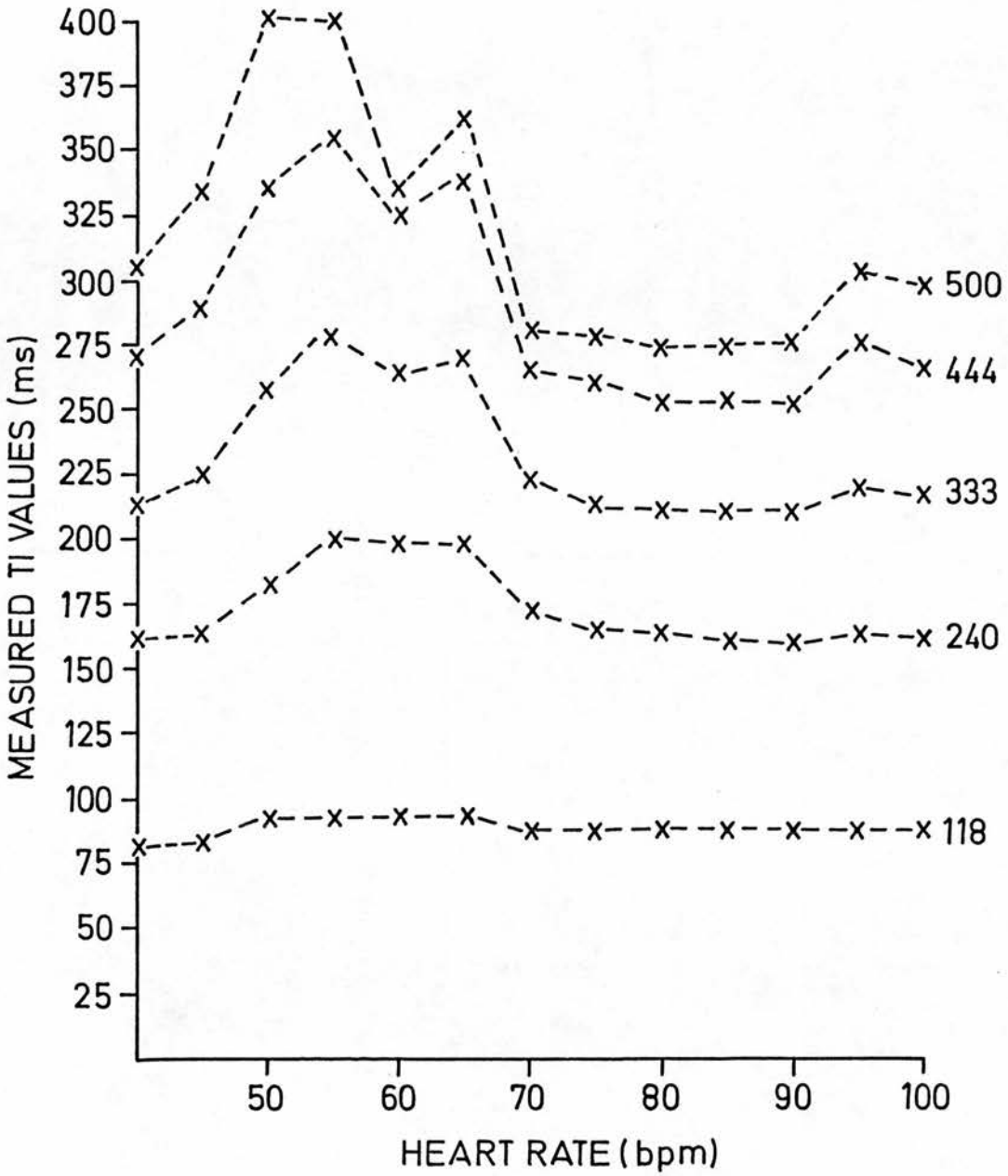


Figure 10. Alteration in signal intensity with heart rate for a series of calibrated phantoms ( T1 values of 118, 240, 333, 444 and 500ms ) using a saturation recovery - inversion recovery pulse sequence ( TR1 = 1000ms; TR2 = 1000ms and TI = 200ms. )

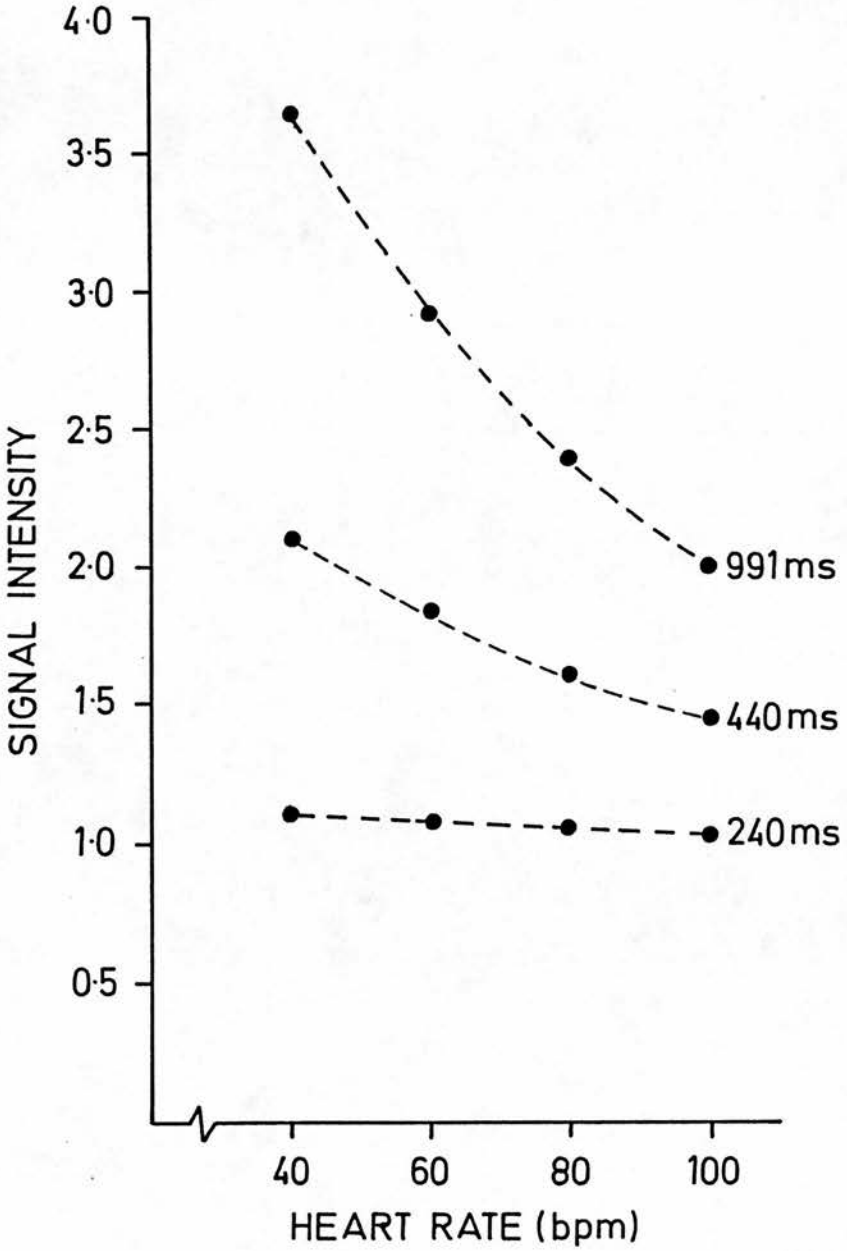


Figure 11. Alteration in theoretical signal intensity with heart rate for three phantoms with calibrated T1 values of 240, 444 and 991ms.

reduction in values with heart rate for the 440ms phantom, but a marked reduction was demonstrated for the 991ms phantom with the signal intensity falling by 45 per cent at a heart rate of 100 bpm compared to 50 bpm.

### T2 Values

The variations in signal intensity of the calibrated phantom objects with heart rate, for both the first- and second-echo images are detailed in Tables 3 & 4, and the results obtained for phantom objects 1, 3 and 4 for both echo images are demonstrated diagrammatically in Figure 12 (a & b). For all phantom objects the measured signal intensity was relatively constant over the 45 to 75 bpm time interval. Between 80 to 90 bpm inclusive, there was a fall in signal intensities, but this returned to previous values at heart rates of 95 and 100 bpm. The fall in signal intensities between 80 to 90 bpm was more marked in the second-echo images for all the phantom objects, with reduction in values by approximately 75 per cent (Figure 12), compared to those obtained for heart rates of 45 to 75 bpm.

The signal intensities obtained by equation for both echoes of the double spin-echo sequence are shown in Figure 13. The curves for both echo times (42 and 120ms) showed a gradual decrease with increasing heart rate.

Table 3

Variation in Signal Intensity of the First-Echo (TE=42ms) of a Double Spin-Echo Pulse Sequence with Heart Rate for a Series of Calibrated T2 Phantom Objects

| Heart rate (bpm) | Calibrated T2 Value (ms) 52 | 105 | 150 | 208 | 236 | 494 |
|---|---|---|---|---|---|---|
| 45 | 123.4 | 201.1 | 214.0 | 217.3 | 204.4 | 198.0 |
| 50 | 120.0 | 181.2 | 194.3 | 205.7 | 195.5 | 187.2 |
| 55 | 130.5 | 193.6 | 219.2 | 230.1 | 218.5 | 208.6 |
| 60 | 132.1 | 182.8 | 206.5 | 221.8 | 210.8 | 206.0 |
| 65 | 135.7 | 183.6 | 212.7 | 225.9 | 212.8 | 210.1 |
| 70 | 123.7 | 159.3 | 190.0 | 210.3 | 192.2 | 191.3 |
| 75 | 120.2 | 150.1 | 183.7 | 195.1 | 185.4 | 183.8 |
| 80 | 106.5 | 130.2 | 158.6 | 165.2 | 162.4 | 167.8 |
| 85 | 94.9 | 109.6 | 131.8 | 148.9 | 138.9 | 141.3 |
| 90 | 87.6 | 95.7 | 124.5 | 137.3 | 125.8 | 133.5 |
| 95 | 147.2 | 158.6 | 203.2 | 216.9 | 214.1 | 218.9 |
| 100 | 146.1 | 156.5 | 203.6 | 216.2 | 213.2 | 220.3 |

Table 4

Variation in Signal Intensity of the Second-Echo (TE=120ms) of a Double Spin-Echo Pulse Sequence with Heart Rate for a Series of Calibrated T2 Phantom Objects

| | Calibrated T2 Value (ms) | | | | | |
|---|---|---|---|---|---|---|
| Heart rate (bpm) | 52 | 105 | 150 | 208 | 236 | 494 |
| 45 | 65.9 | 220.0 | 215.8 | 221.7 | 189.2 | 162.5 |
| 50 | 71.7 | 221.2 | 221.5 | 224.8 | 201.4 | 173.4 |
| 55 | 72.2 | 216.4 | 222.5 | 229.1 | 199.2 | 174.9 |
| 60 | 75.0 | 208.7 | 216.5 | 222.8 | 196.0 | 175.7 |
| 65 | 78.1 | 212.0 | 222.9 | 233.0 | 208.3 | 187.5 |
| 70 | 62.8 | 163.7 | 178.4 | 190.2 | 166.2 | 144.0 |
| 75 | 73.6 | 186.1 | 199.5 | 205.8 | 187.9 | 166.4 |
| 80 | 39.8 | 103.3 | 109.3 | 115.1 | 107.4 | 95.3 |
| 85 | 19.0 | 47.2 | 53.1 | 55.4 | 51.5 | 47.5 |
| 90 | 36.3 | 83.9 | 96.8 | 102.1 | 93.3 | 88.6 |
| 95 | 48.0 | 104.7 | 120.3 | 132.1 | 118.3 | 110.4 |
| 100 | 86.4 | 178.3 | 215.8 | 223.3 | 210.1 | 197.0 |

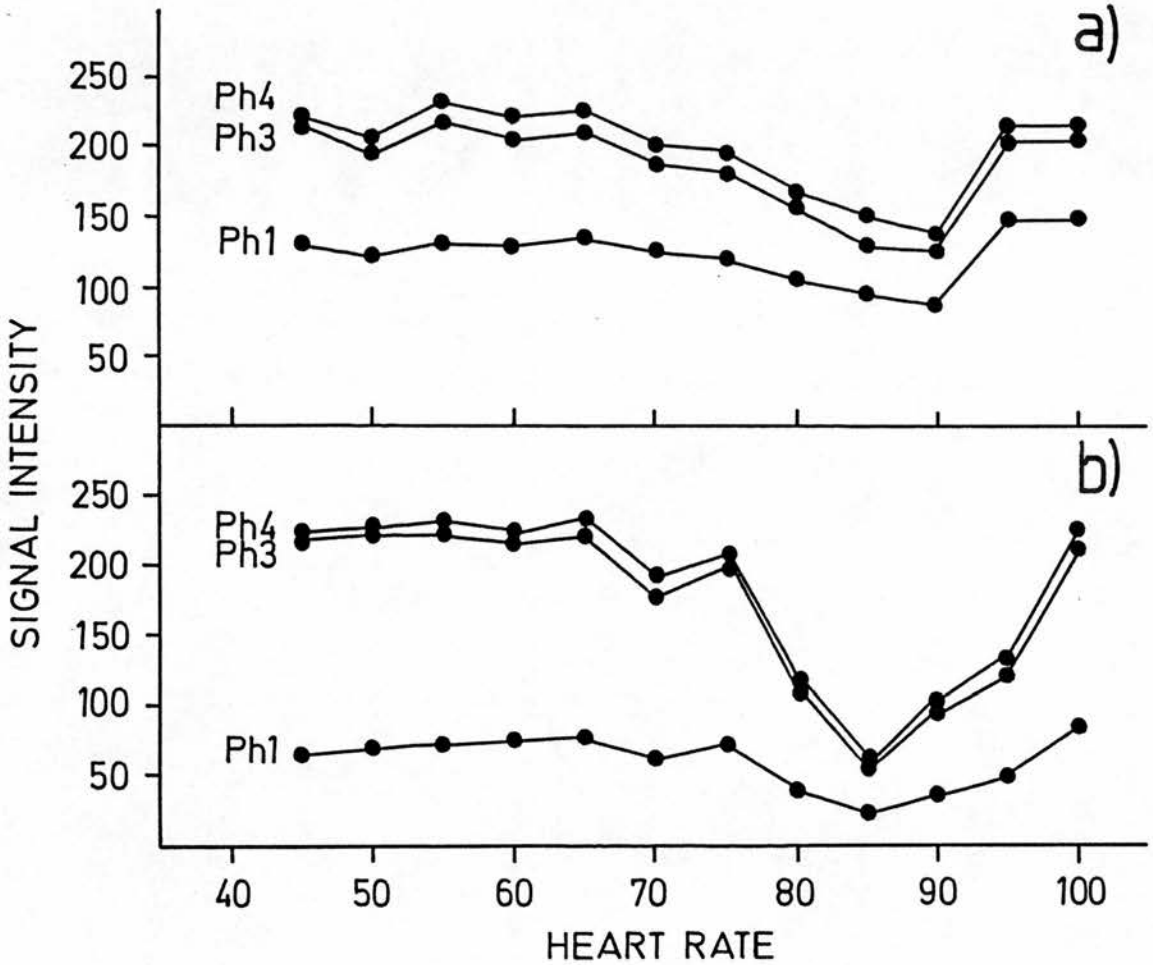


Figure 12. Alteration in signal intensity of phantom objects 1, 3 and 4 using a double spin-echo pulse sequence a) first echo = 42ms b) second echo = 120ms, and a variable heart rate (bpm).

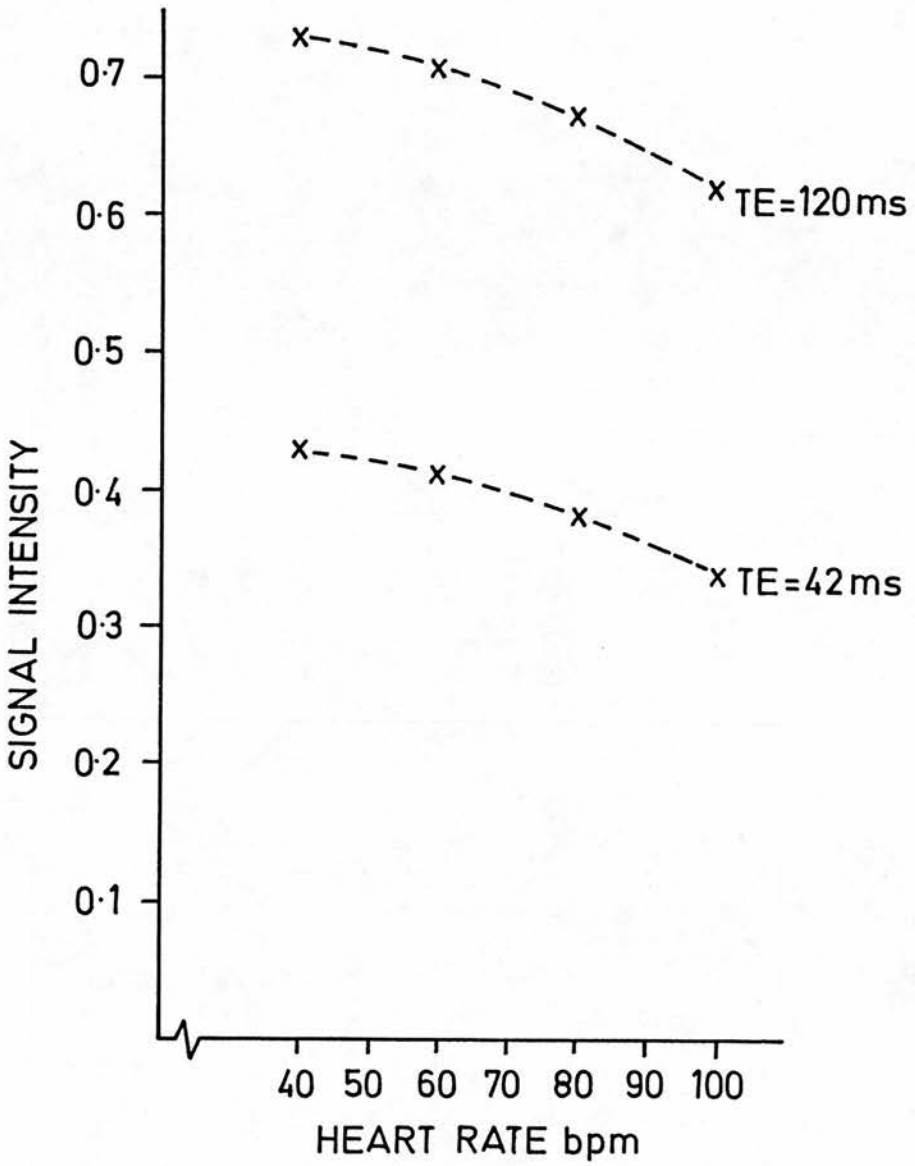


Figure 13. Alteration in theoretical signal intensity for spin-echo images with a TE of 42 and 120ms for a calibrated phantom (T1 = 333ms and T2 = 150ms).

### 3D.3 Conclusions

The shape of the curve obtained for the measured signal intensity for the spin-echo pulse sequence compared favourably with the predicted results over a range of heart rates from 40 to 75 bpm. The sudden decrease in measured signal intensities for both the first- and second-echoes at heart rates between 80 to 95 bpm can be explained by a re-scaling of signal intensities carried out arbitrarily by the computer system software. The computer software arbitrarily scaled the signal intensities on the display consol according to the greatest signal intensity present, rather than to predetermined values.

The results obtained for the measured signal intensities for the saturation recovery-inversion recovery pulse sequence, bore no resemblance to the predicted values. Not only did the curves show considerable disparity in appearance, but the measured T1 values were considerably lower than those expected from previous calibration work, although this was less marked over the 50 to 60 bpm range. The reason for such divergence in results is unknown, but may be due to the use of a fixed repetition time (TR = 1000ms) for generation of the look-up tables in the computer software.

## 3E EFFECT OF SLICE ANGULATION ON T1 MEASUREMENTS

### 3E.1 Methods

A perspex phantom consisting of six tubes containing varying concentrations of an aqueous solution of manganese chloride was employed. The T1 values of the solutions were previously calibrated using an interleaved saturation recovery-inversion recovery pulse sequence (TR1 = 1000ms, TR2 = 1000ms and TI = 200ms), employing a field-of-view of 384, slice resolution of 128 x 64, a slice thickness of 12mm and using a single slice technique. The heart rate was varied, using an electrocardiograph simulator, from 55 to 95 bpm in 5 bpm increments. To assess the effect of slice angulation on T1 measurements, four imaging planes were examined varying from transverse images to a $30^{o}$ anti-clockwise angulation, in $10^{o}$ increments. The pulse sequence employed was an interleaved saturation recovery-inversion recovery pulse sequence, with a TI = 42ms. This particular sequence was chosen as it was used in routine cardiac imaging.

### 3E.2 Results

The variation in measured T1 values with heart rate and slice angulation are tabulated individually for the six calibrated T1 phantoms in Tables 5 to 10 (Appendix 1).

For a calibrated T1 value of 118ms there was no significant alteration in the measured T1 values with either variation in the

heart rate or the degree of angulation from the transverse plane. For the 240ms calibrated phantom, there was a gradual reduction in measured T1 values with increasing heart rate for all imaging planes, but a gradual increase in T1 values with increasing angulation from the transverse plane for all heart rates.

At calibrated T1 values of 333 and 444ms there was a gradual reduction in the measured T1 values with increasing heart rate. However between heart rates of 55 to 65 bpm inclusive, there was a rise in measured T1 values with increasing angulation up to $20^{o}$, with a slight fall at $30^{o}$ angulation. Between 70 and 95 bpm there was a continuing increase in T1 values with a $30^{o}$ angulation. A similar picture was present for the calibrated T1 values of 500 and 991ms, although a slight fall in measured T1 values at $30^{o}$ angulation was present with heart rates from 55 to 75 bpm inclusive.

### 3E.3 Conclusions

This alteration in measured T1 value is presumed to be due to the method of calculation of individual T1 values. In an interleaved saturation recovery-inversion recovery pulse sequence, T1 values are calculated from the signal amplitudes obtained from the saturation recovery and the inversion recovery images.

From Redpath (1982), the signal magnitude for the SR pulse sequence, SRi, immediately following a $90^{o}$ pulse is given by equation (1) and that for the IR pulse sequence, IRi, is given by

equation (2).

$$SRi = k\ Mo\ [1-\exp\ (-TR/T1] \qquad (1)$$

$$IRi = k\ Mo\ [1-2\exp\ (-TI/T1) + \exp\ (-TR/T1)] \qquad (2)$$

where k is a machine-specific constant, Mo is the magnetisation at equilibrium, TR is the time interval between two $90^{o}$ pulses, and TI is the delay between the inversion pulse and the following $90^{o}$ pulse. The "difference" signal data is produced by subtracting the IR signal data from the SR signal data before the images are reconstructed. The signal intensity of the T1 images is then produced by dividing the SR signal data by the "difference" signal data. This number is then converted to a T1 value by comparison with look-up tables which are generated from equation 3.

$$S \propto \frac{\exp\ (-TI/T1) - \exp\ (TR/T1)}{1 - \exp\ (-TR/T1)} \qquad (3)$$

where S is the signal intensity of the T1 image. However these tables are based on a finite value of TR, and do not take into account any possible variation.

In addition the alteration in T1 values obtained with varying degrees of angulation may be secondary to the 2-D Fourier transformation which converts the nuclear magnetic resonance signal into a 2-dimensional image.

## 3F MEASUREMENT OF PARTIAL VOLUME EFFECTS

The final signal intensity that appears in the voxel of an image is dependent on all the parameters of the tissues included, and on additional factors such as the presence of blood flow. In typical imaging circumstances the slice thickness is substantially greater than either of the dimensions of the voxel, so the signal is derived from a mixture of tissues. This results in partial volume effects. In order to measure the magnitude of partial volume effects phantom studies were carried out.

### 3F.1 Methods

A glass jar containing an aqueous solution of copper sulphate (T1 = 980ms) sealed with a single layer of commercially available cling film, was immersed in a tank of water (T1 = 500ms). Using an interleaved saturation recovery-inversion recovery pulse sequence (TR1 = 1000ms, TR2 = 1000ms and TI = 200ms), images were obtained perpendicular and at a $30^{o}$ angulation to the water/copper sulphate interface, using a 12mm slice thickness. A field of view of 384 was employed and each acquisition consisted of 64 phase encoding steps and 128 frequency encoding steps, resulting in a pixel size of 3 x 6mm. This was interpolated to a 128 x 128 matrix (3 x 3mm) for analysis on the final display monitor. Measurements of the "boundary" between copper sulphate and water were made using commercially available software. The distance between two arrows placed on the outer edges of the "boundary" were measured three times and the mean value obtained.

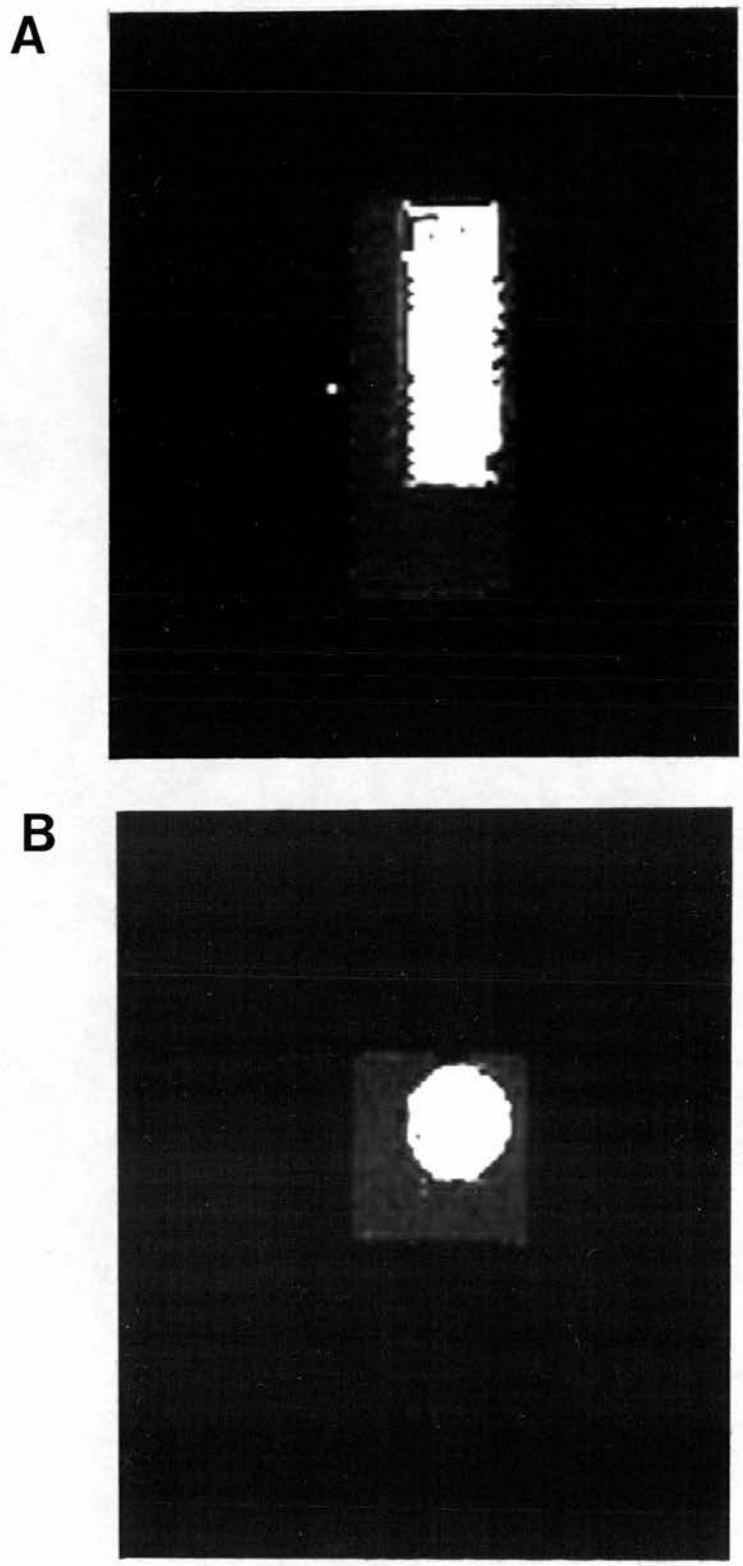


Figure 14. a) Coronal and b) 30° angled transverse T1 map images showing pixel loss at water / copper sulphate boundary. ( TR = 1000ms; TI = 200ms. )

### 3F.2 Results

Figure 14a shows the coronal image which was obtained perpendicular to the fluid interface and Figure 14b shows the 30° angled transverse image. Both images show "pixel loss" at the boundary of water and copper sulphate. This boundary effect had a maximum value of 3mm and a mean value 2.5mm in thickness. It was particularly noticeable on the 30° angled transverse section where the circular image had an irregular "jagged" edge. The interface material itself was too thin to be visualised.

### 3F.3 Conclusions

The actual grey scale level of any individual pixel is determined by the average signal intensity of the various chemical constituents contained within the corresponding voxel. Therefore in voxels containing both copper sulphate solution and water, the signal intensity represents their average value and is not characteristic of either component. In this phantom experiment the "boundary" between solutions had a mean value of 2.5mm which is approximately the size of an individual pixel for a 128-acquisition matrix.

However it is assumed that these partial volume effects will cancel out when measurements of volume are obtained from irregular regions of interest. This will be particularly true when relatively large volumes are measured.

## 4. RADIONUCLIDE CARDIAC IMAGING

Until recently right ventricular performance could only be accurately assessed by cardiac catheterisation and contrast ventriculography. Although right heart catheterisation is less risky than arterial puncture, complications occur in 25 per cent of cases, 4 per cent of which are serious (Boyd 1983). The injection of hypertonic contrast media carries a significant risk and because of the marked variability of the normal right ventricular shape and configuration (Dotter 1953) quantitative measurements of right ventricular volume and of the right ventricular ejection fraction are extremely difficult to obtain. Moreover this invasive technique is not suitable when repeated measurements are required or when large populations are studied.

Two basic techniques are available for functional cardiac imaging, namely the first pass bolus technique and equilibrium ventriculography. The first pass technique is of particular use in studying right ventricular function and dimensions, while equilibrium ventriculography is more suitable for studying left ventricular function. These two techniques will be discussed separately.

### 4A FIRST PASS BOLUS TECHNIQUE

The first pass bolus technique attempts to avoid the geometric variability of the right ventricle. This technique employs a right anterior projection to separate the right atrium from the right

ventricle (Berger 1978). Counts from the overlapping left ventricle can be prevented by detecting the bolus of radioactive tracer only as it passes through the right heart and by stopping the acquisition before it reaches the left atrium. Measurement of the right ventricular ejection fraction is then made from the time activity curve. The main advantages of the first pass technique include:

i) Good temporal and spatial separation between the right and left ventricle (Reduto 1978). This is particularly important in determining the right ventricular silhouette and can be accomplished with a relatively short data acquisition time of between 20-30 seconds.

ii) When studying the right ventricle in isolation, the acquisition of data can be stopped before the bolus of radio tracer enters the lungs thus reducing the background counts.

However there are a number of disadvantages of the first pass technique, which include:

i) Only a single measurement of right ventricular ejection fraction can be made following each injection of radio tracer, and repeated injections cannot be carried out for 2-3 days because of the accumulative radiation burden.

ii) Before injection of the radionuclide the camera must be in a satisfactory position for recording as it is impossible to adjust

the position of the camera during the examination.

iii) It is important to achieve a good bolus of radio tracer in order to get acceptable radioactive counts.

iv) It is assumed that there is adequate mixing of radio tracer within the blood pool in the cardiac chambers.

v) Even with a good bolus injection count rate limitations make the first pass technique less suitable to conventional gamma cameras and a multi-crystal scintillation camera with high count rate capabilities is often required to obtain statistically reliable data (Berger 1978).

vi) The right ventricle has an extremely irregular shape which makes assignment of an accurate region of interest more difficult.

vii) There is often a variable contribution of counts from the right atrium, the exact percentage depending on the right atrial size.

## 4B EQUILIBRIUM VENTRICULOGRAPHY

Strauss et al (1971) first described a technique which allowed a serial evaluation of left ventricular performance. This technique used a cardiac gated mechanism to trigger repeated acquisitions of data at end-systole and end-diastole after the injection of a radio tracer had completely equilibrated in the blood pool.

In this centre, radionuclide ventriculography was performed in the supine position and imaging performed in approximately a $30^{o}$ left anterior oblique projection with a $10^{o}$ caudal tilt. The precise angle was chosen to optimise the separation between the left and right ventricle. After injection of 700MBq 99m-technetium human serum albumen, imaging was carried out using a Siemens low energy mobile gamma camera and the data collected by a micro delta computer.

By gating picture frame images from short time intervals distributed throughout the cardiac cycle, images from 500 sequential heart beats can be summated and viewed in movie format (Muir 1977). The first 20ms accumulation of data, triggered by the upstroke of the R wave thus produces the first frame which represents end-diastole. Further accumulations of data are obtained at 20ms intervals throughout the cardiac cycle. Since radioactive counts are proportional to the chamber volume, if complete mixing has occurred the ejection fraction can be calculated after a suitable correction for non-cardiac background activity.

The multi-gated acquisition technique has several advantages:

i) Most gamma cameras with either single or multiple crystals can be used with minimal additional instrumentation.

ii) Repeated studies can be performed with no additional radiation burden.

iii) The camera can be moved between data acquisitions thus allowing the effects of therapy to be monitored.

iv) Multiple scans can be acquired over three hours without loss of the tracer into the extra-vascular space, provided that a high quality electrolytically labelled human serum albumen preparation is used.

v) Since data is acquired over 500 heart beats the statistics are more reliable than for the first pass technique.

Disadvantages of this technique include:

i) The routine left anterior oblique position may not produce adequate separation between the left and right ventricle.

ii) Poorer results are obtained if the patient is not in sinus rhythm although it is possible to obtain computer programmes to eliminate data collected from ectopic beats.

iii) There is a relatively long acquisition time (10-15 minutes).

## 5. CHRONIC BRONCHITIS AND EMPHYSEMA

Chronic bronchitis is defined clinically as the expectoration of sputum on most days during at least three consecutive months in more than two successive years. Varying degrees of emphysema commonly accompany chronic bronchitis, which is most accurately defined in pathological terms as an increase in the size of the respiratory bronchioles and alveoli resulting from dilatation of airspaces or destruction of their walls.

The basic abnormality in chronic bronchitis is the excessive production of mucous in the bronchi. This excess, probably in conjunction with the direct action of smoking and pollution on the cilia, interferes with the clearance mechanisms of the respiratory tract which renders it susceptible to infection. Recurrent infection is largely responsible for exacerbations of the disease, which cause further damage and destruction of tissue, resulting in dilated, distorted and obliterated bronchioles. The airways obstruction which develops is due to a combination of mucous secretion, thickening of the mucous membranes, spasm and hypertrophy of the bronchial muscle and distortion of the peripheral airways by scarring, air-trapping and emphysema. The ensuing functional abnormality is a ventilation-perfusion imbalance, secondary to poor ventilation of relatively well perfused alveoli, which leads to the development of hypoxaemia.

The classical view holds that hypoxia results in pulmonary vasoconstriction which in turn leads to pulmonary hypertension

(Morley 1947, Wescott 1951, Abrahams 1967). The consequence of this increased pressure load is the development of right ventricular hypertrophy and eventually the clinical signs of right ventricular failure appear, often during an acute exacerbation. The term cor pulmonale is often loosely interpreted as meaning either peripheral oedema, raised jugular venous pressure or right ventricular enlargement, but it was defined by the World Health Organisation in 1963 as "right ventricular enlargement secondary to diseases that affect either the structure or function of the lungs" and this definition remains unchanged at the present time. The development of cor pulmonale in patients with chronic bronchitis and emphysema is invariably associated with a poor prognosis.

## 5.A INCIDENCE

Chronic bronchitis is very prevalent in Britain especially in the Forth-Clyde valley, the industrial Midlands and South Wales, but it occurs in all industrial communities and the prevalence rises with increasing density of urbanization, overcrowding and atmospheric pollution. In the UK chronic obstructive pulmonary disease is one of the most common causes of absence from work, being surpassed only by upper respiratory tract infections and influenza. In England and Wales bronchitis leads to the loss of 30 million working days per year, that is about 10 per cent of all days lost from work due to sickness. A survey carried out by the Royal College of General Practitioners showed that, on clinical grounds alone, 17 per cent of men and 8 per cent of women in the 40-64 year age group, had chronic bronchitis. Similarly, a survey of 18,000

male civil servants in London revealed that 10 per cent of subjects had symptoms suggestive of chronic bronchitis although few had a significant reduction in ventilatory capacity (Office of Health Economics 1977).

In Scotland, chronic bronchitis and emphysema results in 46.5 deaths per 100,000 of the population (Register General 1982). However, in the presence of cor pulmonale, chronic bronchitis and emphysema results in an even higher mortality, with only 45 per cent of such patients surviving for two years compared to a 69 per cent survival rate in patients without cor pulmonale (Renzetti 1966). In 1981, Weitzenblum et al, showed that patients with a normal pulmonary arterial pressure (less that 20mm Hg) had a four year survival of 72 per cent compared with a 49 per cent four year survival in those with a pulmonary arterial pressure greater than 20mm Hg. In a longitudinal study of 50 patients with chronic obstructive pulmonary disease, Burrows et al in 1965 showed that the level of pulmonary vascular resistance correlated best with survival, and that no patients whose pulmonary vascular resistance exceeded 500 dynes sec $cm^{-5}$ survived for 7 years.

## 5.B RIGHT VENTRICULAR ANATOMY

It is known from autopsy (Mitchell 1976, Scott 1941, Spatt 1948) and cineangiofluoroscopic data (Reedy 1963) that the right ventricle has a complex and varied internal structure. It is divided into two parts, namely the in-flow and out-flow tracts both of which can be clearly demonstrated at angiography. The in-flow

tract is conical, trabeculated and its base which is formed by the tricuspid valve, lies posteriorly and opens antero-medially. A large muscular orifice connects the posterior in-flow and the anterior out-flow tracts. Above it, is the prominent crista supra-ventricularis which merges with the septal and parietal bands which are thick ridges of muscle running along their respective ventricular walls. Inferiorly the septal band continues as a large trabeculum, the moderator band, and completes the circle by joining the parietal band on the right parietal wall. The posterior papillary muscles are variable and difficult to define but there is a large constant papillary muscle arising at the point where the moderator joins the parietal band. The medial papillary muscle is small but constant and arises where the crista supra-ventricularis merges with the septal band. The out-flow tract is triangular in the postero-anterior view and semilunar laterally and is formed by the free wall of the heart anteriorly and the crista supra-ventricularis and in-flow tract posteriorly. About a third of the outflow tract which is termed the infundibulum, is above the in-flow tract and this becomes progressively smoother as it approaches the pulmonary valve.

## 5.C PATHOLOGICAL CHANGES IN CHRONIC OBSTRUCTIVE PULMONARY DISEASE

As a result of chronic hypoxia vasoconstriction and subsequent muscularisation of the terminal portions of the pulmonary arterial tree occurs. This has also been found in centrilobar and panacinar emphysema, in normal Quechua Indians born and living at high altitude in the Peruvian Andes, in sufferer's from Monge's disease,

in the Pickwickian syndrome and kyphoscoliosis.

But the most potent stimulus for pulmonary vasoconstriction is alveolar hypoxia which acts directly on adjacent small pulmonary arteries and arterioles. It is known that the alveolar gas composition influences the composition of blood in vessels as large as the muscular pulmonary arteries (Duling 1970), and Hasleton in 1968, demonstrated that the pulmonary arterioles were closely related to those segments of the bronchiole tree which come into immediate contact with alveolar air. Systemic arterial hypoxaemia supplements the local effects of alveolar hypoxia indirectly, by way of the sympathetic nerves to the pulmonary circulation, which further stimulate vasoconstriction. In chronic hypoxia the effects may be augmented by increased viscosity of the blood arising from secondary polycythaemia. Experiments in dogs indicate that severe acidosis (pH <7.2) also elicits pulmonary vasoconstriction and this has been confirmed in man, in whom acidosis has been shown to act synergistically with hypoxia.

Muscularisation of the terminal portions of the pulmonary arterial tree eventually results in elevation of the pulmonary vascular resistance and progressive increase in right ventricular weight (Abraham 1967, Heath 1973), secondary to muscular hypertrophy. In the normal resting individual, the pulmonary circulation is a highly distensible, low-resistance circuit, which accommodates the same blood flow as the systemic circulation but at approximately one-fourth the mean blood pressure. During exercise when the blood flow increases considerably, only slight elevation of the pulmonary

arterial pressure results. However when the pulmonary vascular reserve is depleted by progressive reduction in the extent and distensibility of the pulmonary vascular tree, even the increments in blood flow associated with day-to-day activities, result in marked increase in pulmonary arterial pressure.

At first, the pulmonary hypertension during exercise or during a bout of acute hypoxia is associated with normal end-diastolic right ventricular pressure. However if the pulmonary hypertension is prolonged or becomes severe, abnormally high filling-pressures develop in the right ventricle, due to a combination of ventricular dilatation and diminished ventricular compliance associated with right ventricular hypertrophy. This eventually leads to right ventricular failure, which is characterised by an abnormally high resting end-diastolic pressure, failure to increase the cardiac output during minimal exercise and engorgement of the systemic veins reflecting the inability of the right ventricle to pump adequately.

Pathologists have for a long time debated on the optimal methods for determining right ventricular hypertrophy. A surprising number of studies, one as recently as 1965, have been based on measurement of right ventricular wall thickness alone (Fowler 1965, Michelson 1960, Scott 1941, Spain 1946, Zimmerman 1951). However many studies have shown that measurement of right ventricular thickness correlates only roughly with right ventricular weight and is misleading in determining the size of the ventricle (Lamb 1973, Astorri 1971, Fulton 1952, Reiner 1959). The reliability of this

measurement was tested by Mitchell et al (1976), who correlated right ventricular thickness, measured 2cm below the tricuspid valve on the lateral wall (excluding trabeculae and papillary muscles) with the right ventricular weight, obtained after removal of fat, valves and atria in 106 autopsy cases. Although a significant correlation was obtained ($r = 0.65$), the relationship was poor in an appreciable number of cases, eg a 100g right ventricle could measure from 3 to 11mm, whereas a right ventricle measuring 5mm thick could weigh from 30 to 120g.

The discrepancy in findings between research groups can perhaps be explained by the many different methods of measurement employed as well as by the effect of ventricular dilatation. An additional problem is the regional variation in wall thickness encountered during right ventricular hypertrophy.

In the course of right ventricular hypertrophy the wall of the outflow tract or the parts around the crista supra-ventricularis hypertrophy first, especially in patients with right ventricular pressure overload. These hypertrophic changes subsequently extend to the other parts of the right ventricular wall. Hence, estimation of the thickness of only the inflow tract will be inaccurate for the diagnosis of early right ventricular hypertrophy.

Some investigators, in particularly Bove and associates (1966), have favoured the use of a ratio - either left ventricle including the interventricular septum against the right ventricular weight

(LVS/RV); or a direct comparison of the right ventricle with the left ventricle (RV/LV) - rather than absolute ventricular weights, to establish right ventricular hypertrophy. But, in general the individual right ventricular weight measured after removal of atria, valves and fat is considered to be the most sensitive and reliable index of hypertrophy (Fulton 1952, Mitchell 1976) and is currently the method of choice for assessing right ventricular hypertrophy pathologically.

Although some workers (Cromie 1961, Cullen 1970, Murphy 1974) have found correlations between right ventricular weight and the severity of emphysema and with reduction in diameter of small airways, many have found only a weak correlation (Mitchell 1976, Kountz 1936, Scott 1941, Spain 1946). This is perhaps not surprising considering that chronic lung disease is related to the severity and duration of hypoxaemia and that the severity of hypoxaemia has no linear relationship to the severity of emphysema per se.

## 5.D TECHNIQUES USED TO ASSESS RIGHT VENTRICULAR HYPERTROPHY

Evaluation of the structure of the right ventricle by available imaging methods presents a formidable problem. This is partly due to the complex geometry of the chamber, which consists of a separate outflow and inflow tract and the main body which is crescentic and truncated (Foale 1982). The right ventricular "free" wall also has a variable trabecular pattern that further limits precise measurement of cavity size and wall thickness.

Additional factors such as the retrosternal position and an anterior relation to the left heart that may vary according to the cardiac axis, make the right ventricle less accessible to the diagnostic techniques which depend upon external landmarks for orientation.

Many techniques have been used to assess right ventricular hypertrophy, including plain x-rays of the chest, electrocardiography, thallium-201 myocardial perfusion imaging, echocardiography and magnetic resonance imaging. The advantages and disadvantages of these techniques will be discussed separately.

### 5D.1 Chest Roentgenology

On the standard postero-anterior radiograph, when the right ventricle enlarges it is almost always accompanied by right atrial enlargement which produces rotation of the heart to the left. On the postero-anterior view the right ventricle takes over the left cardiac border from below upwards. With moderate enlargement, the left ventricle still forms the apex of the heart which is characteristically "turned up" above the diaphragm. When there is severe enlargement, the right ventricle takes over the left cardiac border which becomes straight and is difficult to distinguish from left ventricular enlargement. On the lateral projection the antero-posterior diameter of the heart is increased and there is obliteration of the retro-sternal space from below upwards and displacement of the inferior vena cava backwards. Indirect signs of right ventricular enlargement include prominence of the azygous

vein and of the left atrial appendage on the lateral view.

However many reports in the literature have commented on the difficulty in diagnosing right ventricular hypertrophy from chest radiographs. Thurlbeck et al (1970) noted a frequent discrepancy between the radiological assessment of right ventricular hypertrophy and the presence of right ventricular failure at autopsy. Only in the grossest degree of right ventricular hypertrophy was there unanimity of opinion. In this retrospective study, 10 of the 61 cases studied demonstrated right ventricular enlargement at post mortem but the radiographs showed none of the typical diagnostic features. Seven of the 10 hearts were dissected at autopsy and the right ventricular weights varied from 75 to 118g, with an average weight of 87g. By contrast those patients with right ventricular hypertrophy both radiologically and at autopsy had much larger right ventricles, which ranged from 83 to 158g with a mean of 116g. Thus, although the most obvious right ventricular hypertrophy was found in patients with severe emphysema, there were many exceptions.

### 5D.2 Electrocardiography

The criteria for right ventricular hypertrophy proposed by Wilson 1944), Goldberger (1947), Myers (1948), Sokolow and Lyon (1949) and Myers (1950) are now generally accepted. They consist of a dominant R wave in the praecordial lead (V1) with an intrinsicoid deflection and often with T wave inversion. The R wave may be preceded by a Q wave (Fowler 1952) and complete or partial bundle

branch block patterns may also occur. The so-called extreme clockwise rotation indicated by a dominant S wave in V5, and in many cases a dominant R wave in VR, completes the picture of severe right ventricular hypertrophy.

The ECG in chronic lung disease is characterised by poor progression of the R wave from leads V1 to V3 and usually an S wave in lead V5 which is approximately the same amplitude as the R wave in the same lead. Right ventricular hypertrophy can be mimicked by true posterior infarction, but the prominent R wave in lead V1, also found in Wolff-Parkinson-White syndrome with a left sided accessory pathway, can be distinguished by the presence of widened QRS complexes, while dextrocardia can be anticipated by the finding of inverted P waves, rS complexes and inverted T waves in lead 1.

However despite the criteria mentioned above, right ventricular hypertrophy can be a difficult diagnosis to make electrocardiographically. In 1955, Walker et al, compared the electrocardiographic findings with the thickness of the right ventricle in 22 cases of right ventricular hypertrophy and found that only 5 fulfilled at least one of the criteria of Sokolow and Lyon. Similarly in 1951, Thomas showed that the electrocardiogram in pneumoconiosis, in which right ventricular hypertrophy commonly occurs, may often be normal, and Mounsey (1952) reported that the R wave in V4R may increase during an exacerbation of heart failure in cor pulmonale, and then return to normal on recovery. Further evidence of the problems encountered was provided by Davies (1953) and Goodwin (1955) using a simple electrocardiographic grading of

severity of right ventricular hypertrophy in mitral valve disease. They found that appreciable or severe electrocardiographic right ventricular hypertrophy only occurred with considerable or gross pulmonary hypertension and that with moderate pulmonary hypertension the electocardiogram was often virtually normal.

The explanation for this discrepancy in findings is that the QRS complex is the resultant of the electrical forces generated by the left and by the right ventricle, and except at birth the left ventricular mass is much greater than the right. The net effect of this imbalance is that the electrical forces produced by the left ventricle tend to swamp those from the right ventricle. Consequently quite considerable hypertrophy of the right ventricle must occur before an electrocardiographic diagnosis of right ventricular hypertrophy can be made.

### 5D.3 Thallium-201 Myocardial Perfusion Imaging

Although the right ventricle is usually not well visualised during thallium-201 myocardial perfusion scanning, Cohen (1976), observed that this technique was more useful than electrocardiographic criteria for the determination of right ventricular hypertrophy in patients with chronic pulmonary hypertension.

In normal individuals the left ventricle has a much greater muscle mass and consequently blood flow, so there is usually very little uptake of radionuclide by the right ventricle, the image being saturated by the left ventricle. In a series by Khaja (1979), the

right ventricle was not visualised in 20 consecutive patients with normal right ventricular and pulmonary arterial pressures.

However in a further 33 patients, 28 of whom had haemodynamic evidence of right ventricular hypertension with a systolic pressure equal to or greater than 30mm Hg, the right ventricle was clearly visualised. This compared to pick-up rates of 58, 36 and 15 per cent for chest roentgenology, echocardiography and electrocardiography respectively.

Cohen et al (1976) reported visualisation of the right ventricle in resting thallium-201 scans in 18 patients with pulmonary hypertension resulting from a variety of causes and noted that the right ventricular thickness was greater than 1.1cms. However the right ventricle was also visualised in two patients with normal pulmonary artery pressures, although the wall thickness was less than 1cm. They cautioned that the right ventricle may be observed in patients with normal resting pulmonary artery pressures when hypertension was induced either by exercise or by cardiac arrhythmias.

Although reports suggest that thallium-201 myocardial perfusion imaging may be more sensitive at detecting right ventricular hypertrophy than chest x-rays, electrocardiography or echocardiography, quantitative analysis of muscle mass remains elusive.

## 5D.4 Echocardiography

Echocardiographic measurements of the size of cardiac structures such as the left atrium (Hirata 1969), the left ventricular internal dimensions (Popp 1969, Pombo 1971, Fortuin 1971) and the thickness of the left ventricular posterior wall (Feigenbaum 1968, Sjogren 1970, Askanas 1970) have been reported by many investigators and their accuracy has been confirmed by angiography (Feigenbaum 1972) and at surgery (Feigenbaum 1968).

The morphological changes seen in the right heart secondary to chronic cor pulmonale can also be detected by means of M-mode or two-dimensional echocardiography. Early M mode echocardiographic studies of the right ventricle relied upon an evaluation of a single dimension and wall thickness without consideration of the complex geometry of the chamber and the variable trabecular pattern of its wall (Feigenbaum 1976). Real-time echocardiography provides multiple tomographic views of the heart in a beat-by-beat display, without risk or discomfort to the patient. Using this technique Chang et al (1973) reported that subxiphoid echocardiography was useful in emphysematous or aged patients for recording the mitral valve and the left ventricular posterior wall. In 1986 Foale et al proposed a standardised echocardiographic examination sequence to assess the right ventricle. Because the inflow tract, ventricular body and outflow tract are three distinct regions of the right ventricle that are orientated in different axes, measurements of each region were obtained from separate views. Variable angulation of the transducer in the left parasternal long axis provided views

of the inflow tract , outflow tract and right ventricular body, while parasternal short axis views provided views of the inflow tract immediately below the tricuspid valve leaflets. Positioning of the transducer at either the cardiac apex or subcostally allowed imaging of atria and ventricles in the long axis projection.

Later, in 1977 Matsukubo et al, reported the results of sub-xiphoid echocardiography in the assessment of right ventricular thickness. In this technique the transducer is placed in the sub-xiphoid region and directed superiorly and to the left laterally towards the heart. Measurement of the thickness of the right ventricle was carried out where the tricuspid valve or chordae tendinae were visualised. In this report the right ventricular wall thickness averaged 0.34 $\pm$ 0.08cm, ranging from 0.2 to 0.5cm in 25 normal individuals. This was significantly increased ($p<0.001$) in patients with either right ventricular pressure overload (0.60 $\pm$ 0.13cm) or right ventricular volume overload (0.53 $\pm$ 0.11cm). In addition 32 patients underwent diagnostic right heart catheterisation which revealed a good correlation between the right ventricular wall thickness measured echocardiographically and the right ventricular systolic pressure ($r = 0.84$).

The right ventricular end-diastolic wall thickness was also examined by Foale et al (1986). In a group of normal subjects the mean wall thickness did not exceed 0.4cm, although individual values ranged up to 0.7cm. They noted a variation in thickness of over 25 per cent in some normal subjects particularly on the lateral and diaphragmatic regions. Although differences in the

trabecular pattern explained exaggerated wall thickness in some patients, a limited reproducibility of measurements (< 23 per cent) in regions other than the outflow tract were thought to account for some of the findings.

There are two potential problems with this technique. In echocardiography the right ventricular wall appears to increase in thickness from the base to the apex because of inclusion of the papillary muscles and the oblique passage of the sound beam. An erroneous measurement can be made if the thickness of the right ventricular wall is made at the apex. For this reason criteria have been developed to determine the proper site for this measurement. The direction of the transducer is set so as to visualise echoes from the tricupsid valve or the chordea tendinea attached to it, in the same manner as the thickness of the left ventricular posterior wall is measured. At this location the right ventricular wall is uniform in thickness and the endocardium is easily distinguished from the chordea tendinea. The second problem arises when the transducer is placed in the sub-xiphoid region and the echo beam transects part of the wall of the right ventricular outflow tract. In the course of right ventricular hypertrophy, the wall of the outflow tract or the region around the crista supra-ventricularis hypertrophies first, so it follows that estimation of the thickness of only the wall of the right ventricular inflow tract may not be accurate enough for diagnosis of the early stages of right ventricular hypertrophy. And lastly, echocardiography may have difficulties in visualising the endocardial borders of the right ventricle (Mason 1980) again hindering measurement of right

ventricular thickness.

Although some reports have suggested that the amplitude of the echo cardiographic "a" wave, the pulmonary valve diastolic "E-F" slope, the systolic opening "B-C" slope and the presence of mid systolic notching are of value in diagnosing pulmonary hypertension, this has not been substantiated by other workers (Acquatella 1979). The combination of mid systolic pulmonary valve notching and an absent "a" wave was observed in more advanced degrees of pulmonary hypertension and was specific but not sensitive for that condition.

### 5D.5 Magnetic Resonance Imaging

Magnetic resonance imaging is a relatively new, non-invasive and non-ionising method which offers great potential for simultaneously assessing left and right ventricular anatomy, as well as providing information on tissue characterisation. Although there have been many reports in the literature detailing the benefits of gated magnetic resonance imaging in the evaluation of the left ventricle (Lanzer 1984, Akins 1985), the left atrium, the thoracic aorta (Schafer 1987) and the pericardium (Soulen 1985) there have been few reports on either the normal or pathological right ventricle.

In 1988, Suzuki and colleagues compared M-mode and cross-sectional echocardiography with gated magnetic resonance imaging in the assessment of right ventricular wall thickness in 9 healthy

volunteers, and 20 patients with either hypertrophic cardiomyopathy or pulmonary hypertension. In this study a gated spin-echo pulse sequence (TE = 34ms) was used to obtain short axis images in the paraxial plane ie perpendicular to the coronal plane and to the left ventricular long axis. The thickness of the right ventricle was measured at one centimetre intervals along that part of the ventricular wall in which both the endocardial and epicardial margins were clearly defined. In this study, only 68 per cent of the length of the right ventricular free wall was demonstrated in normal subjects, the remainder being obscured by chemical shift or arrythmia induced motion artefact. There was good agreement between the two techniques with a mean difference between measurements of -0.04cm and a standard deviation of 0.06cm. The 95 per cent confidence interval for the bias was -0.06 to 0.02cm, and the confidence intervals for the lower and upper limits of agreement were -0.02 to 0.12cm and 0.04 to 0.12cm respectively. The mean right ventricular wall thickness for normal volunteers was 0.20 $\pm$ 0.08cm, while patients with hypertrophic cardiomyopathy or pulmonary hypertension showed statistically significant increases at 0.44 $\pm$ 0.12cm and 0.73 $\pm$ 0.27cm respectively.

Although the study of Suzuki showed good agreement between magnetic resonance imaging and echocardiography, the same limitations exist concerning measurement of only the right ventricular wall thickness, as mentioned previously in Chapter 5D.4. Indeed it should be remembered that echocardiographic data has shown a regional variation of 0.2cm to 0.7cm in certain views even in normal individuals (Foale 1986). This variation would prohibit the

use of right ventricular "free" wall thickness particularly if the response to therapeutic measures was to be evaluated.

## 5.E TECHNIQUES USED TO ASSESS RIGHT VENTRICULAR CHAMBER VOLUME

Right ventricular volumes have been measured by both invasive and non-invasive methods, including contrast angiography, radionuclide angiography, echocardiography and recently magnetic resonance imaging. The various techniques will be discussed in sequence.

### 5E.1 Contrast Angiography

Many investigators have shown that biplane cine-ventriculography of right ventricular casts yield calculated right ventricular volumes that correlate with cast volumes measured by water displacement. Ferlinz et al (1976, 1975) reported an excellent correlation between right ventricular cast and biplane cine-ventriculographic volumes using a pyramid on a triangular base as the geometric model to calculate right ventricular volumes. Fisher et al (1975) also demonstrated a good correlation with right ventricular cast volumes using a similar geometric model, a prism on a triangular base. Arcilla (1971) and Slutsky (1982) using biplane cine-ventriculography of ventricular casts showed that a simple area-length method to calculate right ventricular volume, provided a reasonable correlation with actual cast volumes. Thus the various geometric models produce accurate volume calculations when the right ventricle is of normal size.

However, as the right ventricle enlarges secondary to volume overload or becomes hypertrophic due to pressure overload, its

intracavitary configuration may become deformed and no longer equates to a simple geometric model.

Simpson's rule algorithm should in theory provide a more accurate measurement of volume in normal as well as enlarged hearts, since in this model, the cardiac chamber is divided into multiple sub-units, thus minimising errors that arise from geometric assumptions. Using this method Dell' Italia in 1985, demonstrated an excellent correlation between right ventricular cast volumes and those obtained by water displacement.

Gentzler (1974) also imaged right ventricular casts with biplane cine-ventriculography and demonstrated a good correlation between cast volumes calculated by Simpson's rule algorithm and cast volumes measured by water displacement. However using this technique, 50 per cent of the end-diastolic right ventricular volumes, examined in normal subjects, measured over 100mls/$m^2$. All other reports in which right ventricular volumes were calculated in normal individuals quoted values of less than 100ml/$m^2$, casting some doubt on Gentzler's results.

Although Simpson's rule algorithm has provided right ventricular volumes which correlated closely with indicator-dilution techniques and postmortem data, it has not found general acceptance (Ferlinz 1982). It is very laborious and virtually necessitates computer analysis. In addition cine-ventriculography is an invasive technique that poses some risk to patients, and it cannot be used serially to evaluate the effect of therapy or progression of

disease.

Biplane cine-ventriculography is generally accepted as the gold standard for left ventricular volume measurements, but there are no comparable firm standards for right ventricular cine-ventriculographic volume indices. In 1971, Carlsson et al, compared right and left ventricular stroke volumes by angiography in 17 patients, and found that only when the right ventricular stroke volume was corrected for filling time did the left and right ventricular stroke volumes equate. Moreover, they found that the injection of contrast into the right ventricle produced temporary volume changes, particularly in end-diastole.

Thus, although conventional contrast cine-ventriculography has been used in the past to measure right ventricular volumes, the technique has lost favour due to dependence on geometric methods, the alteration in chamber volumes during contrast injection, and the inability to perform sequential studies.

### 5E.2 Radionuclide Angiocardiography

Recently, several radionuclide techniques have been used to evaluate right ventricular function. The right ventricular ejection fraction has been calculated by first pass (Berger 1978), gated first pass (McKusick 1978, Twieg 1979, Harolds 1981) and gated equilibrium blood pool techniques (Maddahi 1979, Slutsky 1980). With all these techniques the changes in right ventricular activity are directly proportional to the blood volume, so that

problems arising from the irregular shape of the right ventricle are avoided. Unfortunately overlap by other cardiac chambers may make the assessment of the right ventricle using equilibrium techniques difficult. These anatomical problems are avoided with first pass studies, which allow separation of the right ventricle both temporally and spatially from surrounding cardiac structures. However, the calculation of right ventricular volume by a first pass technique ideally requires biplane images and complicated formulae similar to those required for contrast angiography.

In 1981, Dehmer et al developed a methodology originally devised for calculating left ventricular volumes (Slutsky 1979, Massie 1981, Ong 1980) from the time-activity data derived from gated equilibrium blood pool scans. In this technique volumes were measured from gated blood pool scintigrams by quantitating the background-corrected and volume-normalised ventricular activity at end-diastole and end-systole. Scintigraphic volume estimates were calculated by this equation

$$\text{Volume estimate} = \frac{\text{Background corrected ventricular counts}}{\text{Total acquisition time/frame(s)}} \Big/ \frac{\text{Peripheral blood activity} \times e^{-\lambda t}}{\text{(counts/ml/s)}}$$

where $e^{-\lambda t}$ is the expression for isotope decay, $\lambda = 0.693/T1/2$, $t$ = time (min) from counting the peripheral blood sample to the

midpoint of the gated study, and T1/2 is the half-life of the radionuclide employed. In the study by Dehmer et al (1981), the results of scintigraphy were correlated with thermodilution determinations of stroke volume. The best correlation ($r = 0.88$, $p < 0.0001$) was obtained for studies acquired with a $25^{o}$ rotating slant hole collimator positioned in a 10 to $15^{o}$ left anterior oblique position with the collimator slant directed toward the cardiac apex along the axis of the interventricular septum. However, using this technique volumes were obtained by regression equation correction of the corresponding volumes that were not corrected for photon attenuation. Theoretically, a method that is highly dependent on regression equation correction may yield estimates of left or right ventricular volumes that are imprecise, since each patient has variable photon attenuation, because of the composition of the intervening body tissue, and the distance between the ventricles and the gamma camera.

In 1985 Dell'Italia used a simple geometric method to obtain the distance from the camera to the centre of the right ventricular mass, and then used the measured distance to calculate attenuation-corrected radionuclide right ventricular volumes. These radionuclide volumes correlated highly with the corresponding cast-validated biplane cine-ventriculographic volumes ($r = 0.91$; SEE = 27ml).

Although this technique has advantages over previous methods there are however several potential sources of error including the reproducibility of blood sample counts, measurement of distance and

the use of the linear attenuation coefficient of technetium-99m photons in water as the physiological composition of the body. Furthermore right ventricular end-diastolic and end-systolic counts are highly dependent on hand drawn regions of interest, which can be influenced by the subjective positioning of the right atrio-ventricular border and the pulmonary valve plane. This can partially be resolved by use of phase analysis to define the cardiac borders. Lastly, the use of a left paraventricular region of interest for background correction may include scatter from the left ventricle and the pulmonary vascular bed giving a falsely high level, whilst right ventricular counts may be falsely high due to an overlying right atrium (Maddahi, 1979).

### 5E.3 Echocardiography

Although M-mode echocardiography can document the presence of a variety of cardiac disorders, including valvular heart disesase, myxomas and pericardial disorders the relatively inaccessible intra-thoracic position and the irregular geometric shape of both the right atrium and ventricle prevent adequate assessment. With the advent of 2-D echocardiography the anatomical difficulties have been overcome.

In 1979, Bommer et al performed 2-D echocardiography on 8 human right heart casts obtained at autopsy. Measurements of individual long and short axes dimensions of the right atrium and ventricle from the right heart casts correlated well with the volume of these structures measured by water displacement. He also studied 50

patients who had undergone right and left heart catheterisation. Values for right ventricular short-axis and planimetric area distinguished normals from patients with right ventricular volume overload, with minimal overlap between the groups. However there was no difference in the right ventricular long-axis measurement between groups. This limitation was explained by the inability to image the entire expanse of the enlarged right ventricle, although this study did not correlate the results with another technique that was independent of geometry.

Starling and collegues in 1982, compared the results obtained from resting 2-D echocardiography with radionuclide angiography, in patients with chronic obstructive pulmonary disease. They showed a good correlation between echocardiographic right ventricular end-diastolic area measurements and radionuclide end-diastolic count data ($r = 0.76$) and equally good correlations were obtained with end-systolic and ejection fraction results. However certain limitations of 2-D echocardiography must be recognised. Firstly, high-quality images of the right ventricle in both planes can only be obtained in approximately 64 per cent of patients with chronic obstructive pulmonary disease (Starling, 1982). Secondly, the presence of segmental ventricular wall dysfunction has not been examined but may alter volumetric analysis. Finally, the identification of the right ventricular endocardium is difficult because of extensive trabeculations, and this may affect the reproducibility of serial measurements, particularly between different observers (Mason 1980).

## 5E.4 Magnetic Resonance Imaging

Magnetic resonance imaging has already proved capable of providing accurate determination of cardiac volumes in vitro and in animal studies (Rehr 1985), and Longmore et al (1985), have reported a good correlation between in vitro left ventricular dimensions determined by magnetic resonance imaging and contrast ventriculography. They reported a good correlation with anteroposterior angiograms, but a poorer correlation with the lateral projection due to difficulty in locating the aortic valve. The left and right ventricular volumes were measured by gated magnetic resonance imaging at end-diastole and end-systole by summing the areas of the cavities in multiple contiguous transverse sections. The stroke volume and ejection fraction were then calculated. The ratio of left to right ventricular stroke volume approached the theoretical value of 1, in all cases, with a calculated error in volume measurement of only 2 per cent.

In 1988, Underwood et al published results on the measurement of left ventricular volume and ejection fraction based on measurement of the area and length in a single oblique plane containing the long axis of the ventricle. This technique required a much shorter scanning time. They compared the results obtained using this technique with the multiple contiguous slice technique and obtained a good agreement between the two methods in normal subjects (mean difference 6mls), but in patients with previous infarction the agreement was poorer with a mean difference of 18mls. This discrepancy was greatest in patients with abnormal wall motion and

a low ejection fraction.

To date there is very little published data on right ventricular dimensions using magnetic resonance imaging. In 1988, Mogelvang et al studied right and left ventricular end-diastolic and end-systolic volumes in a mixed group of 12 patients, 2 of whom had pulmonary heart disease. They used oblique short-axis images to obtain the area inside the endocardial surface and long-axis views to measure ventricular length. Ventricular volumes were then calculated using Simpson's rule. They showed a close correlation between right and left ventricular stroke volumes measured by magnetic resonance imaging and the indicator dilution method, with SEE of 10 and 11ml, respectively.

Magnetic resonance imaging has several advantages over pre-existing techniques for assessing the right ventricle. It does not alter the chamber volumes as no contrast injections are required, and the right and left ventricular volumes can be measured simultaneously. In addition, the technique is suitable for repeated investigations allowing the response to therapy to be monitored.

## 5F AIMS

Right ventricular volumes are difficult to measure accurately in man because of the unusual shape of the right ventricle. Previous studies using contrast biplane cineangiography and various geometric formulae to calculate right ventricular volumes have correlated well with actual volume measurements obtained by water displacement from right ventricular casts (Goerke 1967, Arcilla 1971, Gentzler 1974, Ferlinz 1975, Horn 1979). However this method is not wholly applicable in patients under different physiological conditions where repeated measurements are desirable. Radionuclide angiography is suitable for evaluating right ventricular chamber size and performance because it is independent of geometry and can easily be repeated. Unfortunately neither of the above techniques is capable of providing any information regarding right ventricular wall size.

Bommer and co-investigators (1979) reported that 2-D echocardiographic cross-sectional area measurements of right ventricular casts correlated highly with actual cast volumes, and more recently Starling et al (1982) showed a good correlation between 2-dimensional echocardiographic and radionuclide end-diastolic and end-systolic chamber volumes ($r = 0.76$ and 0.82 respectively). Although echocardiography is capable of measuring right ventricular wall thickness, the variability and subjectivity of the measurements particularly in the right ventricle precludes this technique for the assessment of response to therapy.

Magnetic resonance imaging is a relatively new imaging modality which is both non-ionising and non-invasive (Higgins 1985) and has already been shown to be an accurate method for determining left ventricular chamber volumes (Mogelvang 1988; Longmore 1985). The purpose of this study was to :

a) Develop a technique using magnetic resonance imaging to measure the right ventricular chamber and wall volumes, thus satisfying the definition of cor pulmonale, laid down by the World Health Organisation (1963).

b) Magnetic resonance imaging has already been shown to provide accurate information on left ventricular chamber volumes, but is also capable of tissue characterisation. In this study, the T1 values of both the right and left ventricular walls and chambers will be examined in patients with chronic obstructive airways disease and the results compared with patients with ischaemic heart disease, age-matched controls and a group of normal young volunteers.

c) As pulmonary hypertension is traditionally diagnosed by right heart catheterisation, pulmonary haemodynamic data will be compared with the findings from magnetic resonance imaging in patients with airways limitations.

d) Right ventricular chamber volume and ejection fraction are measured routinely by radionuclide ventriculography in patients with chronic obstructive pulmonary disease and this data will be

compared with results obtained by magnetic resonance imaging and cardiac catheterisation.

e) To determine the reproducibility of the technique, patients will be examined on separate occasions, and the day-to-day variability analysed. Similarly intra- and inter-observer error will be closely monitored.

f) As it is frequently important to assess the effects of therapeutic interventions, patients with chronic obstructive airways disease will be examined before and after long-term oxygen therapy, and the effects on right and left ventricular wall and chamber dimensions assessed.

## 5G PATIENTS

### 5G.1 Chronic Obstructive Pulmonary Disease

Sixteen patients (7 female and 9 male) with chronic obstructive pulmonary disease were studied. The mean age was 65.4 years with a range of 40 to 80 years. All patients were being assessed for long term domiciliary oxygen therapy and all had air flow limitation (mean FEV1 0.73 l/min, range 0.3 to 1.4 l/min; mean FVC 2.4 l/min, range 0.9 to 4 l/min) were hypoxic (mean PaO2 6.5kPa, range 4.9 to 8.3kPa) and the majority were also hypercapnic (mean PaCO2 6.5kPa, range 4.9 to 8.8kPa). All patients were clinically stable during the 6 weeks prior to examination and none had evidence of peripheral oedema or had had a recent exacerbation of the condition. All patients had recent chest x-rays which showed evidence of chronic obstructive pulmonary disease with over-inflation of the lung fields but no evidence of focal areas of consolidation or of early pulmonary oedema. The blood gas values, FEV1 and body weight were stable during the pre-study period. With the exception of one female patient, all had a long history of excessive smoking and 2 patients continued to smoke despite their severe airways limitation. A full blood count was obtained in all patients during the pre-study period and most had elevation of the haemoglobin count (mean 16.3g-dl; range 14.9-18.7g/dl). All patients were required to give informed consent prior to the examination.

### 5G.2 Ischaemic Heart Disease

Nineteen patients (4 female and 15 male) with known ischaemic heart disease who had suffered an acute myocardial infarction between 5 to 7 days prior to the examination were studied. The mean age range was 58 years with a range of 33 to 81 years. At the time of the examination all patients were symptom-free with no clinical or radiological evidence of cardiac failure. Although 8 of these patients gave a history of cigarette smoking none had symptoms suggestive of chronic obstructive pulmonary disease.

### 5G.3 Age-Matched Controls

Five patients (4 female, 1 male) whose ages ranged from 63 to 79 (mean 71 years) were studied as age-matched controls. None of these patients had a previous medical history of either cardiac or respiratory disease and all were non smokers.

### 5G.4 Young Normal Individuals

Four individuals whose ages ranged from 30 to 37 (mean 34 years) formed a separate group of healthy young volunteers. None of these individuals had relevant past medical history and all were life-long non smokers.

## 5H METHODS

### 5H.1 Magnetic Resonance Imaging

a) Technique

Magnetic resonance imaging was carried out 2 to 5 days following the cardiac catheterisation using a low field resistive system (M&D Technology) operating at 0.08 Tesla. Patients with a cardiac pacemaker or who had had previous intra-cranial surgery with insertion of metallic arterial clips were excluded. Following removal of all metallic objects the patients were positioned supine on the examination couch. To increase patient comfort the legs were supported slightly flexed on cushions with the head elevated as far as possible. Time was allowed for the patients to rest following any exertion prior to the examination and hence reduce unwanted respiratory movement. When necessary, oxygen was supplied during the examination from a portable oxygen cylinder placed approximately 6 feet away from the centre of the magnet and supplied at a rate of 2l/min via nasal speculae.

Throughout the examination the patient was in full view of the operator and could be removed immediately from the scanner if he or she became dyspnoeic or claustrophobic.

Ungated scout images were carried out in the coronal plane to visualise the left and right ventricles in the longitudinal axis. These images were obtained using a field of view of 384mm, a matrix

of 128 x 64 with no averaging, a short repetition time of 240ms and a field echo time of 22ms. Four slices were obtained using a 16mm slice width and separation to encompass the heart. These scout images were acquired in 31 seconds.

From the coronal scout images, short axis images through the vertical long axis were orientated so that the imaging plane was perpendicular to the inter-ventricular septum. In most patients this required approximately a $30^{o}$ angulation from the transverse plane. A cardiac gating technique was employed to obtain these images. Two carbon fibre electrodes (Abingdon Instruments, Abingdon, Oxon) were placed on the left antero-lateral and right para-sternal chest wall. The exact position of the electrodes was varied to maximise the positive deflection in the QRS complex and to reduce muscle artefact secondary to respiration.

The upslope of the electrocardiographic R-wave was used to synchronise data acquisition during end-systole at approximately 110ms following the upstroke of the R wave. The gating technique has been previously described (Chapter 3.B). An interleaved saturation recovery - inversion recovery pulse sequence (TI = 42ms) was employed from which a T1 map was calculated. The repetition time (TR) varied according to patient's heart rate. Eight slices of 16mm thickness were acquired, using 4 acquisitions, to obtain multiple images from below the cardiac apex to the level of the main pulmonary arteries. Two slices with a 42ms time separation were acquired with each acquisition which consisted of two averages of 64 phase encoding steps, and 128 frequency encoding steps,

resulting in a pixel size of 3 x 6mm. This data was interpolated to a 128 x 128 matrix (3 x 3mm) on the final display matrix, and this used for image analysis. The total examination time which included time for the computer to save information depended on the heart rate but averaged between 30 to 40 minutes.

Further images were acquired in 10 of the 16 patients using the above technique but with a time delay of between 500 to 700ms following the upslope of the R wave so that images were obtained during end-diastole. The time delay varied with the patients heart rate. The right and left ventricular ejection fractions were calculated from the following equation:

$$\text{Ejection fraction (\%)} = \frac{\text{End-diastolic volume } (cm^3) - \text{End-systolic volume } (cm^3)}{\text{End-diastolic volume } (cm^3)}$$

The stroke volume was defined as :

$$\text{Stroke volume } (cm^3) = \text{End-diastolic volume } (cm^3) - \text{End-systolic volume } (cm^3)$$

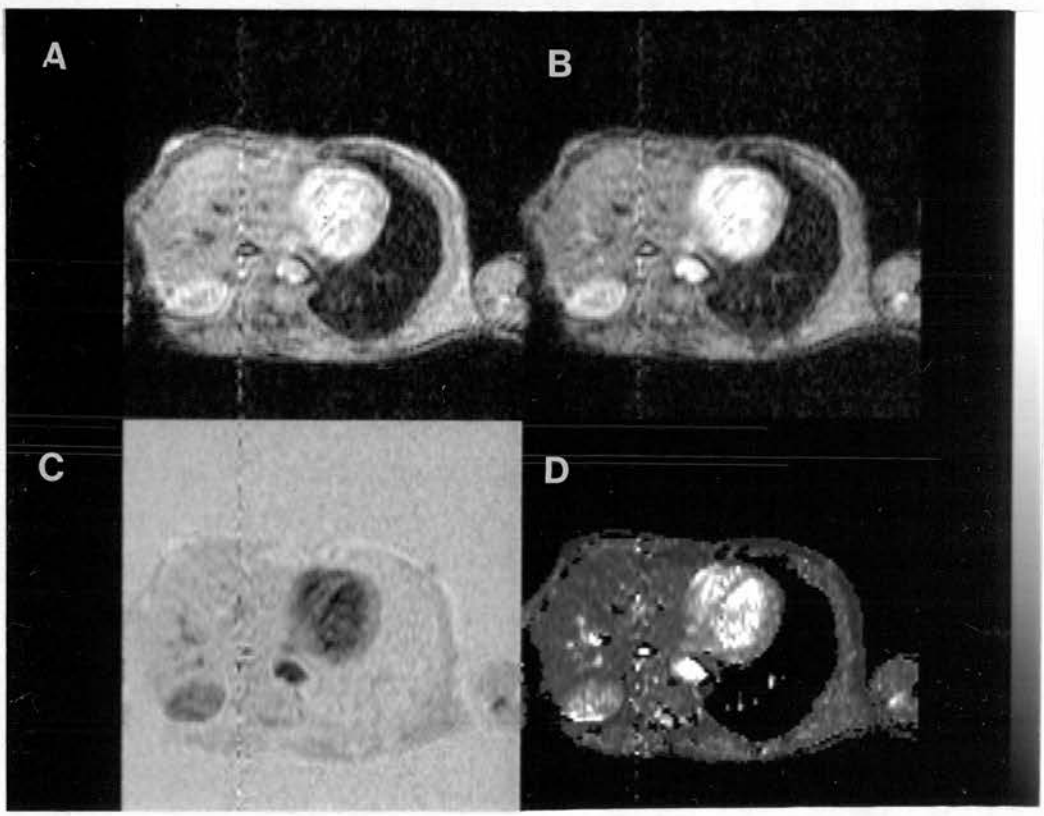


Figure 15. Using a saturation recovery - inversion recovery pulse sequence, four images are obtained:

a) saturation recovery b) inversion recovery

c) difference and d) T1 map image.

b) MR Image Analysis

Of the four images obtained in the saturation recovery - inversion recovery pulse sequence, the proton density and the "difference" images provided insufficient contrast difference between the ventricular wall and contained blood pool for image analysis. Good contrast and satisfactory image resolution was obtained in both the inversion recovery and in the calculated T1 map images (Figure 15). The calculated T1 map provided good delineation between normal myocardium and intra-ventricular blood as well as tissue characterisation and was therefore used to define the myocardial borders. The outlines of the endo- and epicardial borders of the right ventricular "free" wall and the left ventricle including the interventricular septum, were defined inter-actively by using image analysis software to draw an irregular region of interest (Figure 16a and b).

Particular care was taken to accurately outline the irregular trabeculated endocardial surface of the right ventricle and in the left ventricle to include the papillary muscles. Although it was frequently difficult to clearly identify either the mitral or tricuspid valves there was a clear distinction both in wall thickness and in contour between the atria and ventricles which allowed separation. A similar problem was encountered with the aortic and pulmonary valves although the contours of the aorta and the main pulmonary artery could be clearly distinguished.

The point of separation between the right ventricular free wall

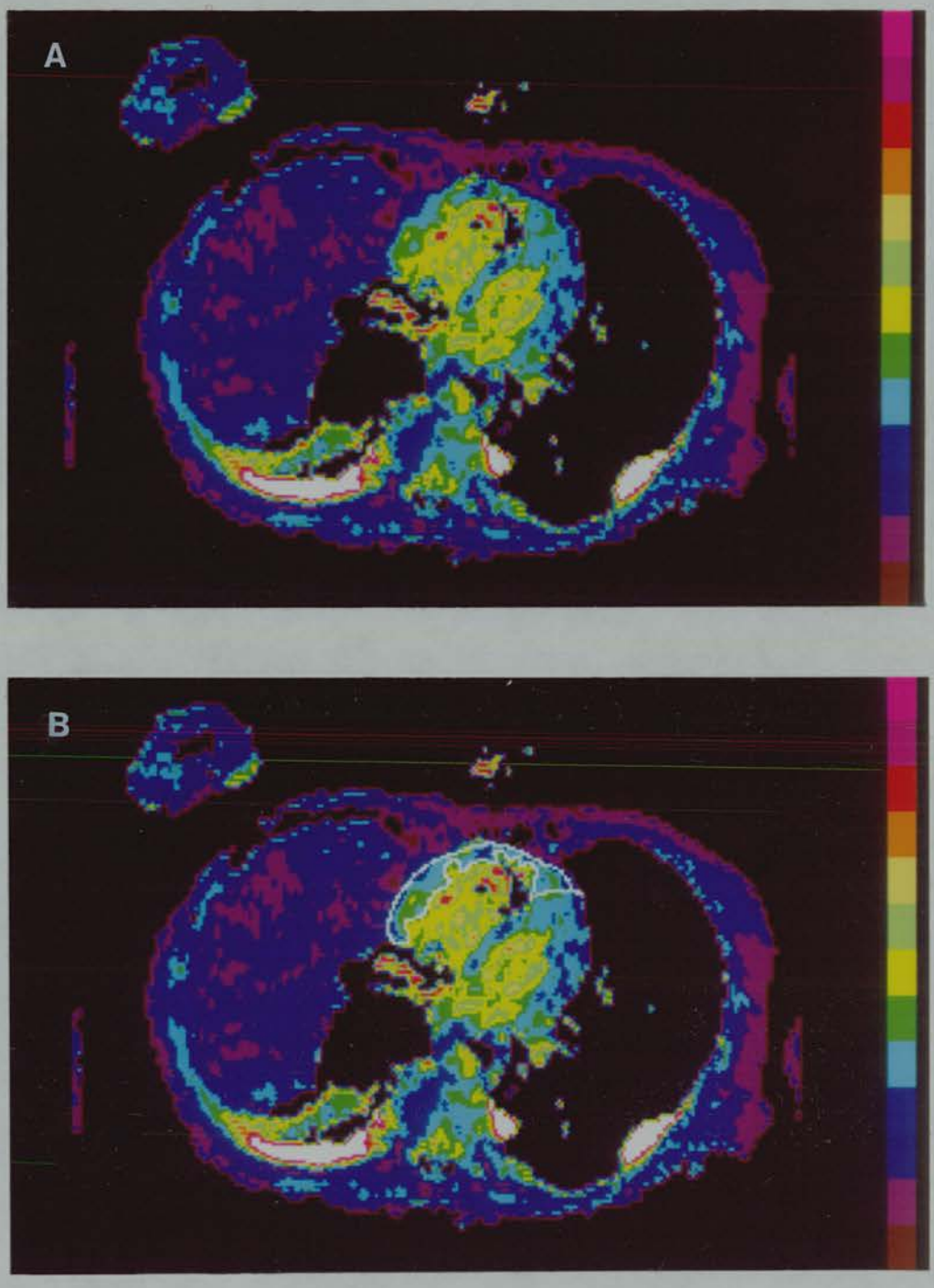


Figure 16. a) T1 map image showing good delineation between normal myocardium and intra-ventricular blood, in a patient with marked right ventricular hypertrophy.

b) The right ventricular "free" wall is outlined in white. Small pleural effusions are seen posteriorly as areas of increased signal intensity.

and the adjacent left ventricular wall and interventricular septum was taken at the intersection of imaginary lines extended from the right lateral wall of the interventricular septum transecting with the epicardial surface of the heart. On several images blood flow artefacts resulted in loss of contrast between the myocardial wall and the blood pool and on these images regions of interest were transcribed from the inversion recovery images on to the T1 maps, providing the necessary chamber outline. A similar method was used to define both ventricular chamber volumes. The value obtained for the ventricular wall and chamber volumes on each individual slice was multiplied by the slice thickness (1.6cm) and the results summated to obtain the total ventricular wall and chamber volumes. The mean T1 and standard deviation were also noted for all regions of interest involving the ventricular walls or chambers. During the examination, the heart rate was recorded intermittently from the consol display monitor and the presence of arrythmias such as supra-ventricular or ventricular ectopic beats noted.

In patients with ischaemic heart disease, particular care was taken to exclude areas of recent infarction from measurements of the T1 value of normal myocardium. This was only necessary for the left ventricle as none of the patients studied had either electrocardiographic, pyrophosphate or magnetic resonance evidence of right ventricular infarction.

In order to determine the intra- and inter-observer variability measurements were performed on all patient examinations on 3 separate occasions by the same observer (LWT) and on 4 different

patient examinations on 3 separate occasions by an independent observer.

The day to day variation in right ventricular volumetric analysis was obtained by carrying out 3 examinations on consecutive days in the 4 normal healthy volunteers.

### 5H.2 Right Heart Catheterisation

This was carried out using the standard Seldinger technique. A 7F Swan Ganz catheter was inserted under local anaesthetic without pre-medication into a right antecubital fossa vein. Pressures were measured while the patients were semi-supine and were zero referenced to a point 5cm below the sternal notch. The mean and systolic pulmonary artery pressures and the pulmonary artery wedge pressure were averaged over three respiratory cycles. Mean pressures were obtained by electrical integration and the cardiac output was measured using a standard thermodilution technique. The mean of 3 values which varied by less than 10 per cent was used in analysis.

### 5H.3 Measurement of Right Ventricular Ejection Fraction

The right and left ventricular ejection fractions were only measured in patients with chronic obstructive pulmonary disease. Ejection fractions were measured using a multi-crystal Maxicamera 400 AT gamma camera (Internation General Electric) and a Micro Delta Plus computer system (Siemens Gammasonics). With the patients supine

750MBq of 99m technetium human serum albumin were injected via an antecubital vein using an 18-gage butterfly needle connected to a three way tap to which were attached syringes containing the radiopharmaceutical and a saline flush. Data was collected at a frame rate of 20 per second over 60 seconds. Dead time and uniformity corrections and temporal smoothing were performed before further analysis. The right and left heart phases of the first pass study were identified and analysed separately. Time activity curves were obtained from regions of interest over the right and left ventricle. End-systolic and end-diastolic images of the right and left ventricle were generated and the ejection fractions obtained. The left ventricular ejection fraction was calculated using the background corrected representative cycle.

Table 11

Mean, Standard Deviation and Range of T1 values for the Right and Left Ventricular Walls and Heart Rates for the Four Patient Groups Studied

| Patient Groups | T1 Values | | | | Heart Rate | |
|---|---|---|---|---|---|---|
| | Right Ventricle | | Left Ventricle | | | |
| | Mean ±SD | Range | Mean ±SD | Range | Mean ±SD | Range |
| Chronic Obstructive Pulmonary Disease (n = 16) | 311.7 ±33.3 | 251.2 - 370.0 | 336.7 ±26.6 | 298.7 - 398.8 | 62 ±31.7 | 45 - 100 |
| Ischaemic Heart Disease (n = 19) | 321.7 ±38.0 | 275.2 - 423.2 | 337.2 ±53.6 | 277.3 - 475.6 | 77 ±14.2 | 55 - 100 |
| Age-Matched Controls (n = 5) | 308.2 ±8.5 | 297.9 - 319.2 | 327.1 ±19.7 | 297.3 - 352.1 | 76 ±6.7 | 65 - 82 |
| Normal Young Volunteers (n = 4) | 315.1 ±14.9 | 301.3 - 333.7 | 318.0 ±14.8 | 307.1 - 339.8 | 79 ±7.8 | 70 - 80 |

## 5I RESULTS

### 5I.1 T1 Values

T1 values of the right and left ventricular walls and chamber contents were calculated separately for all patient groups. Tables 11 and 12 show the mean, standard deviation and range of T1 values for the right and left ventricular walls and chamber contents for the four groups, while individual values are detailed in Tables 13 to 16 (Appendix 2).

#### T1 Value for Ventricular Walls

The mean T1 values obtained for the right ventricular "free" wall for the four patient groups were very similar, ranging from 308.2 $\pm$ 8.5ms for the age matched control group to 321.7 $\pm$ 38.0ms for those with ischaemic heart disease. There was only a small spread of values in both the age-matched control and normal young volunteer groups, but the values obtained in both the chronic obstructive pulmonary disease and ischaemic heart disease groups showed a wide variation from a minimum of 251.2ms in the former group to a maximum of 423.2ms in the latter group.

No significant difference was obtained between the mean T1 values for the left ventricular wall for the four patient groups. These varied from 318.0 $\pm$ 4.8ms for the normal young volunteer group to 387.2 $\pm$ 53.6ms for patients with ischaemic heart disease. Although values varied in all groups, this was least in the normal young

Table 12

Mean, Standard Deviation and Range of T1 values for the Right and Left Ventricular Chamber Contents for the Four Patient Groups Studied

| Patient Groups | T1 Values | | | |
|---|---|---|---|---|
| | Right Ventricle | | Left Ventricle | |
| | Mean ±SD | Range | Mean ±SD | Range |
| Chronic Obstructive Pulmonary Disease (n = 16) | 581.1±104.0 | 499.2 - 910.4 | 565.3±89.2 | 475.8 - 759.6 |
| Ischaemic Heart Disease (n = 19) | 549.9±140.6 | 298.2 - 832.4 | 536.5±112.3 | 343.6 - 753.5 |
| Age-Matched Controls (n = 5) | 737.2±152.1 | 478.6 - 877.7 | 669.9±153.5 | 454.1 - 836.3 |
| Normal Young Volunteers (n = 4) | 770.9±145.4 | 587.2 - 935.6 | 680.7±129.9 | 556.7 - 845.1 |

volunteer group (307.1 - 339.8ms), while values varied considerably in those suffering from ischaemic heart disease (277.3 - 475.6ms). A wide variation but with less marked spread was noted in patients with chronic obstructive pulmonary disease.

## T1 Value of Ventricular Chambers

The mean, standard deviation and range of T1 values for the right and left ventricular chamber contents for the four patient groups are detailed in Table 12, and individual values in Tables 13 to 16, Appendix 2. There was no significant difference in the mean T1 values obtained for either the right or left ventricular blood pool between the groups studied. A wide range of values was noted in all patient groups from a minimum of 298.2ms for the right ventricular chamber in patients with ischaemic heart disease to a maximum of 935.6ms for the right ventricle in the normal young volunteer group.

## Correlation of T1 Values : Ventricular Wall versus Chamber Contents

Using the null hypothesis there was a good correlation between the individual T1 values for the right and left ventricular walls but a better correlation was obtained for the chamber contents (Figure 17a and b), with coefficients of correlation of $r = 0.56$ ($p<0.001$), and $r = 0.86$ ($p<0.001$) respectively. However neither the T1 values for the ventricular walls nor the chamber contents were linearly related.

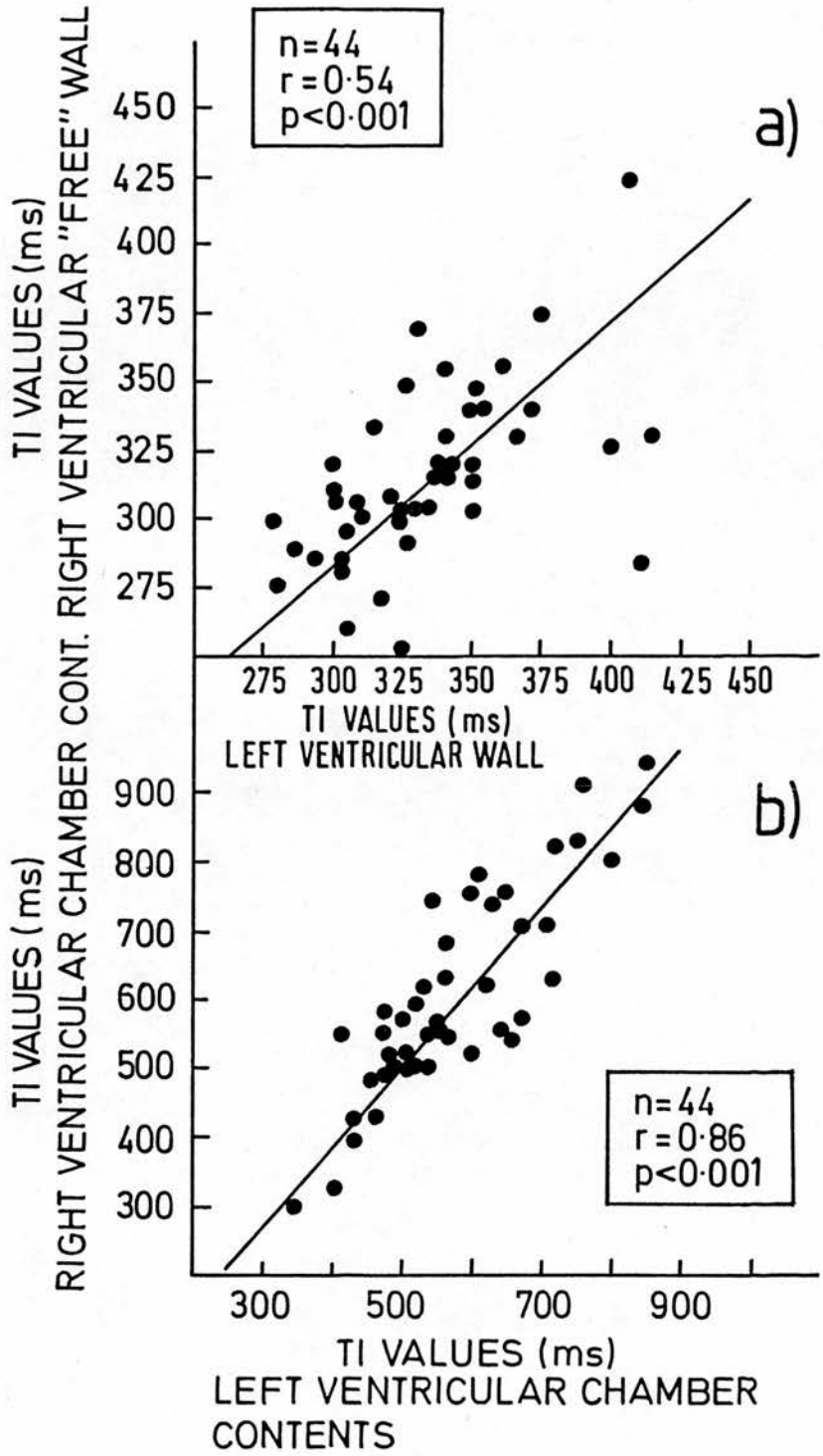


Figure 17. Comparison between T1 values for a) the right and left ventricular walls and b) chamber contents using coefficient of correlation.

The results were further analysed using a plot of the difference between the T1 values for the right and left ventricles against their mean (Figures 18a and b). The mean difference in T1 values for the left compared to the right ventricular walls was 18.4ms and the standard deviation 31.4ms. Hence the 95 per cent confidence limits for the bias were 8.9ms to 28.0ms. The 95 per cent confidence interval for the lower limit of agreement was -60.9ms to -27.9ms, while the upper limit of agreement was 64.7ms to 97.7ms. The results show that although there was a moderately good agreement between T1 values for the right and left ventricular walls, the T1 values for the left ventricle were in general slightly higher than the right ventricle (mean difference 18.4ms).

The mean difference in T1 values for the left compared to the right chamber contents was -27.6ms, and the standard deviation 74.5ms. The 95 per cent confidence limits for the bias were -4.9 to -50.3ms. The 95 per cent confidence interval for the lower limit of agreement was -137.4 to -215.0ms, while the value for the upper limit of agreement was 82.2 to 160.7ms. These figures suggest that T1 values for the right ventricular chamber were greater than the left, and although the coefficient of correlation ($r = 0.86$, $p<0.001$) showed a moderate correlation, the plot of the difference between T1 values against their mean showed considerable discrepancies such that the level of agreement was not acceptable. Of interest the T1 values for the left ventricular chamber were less than those for the right in all the age-matched control and normal young volunteer patients. However in 13 out of the 35 remaining patients with either ischaemic heart disease or chronic

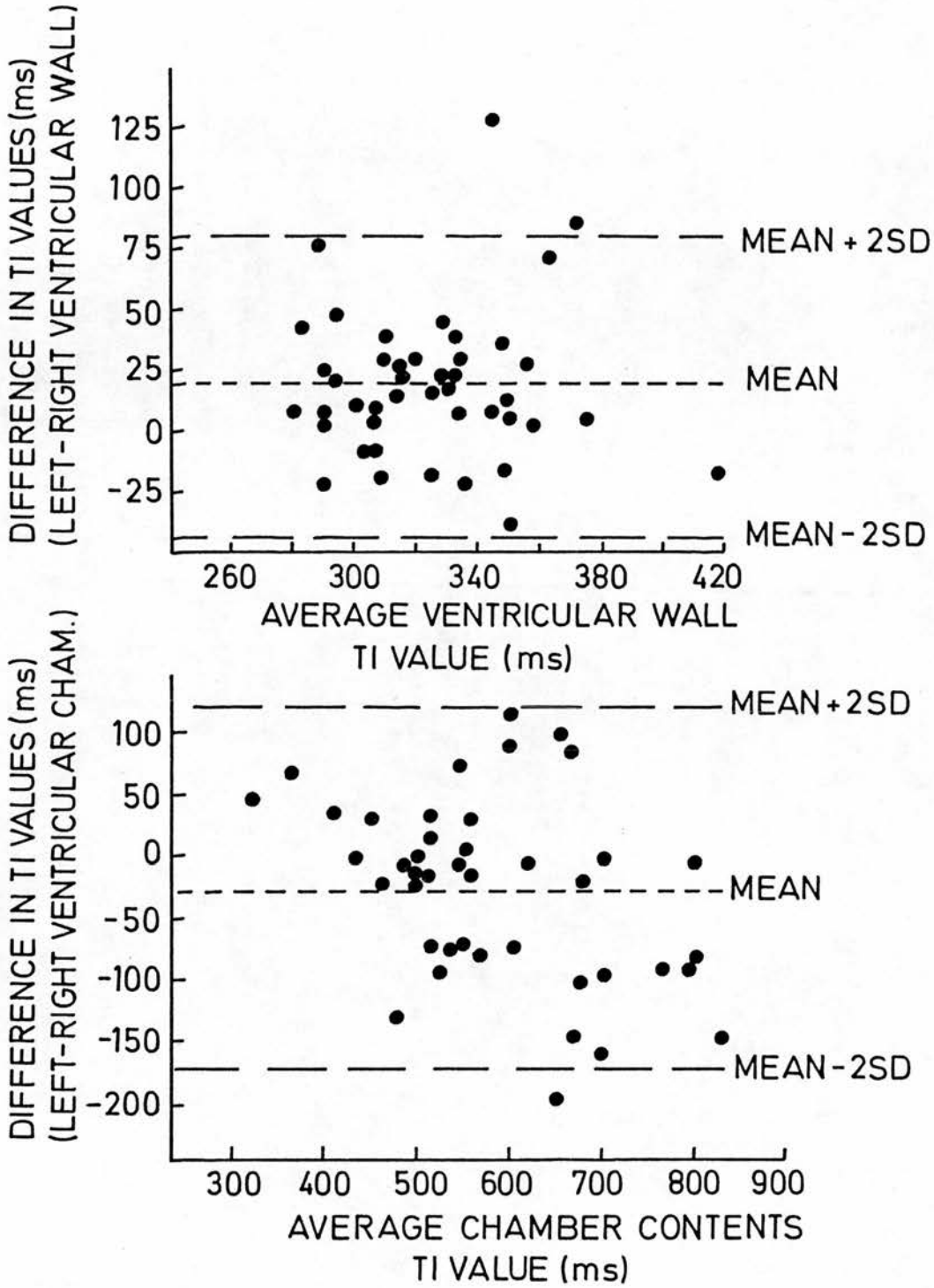


Figure 18. Plot of the difference between T1 values for a) the left and right ventricular walls and b) the chamber contents against their mean values.

obstructive pulmonary disease the values were greater.

### 5I.2 Heart Rate

The mean value for heart rate showed no change between the four groups, ranging from 62 to 79 bpm. However there was a much wider spread of values in the ischaemic heart disease and chronic obstructive pulmonary disease groups, of 45 and 55 bpm respectively compared to a small spread of 17 and 10 bpm for the age-matched control and normal young volunteer groups respectively (Tables 13 to 16, Appendix 2).

In an attempt to correlate changes in T1 values with heart rate, the T1 values for both the right and left ventricular wall were plotted separately (Figure 19a and b). Superimposed on each graph were the measured T1 values for a standard manganese chloride phantom with a known T1 value of 333ms obtained at computer controlled heart rates between 45 to 105ms.

There was considerable spread in T1 values for both the right and left ventricular walls at all heart rates. Although there was a trend towards higher T1 values at lower heart rates, the values obtained showed considerable variation around the graph obtained for the manganese chloride phantom.

### 5I.3 Right Ventricular Chamber Volume

Systolic

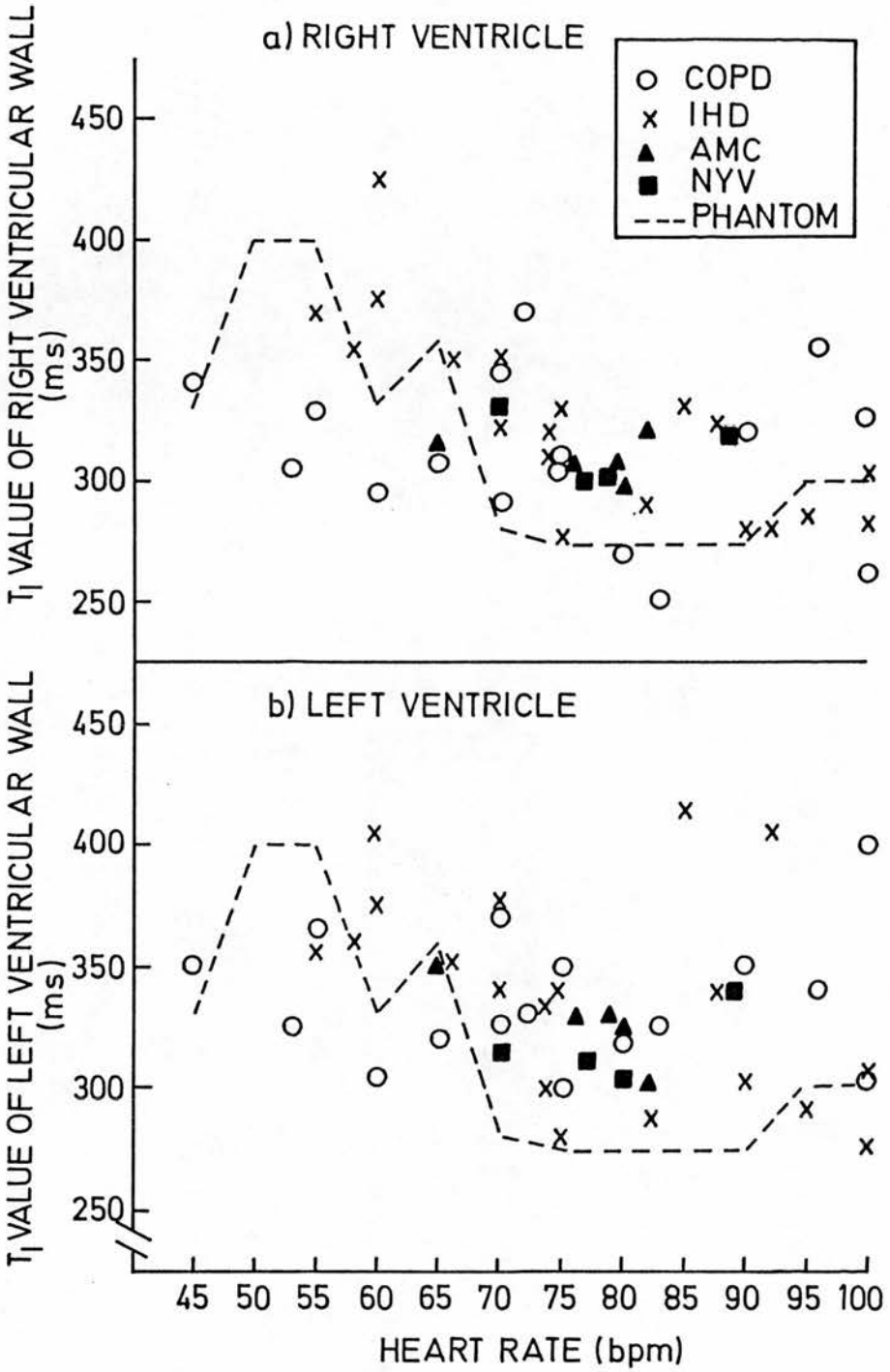


Figure 19. Comparison of T1 values for the right a) and left b) ventricular walls with heart rate for four patient groups studied. Measured T1 values for calibrated phantom (333ms) are superimposed (------).

The mean, standard deviation and range of the values obtained for the right ventricular end-systolic "free" wall and chamber volumes for the four patient groups are detailed in Table 21, and individual results shown in Tables 17 to 20, Appendix 2.

Patients with chronic obstructive pulmonary disease had a mean end-systolic right ventricular chamber volume of 44.8 $\pm$23.4cm$^3$ (range 13.3 to 97.6cm$^3$), while the mean value for patients with ischaemic heart disease was significantly less at 29.1 $\pm$16.3cm$^3$ (range 8.6 to 48.1cm$^3$), $p<0.025$.

The mean right ventricular chamber volume for the age matched control group was slightly, but not significantly less than that obtained for patients with ischaemic heart disease, with a mean value of 23.8 $\pm$11.6cm$^3$ (range 12.8 to 40.9cm$^3$), while the smallest volumes were obtained in the normal young volunteer group, with a mean value of 17.4 $\pm$4.2cm$^3$ (range 12.4 to 21.4cm$^3$).

Table 22 shows a comparison between the right ventricular chamber volumes obtained in the four study groups using an independent student's t-test. The most significant difference between the four groups was obtained between patients with chronic obstructive pulmonary disease and normal young volunteers ($00.5>p>0.02$), with only a slightly less significant difference with the age matched control group.

No statistically significant difference was obtained between patients with ischaemic heart disease and either the normal young

TABLE 21

Mean, Standard Deviation and Range of Right Ventricular End-Systolic Chamber Volumes in the Four Patient Groups Studied

| Patient Groups | Mean ±SD $cm^3$ | Range $cm^3$ |
|---|---|---|
| Chronic Obstructive Pulmonary Disease | 42.3±19.1 | 13.3 - 97.6 |
| Ischaemic Heart Disease | 29.1±16.3 | 8.6 - 48.1 |
| Age-Matched Controls | 23.8±11.6 | 12.8 - 40.9 |
| Normal Young Volunteers | 17.4±4.2 | 12.4 - 21.4 |

TABLE 22

Comparison of Right Ventricular Chamber Volumes in the 4 Patient Groups using an Independent Student's t-test

| | Patient Groups | | |
|---|---|---|---|
| | Ischaemic Heart Disease | Age Matched Controls | Chronic Obstructive Pulmonary Disease |
| Age Matched Controls | SE = 6.85<br>t = 0.33<br>df = 14<br>p = NS | | |
| Chronic Obstructive Pulmonary Disease | SE = 7.79<br>t = 2.40<br>df = 25<br>p <0.025 | SE = 10.98<br>t = 1.91<br>df = 19<br>0.1 > p > 0.05 | |
| Normal Young Volunteers | SE = 6.81<br>t = 1.27<br>df = 13<br>p = NS | SE = 6.81<br>t = 1.03<br>df = 7<br>p = NS | SE = 11.96<br>t = 2.29<br>df = 18<br>0.05 > p > 0.02 |

volunteers or age-matched controls, although a weak difference was demonstrated with patients with chronic obstructive pulmonary disease ($p<0.025$).

Diastolic

Images were also obtained at end-diastole in 10 of the 16 patients with chronic obstructive pulmonary disease. The right ventricular end-diastolic volumes ranged from 71.8 to 172.0$cm^3$, with a mean value of 104.1.$cm^3$.

### 5I.4 Left Ventricular Chamber Volume

Systolic

The mean, standard deviation and individual values for left ventricular end-systolic chamber volumes are shown in Tables 17 to 20, Appendix 2. There was no significant difference in values between patients with chronic obstructive pulmonary disease, the age-matched controls or the normal young volunteer group (49.5 $\pm$26.9$cm^3$, 44.1 $\pm$17.7$cm^3$ and 30.6 $\pm$1.4$cm^3$). However patients with ischaemic heart disease had larger left ventricular chambers, with a mean value of 100.0 $\pm$29.1$cm^3$. This was significantly greater than the remaining 3 patient groups ($0.01>p>0.001$).

### 5I.5 Ejection Fractions and Stroke Volume

Left and right ventricular ejection fractions and stroke volumes were carried out in only 10 of the 16 patients with chronic obstructive pulmonary disease. The mean ejection fractions were

Table 23

Right and Left Ventricular Chamber Volumes Obtained at End-Systole (ESV) and End-Diastole (EDV), the Stroke Volumes (SV) and Calculated Ejection Fractions (EF) in Patients with Chronic Obstructive Pulmonary Disease

| Name | Left Ventricle | | | | Right Ventricle | | | |
|---|---|---|---|---|---|---|---|---|
| | ESV $cm^3$ | EDV $cm^3$ | SV $cm^3$ | EF % | ESV $cm^3$ | EDV $cm^3$ | SV $cm^3$ | EF % |
| MA | 32.3 | 54.3 | 22.0 | 40.5 | 49.9 | 75.4 | 25.5 | 33.8 |
| TH | 81.1 | 181.2 | 100.1 | 55.2 | 56.5 | 172.0 | 115.5 | 67.2 |
| RW | 17.1 | 72.3 | 55.2 | 76.3 | 45.3 | 106.8 | 61.5 | 57.6 |
| WH | 79.4 | 140.8 | 61.4 | 43.6 | 48.3 | 115.0 | 66.7 | 58.0 |
| RH | 42.6 | 79.0 | 36.4 | 46.1 | 56.8 | 89.7 | 32.9 | 36.7 |
| AE | 67.4 | 120.0 | 52.6 | 43.8 | 16.3 | 71.8 | 55.5 | 77.4 |
| MD | 42.4 | ND | ND | ND | 24.6 | ND | ND | ND |
| RC | 35.5 | 77.8 | 42.3 | 54.4 | 41.4 | 90.1 | 48.7 | 54.1 |
| WF | 56.5 | 93.6 | 37.1 | 39.6 | 57.4 | 88.2 | 30.8 | 34.9 |
| TW | 115.8 | ND | ND | ND | 18.7 | ND | ND | ND |
| JW | 40.6 | 112.3 | 71.7 | 63.8 | 22.1 | 89.0 | 66.9 | 72.5 |
| AM | 57.8 | 120.2 | 62.4 | 51.9 | 87.4 | 142.6 | 55.2 | 38.7 |
| RS | 24.6 | ND | ND | ND | 29.1 | ND | ND | ND |
| SD | 37.4 | ND | ND | ND | 40.6 | ND | ND | ND |
| MD | 8.8 | ND | ND | ND | 28.8 | ND | ND | ND |
| MB | 53.4 | ND | ND | ND | 56.2 | ND | ND | ND |

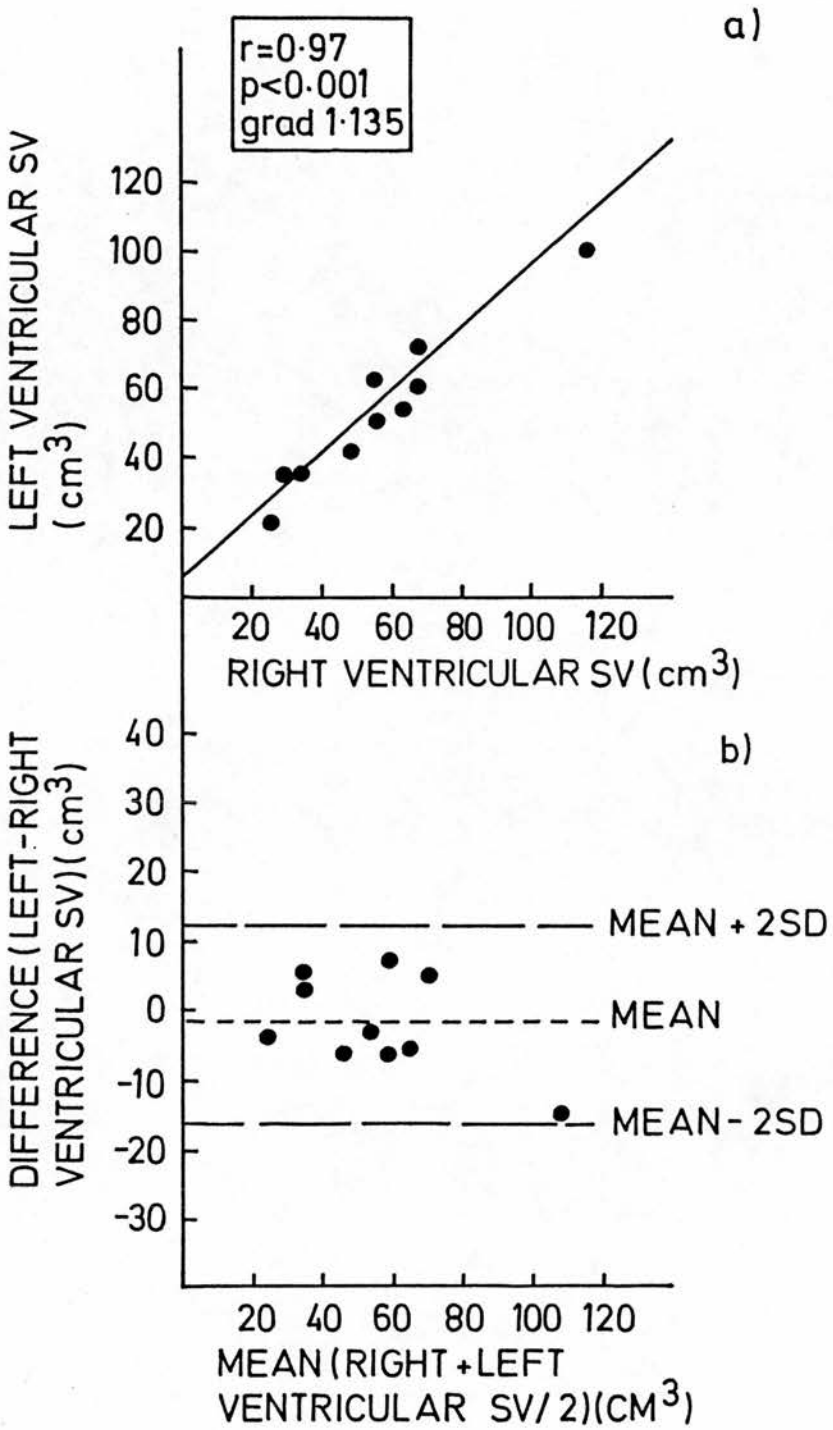


Figure 20. Comparison of right and left ventricular stroke volumes using a) coefficient of correlation and b) difference between left and right ventricular stroke volumes against the mean of the two measurements.

similar for the right and left ventricle at 53.4 per cent (range 33.8 to 77.4%) and 51.5 per cent (range 39.6 to 76.3%) respectively. However there was considerable variation between right and left ventricular ejection fractions in individual patients (Table 23). The stroke volumes for the right and left ventricle were correlated and the results shown in Figures 20a & b. Figure 20a shows a highly significant result using a coefficient of correlation ($r = 0.97$, $p<0.001$), while Figure 20b plots the difference between measurements against the mean of the two measurements. The mean difference between measurements was $- 1.8cm^3$, the standard deviation of the difference $+ 7.2cm^3$, and the standard error of the difference was $+ 2.26cm^3$. The mean difference between measurements did not vary significantly from zero, indicating a satisfactory agreement between measurements of left and right ventricular stroke volume.

### 5I.6 Right Ventricular "Free" Wall Volume

Systolic

The mean, standard deviation and range of values for the right ventricular "free" wall volumes, for the four study groups are shown in Table 24, and individual values in Tables 17 to 20, Appendix 2.

There was no significant alteration in the right ventricular "free" wall volume between patients with ischaemic heart disease (mean $27.2 \pm 6.0cm^3$ ; range 19.0 to $39.4cm^3$), the age matched controls (mean $20.8 \pm 11.0cm^3$; range 9.1 to $31.7cm^3$) or the normal young

TABLE 24

Mean, Standard Deviation and Range of Right Ventricular "Free" Wall Volumes obtained at End-systole in the Four Patient Groups Studied

| Patient Groups | Mean ±SD $cm^3$ | Range $cm^3$ |
|---|---|---|
| Chronic Obstructive Pulmonary Disease | 56.9±22.2 | 11.8 - 96.0 |
| Ischaemic Heart Disease | 27.2±6.0 | 19.0 - 39.4 |
| Age-Matched Controls | 20.8±11.0 | 9.1 - 31.7 |
| Normal Young Volunteers | 28.5±7.5 | 20.7 - 35.6 |

TABLE 25

Comparison of Right Ventricular "Free" Wall Volumes obtained at End-systole in the 4 Study Groups using an Independent Student's t-test

| | Patient Groups | | |
|---|---|---|---|
| | Ischaemic Heart Disease | Age Matched Controls | Chronic Obstructive Pulmonary Disease |
| Age Matched Controls | SE = 4.21<br>t = 1.43<br>df = 14<br>p = NS | | |
| Chronic Obstructive Pulmonary Disease | SE = 6.92<br>t = 4.35<br>df = 25<br>p >0.001 | SE = 10.45<br>t = 3.46<br>df = 19<br>p >0.005 | |
| Young Volunteers | SE = 3.75<br>t = 0.45<br>df = 13<br>p = NS | SE = 6.46<br>t = 1.19<br>df = 7<br>p = NS | SE = 11.47<br>t = 2.48<br>df = 18<br>p = 0.025 |

volunteers (mean 28.5 $\pm$7.5cm$^3$; range 20.7 to 35.6cm$^3$). There was however a significant increase in the right ventricular "free" wall volume in patients with chronic obstructive pulmonary disease with a mean value of 56.9 $\pm$22.2cm$^3$ (range 11.8 to 96.0cm$^3$). This was significantly greater than the other three groups although the difference was greatest between patients with chronic obstructive pulmonary disease and ischaemic heart disease ($p>0.001$), see Table 25.

Diastolic

The right ventricular "free" wall volume was measured both during systole and diastole in 10 of the 16 patients with chronic obstructive pulmonary disease. The diastolic images were in general more difficult to calculate than the corresponding systolic images, due to the relative wall thinning. However the lack of blood flow at this point in the cardiac cycle reduced "flow" artefact, resulting in little or no signal from intra-ventricular blood. This aided delineation of the endo-cardial outline. The mean right ventricle "free" wall volume at end-diastole was 65.9 $\pm$19.3cm$^3$ (range 27.0 to 95.9cm$^3$) compared to the mean systolic value of 56.9 $\pm$22.2cm$^3$ (range 11.8 to 96.0cm$^3$). These values correlated well ($r = 0.70$; $p>0.01$).

### 5I.7 Left Ventricular Wall Volumes

The mean, standard deviation and range of values for the four patients groups are shown in Table 26, and individual values in Table 17 to 20 (Appendix 2). There was no difference between

Table 26

Mean, Standard Deviation and Range of Left Ventricular Wall Volumes In the 4 Patient Groups Studied

| Patient Groups | Mean ±SD ($cm^3$) | Range ($cm^3$) |
|---|---|---|
| Chronic Obstructive Pulmonary Disease | 137.1 ±23.3 | 101.4 - 169.8 |
| Ischaemic Heart Disease | 171.6 ±38.3 | 111.5 - 238.4 |
| Age-Matched Controls | 163.0 ±22.9 | 129.9 - 186.6 |
| Normal Young Volunteers | 145.0 ±27.5 | 116.2 - 180.2 |

Table 27

Comparison of Left Ventricular Wall Volumes ($cm^3$) between 4 Patient Groups Using an Independent Student's t-test

| | Chronic Obstructive Pulmonary Heart Disease | Ischaemic Heart Disease | Normal Young Volunteers |
|---|---|---|---|
| Ischaemic Heart Disease | SED = 15.06<br>t = 5.29<br>df = 25<br>p>0.001 | | |
| Normal Young Volunteers | SED = 13.45<br>t = 0.59<br>df = 18<br>p NS | SED = 28.54<br>t = 2.58<br>df = 13<br>p = 0.025 | |
| Age-Matched Controls | SED = 11.89<br>t = 2.18<br>df = 19<br>p NS | SED = 25.33<br>t = 2.12<br>df = 14<br>p = 0.05 | SED = 16.71<br>t = 1.08<br>df = 7<br>p NS |

measurements obtained for the normal young volunteer(145.0 $\pm$27.5cm$^3$), the age-matched control groups (163.0 $\pm$22.9cm$^3$) or patients with chronic obstructive pulmonary 137.1 $\pm$23.3cm$^3$.

Patients with ischaemic heart disease had a marginally greater left ventricular wall volume at 171.6 $\pm$ 38.8cm$^3$ but this was not significantly larger than the remaining three groups. A comparison of the mean values for the four patient groups is detailed in Table 27.

### 5I.8 Comparative Results

(a) Right Ventricular End-Systolic Chamber Volume

Multiple correlations were carried out between the right ventricular end-systolic chamber volume, the right ventricular "free" wall volume, the pulmonary haemodynamic measurements, the left ventricular measurements and the data obtained from radionuclide ventriculography in the patients with chronic bronchitis and emphysema (Table 28).

Pulmonary Haemodynamic Data

No significant correlation was obtained between either the systolic pulmonary arterial pressure or the pulmonary vascular resistance and the right ventricular end-systolic chamber volume. Only a weak correlation was obtained between the right ventricular end-systolic chamber volume and the mean pulmonary arterial pressure ($r = 0.50$; $p<0.05$).

TABLE 28

Correlations with Right Ventricular End-Systolic Chamber Volume, in 16 Patients with Chronic Bronchitis and Emphysema

| | RV End-Systolic Chamber Volume | |
|---|---|---|
| | r | p |
| Systolic Pulmonary Artery Pressure | 0.47 | NS |
| Mean Pulmonary Artery Pressure | 0.50 | <0.05 |
| Pulmonary Vascular Resistance | 0.32 | NS |
| Pa CO2 | 0.23 | NS |
| Pa O2 | -0.37 | NS |
| RV "Free" Wall Volume | 0.71 | <0.01 |
| RV End-Diastolic Chamber Volume | 0.88 | <0.001 |
| Radionuclide RV Ejection Fraction | -0.19 | NS |
| Radionuclide RV End-Systolic Chamber Volume | 0.54 | 0.05>p>0.02 |

(Abbreviations: RV, right ventricle; Pa, pulmonary arterial tension)

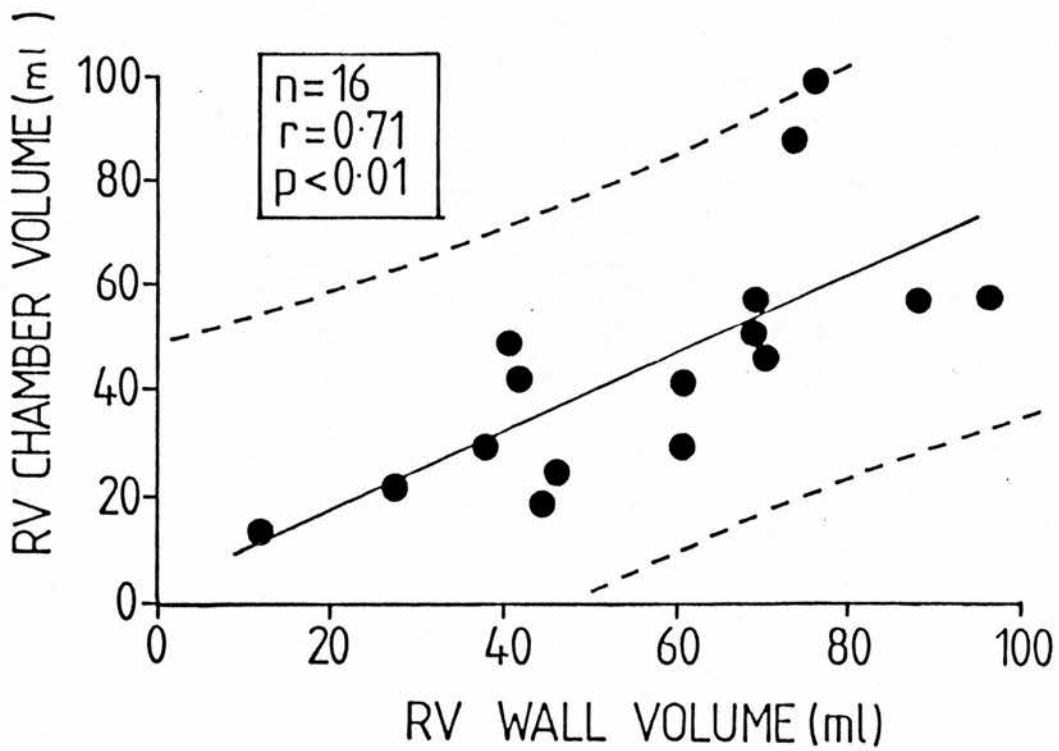


Figure 21. Relationship between right ventricular "free" wall volume and right ventricular chamber volume in patients with chronic obstructive pulmonary disease.

Blood Gas Results

No significant correlation was obtained with either the arterial carbon dioxide or oxygen saturation pressures and the right ventricular end-systolic chamber volumes with correlation coefficients of 0.23 and -0.37 respectively.

Magnetic Resonance Measurements

There was a highly significant correlation ($r = 0.71$; $p<0.01$) between the right ventricular end-systolic chamber volume and the right ventricular "free" wall volume also measured during end-systole (Figure 21). As the right ventricular "free" wall hypertrophied there was a corresponding dilatation of the ventricular chamber. Similarly, as the right ventricular end-systolic chamber volume increased there was a corresponding increase in the right ventricular end-diastolic chamber volume ($r = 0.88$; $p<0.001$). No significant correlation was obtained between the left and right ventricular end-systolic chamber volumes.

Radionuclide Ventriculograpy

Comparison was made between the right ventricular end-systolic chamber volume measured by magnetic resonance and that obtained by radionuclide ventriculography using a first pass bolus technique. This showed only a moderate correlation between the two values with a correlation coefficient of 0.54, ($p>0.05>0.02$). However there was no significant correlation between the right ventricular chamber volume measured by magnetic resonance and the radionuclide right ventricular ejection fraction.

TABLE 29

Correlations with Right Ventricular "Free" Wall Volume, in 16 Patients with Chronic Bronchitis and Emphysema

| | RV "Free" Wall Volume (systole) | |
|---|---|---|
| | r | p |
| Systolic Pulmonary Artery Pressure | 0.74 | <0.01 |
| Mean Pulmonary Artery Pressure | 0.72 | <0.01 |
| Pulmonary Vascular Resistance | 0.65 | <0.01 |
| Pa CO2 | 0.56 | <0.02 |
| Pa O2 | -0.25 | NS |
| RV "Free" Wall Volume (diastole) | 0.70 | <0.01 |
| LV "Wall" Volume (systole) | 0.19 | NS |
| Radionuclide RV Ejection Fraction | -0.09 | NS |

(Abbreviations: RV, right ventricle; LV, left ventricle; Pa, pulmonary arterial tension).

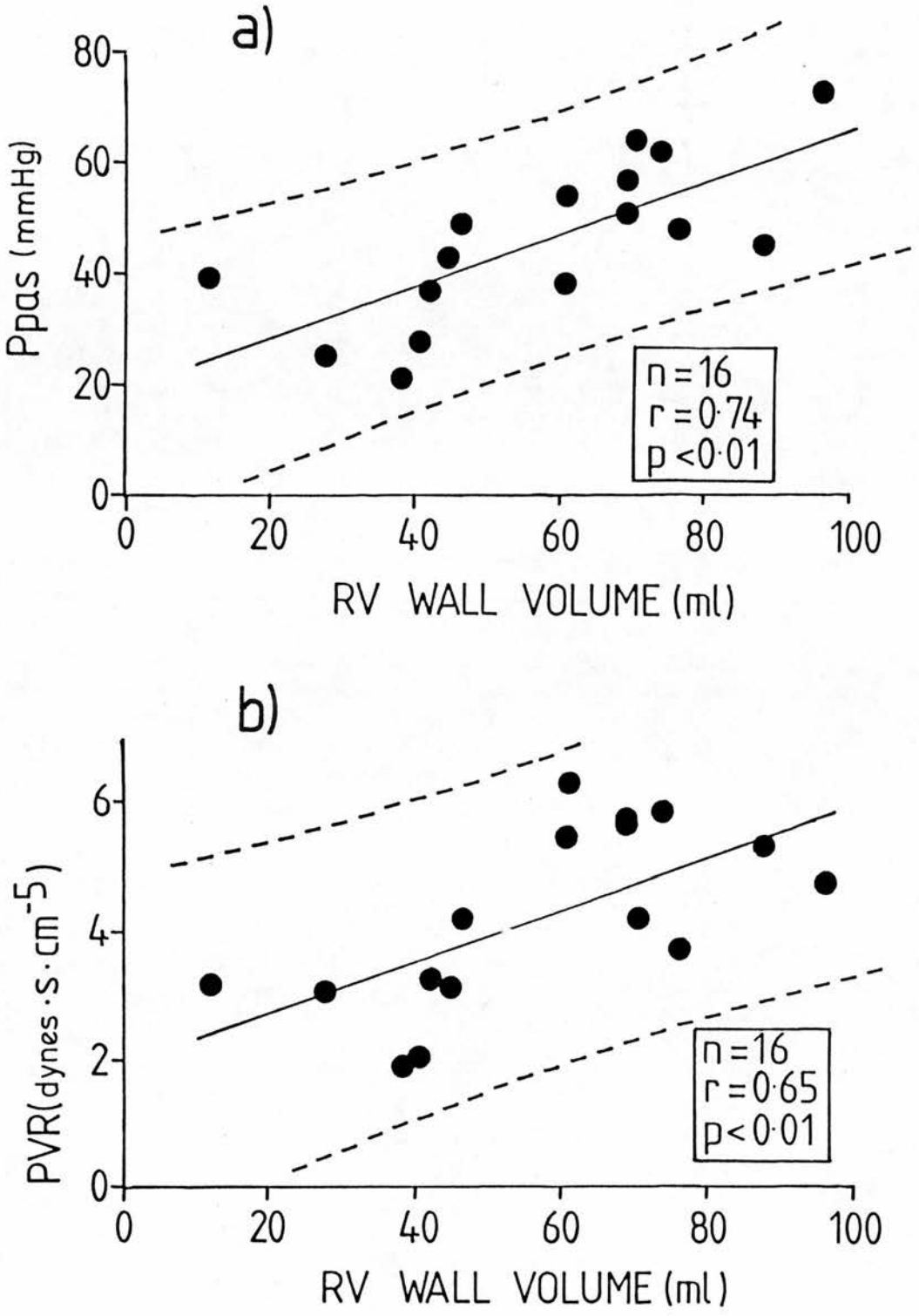


Figure 22. Relationship between right ventricular "free" wall volume and a) the systolic arterial pressure and b) the pulmonary vascular resistance in patients with chronic obstructive pulmonary disease.

(b) Right Ventricular "Free" Wall Volume

Multiple correlations were obtained between the right ventricular "free" wall volume and the pulmonary haemodynamic data, blood gas results, left ventricular wall volume measurements and radionuclide ventriculography (Table 29).

Pulmonary Haemodynamic Data

Both the systolic and the mean pulmonary arterial pressures correlated with the right ventricular "free" wall volume with correlation coefficients of 0.74 (Figure 22a) and 0.72 respectively. Similarly a significant although slightly weaker correlation was obtained between the pulmonary vascular resistance and the right ventricular "free" wall volume ($r = 0.65$; $p<0.01$), Figure 22b.

Blood Gas Results

The right ventricular "free" wall volume correlated significantly with the arterial carbon dioxide tension ($r = 0.56$; $p<0.02$) but not with the arterial oxygen tension, measured when breathing air (Figure 23).

Magnetic Resonance Measurements

There was a good correlation between measurements of the right ventricular "free" wall volume obtained during end-systole and end-diastole ($r = 0.70$, $p<0.001$) but there was no significant correlation between the right ventricular "free" wall volume and the left ventricular wall volume which included the inter-

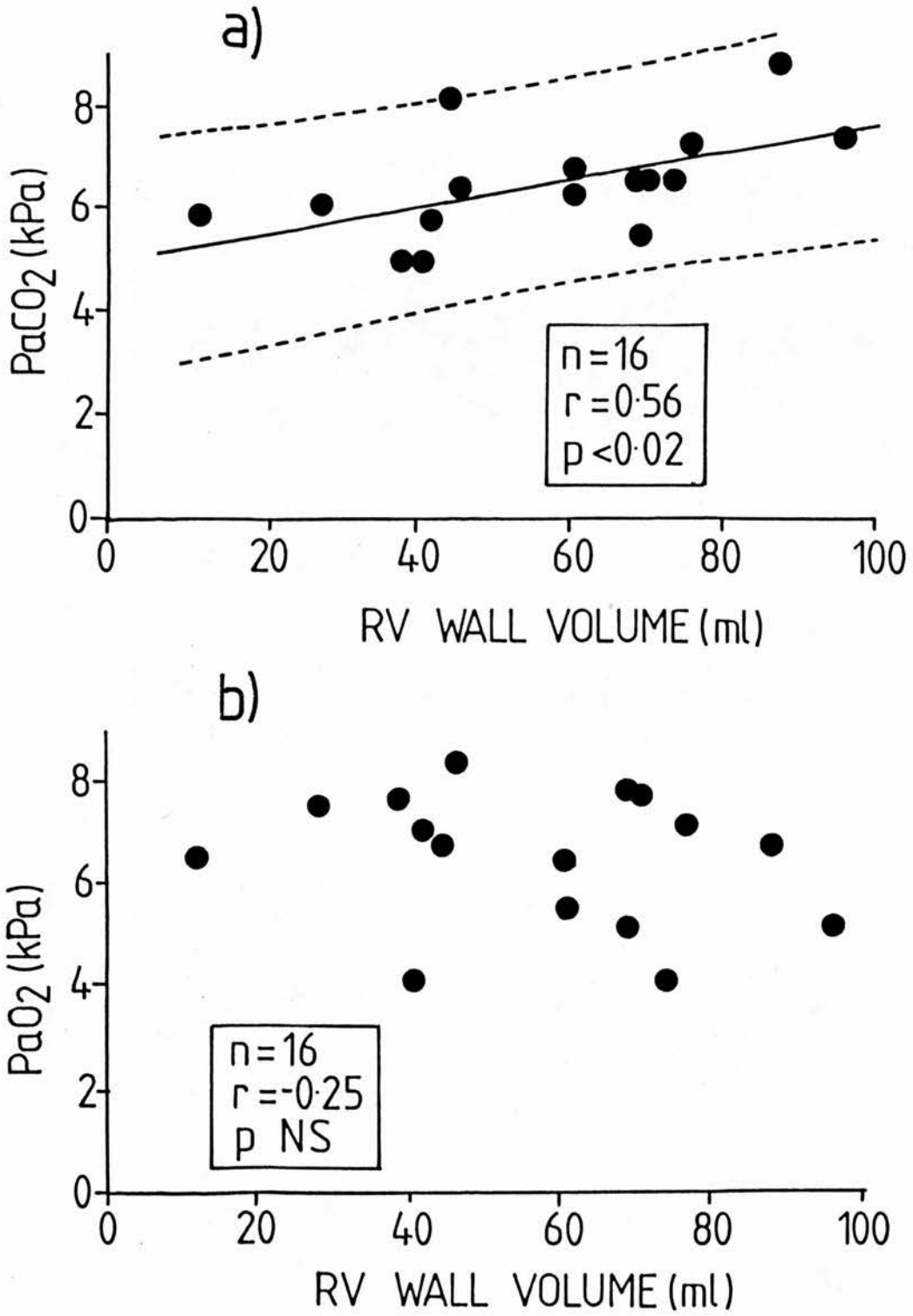


Figure 23. Relationship between right ventricular "free" wall volume and a) arterial carbon dioxide tension and b) arterial oxygen tension in patients with chronic obstructive pulmonary disease.

ventricular septum.

Radionuclide Ventriculograpy

The right ventricular ejection fraction measured using a first pass bolus technique showed no correlation with the degree of right ventricular hypertrophy measured by magnetic resonance imaging.

(c) Right Ventricular Radionuclide Ventriculography

Further correlations were obtained between the radionuclide right ventricular ejection fractions in 15 of the 16 patients with chronic obstructive pulmonary disease and the pulmonary haemodynamic and blood gas data (Table 30).

Pulmonary Haemodynamic Data

There was no correlation between either the systolic pulmonary arterial pressure or the pulmonary vascular resistance and there was only a weak negative correlation with the mean pulmonary arterial pressure ($r = -0.49$; $p>0.05$).

Blood Gas Results

The right ventricular ejection fraction measured by radionuclide ventriculography showed no correlation with either the arterial carbon dioxide or oxygen saturation pressures. The correlations obtained are shown in Table 30.

Table 30

Correlations with Radionuclide Right Ventricular Ejection Fraction,

in 15 of the 16 Patients with Chronic Bronchitis and Emphysema

| | Radionuclide RV Ejection Fraction | |
|---|---|---|
| | r | p |
| Systolic Pulmonary Artery Pressure | r = -0.42 | NS |
| Mean Pulmonary Artery Pressure | r = -0.49 | >0.05 |
| Pa C02 | r = -0.17 | NS |
| Pa O2 | r = -9.64 | NS |

(Abbreviations: Pa, pulmonary arterial tension)

## 5I.9 Reproducibilities

To determine the day-to-day reproducibility, right ventricular "free" wall volumes were measured from scans obtained on three separate occasions, in the four normal healthy volunteers. The mean percentage difference in the measurement of right ventricular "free" wall volume was 3 per cent with a range of 1.1 to 7.0 per cent (Table 31).

The intra-observer variability for LWT and HMcR which was calculated by measuring the same three scans on three separate occasions was 6.0 and 7.0 per cent respectively. The inter-observer variability for the right ventricular "free" wall volume by mean percent difference was 14.0 per cent.

Table 31

Variation in Right Ventricular "Free" Wall Volume Obtained at End-systole in 4 Normal Volunteers on 3 separate occasions

| Volunteer No | RV "Free" Wall Volume $cm^3$ Scan Number | | | Variability (max % difference from mean value) |
|---|---|---|---|---|
| | 1 | 2 | 3 | |
| 1 | 20.4 | 22.2 | 19.6 | 7.2 |
| 2 | 24.0 | 22.6 | 23.9 | 3.8 |
| 3 | 35.0 | 35.8 | 36.0 | 1.7 |
| 4 | 34.6 | 34.4 | 33.3 | 2.3 |

## 5J EFFECTS OF LONG TERM DOMICILIARY OXYGEN THERAPY

### 5J.1 Patients

Eight of the 16 patients with chronic obstructive airways disease underwent magnetic resonance imaging on a second occasion, between 6 to 20 months (mean = 9.4 months) following the initial examination. All patients with the exception of one (RH) had received domiciliary oxygen therapy for between 6 to 20 months (mean 9.4 months). Oxygen was supplied at a low flow rate (2l/min) via nasal cannulae for approximately 16 hours per day. All patients had apparently refrained from smoking since commencing long term oxygen therapy and, at the time of repeat examination, were both clear of cardiac failure and had not experienced an exacerbation of their condition within the preceeding four weeks. Of the eight patients who were not re-examined, five died before a repeat examination could be performed and three refused further investigation.

### 5J.2 Methods

Magnetic resonance imaging was carried out as described previously in Chapter 5H.1. Using cardiac gating, an interleaved saturation recovery-inversion recovery pulse sequence was employed to acquire T1 map images during end-systole. The method of image analysis has already been described in detail. A typical example of images obtained before and after long term oxygen therapy is shown in Figure 24.

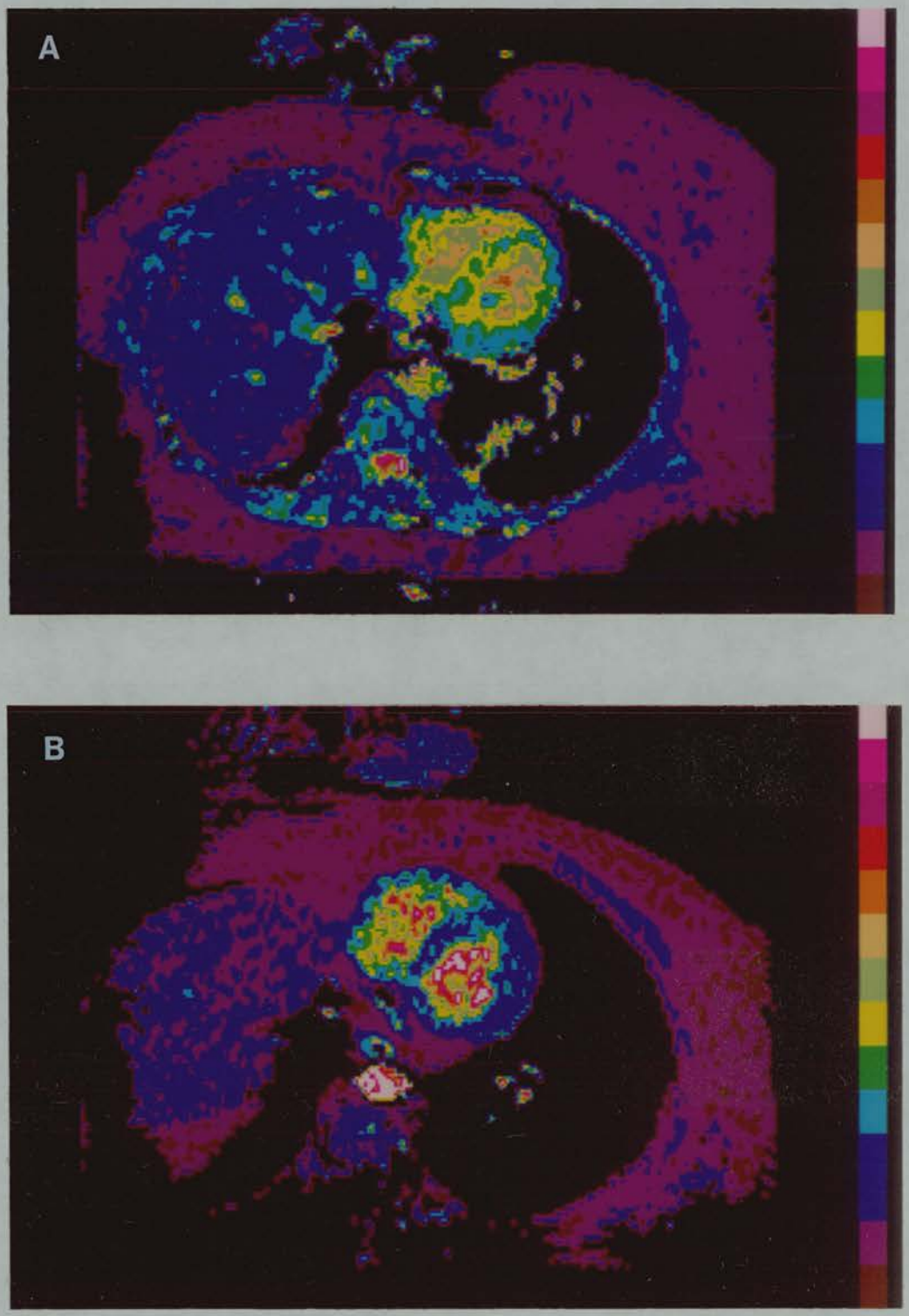


Figure 24. Typical example of an transverse T1 map image obtained at the level of the right ventricle, showing significant increase in right ventricular "free" wall volume after long term oxygen therapy (b), compared to the pre-treatment examination (a).

TABLE 32

Alterations in Right and Left Ventricular Wall Volume in 8 Patients with Chronic Obstructive Pulmonary Disease after Long-Term Oxygen Therapy

| Patient | Time Interval Between Scans (months) | Wall Volume (ml) | | | | | |
|---|---|---|---|---|---|---|---|
| | | Right Ventricle | | | Left Ventricle | | |
| | | Pre | Post | Increase (%) | Pre | Post | Increase (%) |
| AE | 20 | 11.8 | 48.3 | +309.3 | 101.4 | 176.17 | +73.8 |
| AM | 8 | 13.6 | 93.4 | +26.9 | 120.3 | 196.51 | +63.3 |
| TW | 10 | 44.5 | 84.1 | +89.0 | 115.8 | 253.76 | +119.2 |
| WF | 6 | 76.0 | 70.48 | -7.2 | 154.7 | 205.31 | +32.7 |
| WH | 8 | 40.6 | 87.31 | +115.0 | 102.6 | 218.11 | +112.6 |
| JB | 6 | 87.8 | 114.57 | +30.5 | 78. 4 | 162.67 | +107.5 |
| RW | 8 | 70.4 | 52.88 | -24.8 | 57.8 | 96.25 | +66.6 |
| RH | 11 | 96.0 | 74.56 | -22.3 | 169.4 | 149.42 | -11.8 |

(* only patient not receiving long-term domiciliary oxygen therapy)

## 5J.3 Results

Individual values for the right and left ventricular wall and chamber volumes and the percentage change during treatment are detailed in Tables 32 and 33.

Figures 25 and 26 show the right and left ventricular wall and chamber volumes for the 7 patients examined before and after oxygen therapy and detail the 95 per cent confidence interval for the difference between measurements.

### a) Ventricular Wall Volumes

Right Ventricular "Free" Wall Volumes

Five of the 7 patients who received long-term domiciliary oxygen therapy demonstrated an increase in right ventricular "free" wall volume, ranging from 26.9 to 309.3 per cent (mean +114.1%), compared to the initial examination, while in the remaining 2 patients there was a fall in right ventricular "free" wall volumes of 7.2 and 24.8 per cent respectively (mean 18.1%). The only patient (RH) who did not receive domiciliary oxygen therapy showed a decrease in the right ventricular "free" wall volume by 22.3 per cent.

The overall mean change in volumes was 29.6cm$^3$. The 95 per cent confidence interval for the difference before and after oxygen therapy centred on the mean change of $\pm$29.6cm$^3$, extended from -0.7

to + 59.9cm$^3$ (Figure 25). As the confidence interval includes zero this result is equivalent to a significance test that gives a non-significant result. However the upper limit of the confidence interval (+ 59.9cm$^3$) draws attention to the possibility that the average increase might be clinically important.

Left Ventricular Wall Volumes

With the exception of the single patient who did not receive oxygen therapy, and who showed a decrease of 11.8 per cent in the left ventricular wall volume, all the remaining patients demonstrated left ventricular hypertrophy, the increases ranging from 32.7 to 119.2 per cent (mean +82.2%). The actual mean change in left ventricular wall volumes was 81.4cm$^3$, with 95 per cent confidence intervals of 46.8 to 115.4cm$^3$ (Figure 25). This is highly significant.

b) Ventricular Chamber Volumes

Right Ventricular Chamber Volumes

Six of the 7 patients who received long-term oxygen therapy demonstrated an increase in the right ventricular chamber volume of between 21.0 to 307.0 per cent, while the remaining patients showed a slight decrease of 24.5 per cent (mean +135.9%). The only patient not on long-term oxygen also showed an increase in right ventricular chamber size of 131.7 per cent. The mean change in right ventricular chamber volume was + 48.0cm$^3$, while the 95 per

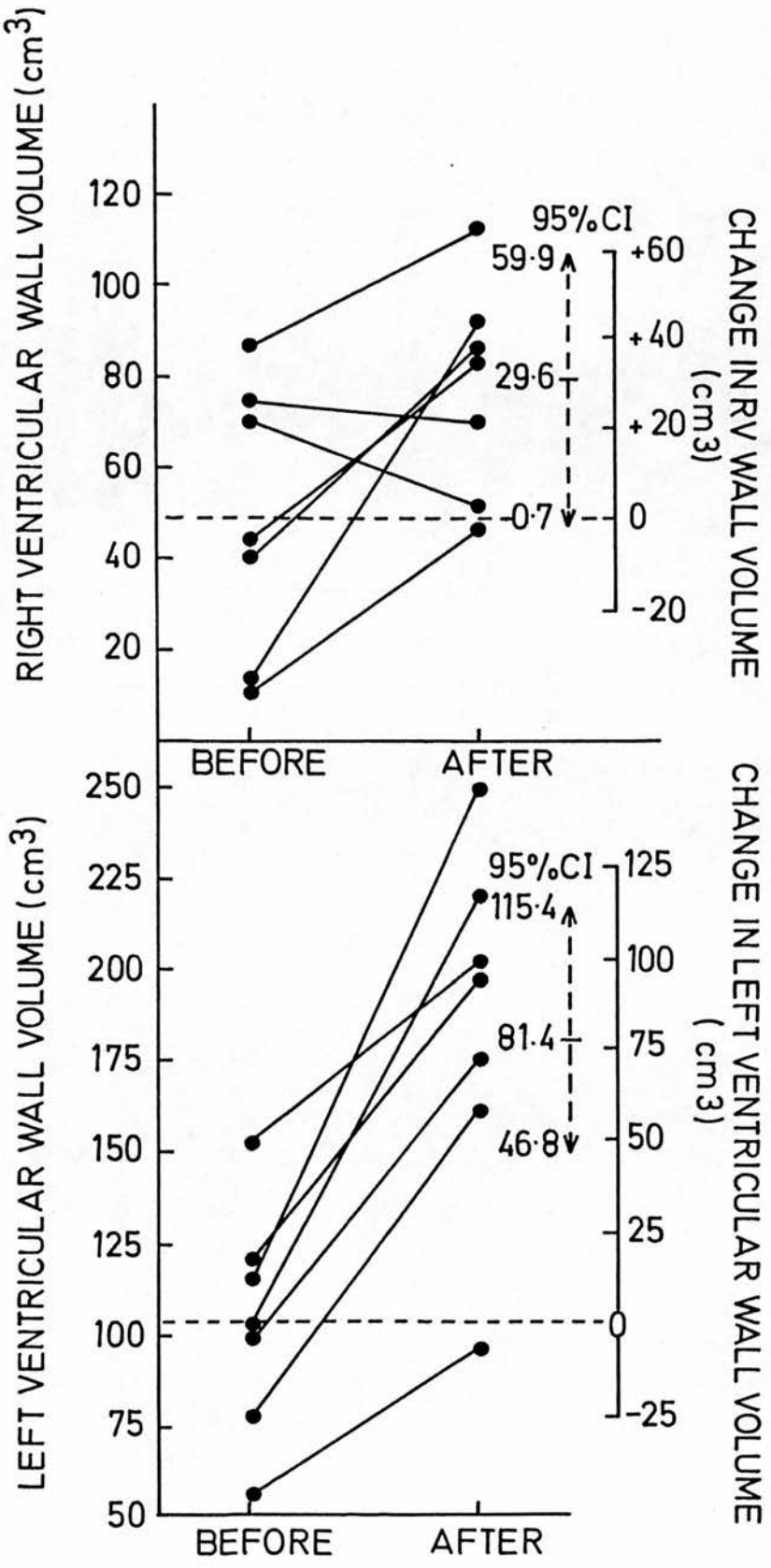


Figure 25. Comparison of right and left ventricular wall volumes before and after domiciliary oxygen therapy.

cent confidence intervals ranged from 12.5 to 83.5cm$^3$ (Figure 26). This shows a highly significant increase in the right ventricular chamber volume despite long-term oxygen therapy.

Left Ventricular Chamber Volumes

Five of the 7 patients on long-term oxygen therapy showed a rise in the left ventricular chamber volume, ranging from only 0.7 to 125.1 per cent, while 2 patients demonstrated a fall in chamber size of 20.1 and 36.4 per cent (mean +51.3%). The single patient on no therapy showed virtually no change in chamber volume with an increase of only 0.9 per cent. The actual mean change in left ventricular chamber volume was +18.5cm$^3$, with 95 per cent confidence intervals of -11.3cm$^3$ to + 48.3cm$^3$. The results show no significant change in chamber volume during long-term oxygen therapy (Figure 26).

There was no significant correlation between the degree of left ventricular hypertrophy and the alteration in left ventricular chamber size. However using an independent student's t-test there was a moderately significant correlation between the degree of right ventricular hypertrophy and right ventricular dilatation present ($r = 0.62$, $p = 0.05$).

TABLE 33

Alterations in Right and Left Ventricular Chamber Volumes in 8 Patients with Chronic Obstructive Pulmonary Disease after Long-Term Oxygen Therapy

| Patient | Time Interval Between Scans (months) | Chamber Volume (ml) | | | | | |
|---|---|---|---|---|---|---|---|
| | | Right Ventricle | | | Left Ventricle | | |
| | | Pre | Post | Increase (%) | Pre | Post | Increase (%) |
| AE | 20 | 13.3 | 44.9 | +237.6 | 67.4 | 42.9 | -36.4 |
| AM | 8 | 87.4 | 145.8 | +66.8 | 51.8 | 117.6 | +127.0 |
| TW | 10 | 18.7 | 76.2 | +307.0 | 115.8 | 92.5 | -20.1 |
| WF | 6 | 97.6 | 118.1 | +21.0 | 45.1 | 81.4 | +80.5 |
| WH | 8 | 48.3 | 123.3 | +155.3 | 138.1 | 139.1 | +0.7 |
| JB | 6 | 56.2 | 162.1 | +188.4 | 53.4 | 97.5 | +82.6 |
| RW | 8 | 45.3 | 34.2 | -24.5 | 17.1 | 38.5 | +125.1 |
| *RH | 11 | 56.8 | 131.6 | +131.7 | 42.6 | 42.2 | -0.9 |

(* only patient not receiving long-term domiciliary oxygen therapy)

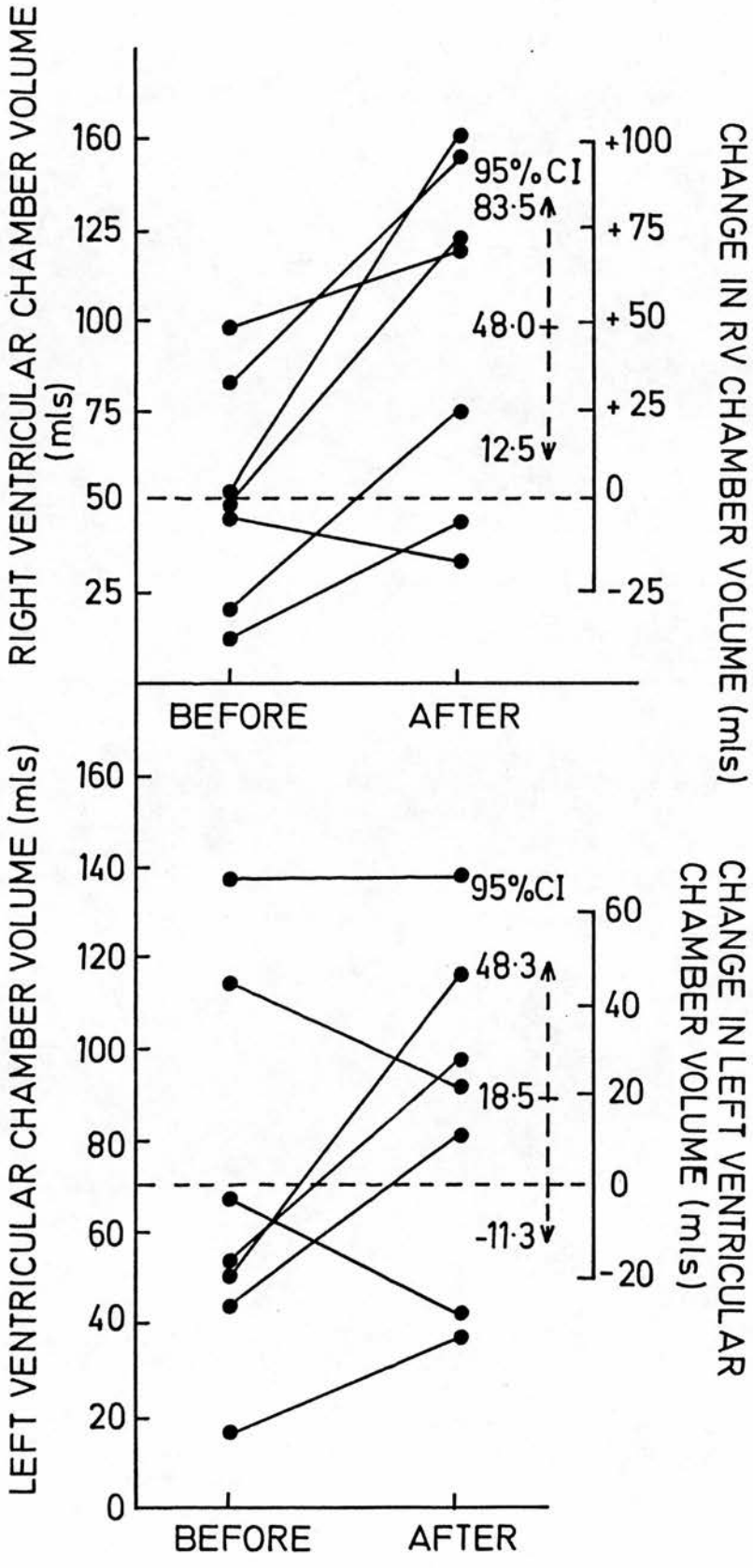


Figure 26. Comparison of right and left ventricular chamber volumes before and after domicillary oxygen therapy.

## 5K DISCUSSION

For any new diagnostic technique to gain acceptance as a method for complete evaluation of cardiac disease it must be capable of evaluating not only cardiac function but also anatomy. The depiction of cardiac anatomy requires good spatial resolution but the assessment of function also necessitates sufficient temporal resolution that images can be obtained at any desired point during the cardiac cycle.

Traditionally this dual role was dependent upon cardiac catheterisation and angiography. Invasive techniques based on x-ray contrast ventriculography have been used for many years for assessment of left ventricular function and anatomy, and they assume that the left ventricle is either an ellipsoid or a prolate spheroid. The first method which was proposed by Chapman in 1958 used a multi-slice technique in which the areas of sections through the left ventricle were summed. This method was too tedious for routine use and was superseded by the methods of Arvidsson (1961) and Dodge (1960) in which the minor axes of the ellipsoid were either measured directly or were calculated from the projected area of the left ventricle. Adaptation of the technique for single plane ventriculography (Sandler 1968) and for oblique bi-plane ventriculography (Wynne 1978) has been reasonably successful and the subject has been well reviewed.

Because of the complexity of the right ventricle a number of different formulae have been devised to compute chamber size. The

angiographic models have included pyramids (Ferlinz 1975), stacks of cylinders (Gentzler 1974), slices of ellipsoids (Graham 1973), and divided chambers (Graham 1973) with volume estimations using Simpson's rule (Gentzler 1974, Graham 1973), area-length determinations (Ferlinz 1975, Graham 1973, Arcilla 1971) and area sum and product calculations (Arcilla 1971). Despite the obvious dissimilarity of the shape of the models from that of the right ventricle, good correlations with chamber volume have been obtained with each model. One of the explanations for this finding may be the constancy in shape of the right ventricle through the cardiac cycle, indeed amongst normal ventricles a relationship exists between any standard dimension and the corresponding right ventricular volume (Bommer 1979). However this technique is of limited usefulness - not only is it very tedious to perform, but sequential studies cannot be carried out and there is a potential for alteration in chamber size following contrast injection.

In recent years, non-invasive methods such as two dimensional echocardiography have been proposed as alternatives with less risk and discomfort for the patients. Two dimensional echocardiography can be used to measure right ventricular chamber volumes and has been shown to correlate well with in-vitro measurements of right-heart casts (Bommer 1979) and radionuclide angiocardiography (Starling 1982). Sub-xiphoid echocardiography can also be used to measure right ventricular wall thickness, but such measurements are usually made from only a limited number of points on the right ventricular "free" wall. Recently measurements of right ventricular wall thickness have been made from multiple points on

the "free" wall using magnetic resonance imaging and have been shown to correlate with the echocardiographic findings (Suzuki 1988). Nevertheless, measurements of right ventricular wall thickness have important limitations in monitoring sequential changes. Small variations in wall thickness are difficult to detect and may be due to alterations in the position or obliquity of the scan, and changes which result in ventricular dilatation will alter the right ventricular wall thickness. Autopsy studies have also shown that right ventricular wall thickness correlates poorly with the right ventricular weight and should not be considered a good indicator of right ventricular hypertrophy (Fulton 1952). Moreover this technique has major limitations with respect to patients with chronic obstructive pulmonary disease, as in at least 40 per cent of these patients over-inflation of the lung fields precludes a satisfactory examination (Matsukubo 1977, Weitzenblum 1983).

Magnetic resonance imaging fulfils many requirements of previous imaging techniques and has a number of additional important attributes which makes it suitable for imaging the cardiovascular system. Firstly, the natural contrast between blood and cardiac tissue allows accurate assessment of both the ventricular wall, and the chamber size (Longmore 1985). Secondly, since magnetic resonance imaging is essentially a three dimensional imaging process, its accuracy is not dependent upon geometric models and assumptions which influence the accuracy of single or bi-plane angiography, particularly in the presence of regional myocardial dysfunction. And lastly, with the development of cardiac gating,

images of the heart can be acquired at multiple levels at a set time interval during the cardiac cycle, or alternatively multiple images can be acquired at a single pre-selected level at multiple time intervals following the QRS complex.

Previous studies have already shown that magnetic resonance imaging is capable of providing accurate information on the left ventricular wall and chamber dimensions (Longmore 1985), but little information exists on right ventricular dimensions. These considerations led to the development of a method of measuring right ventricular wall and chamber volumes and to study patients prone to develop right heart disease, namely patients with chronic obstructive pulmonary disease. As pulmonary hypertension is known to result in right ventricular hypertrophy, the pulmonary haemodynamic data available on these patients was compared with the findings from magnetic resonance imaging. Patients with ischaemic heart disease, age-matched controls and a small group of normal young volunteers were studied for comparison.

The method described here has good reproducibility in normal subjects. In order to determine the day-to-day reproducibility and the effect of unavoidable changes, both in the position of the patient on the examination couch and on the exact level at which angled transverse images were obtained through the ventricles, four individuals were examined on three separate occasions. The mean variability of 3 per cent was satisfactory. Undoubtedly, the day-to-day variability in patients with chronic airways disease would exceed this value, primarily due to the poorer image quality

obtained in such patients.

The intra-observer variability of this method was satisfactory, but the poorer inter-observer variability reflected the degree of subjectivity involved in outlining the right ventricular wall. This was particularly noticeable in patients with chronic obstructive pulmonary disease in whom exaggerated respiratory excursion created movement artefact and a pronounced Valsalva effect. This in turn resulted in cyclical variations in the R-R interval which inevitably would have produced variations in ventricular chamber filling.

Prior to examining patients, long axis images in the coronal plane, short axis images in the paraxial plane, short axis images perpendicular to the vertical long axis, and transaxial images were obtained in normal volunteers. Descriptions of the images obtained are detailed in Chapter 3A, but in all subjects short axis images perpendicular to the vertical long axis provided the best depiction of right ventricular outline.

In this study the entire right ventricle could be imaged in all patients, whereas Suzuki et al in 1988 reported clear visualisation of only 68 per cent of the length of the right ventricular "free" wall in normal subjects using magnetic resonance imaging. Several factors may explain this discrepancy. Short axis images perpendicular to the vertical long axis of the heart were employed in this study in contrast to the short axis images in the paraxial plane used in the study by Suzuki. In contrast to Suzuki's cohort

of normal volunteers, the patients with chronic obstructive airways disease had hyper-inflated lungs with a resulting increase in the retrosternal air space, aiding the distinction between the right ventricular "free" wall and the retrosternal soft tissues.

The right ventricular end-systolic volume, calculated by magnetic resonance imaging, slightly underestimated the true chamber volume. This is because the technique described excluded the right ventricular outflow tract, since accurate delineation of the pulmonary valve within the outflow tract was not possible in the majority of patients with chronic obstructive pulmonary disease. The contribution which the right ventricular outflow tract made to the total right ventricular chamber would have varied in patients with and without pulmonary hypertension and almost certainly accounted for the poor correlation between the radionuclide and magnetic resonance measurements of right ventricular end-systolic chamber volume.

At present no generally agreed gold standard exists for right ventricular chamber volumes in either normal subjects or in those with chronic obstructive pulmonary disease. Data obtained from normal volunteers using bi-plane angiography have produced right ventricular end-systolic chamber volumes of 39 $\pm$ 9ml (Arcilla 1971) and 26 $\pm$ 6ml (Gentzler 1974), whereas the end-systolic chamber volumes determined by magnetic resonance imaging have ranged from 43 to 72ml (Longmore 1985) in normal volunteers.

Although the right ventricular end-systolic chamber volumes

measured in all four patient groups lay within this rather wide spectrum of values, patients with chronic obstructive pulmonary disease had significantly greater chamber volumes than the age-matched control or normal young volunteer groups. Patients with ischaemic heart disease also had marginal elevation of the right ventricular chamber size compared to the control groups although the difference was not statistically significant.

MacNee and co-workers (1984) used radionuclide ventriculographic data to determine right ventricular chamber volumes in normal healthy subjects. These were then corrected for body surface area. From the mean right ventricular ejection fraction, together with normal values for cardiac output and intracardiac pressure, they calculated the mean right ventricular end-diastolic volume index to be 79mls.$m^{-2}$ and the normal right ventricular end-systolic volume index to be 33mls.$m^{-2}$. They subsequently studied a group of 8 patients with stable chronic obstructive pulmonary disease (MacNee 1988) and they showed that despite the presence of pulmonary arterial hypertension the right ventricular end-systolic and end-diastolic volume indexes remained relatively normal with values of 39 $\pm$ 21 and 69 $\pm$ 26 mls.$m^{-2}$. However in the patients with decompensated cor pulmonale, these indexes rose considerably to 183 $\pm$ 162 ml.$m^{-2}$ and 218 $\pm$ 166 mls.$m^{-2}$. This increase in volume indexes resulted in preservation of a normal right ventricular stroke volume despite a very low ejection fraction. When the mean right ventricular end-systolic value in this study (42.3 $\pm$ 18.1$cm^3$) was corrected for body surface area a value of 39.2 $\pm$ 15.3$cm^3$ was obtained. This compared very favourably with the data from

radionuclide ventriculography despite exclusion of the right ventricular outflow tract in chamber measurements. In addition it would confirm the findings of MacNee (1988) who showed that in patients with chronic obstructive pulmonary disease, who had no evidence of decompensated cor pulmonale, the right ventricular function, as assessed by radionuclide ventriculography, was well preserved. Similarly Khaja and Parker (1971) showed that these patients had a normal right ventricular response to exercise.

In this study magnetic resonance measurements of left ventricular end-systolic chamber volume in patients with chronic obstructive pulmonary disease and in normal subjects were similar to those obtained by Longmore (1985) in normal volunteers. He quoted a left ventricular end-diastolic volume of 132.0 $\pm$ 14.7mls, and stroke volume of 81.6 $\pm$ 16.2mls, resulting in an end-systolic volume of 50.4mls, which was very similar to the values obtained in this study of 44.8 $\pm$ 23.4mls in patients with airflow limitation and 44.1 $\pm$ 17.7mls and 30.6 $\pm$ 1.4mls for age-matched and normal young volunteer control groups. It was not surprising that the left ventricular chamber volume in patients with ischaemic heart disease were substantially greater than the other three groups. Most of these patients had either electrocardiographic or enzymatic evidence of acute myocardial infarction in the 5 to 7 day period preceeding the magnetic resonance examination, and many had significant left ventricular dysfunction as assessed by equilibrium radionuclide ventriculography.

In all techniques in which both right and left chamber volumes can

be measured simultaneously, there is an internal standard by which the accuracy of measurements can be judged. In the absence of valvular regurgitation or intra-cardiac shunting the left and right ventricular stroke volumes must be identical. In this study the mean difference between left and right ventricular stroke volumes was $-1.8 \pm 7.2cm^3$, indicating satisfactory measurement of chamber volumes.

Early studies on human volunteers using ungated cardiac images displayed a decrease in the relaxation parameter, T1, of blood within the left ventricular cavity when subjects breathed 100% oxygen (Bydder 1982). Subsequent studies demonstrated a progressive decrease in T1 values when breathing 21, 40, 60 and 100 per cent oxygen. A similar decrease in T1 with increased oxygen tension was demonstrated in further studies in dogs. Dissolved oxygen within the plasma has been proposed as an explanation for this finding, as free oxygen is paramagnetic and would be expected to shorten the T1 of blood when its concentration is increased (Steiner 1983).

In this study all of the age-matched controls and normal young volunteers demonstrated a decrease in the T1 value of blood within the left ventricle, compared to the right ventricle. This effect might have been expected to be more pronounced in patients with airflow limitation, but in 13 out of the 35 patients with either ischaemic heart or chronic obstructive pulmonary disease the T1 value of blood in the right ventricle was decreased. It is known that blood flowing at slower velocities results in a more intense

signal than fast flowing blood (Kaufman 1983, George 1984), which raises the possibility that either regional akinesis or dyskinesis within the left ventricular wall may account for these findings. There was no significant difference in T1 values between the right and left ventricular walls in individual patients although there was considerable variation in the T1 value of myocardium with heart rate. This was discussed in greater detail in Chapter 3D.

The right ventricle is normally thin-walled, compliant and capable of distention. The response of the right ventricle to progressive increases in afterload has been sparsely studied and most of the data for the difference in the response of the ventricle to changes in pressure or volume has come from animal work. The traditional view is that as cor pulmonale progresses, high filling pressures develop in the right ventricle in order to maintain the cardiac output. This is particularly pronounced during exercise in the early stages, but eventually elevated right ventricular diastolic pressures are present at rest (Fishman 1976) leading to the development of right ventricular hypertrophy. However even in the presence of elevated end-diastolic pressures, the right ventricular chamber volume may be normal, until right ventricular failure develops. Thus from an imaging point-of-view unless the right ventricular wall volume can be determined, the diagnosis of cor pulmonale is in doubt.

The rate at which such changes occur with moderate levels of pulmonary arterial hypertension in patients with chronic obstructive pulmonary disease is unknown. Animal studies suggest

that the ability of the right ventricle to compensate as the pulmonary arteries constrict is determined by a number of variables including its ability to increase the force of contraction, the adequacy of the coronary circulation, the presence of neurohumoral substances which increase the force of contraction and by alterations in the circulating blood volume which can augment the right ventricular end-diastolic pressure.

In order to satisfy the definition of cor pulmonale laid down by the World Health Organisation, magnetic resonance imaging was carried out to measure right ventricular "free" wall volumes. Initially measurements were obtained at end-systole and end-diastole to determine which image provided the best information and also to assess the reproducibility of the technique. Although the right ventricular "free" wall volumes, measured at end-systole and end-diastole were similar, the relative thinning of the ventricular wall during diastole required more precision in outlining the endo- and epicardial borders. The systolic images were therefore used routinely for analysis.

In this report all patients whose systolic pulmonary artery pressures measured over 40mm Hg had right ventricular "free" wall volumes above the range seen in normal subjects, whereas some of those with lower pulmonary artery pressures (<40mm Hg) had values within the normal range. Although measurements of right ventricular "free" wall volume correlated well with systolic pulmonary artery pressure, the relationship was not sufficiently strong to allow an accurate non-invasive measurement of pulmonary

artery pressure. The lack of a strong relationship was not entirely unexpected as pulmonary arterial pressure is not a true measure of the right ventricular afterload, and in individual patients pulmonary hypertension may have been present for variable periods of time.

The association of left ventricular hypertrophy with chronic obstructive pulmonary disease is controversial. Although most workers now accept that left ventricular hypertrophy does occur in many patients, at least one study by Foraker and colleagues (1970) showed a decrease in left ventricular weight in patients with severe emphysema. In many patients left ventricular hypertrophy is thought to occur secondary to such obvious causes as hypertension, arteriosclerotic cardiovascular disease or calcific aortic stenosis (Murphy 1974).

At the start of this study, the mean left ventricular wall volume was similar to normal subjects. However following a mean interval of nine months on long-term oxygen therapy, the left ventricular wall volume increased by a mean of 81.4cm$^3$. It remains unclear whether left ventricular hypertrophy in these patients, who had no other obvious pathology, was due merely to associated right ventricular hypertrophy or to metabolic and haemodynamic alterations secondary to chronic pulmonary disease. In a review of this topic, Fishman (1976) suggested that left ventricular hypertrophy in these patients may be due to a combination of factors, among them metabolic myocardial dysfunction secondary to hypoxaemia and acidosis, reduced right ventricular compliance,

increased intra-thoracic pressure and work hypertrophy secondary to chronic polycythaemia.

Previous studies have suggested a correlation between the right and left ventricular ejection fractions (MacNee 1983) and in this study there was simultaneously development of right and left ventricular hypertrophy during long-term oxygen therapy. This would suggest interdependence between ventricles possibly as a result of decreased right ventricular compliance, but this remains to be confirmed.

The correlation between pulmonary arterial pressure and arterial oxygen saturation pressures was first reported by Harvey (1951) and has been confirmed by many others. More recently data from a large European multicentre study of almost 1,000 patients suffering from common chronic lung diseases, of whom 595 had chronic bronchitis and emphysema, showed a highly significant correlation between pulmonary arterial pressure and pulmonary arterial oxygen tension (Bishop 1981). Although it is known that acute hypoxia produces pulmonary vasoconstriction both in normal subjects and in those with chronic lung disease, this relationship is not proof that chronic hypoxia is the only cause of pulmonary hypertension. In this study there was no correlation between the right ventricular "free" wall volume and the pulmonary arterial oxygen tension. This is perhaps explained by the relatively small number of patients studied and by the narrow range of arterial oxygen tensions within this group of patients.

Previous data has also suggested a positive correlation between pulmonary arterial carbon dioxide tension and the mean pulmonary arterial pressure (Aber 1963, Harvey 1951, Horsefield 1968), although in this study only a weak correlation was obtained. However in studies where increasing concentrations of inspired carbon dioxide were given to patients with chronic bronchitis and emphysema, it has been suggested that elevation of the pulmonary arterial pressure secondary to vasoconstriction may have been due to increase in carbon monoxide levels rather than the level of carbon dioxide (Fishman 1952, Kilburn 1969). Moreover in only one of these studies did the pulmonary vascular resistance increase significantly in response to breathing hypercapnic gas mixtures (Kilburn 1969). There is now some evidence to suggest that increased alveolar carbon dioxide levels potentiate rather than initiate hypoxic vasoconstriction (Durand 1970).

It is known from animal experiments that hypoxic hypertensive pulmonary disease is reversible. In one experiment rats were maintained at a pressure of 380mm Hg for 33 days, followed by 37 days of recovery at atmospheric pressure (Abraham 1971). Rats were sacrificed at intervals during the recovery period. In the hypoxic phase of the experiment, there was a progressive increase in right ventricular weight and muscularisation of the pulmonary arterioles. During the recovery phase there was a progressive reduction in right ventricular mean pressure with concommitant regression of the right ventricular hypertrophy and pulmonary vascular changes. Similar results were obtained by other workers, including Heath (1973).

Two controlled trials have now shown that long-term oxygen therapy can prolong survival in patients with chronic hypoxic respiratory failure although the method of action remains controversial (MRC Working Party 1981; NOTT Group 1980). In neither of the initial trials was any reduction in the mean pulmonary arterial pressure demonstrated. More recently Ashutosh et al (1983) showed a fall in the mean pulmonary artery pressure in response to 48 hours of continuous oxygen although there was no change in right ventricular function as measured by the ejection fraction. Others (Morrison 1986) have shown an improvement in the right ventricular ejection fraction after 3 weeks of continuous oxygen therapy but no reduction in the pulmonary vascular resistance.

Recently the Nocturnal Oxygen Therapy Trial has shown a significant haemodynamic response to continuous oxygen therapy administered over a 3 to 6 month period, and improved survival (Timms, 1985). This study, which was carried out at six centres in America, examined 203 patients with stabilized hypoxaemic chronic obstructive pulmonary disease who were receiving either continuous or nocturnal (12 hours/day) oxygen therapy. Neither oxygen therapy programme resulted in correction or near-correction of the baseline haemodynamic abnormalities. Nocturnal oxygen therapy was associated with significant decreases in the mean pulmonary artery pressures (-4 $\pm$ 11mmHg) and the pulmonary vascular resistance (-47.9 $\pm$ 117.8 dyne s $cm^{-5}$) during exercise, although the absolute differences were small. More significant results were obtained for continuous oxygen therapy, where the improvement in pulmonary vascular resistance was associated with improved cardiac function,

as evidenced by an increase in baseline and exercise stroke volume indexes. For both groups there were improved survival rates, after adjustment for the baseline mean pulmonary artery pressure.

Several workers have now shown a small but significant haemodynamic response to acute oxygen administration, in patients without decompensated cor pulmonale (MacNee 1988), although the cardiac and stroke indexes were unaltered. This would suggest that the improved right ventricular ejection fraction, demonstrated by some workers (Olvey 1980) after acute oxygen therapy, is due to acute reduction in the right ventricular afterload. The lack of improvement in stroke index either at rest or during exercise would imply that the improved right ventricular ejection fraction is not due to reversal of right ventricular myocardial ischaemia. Indeed most patients with chronic obstructive pulmonary disease, who are clinically stable, have normal right ventricular contractility (MacNee 1984).

In this small group of patients only 2 of the 7 patients on nocturnal oxygen therapy demonstrated a significant reduction in right ventricular "free" wall volume. Interestingly, Timms et al (1985) were able to define two roughly equal groups of oxygen responders and non-responders. Patients with at least a 25 per cent improvement in resting or exercise pulmonary vascular resistance after 6 months of therapy were considered to be oxygen responders, whereas a 5 per cent or less improvement was considered to be a non-responder. The only difference between these groups was a marginally greater baseline awake arterial oxygen-haemoglobin

saturation level in the responder group.

It is known that haemodynamic abnormalities in younger, less hypoxic patients with chronic obstructive pulmonary disease are slowly progressive (Weitzenblum 1979, Schrijen 1978) and it is likely that in older patients with greater airflow limitation and hypoxia, there is a faster progression of haemodynamic abnormalities without treatment. The obvious progression of disease in 5 of the 7 patients examined here, would indicate either inadequate oxygen therapy or poor compliance with treatment, or alternatively, that at least some of the patients were non-responders as defined by Timms and colleagues (1985). The relentless progression of left ventricular hypertrophy, which is thought to be due to an interdependence between ventricles, would also attest to the lack of response to therapy.

Since the installation of the M & D system there have been considerable advances in magnetic resonance technology. The recent advent of dynamic or "cine" magnetic resonance imaging software makes the acquisition of combined functional and structural studies of the heart practical. It is now possible to obtain a three-dimensional evaluation of cardiac structure and biventricular function in practical study times. The original pulse sequence employed was an electrocardiogram gated spin-echo sequence, using either a cycled multi-slice or rotating gated spin-echo technique (Crooks 1984) which resulted in a prolonged acquisition time of 40 to 50 minutes. This has subsequently been modified by Pettigrew (1988) who used a dual rather than single spin-echo, for each $90^{o}$

pulse excitation, which reduced the acquisition time by a factor of two. With this approach, typically six or seven consecutive slices through the cardiac chambers are obtained, with each slice being imaged at 12 to 14 phases of the cardiac cycle.

Although the spin-echo pulse sequence was not available at the commencement of this study, it is now widely accepted that these images provide better anatomical detail than T1 map images. The first echo (typically 30ms) of a spin-echo pulse sequence provides good contrast between epicardial fat and myocardium and the flow void seen with rapidly flowing blood, improves the delineation of the endocardial border outline. In addition the use of higher field strengths, typically 0.5 to 1.5 Tesla, and a 128-acquisition matrix would considerably improve image resolution. This would allow more accurate assessment of both the right ventricular wall volume and the response to various therapeutic options, and hopefully, would provide a better correlation between ventricular size and haemodynamic measurements.

## 6 MEASUREMENT OF MYOCARDIAL INFARCT SIZE

The early and late morbidity and mortality rates after acute myocardial infarction are considerably influenced by the amount of myocardial damage. The importance of infarct size is attested to by the numerous positive correlations between the amount of myocardium destroyed, and the incidence of cardiogenic shock and cardiac failure (Braunwald 1967, Harnarayon 1970 and Page 1971), the frequency of ventricular arrhythmias (Roberts 1975 and Cox 1976), the severity of haemodynamic abnormalities (Bleifield 1977), and the prognosis both in-hospital (Sobel 1972) and after discharge (Geltman 1979 & Thompson 1979).

Since the 1960's when coronary care units were introduced, there has been improved recognition and treatment of the electrical complications of myocardial ischaemia and necrosis. However, although there has been considerable reduction in in-hospital mortality from arrhythmias there has been little reduction in deaths from re-infarction, heart failure and cardiogenic shock (Alonso 1973) which tend to occur in patients with large areas of infarction, who frequently have poor left ventricular function (Sobel 1972).

### 6A METHODS OF REDUCING MYOCARDIAL INFARCT SIZE

Given the adverse consequence of large infarcts, a number of interventions have been evaluated for their ability to limit infarct size and thereby improve prognosis. In the 1960's and

1970's, attention centred on the use of B-adrenergic blocking agents, which reduce total myocardial (Mueller 1974) and ischaemic myocardial oxygen consumption (Haneda 1973) by negative chronotropic and inotropic effects (Epstein 1966).

Both propranolol, and practolol which is a cardioselective B-adrenergic blocker, have been shown to decrease acute myocardial ischaemia after experimental coronary artery occlusion in dogs. Reimer and associates (1973) have documented anatomic salvage of ischaemic myocardium by propranolol when treatment was combined with coronary reperfusion, and Hillis et al (1976) found less epicardial R-wave loss and Q-wave development in propranolol treated dogs than in controls after permanent coronary artery occlusion. Pathologically documented reduction in infarct size has also been reported by other investigators (Pierce 1973, Rasmussen 1977, Miura 1979) although not all have confirmed this effect (Peter 1978).

Early clinical studies of B-blockade focussed on alterations in clinical course and mortality as end points. Although Snow (1965) reported reduced mortality in patients treated for 3 weeks after acute myocardial infarction with propranolol, these results were not duplicated by other randomized, double-blind trials (Norris 1968, Balcon 1966). More recent studies on B-blockade in the post-infarction period have shown a decreased incidence of sudden death with alprenolol (Wilhelmsson 1974), a decreased mortality in patients with anterior myocardial infarction treated with practolol (Green 1977), and decreased mortality in randomized

survivors of acute infarction treated with timolol (Norwegian MSG, 1981). However these studies, although relevant to the long-term management of ischaemic heart disease, do not provide data on acute limitation of infarct size, as treatment was begun days to weeks after onset of infarction.

Objective evidence of the beneficial effects of B-blockers on acute myocardial ischaemia in humans has been reported by many investigators using various modifications of the praecordial ST segment technique. Patients with anterior transmural infarction treated with intravenous propranolol (Waagstein 1975), showed a significant reduction in praecordial ST segment elevation and a marked sudden reduction in chest pain within minutes of drug administration. Waagstein and Hjalmarson (1975) showed similar results in a double-blind controlled study using practolol and metoprolol. Intravenous pindolol, a B-blocker with some intrinsic sympathomimetic activity, reduced ST segment elevation and was shown to improve regional wall motion (Heikkila 1978). In addition, both propranolol (Peter 1978) and atenolol (Yusuf 1980) when given intravenously a median of 4 hours after onset of symptoms, have been reported to decrease serum creatine kinase-MB release.

Nitroglycerin and other nitrate preparations have been used in the aggressive management of unstable angina pectoris, congestive heart failure and coronary spasm. Animal studies have shown that intravenous nitroglycerin can ameliorate myocardial ischaemia (Smith 1973, Bussmann 1979) and reduce the extent of myocardial

necrosis after coronary artery occlusion (Epstein 1975, Hirshfeld 1974, Jugdutt 1981). Chiche and associates in 1979, reported preliminary results of a randomised trial of prolonged nitroglycerin infusion in patients with acute myocardial infarction. Praecordial ST segment mapping in those with acute infarction showed a 30 per cent decrease in ST segment elevation, 30 minutes after start of therapy, and praecordial maps at 7 days showed less R-wave fall at initially ischaemic sites. Later, Bussman (1979) showed significantly lower values of peak serum creatine kinase-MB release in nitroglycerin treated patients, especially when treatment was started within 8 hours of symptoms. Other workers have shown an improvement in myocardial perfusion measured with 201 Thallium scintigraphy following intravenous nitroglycerin (Flaherty 1980). However, Bussmann (1979) also showed that although ST segment elevation diminished with infusion rates of 50mg/min, this effect was partially reversed at 100mg/min. Other workers (Bowen 1979) have found no decrease in infarct size as measured by serum creatine kinase-MB release. Thus doubt exists about the ability of nitroglycerin to limit infarct size.

The most effective way to limit myocardial necrosis may be the early restoration of coronary artery blood flow. Recent observations at coronary angiography, performed within a few hours after transmural myocardial infarction in man, have revealed a high incidence of coronary arteries occluded by thrombus (DeWood 1980, Phillips 1979). This is in accordance with postmortem findings of occlusive thrombi in 88 to 97 per cent of patients dying of acute transmural myocardial infarction (Chandler 1974, Davies 1976,

Ridolfi 1977) and with the retrieval of thrombus in most patients undergoing bypass surgery because of acute myocardial infarction (Phillips 1979). If the coronary blood supply is permanently interrupted, irreversible cell necrosis will inevitably follow, with most of the damage occurring within the first few hours. The role of thrombolysis therefore, is not only to unblock the occluded artery and re-establish blood flow, but also to salvage myocardial tissue before it becomes necrotic, thereby preserving regional and global myocardial function.

In 1949, Tillett and Sherry demonstrated that streptokinase could effectively dissolve extra-vascular clots in humans. This was followed in 1959 by the first controlled study, in which ischaemic ST segment elevation in patients with acute myocardial infarction was reduced by the intravenous administration of hyaluronidase (Martins De Oliveira 1959). Subsequent studies on experimental animals showed that hyaluronidase reduced infarct size as reflected by histological analysis, myocardial creatine kinase-MB measurements and epicardial QRS mapping (Hillis 1976, Maroko 1972, Kloner 1978). Over the next twenty years streptokinase became the most extensively studied thrombolytic agent, although thrombolysis was not adopted routinely in the management of acute myocardial infarction.

Interest in thrombolysis has been rekindled in recent years and many clinical studies have now shown early re-opening of thrombolytically occluded arteries (Ganz 1981, Mathey 1980). Ganz and colleagues showed reperfusion in 19 out of 20 patients

following intracoronary thrombolysis using a combination of streptokinase and plasmin, whereas Schroder (1983) demonstrated an 84 per cent patency rate by angiography in the fourth week following short-term intravenous infusion of streptokinase in 93 patients treated within 6 hours after onset of symptoms. Many other reports have confirmed these findings (Neuhaus 1983, Spann 1984, Ganz 1983, Schaper 1983, Ellis 1983).

As time may be lost between the onset of chest pain and the adminstration of lytic agents via an intracoronary catheter, the intravenous administration of drugs is now preferred. New thrombolytic agents are now available and the results from very large controlled clinical trials have established beyond doubt that there is a significant reduction in mortality rate.

Many thrombolytic agents have now been closely evaluated for the treatment of acute myocardial infarction. These include streptokinase, anisoylated plasminogen-streptokinase activator complex (APSAC), urokinase, tissue plasminogen activator (t-PA) and pro-urokinase.

The results of mortality rates for the key thrombolytic agents either given alone or in combination with other treatments, all show significant reduction. In the APSAC intervention mortality study (AIMS, 1988) there was a 46 per cent reduction in mortality in the APSAC group at 30 days with an estimated one year reduction in mortality of 44 per cent for treatment within 6 hours. In the International Study of Infarct Survival (ISIS-2, 1988) there were

23, 25 and 42 per cent reductions in the aspirin, streptokinase and combined aspirin/streptokinase groups respectively at 5 weeks for treatment within 24 hours from the onset of chest pain. Similarly in the Anglo-Scandinavian Study of Early Thrombolysis with Tissue Plasminogen Activator (ASSET) there was a 26 per cent reduction in mortality rate in the t-PA group at one month, following treatment administered within 5 hours. As it is very difficult to extrapolate between studies, a "head-on-trial" which would compare all available thrombolytic treatments, would be required to determine which agents are superior.

Reperfusion after coronary artery occlusion can be achieved with revascularization surgery. In dogs, reperfusion of ischaemic myocardium within 20 minutes of onset of ischaemia prevented anatomic and electrocardiographic evidence of necrosis and preserved myocardial function (Banka 1974). Reperfusion up to 3 hours after coronary occlusion in dogs resulted in reduction in myocardial necrosis assessed both 1 and 7 days later (Maroko 1972, Ginks 1972). However, by 6 hours after coronary ligation, little salvageable myocardium remains (Reimer 1977). Although a prospective, controlled randomised trial is needed to determine whether acute revascularisation should be used routinely, early reports suggest a beneficial effect. DeWood et al (1980), reported a 5.8 per cent in-hospital mortality rate, in patients operated on soon after symptoms, compared to a 9.3 per cent rate in a medical control group.

Most studies of thrombolytic agents have used patency rates of the

infarct related vessel and mortality as study end points, but in the multi-centre APSIM study the left ventricular function, and pyrophosphate uptake were assessed following APSAC or intravenous heparin in a double blind fashion in 231 patients. All patients in this study presented within 5 hours of onset of symptoms and all underwent left ventricular angiography and coronary arteriography within one week of treatment, and radionuclide ventriculography and pyrophosphate scanning with single photon emission computed tomography within 3 weeks. All patients receiving APSAC had a 77 per cent patency rate of the infarct related artery compared with a 37 per cent patency rate in those receiving heparin. Left ventricular ejection fraction determined by radionuclide ventriculography was significantly higher in the APSAC group compared with the heparin group for both anterior and inferior wall infarcts. Infarct size estimated from emission tomography was significantly lower in the APSAC group with an overall reduction of 30 per cent compared to the heparin group. However, although there was a 36 per cent reduction in the anterior wall infarction group, there was no significant difference between groups for inferior wall infarction.

Post-mortem studies carried out within 30 days of acute myocardial infarction have shown that 72 per cent of hearts have infarct stretching, thinning or dilatation (Hutchins 1978). This is common in the first week particularly after anterior or anteroseptal infarction (Hutchins 1978) and is associated with increased early mortality (Hochman 1982, Eaton 1981). In approximately one third of hearts with transmural infarcts there is marked expansion of the

infarcted zone resulting in obvious cardiac dilatation (Hutchins 1978). One of the neurohumoral consequences of acute myocardial infarction (McAlpine 1986) is the release of catecholamines which stimulate the heart and increase systemic and coronary vascular resistance. As a result, myocardial oxygen requirements are increased, but oxygen supply decreases, which may lead to extension of the infarct. In addition, increases in the afterload may "stress" large transmural infarcts leading to progressive cardiac dilatation and aneurysm formation.

Activation of the renin angiotensin system leading to elevation of the plasma renin and angiotensin II levels has also been observed following coronary artery ligation in animals, and evidence is accumulating for a similar release following acute myocardial infarction in man whether complicated by heart failure, or uncomplicated. Experimental studies of converting enzyme inhibitors such as captopril, enalapril and lisinopril, which block renin angiotensin system activation, have provided early evidence of a reduction in infarct size either directly or measured by the release of cardiac enzymes (Liang 1982, Ertl 1982, Pfeffer 1985), and reduction in both the preload and afterload. Moreover, a substantial improvement in left ventricular function has been reported during the later recovery phase of acute myocardial infarction (Sharpe 1988).

Prognosis after acute myocardial infarction depends on the extent of myocardial damage and on the residual left ventricular function. Although the left ventricular function at the end of the acute

phase following myocardial infarction has been shown to be the best predictor of the one year mortality rate (Dewhurst 1983), there are discrepancies between survival rates following reperfusion and the residual left ventricular function (White 1987). It has been suggested that the beneficial effects of thrombolysis may be more complex than a simple reduction in infarct size. At the present time ventricular function is used as an indirect indicator of the mass of ventricle surviving but particularly in patients with previous infarction this relationship is distorted. More direct measurements of infarct size are required to clarify the effects of interventional therapy.

## 6B TECHNIQUES USED TO QUANTIFY MYOCARDIAL INFARCT SIZE

Many techniques have been investigated in an attempt to quantify infarct size. Of the standard techniques used including electrocardiographic mapping, cardiac enzyme release and echocardiography, only radionuclide imaging using infarct avid agents attempts to provide direct quantitation of the mass of damaged myocardium. X-ray computed tomography and magnetic resonance imaging are more recent techniques which are still to be fully evaluated.

### 6B.1 Electrocardiography

ST segment mapping provides information on the severity of injury from acute myocardial ischaemia, whereas QRS mapping provides semi-quantitative data on the extent of myocardial necrosis. Epicardial ST segment mapping was the first technique used to show pharmacological protection of ischaemic myocardium (Maroko 1971 and 1972) but the technique has a number of disadvantages. Because there is considerable variation among different patients in the attenuation of epicardial potentials as they are recorded from the praecordium, the method is used to measure changes occurring in individual patients after an intervention rather than as an absolute quantitative index of ischaemic injury. Also, as there is a normal reduction in ST segment elevation with time, comparison of results with an untreated control group is desirable. Furthermore this technique is only applicable to patients with transmural anterior or lateral acute infarction, and patients must be free of

intraventricular conduction defects, pericarditis and serum electrolyte disturbances and must survive for almost 7 days for post-treatment QRS map to be obtained.

### 6B.2 Enzymatic Estimation

Since Karmen and collegues in 1955 described elevation of serum transaminase in acute myocardial infarction, attempts have been made to correlate the release of various enzymes, particularly creatine kinase-MB with the clinical severity of infarction and patient prognosis.

In experimental studies in healthy dogs the release of serum creatine kinase-MB correlated almost perfectly with depletion of creatine kinase-MB in the infarcted myocardium. (Shell 1971, Shell 1973). Shell et al using the conscious dog model, showed that quantitative estimates of infarct size could be obtained not only by measurements of tissue creatine kinase-MB but also by analysis of serial creatine kinase-MB in systemic venous blood. A mathematical model was developed on the basis of the rate of release of myocardial creatine kinase-MB, its volume of distribution and clearance rate. Using this method, studies of acute myocardial infarction in man have demonstrated reasonable agreement between infarct size estimated by serum creatine kinase-MB and the left ventricular haemodynamics, prognosis and post mortem macroscopic infarct size measurements (Sobel 1972, Thompson 1979).

However the mathematical model used remains an empirical and simplified method of characterising a complex biological phenomenon that may be affected by many variables in individual experimental animals and in man.

### 6B.3 Echocardiography

Since the advent of two-dimensional echocardiography, acute alterations in cardiac topography can be detected by serial examinations. It is now possible to analyse regional myocardial function and to differentiate akinetic and dyskinetic segments. The dimensions of the left ventricle can be analysed and wall thickness determined (Ross 1976).

However there are certain problems. Firstly, for technical reasons it is not always possible to acquire adequate views of the ventricles in all patients. Secondly, the area of infarction is only defined by virtue of the change in myocardial contractility, and areas of reversible ischaemia can mimic infarction. And lastly, the reproducibility of serial measurements is critically dependent on the ability to image the same area of the heart in each study. This method, which is referenced to external body landmarks, is a potential source of error and assumes that no substantial changes in the position of the heart within the chest have occurred.

## 6B.4 Radionuclide Imaging

In infarct avid scintigraphy, radiopharmaceuticals are sequestered by acutely infarcted myocardium, producing regions of increased myocardial uptake. Based on the phenomenon that irreversibly injured myocardial tissue accumulates calcium ions, Bonte et al (1974), proposed the use of 99m-technetium stannous pyrophosphate for imaging myocardial infarction. At the present time this is the radiotracer of choice for imaging acute myocardial infarction in man (Parkey 1974, Holman 1976). The tissue uptake of 99m-technetium pyrophosphate is localised selectively to sites with elevated calcium levels, although a constant linear relationship does not exist between the total tissue calcium concentration and the level of pyrophosphate uptake. This appears to result mainly from local differences in blood flow as well as from the composition and physiological properties of tissue calcium stores.

Using planar imaging, 99m-technetium pyrophosphate imaging is only accurate in the diagnosis of anterior and transmural lesions that weigh more than 3g (Poliner 1977), but since the introduction of single photon emission computed tomography, posterior, inferior, right ventricular and small sub-endocardial infarcts can be accurately identified irrespective of their location (Lewis 1984). However pyrophosphate imaging with single photon emission computed tomography has certain limitations. The study should ideally be carried out within 24 to 72 hours after onset of symptoms and usually becomes negative by 7 days after infarction (Parkey 1974). Furthermore tomographic acquisitions are normally limited to 180$^{o}$

in order to maintain the imaging time at approximately 40 minutes, but this prohibits correction for attenuation. Although the absence of attenuation correction may result in an underestimation of activity near the base of the ventricle compared to the apex (Jaszczak 1979 and 1981) previous work has suggested the practical consequences of this limitation on volume or mass determinations are probably small (Lewis 1984).

Other problems associated with single photon emission computed tomographic measurements of infarct size include artefacts and residual blood pool radioactivity. Relatively high radioactivity in the ribs can create significant back projection artefacts which interfere with the performance of a back projection algorithm. This may be improved by selective filtering. Residual radioactivity in the cardiac blood pool may be masked by subtracting corresponding sections of an ungated blood pool tomogram (Corbett 1982, Pizer 1978). This also permits more accurate definition of the endocardial border. The measurement of pyrophosphate infarct size also depends on the timing of imaging relative to the infarction, the presence of reperfusion, the quality control of the radiopharmaceutical used, the resolution of the imaging system and most importantly the criteria used to define the boundary of pyrophosphate uptake. In all examinations the calibration of volume measurement is mandatory.

Recently it has been shown that single photon emission computed tomography with blood pool overlay significantly increases the sensitivity of pyrophosphate detection especially for non-

transmural infarcts (Corbett 1984). Although from a theoretical standpoint one would expect small infarcts to be overestimated by single photon emission computed tomography, using a "hotspot" marker in animal studies, small infarcts have been both over and underestimated. This probably reflects the more patchy necrosis in small infarcts, the less well defined margins and a much greater relative error in defining the boundaries of small lesions from tomographic images.

### 6B.5 X-ray Computed Tomography

X-ray computed tomography has also been used to determine myocardial infarct size. Gray et al (1978), showed a good correlation between histological infarct size and the infarct size determined by computed tomography after animals had been given iodinated water soluble contrast intravenously immediately prior to sacrifice, to increase tissue contrast. The potential of this technique will only be fully assessed in man when cardiac gating techniques are available to reduce motion-induced artefact.

### 6B.6 Magnetic Resonance Imaging

The most recent technique to be used to detect acute myocardial infarction is magnetic resonance imaging.

In 1980, Williams and colleagues demonstrated an increase in the T1 relaxation time of acutely infarcted canine myocardium using proton spectroscopy. This increase in relaxation time correlated well

with the increased water content of the tissue due to haemorrhage and oedema. Subsequent studies by Herfkens (1983) in Sprague-Dawley rats with experimentally induced infarction of the lower extremities, showed an increase in both the T1 and T2 values immediately following infarction, although the contrast difference substantially increased by 24 hours. This work was carried out using a 6.5cm aperture imager with a field strength of 0.3 Tesla. Confirmation of this finding was reported by Higgins et al (1983) who showed an increase in both the T1 and T2 values in excised hearts, 24 hours following acute myocardial infarction in dogs. This ex-situ study was carried out using a 6.5ml bore resistive imager operating at 0.35 Tesla. However these findings were not confirmed by all workers. Brady and colleagues (1982) attempted to image ex-situ infarcted canine hearts using a steady-state-free-precession technique but failed to discriminate infarcted from normal myocardium unless the contrast medium, manganese chloride was administered. A similar finding was reported by Buonanno et al (1983), again using a steady-state-free-precession technique, who were also unable to demonstrate myocardial infarction without the use of manganese chloride as a paramagnetic contrast agent to enhance the images.

Such discrepancy in findings has not been reported in in-vivo studies. In 1984, Wesby and colleagues demonstrated that cardiac gated magnetic resonance imaging of the canine heart in-vivo could distinguish normal from infarcted myocardium without the use of intravenous paramagnetic contrast agents. They showed a significant increase in the T2 relaxation time between 2 to 7 days

after ligation of the left anterior descending coronary artery. Regions of prolonged signal intensity corresponded to areas of myocardial infarction demonstrated at post mortem examination. In the same year Pflugfelder (1985) studied canine hearts before and serially for up to 6 hours after anterior descending or circumflex coronary artery ligation in-vivo, using a 0.15 Tesla resistive magnet and single spin-echo and modified inversion recovery pulse sequences. By 4 hours after coronary artery occlusion the signal in the infarct zone increased by 36 per cent compared to that in the adjacent normal myocardium for the TE 30ms sequence and by 116 per cent for the TE 60ms sequence. Both of these sequences are T2 weighted. However the inversion recovery image, which produces a heavily T1 weighted image, did not show areas of ischaemia. This was explained by the opposing effects of T1 and T2 on signal intensity in the inversion recovery images, which although heavily T1 weighted, had a substantial contribution from T2 signal. The lack of any significant change in signal in the infarct zone by this technique suggested an unchanged or only slightly altered T1 signal within the infarct or alternatively cancellation of the signal reduction produced by T1, by signal enhancement by an increased T2 value.

In the same year Johnston et al (1985) demonstrated significant increases in both the T1 and T2 relaxation times by spectroscopy in excised canine hearts as early as 3 hours after coronary artery occlusion. This rapid evolution of changes was confirmed in 1986 by Tscholakoff and colleagues using a superconductive system operating at 0.35 Tesla. They were able to detect an increase in

the T2 value of canine myocardium as early as 30 minutes after re-establishing blood flow to non-perfused tissue. The area of increased signal intensity conformed to the site of myocardial infarction found at autopsy.

By 1985 McNamara et al had evaluated the capability of magnetic resonance imaging to detect and characterise alterations in the T2 relaxation time in acutely infarcted myocardium in humans. Patients were examined between 5 to 12 days following the onset of symptoms. All the areas of acutely infarcted tissue demonstrated significant prolongation of the T2 relaxation time relative to normal myocardium which corresponded anatomically to the site of infarction defined by the electrocardiographic changes. McNamara used a double-echo spin-echo pulse sequence performed with echo delays of either 28 or 56ms between the application of the initial radiofrequency pulse and the receipt of the corresponding signal. Using this sequence a region of high signal intensity was visible on both the first and second-echo images, but in general was more intense relative to normal myocardium on the second echo image (mean increase 70 per cent compared with 27 per cent on the first echo image). In the same year Been et al (1985) using a low field resistive system operating at 0.08 Tesla and a saturation recovery-inversion recovery pulse sequence, showed a significant increase in the T1 value of acutely infarcted myocardium in man within the first week following acute myocardial infarction.

That magnetic resonance imaging is capable of detecting and characterising ischaemically damaged myocardium both in-vitro and

in-vivo is now well established in both animals and man. The findings of prolongation of T1 and T2 in acutely infarcted myocardium are probably related to local changes in tissue water content resulting from myocardial oedema and a number of investigators have shown a significant increase in the percentage of water present in infarcted myocardium compared with normal tissue (Higgins 1984, Wesby 1984).

Although transmural myocardial infarcts are readily characterised, there is a potential pitfall in the diagnosis of infarcted sub-endocardial regions of the myocardial wall by magnetic resonance imaging. Reports from Higgins et al (1984) and McNamara et al (1985) have shown that high signal intensity can also be caused by stasis of blood adjacent to akinetic or dyskinetic regions of myocardium on the second spin-echo images. However using region of interest analysis software it is possible to differentiate between flow signal and adjacent infarcted myocardium by recognition of the prolonged positive T2 value of flow signal. Although this signal suggests stasis as a consequence of regional myocardial abnormalities in patients with acute myocardial infarction, this finding is not specific.

## 6C AIMS

The aims of this chapter:

a) To develop a method to measure myocardial infarct size and to compare this with currently available techniques including $^{99m}Tc$ - pyrophosphate scanning with single photon emission computed tomography and with indirect methods of myocardial infarct sizing namely measurement of "peak" and total serum creatine kinase - MB release and with the residual left ventricular function measured by radionuclide equilibrium ventriculography.

b) As most other centres currently use a first or second-echo image from a spin-echo pulse sequence to visualise areas of myocardial infarction, as opposed to an interleaved saturation recovery - inversion recovery pulse sequence from which a T1 map is generated, comparison of these two pulse sequences was carried out to assess their respective advantages and disadvantages.

c) Since previous studies have shown an increase in the T1 value of areas of infarcted myocardium up to three months following the onset of symptoms, this study sought to determine the alteration in infarct size following a six week convalescent period, in a group of patients treated with thrombolysis and then randomly allocated to placebo or vasodilator therapy.

d) As magnetic resonance imaging provides information on both tissue characterisation and cardiac anatomy the effects of

peripheral vasodilator therapy, namely captopril and isosorbide dinitrate, on myocardial infarct size and left ventricular volume were examined in a group of subjects, who had experienced an uncomplicated first myocardial infarction and compared with a placebo group.

## 6D ESTIMATION OF MYOCARDIAL INFARCT SIZE FROM T1 IMAGES

### 6D.1 Patients

Nineteen patients (14 male; 5 female) whose ages ranged from 39 to 72 years (mean 55yrs) were examined. All patients had sustained their first myocardial infarction, and at the time of examination were clinically stable, with no evidence of low-output cardiogenic shock or acute pulmonary oedema. The patients were all in sinus rhythm, and none had previously required electrical conversion for ventricular arrhythmia. None of the patients had received either intracoronary or intravenous thrombolytic therapy. The diagnosis of acute myocardial infarction was made on the basis of presenting history and typical electrocardiographic changes, and was confirmed by serum creatine kinase-MB measurements. None of the patients gave a history suggestive of either previous myocardial ischaemia or infarction and none had co-existing chronic medical conditions.

Prior to entering the study all patients gave informed consent.

### 6D.2 Methods

a) Magnetic Resonance Imaging

Technique

Magnetic resonance imaging was carried out 5 to 7 days following

the onset of chest pain using a low field system (M&D Technology) operating at 0.08 Tesla. Patients with either temporary or permanent cardiac pacemakers, prosthetic heart valves or previous intra-cranial surgery had previously been excluded from the study. Watches and jewellery were removed prior to entering the scanner. Scout images were initially carried out in the coronal plane to visualise the long axis of the ventricles. These images were obtained using a field of view of 384mm, a matrix of 128 x 64 with no averaging, a short repetition time of 240ms, and a field echo time of 22ms. Four slices were obtained using a 16mm slice thickness and separation. From these images, short axis views through the vertical long axis of the ventricular chambers were positioned. A cardiac gating technique was employed using either non-ferromagnetic (pre-wetted silver chloride electrodes) or carbon fibre electrodes (Abingdon Instruments, Abingdon, Oxon), placed on the left anterolateral and the right para-sternal chest wall. The upslope of the electrocardiographic R-wave was used to synchronise data acquisition during end-systole at approximately 110ms following the upstroke of the R-wave. An interleaved saturation recovery-inversion recovery pulse sequence was employed using a TI = 42ms with a variable TR, depending on the R-R interval. Eight to ten slices of 12mm thickness were acquired, using four acquisitions, to obtain multiple images from below the cardiac apex to the level of the aortic arch. Two slices with a 42ms time separation were obtained with each acquisition which consisted of two averages of 64 phase encoding steps, and 128 frequency encoding steps, resulting in a pixel size of 3 x 6mm. This data was interpolated to a 128 x 128 matrix (3 x 3 mm) and smoothed on the

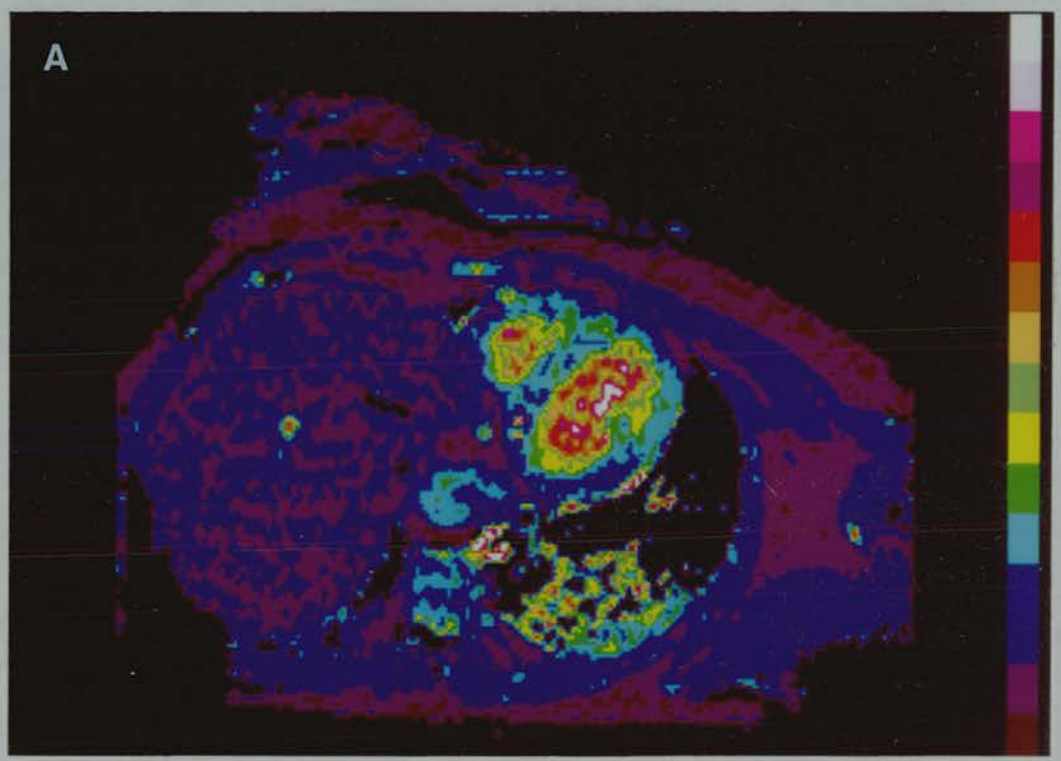


Figure 27(a). Angled transverse T1 map image at the level of the ventricles showing good contrast between myocardium, pericardial soft tissues and chamber contents.

The increased signal intensity (light blue/green areas) seen in the interventricular septum, anterior wall of the right ventricle and anterolaterally on the left ventricle represents extensive infarction.

final display monitor for image analysis.

Analysis

The calculated T1 map showed good contrast between normal and ischaemic myocardium, pericardial soft tissues and chamber contents and was therefore used to define the myocardial border (Figure 27a). The outlines of the endo- and epicardial interfaces of the left ventricle, including septum, were defined interactively by using image analysis software to draw an irregular region of interest (Figure 27b). The endocardial outline was frequently not visualised on the apical slice and, if not, these images were excluded from the measurement. The images were first "windowed" so that areas of the left ventricular wall, including the inter-ventricular septum, with the shortest T1 values were depicted. The mean T1 and standard deviation were then measured from regions of a fixed size ($2cm^3$ or greater), placed within "normal myocardium", on all slices which included the left ventricle. An upper limit of normal was then derived for each individual patient, by taking the mean T1 value, plus two standard deviations, for each slice and averaging this value over all the slices measured. Regions within the myocardium having a T1 value greater than this limit were then generated by the computer (Figure 27c) and their areas were measured. These values were multiplied by the slice thickness to obtain the volume of infarcted myocardium on each slice. The volumes obtained from all the slices were summed to obtain the total volume of infarcted myocardium.

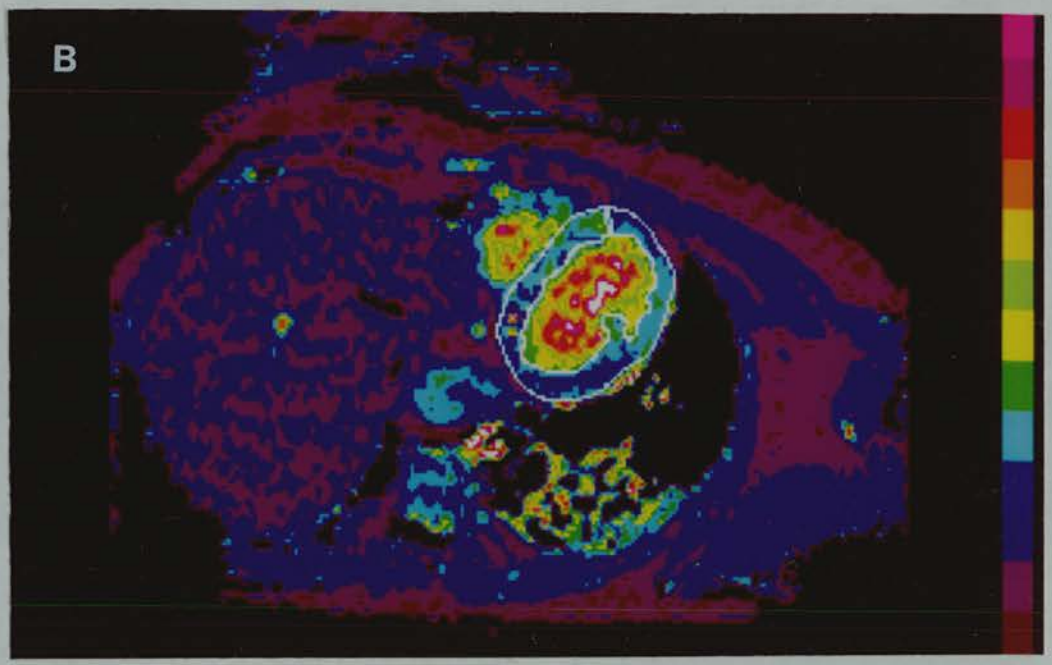


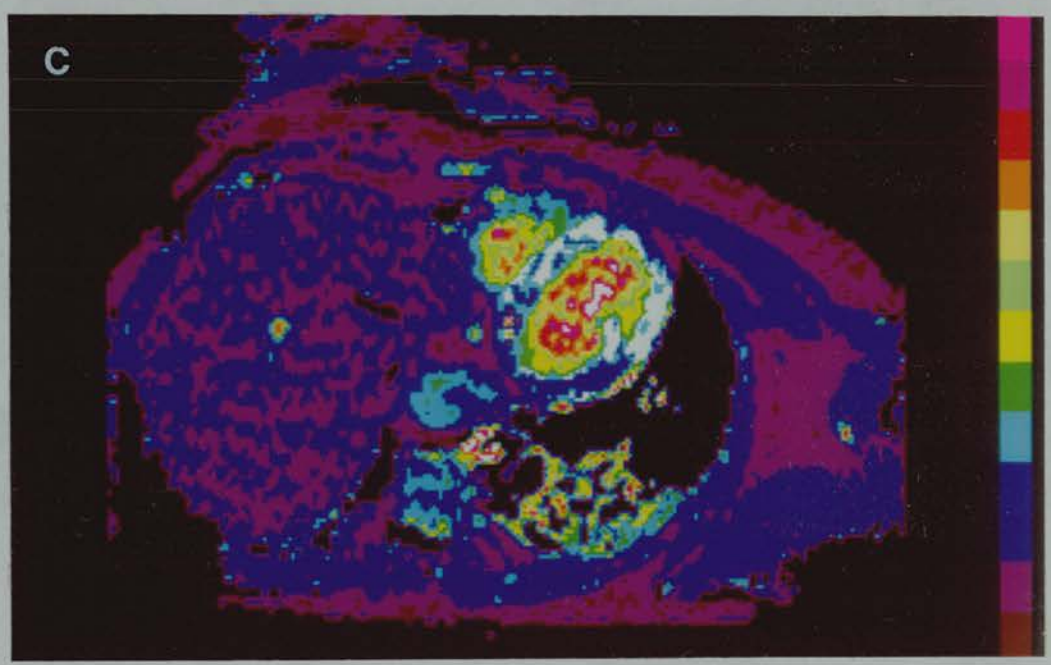


Figure 27. Extensive anterolateral myocardial infarction, shown as a large semi-circular area of increased signal intensity. (b) The left ventricular endo- and epicardial borders are outlined in white. (c) Areas within the left ventricular myocardium with a T1 value two standard deviations or more above the mean T1 value for normal myocardium are shown in white.

Reproducibility

In order to determine the intra- and inter-observer variability measurements were performed on the same four patient examinations on three separate occasions by two independent observers.

b) 99m Technetium Pyrophosphate Scanning

Radioisotope scanning with 99m-technetium pyrophosphate was performed using a MaxiCamera 400AT Gamma Camera, equipped with a low-energy, general purpose, parallel hole collimator (International General Electric) and a MicroDelta Plus computer system (Siemens Gammasonics). Patients were imaged between 24 and 36 hours after admission to hospital and two hours following adminstration of 600 MBq 99m-technetium pyrophosphate. Patients were positioned supine with both arms positioned beside the head. Single photon emission tomography was performed with a set of sixty four, 64 x 64 images taken over a $360^{o}$ arc, with the radius of rotation selected to minimise the distance from detector to the chest wall. Each image was collected for a preset time of 10 seconds and in addition to the "auto-tune" facility, the camera was further corrected for uniformity (using a 30 million count 99m-Tc flood) and for the centre of rotation. Transverse images, one pixel thick were reconstructed "on line" using a Butterworth filter of order 5, with a cut-off frequency of 0.5 Nyquist. Myocardial uptake of pyrophosphate was determined from the transverse images by a simple three-dimensional thresholding procedure operating at 65 per cent of the peak voxel value within the infarct volume. The

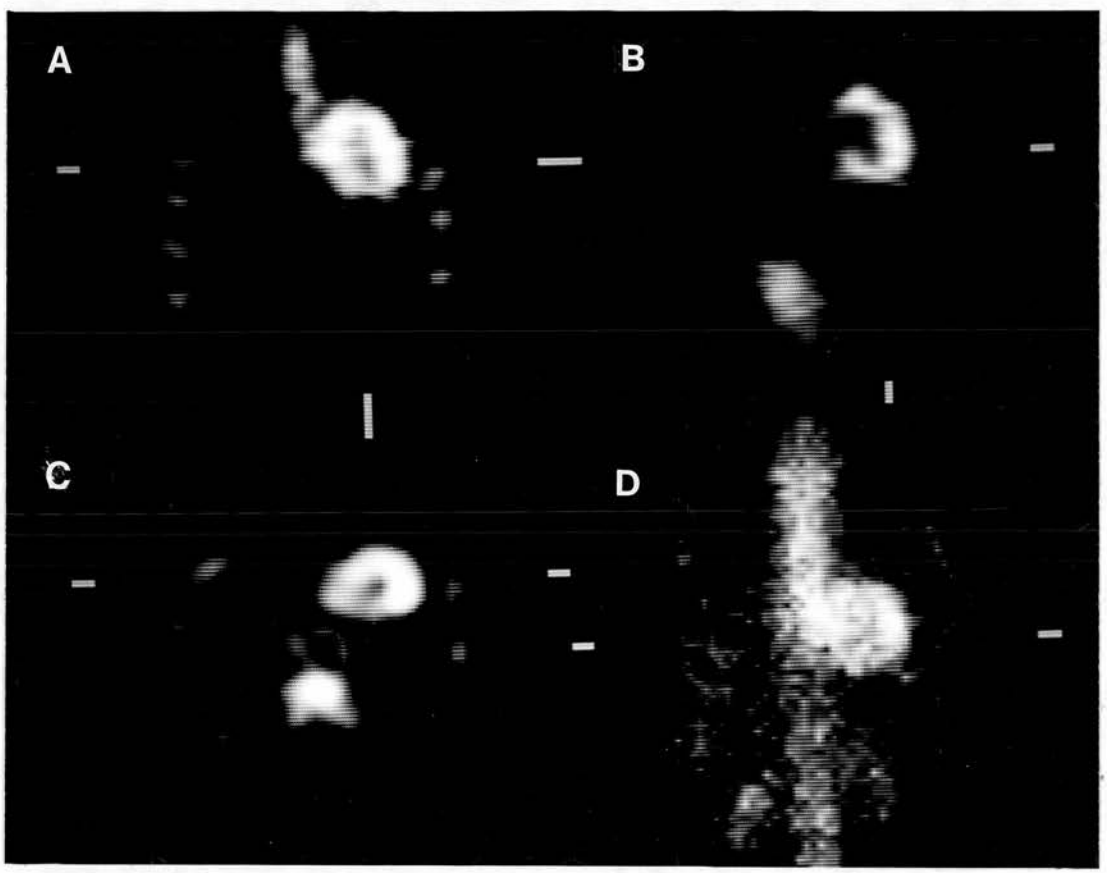


Figure 28. Single photon emission tomographic images of 99m-Tc pyrophosphate uptake in the myocardium of the same patient seen in Figure 27a to c, with an extensive anterolateral myocardial infarction. The four images are: a) coronal section, b) sagittal section, c) transverse section and d) scout image roughly equating to a planar anterior view.

threshold value of 65 per cent has been shown by other workers (Jansen 1985), from phantom studies to be the optimal value. The peak value in the volume of interest was found after each transverse slice had been smoothed twice by a nine point filter. Myocardial uptake was analysed by drawing a cuboid region of interest around the heart and counting the number of voxels above 65 per cent of the peak value within that volume (Figure 28). The digital resolution of reconstructed slices was 64 x 64, and the voxel size 0.24cm$^3$. The "infarct voxels" were then summed and the size of infarction determined by multiplying the number of infarct voxels by 0.24cm$^3$/voxel.

Prior to calculating infarct volume, each transverse image was reviewed and the region of interest modified if necessary to exclude areas of non-cardiac uptake, such as the sternum or ribs.

d) Serum Creatine Kinase-MB

Serum creatine kinase-MB was measured using an optimised kinetic spectrophotometer assay. In 11 of the 19 patients, 4 to 8 blood samples were obtained during the period from 8 to 48 hours following the onset of chest pain. This allowed calculation of the total creatine kinase-MB release. In the remaining 8 patients only 3 blood samples were obtained and the highest value was used to express a "peak" creatine kinase-MB release. Both the total and peak creatine kinase-MB release were used in the correlations.

e) Radionuclide Ventriculography

Equilibrium radionuclide ventriculography was carried out on the day prior to discharge from hospital (mean = 7 days), when the patients were clinically and radiologically clear of cardiac failure. All the patients were studied in the supine position and cardiac imaging was performed in approximately a $30^{o}$ anterior oblique projection with a $10^{o}$ caudal tilt. The precise angle was chosen to optimise separation of the ventricles. After injection of 700 MBq of 99m-technetium human serum albumen, imaging was carried out using a Siemens low energy mobile gamma camera and the data was collected by a MicroDelta Plus computer system. The left ventricular ejection fraction was calculated using a gated blood pool technique (Muir 1980).

f) Statistical Methods

In order to determine the agreement between myocardial infarct size measured by magnetic resonance imaging and pyrophosphate scanning, a plot of the difference between the values obtained using the two methods, against their mean value (Bland 1986) was carried out. The lack of agreement was summarised by calculating the bias, estimated by the mean difference (d) and the standard deviation of the differences (s). The precision of estimated limits of agreement (ie d +/- 2s) was examined using standard errors and confidence intervals. The standard error of d, was calculated from $\sqrt{(s2/n)}$, were n is the sample size, and the standard error of d - 2s and d + 2s from $\sqrt{3s2/n}$. Ninety-five per cent confidence intervals were calculated by finding the appropriate point of the t-distribution with n-1 degrees of freedom, and then the confidence

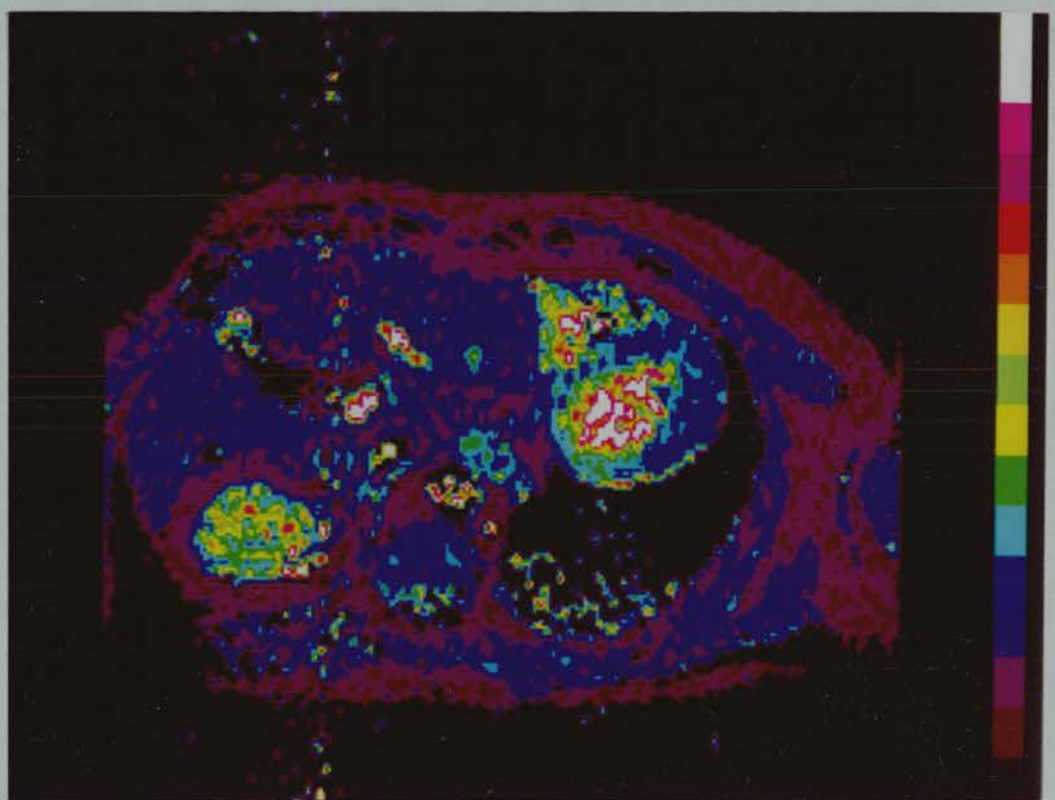

Figure 29. Angled transverse T1 map image showing an area of increased signal posteroinferiorly (represented by blue/green area), secondary to myocardial infarction.

interval determined from the observed value minus t standard errors to the observed value plus t standard errors.

Correlation analysis using Pearson's correlation coefficient (r) was also used to assess whether the values of two variables were associated.

### 6D.3 **Results**

a) Electrocardiography

On admission to hospital, electrocardiograms demonstrated 10 anterior or anterolateral, 5 inferior, and 2 posterior infarcts and in one patient no abnormality was demonstrated. An example of a posteroinferior infarct is shown in Figure 29. In a further patient the electrocardiogram was indeterminate due to the presence of a left bundle branch block (Table 34). The location of the infarct was clearly demonstrated and was identical using both pyrophosphate scanning and magnetic resonance imaging in 17 of the 19 patients. No abnormality was demonstrated by either imaging technique in one patient, whilst in a second, pyrophosphate imaging showed only a very small area of increased uptake anteriorly, but magnetic resonance imaging failed to demonstrate any abnormality. In the first of these 2 patients the electrocardiogram was normal and in the second indeterminate due to the presence of left bundle branch block. Both patients demonstrated only a minor rise in the peak serum creatine kinase- MB values of 172 and 522 units per litre respectively.

TABLE 34

Location of Myocardial Infarct, T1 Values of Normal and Infarcted Myocardium and Heart Rate for 19 Patients with First Untreated Infarct

| Name | Location of Infarct | T1 Values of Left Ventricle (ms) | | Heart Rate |
|---|---|---|---|---|
| | | Normal | Infarcted | |
| EC | Anterolateral | 298.2 ± 43.8 | 418.3 ± 27.4 | 55 |
| JB | Posterior | 272.6 ± 31.6 | 361.2 ± 25.3 | 90 |
| SC | Lateral | 306.1 ± 38.7 | 399.8 ± 18.4 | 63 |
| WS | Anterolateral | 259.8 ± 19.6 | 329.2 ± 27.5 | 85 |
| GH | Anterolateral | 330.3 ± 35.0 | 431.7 ± 17.2 | 60 |
| TN | L B B B * | 318.4 ± 22.6 | - | 50 |
| JD | Lateral | 320.3 ± 44.6 | 440.0 ± 24.9 | 60 |
| DO | Anterolateral | 278.3 ± 23.4 | 347.2 ± 23.2 | 100 |
| BI | Anterolateral | 296.9 ± 25.6 | 372.2 ± 22.7 | 74 |
| MW | Anterolateral | 342.3 ± 36.4 | 448.3 ± 25.3 | 55 |
| JH | Anterior | 259.0 ± 14.6 | 315.7 ± 29.6 | 75 |
| ElC | Inferior | 304.8 ± 33.7 | 408.9 ± 32.7 | 75 |
| HW | No infarct | 321.1 ± 37.3 | - | 65 |
| JG | Inferior | 297.5 ± 27.7 | 366.7 ± 20.0 | 62 |
| FF | Posterior | 343.9 ± 30.9 | 437.2 ± 26.4 | 48 |
| MMcM | Inferior | 321.4 ± 49.3 | 445.2 ± 20.3 | 72 |
| KG | Anterolateral | 317.8 ± 29.1 | 405.1 ± 27.2 | 58 |
| MS | Inferior | 273.3 ± 23.7 | 336.7 ± 19.1 | 86 |
| MC | Inferior | 311.3 ± 24.1 | 390.3 ± 30.0 | 70 |
| Mean | | 303.4 ± 31.1 | 391.4 ± 24.5 | |

* (L B B B : Left bundle branch block)

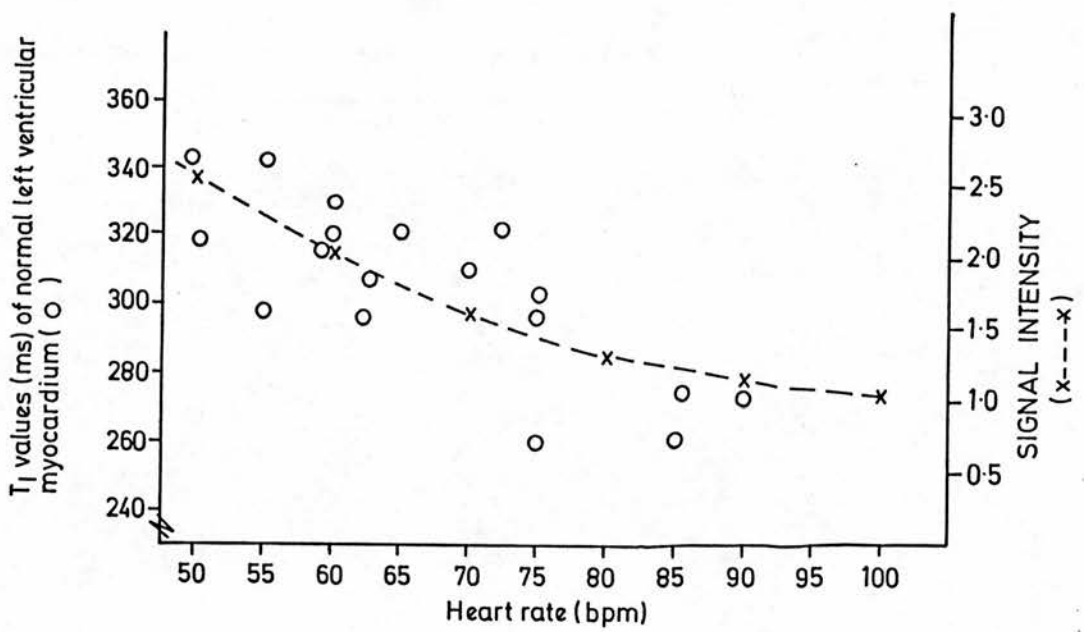


Figure 30: Comparison of T1 values (ms) of normal left ventricular myocardium against heart rate (bpm). Theoretical signal intensity is superimposed on graph (x-----x).

b) T1 Values

The individual T1 values for normal and infarcted myocardium for the 19 patients are detailed in Table 34. There was a wide variation in the T1 values of normal left ventricular myocardium within the group of patients. The T1 values ranged from 259.0 $\pm$ 14.6ms to a maximum of 343.9 $\pm$ 30.9ms, with a mean value of 303.4 $\pm$ 31.1ms. There was also a wide variation in the heart rates recorded at the time of magnetic resonance imaging and these ranged from 48 to 100 bpm.

Figure 30 shows the variation in the T1 value of normal left ventricular myocardium against the patient's heart rate. Although there was a wide spectrum of values , there was a trend towards higher T1 values at lower heart rates, and lower T1 values at higher heart rates, particularly between 85 to 100 bpm. Superimposed on this graph are the theoretical values for signal amplitude, SIR, for a variable repetition time (TR), obtained from to the equation:

$$S = kp \frac{[\exp(-TI/T1) - \exp(-TR/T1)]}{1-\exp(-TR/T1)}$$

where k is a machine specific constant, p is the proton density, TI is the time to inversion (42 ms) and TR is the repetition time which varied from 600 to 1200ms. The signal amplitude is calculated for the calibrated T1 phantom of 300ms, which is approximately the mean T1 value of normal left ventricular

TABLE 35

Myocardial Infarct Size, Measured by Magnetic Resonance Imaging (MRI), Pyrophosphate Scanning (PYP) and Creatine Kinase - MB Release in 19 Patients after First Uncomplicated Infarction

| Patients | Myocardial Infarct Size ($cm^3$) | | Creatine Kinase Units/l | |
|---|---|---|---|---|
| | MRI | PYP | Peak | Total |
| EC | 71.9 | 97.2 | 3715 | 109292 |
| JB | 70.7 | 64.3 | 1719 | 39140 |
| SC | 15.0 | 12.7 | 400 | ND |
| WS | 69.6 | 76.6 | 2950 | ND |
| GM | 33.7 | 26.6 | 1419 | 24612 |
| TN | 0 | 7.9 | 522 | 18224 |
| JD | 33.1 | 25.0 | 1317 | ND |
| DO | 49.0 | 46.1 | 6955 | 104976 |
| BI | 69.8 | 77.5 | 4225 | 80416 |
| MW | 32.3 | 45.1 | 6255 | 101716 |
| JH | 30.0 | 27.4 | 1995 | 42340 |
| ElC | 46.8 | 36.7 | 1364 | 29592 |
| HW | 0 | 0 | 172 | ND |
| JG | 26.4 | 26.6 | 1516 | ND |
| FF | 65.1 | 57.8 | 2850 | ND |
| MMcM | 8.6 | 12.2 | 258 | 8728 |
| KG | 16.8 | 21.4 | 1817 | ND |
| MS | 10.8 | 19.7 | 657 | 17721 |
| MC | 73.8 | 95.8 | 2091 | ND |

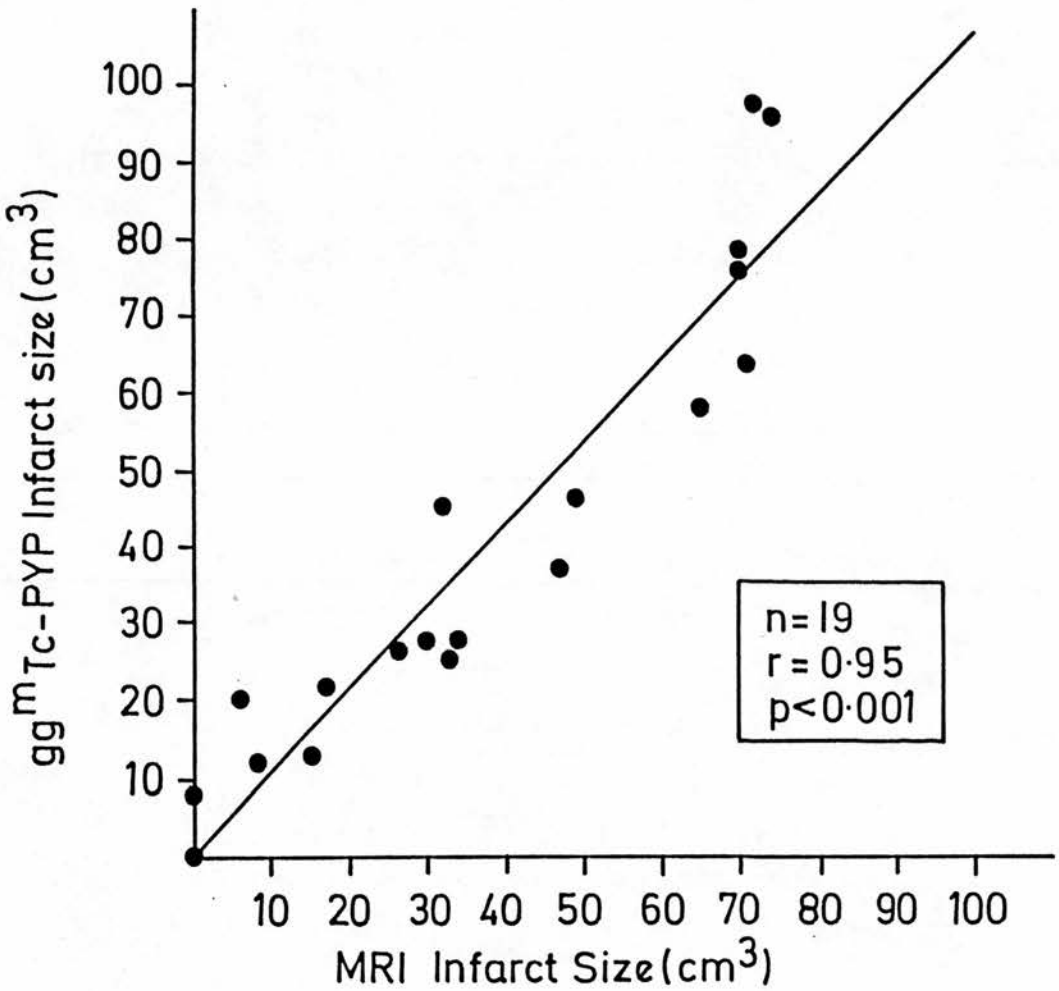


Figure 31. Comparison of myocardial infarct size measured by magnetic resonance imaging and pyrophosphate scanning using a coefficient of correlation.

myocardium.

As no infarct was demonstrated in 2 patients, the T1 value of infarcted myocardium was recorded in only 17 of the 19 patients. Again there was a wide spread of values from 315.7 $\pm$ 29.6ms to 448.3 $\pm$ 25.3ms, with a mean T1 value of 391.4 $\pm$ 24.5ms for infarcted left ventricular muscle (Table 34).

c) Myocardial Infarct Size

The individual patient values for myocardial infarct size measured by magnetic resonance imaging, pyrophosphate scanning and the "peak" and total creatine kinase-MB release are detailed in Table 35. The myocardial infarct size measured by magnetic resonance imaging ranged from 0 to 73.8cm$^3$ with a mean value of 38.1cm$^3$, while infarct size assessed by pyrophosphate scanning ranged from 0 to 97.2cm$^3$, with a mean value of 40.9cm$^3$.

The "peak" creatine kinase-MB release ranged from 172 to 6955 units/l, while the total creatine kinase-MB release, which was only measured in 11 of the 19 patients, ranged from 8728 to 109292 units.

d) Left Ventricular Ejection Fraction

The mean left ventricular ejection fraction was 40.0 per cent while values ranged from 15 to 71 per cent.

e) Correlations

Table 36 shows the correlations obtained between the variables examined. Using a coefficient of correlation there was an excellent agreement between the myocardial infarct size measured by magnetic resonance imaging and pyrophosphate scanning ($r = 0.95$, $p < 0.001$), Figure 31. The same data was also expressed as a plot of the difference between the two values against the mean infarct size obtained by averaging the two values (Figure 32). This revealed a mean difference between the magnetic resonance and pyrophosphate infarct size of $2.7cm^3$, while the standard deviation of the difference was $9.9cm^3$. From these values the "limits of agreement" lay between -22.5 and 17.1 $cm^3$, and the standard error of the mean was $2.27cm^3$. For 19 degrees of freedom the t value was 2.10. Hence the 95 per cent confidence interval for the bias was -7.4 to $-2.1cm^3$. The standard error of the limit was $3.93cm^3$. The 95% confidence interval for the lower limit of agreement was -30.8 to $-14.3cm^3$, whilst for the upper limit of agreement the 95 per cent confidence interval was 8.9 to $25.4cm^3$. These intervals show moderately good agreement between the two methods, which are reasonably consistent over the range of values encountered, although discrepancies exist particularly with larger infarct sizes ie greater than $80cm^3$ .

The residual left ventricular function measured in 18 of the 19 patients by radionuclide equilibrium ventriculography correlated negatively with the volume of infarct measured by both magnetic resonance imaging ($r = -0.71$; $p<0.001$) and with pyrophosphate

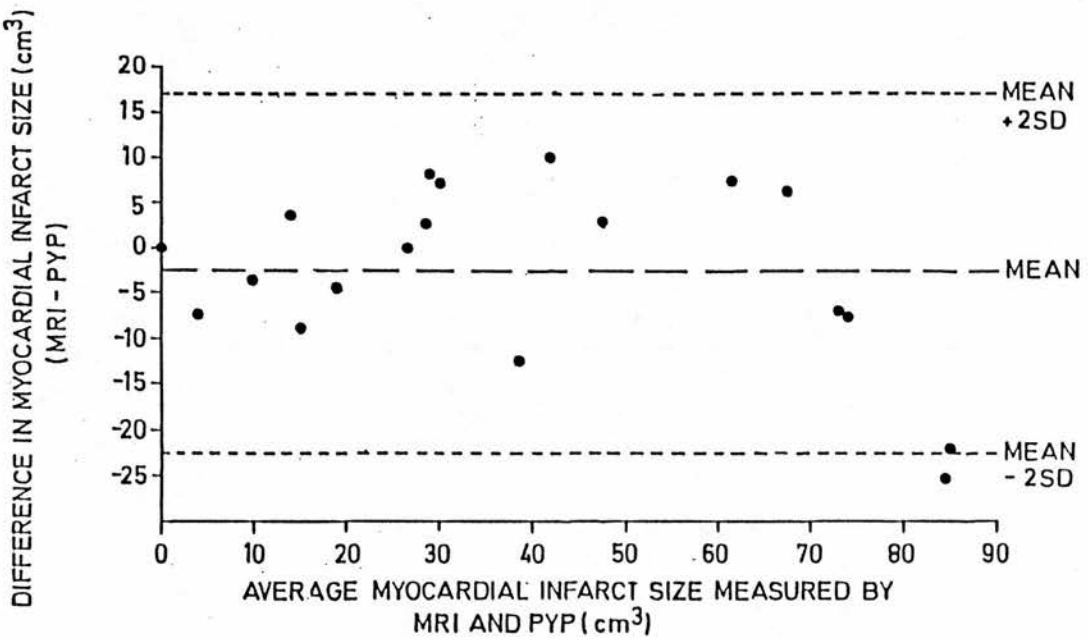


Figure 32. Comparison of myocardial infarct size measured by magnetic resonance imaging and pyrophosphate scanning using a plot of the difference between the two values against the mean of the two values.

scanning ($r = -0.79$; $p<0.001$).

Although the total creatine kinase-MB release curves could only be calculated in 11 patients, there was a good correlation between the "peak" and total creatine kinase-MB values obtained ($r = 0.93$; $p < 0.001$). The size of the infarct measured by "peak" creatine kinase correlated only moderately with either the volume of infarct measured by magnetic resonance imaging ($r = 0.58$; $p = 0.012$), or with the volume obtained by pyrophosphate scanning ($r = 0.53$; $p = 0.0023$). Both of these correlations were weakened by the presence of two particularly high creatine kinase-MB results, which were considerably greater than the remainder of the values at 6955 and 6255 units/l respectively. However the total creatine kinase-MB release which included these two values demonstrated a better correlation both with infarct size measured by pyrophosphate ($r = 0.75$; $p = 0.008$) and with magnetic resonance imaging ($r = 0.70$; $p = 0.02$).

As anticipated, there was also a moderate negative correlation between the left ventricular ejection fraction and the "peak" creatine kinase-MB level ($r = -0.63$; $p = 0.007$), but a stronger correlation was obtained with the total creatine kinase-MB release ($r = -0.78$; $p = 0.005$).

f) Reproducibility

The reproducibility of the technique was affected by several variables namely the mean and standard deviation of T1 values for

TABLE 36

Correlations obtained between measurements of infarct size, left ventricular ejection fraction (%) and creatine kinase-MB release (units/l)

| | MRI Infarct Size | 99m-Tc PYP Infarct Size | LV Ejection Fraction | Peak Creatine Kinase |
|---|---|---|---|---|
| 99m-Tc PYP Infarct Size | n = 19<br>r = 0.95<br>p < 0.001 | | | |
| LV Ejection Fraction | n = 18<br>r = -0.79<br>p < 0.001 | n = 18<br>r = -0.79<br>p < 0.001 | | |
| Peak Creatine Kinase | n = 18<br>r = 0.52<br>0.05>p>0.02 | n = 18<br>r = 0.53<br>0.02>p>0.001 | n = 17<br>r = -0.63<br>0.01>p>0.001 | |
| Total Creatine Kinase | n = 11<br>r = 0.62<br>0.05>p>0.02 | n = 11<br>r = 0.75<br>0.01>p>0.001 | n = 11<br>r = -0.78<br>0.01>p>0.001 | n = 11<br>r = 0.93<br>p < 0.0001 |

normal myocardium, and the identification of the endo- and epicardial borders of the left ventricle.

As the T1 values of normal myocardium varied considerably with the heart rate, it was necessary to measure the upper limit for normal myocardium for each patient individually. The inter-observer variability depended considerably on the measurement of the upper threshold for the T1 value of normal myocardium. Whilst the mean T1 values showed only a 2 per cent difference, the standard deviations varied by up to 13.5 per cent. This was explained by the size of the region of interest used by the different observers to measure normal myocardial T1 values. The size of the region-of-interest was therefore standardised at $2cm^3$ or greater.

When the same threshold value for normal myocardium was used by both observers, the volume of infarcted myocardial tissue varied by a mean of 10.1 per cent between observers, while the intra-observer variability was 6.8 and 10.4 per cent respectively. The measurements of infarct size obtained on several occasions for both observers as well as the inter-observer variability are shown in Table 37.

Table 37

Comparison Between Measurements of Myocardial Infarct Size ($cm^3$) for 4 Patients, obtained on 3 Occasions by 2 Observers, and the Inter-observer Variability

| Patient | Observers | | | | Inter-observer Variability % difference between mean myocardial infarct size |
|---|---|---|---|---|---|
| | JPR | | LWT | | |
| | Repeated | Mean Values | Repeated | Mean Values | |
| JH | 30.1<br>26.6<br>32.4 | 29.7 | 32.4<br>28.7<br>28.9 | 30.0 | 1.0 |
| BI | 72.3<br>79.0<br>72.5 | 74.6 | 74.6<br>71.3<br>63.5 | 69.8 | 6.9 |
| MW | 27.5<br>27.8<br>26.4 | 27.2 | 29.9<br>30.1<br>36.9 | 32.3 | 15.8 |
| DO | 41.5<br>37.6<br>43.4 | 40.8 | 54.0<br>47.6<br>45.4 | 49.0 | 16.5 |

## 6E COMPARISON OF T1 AND T2 IMAGES IN THE ESTIMATION OF MYOCARDIAL INFARCT SIZE

### 6E.1 Patients

Ten patients (8 male; 2 female) whose ages ranged from 41 to 77 years and who had sustained their first uncomplicated myocardial infarction were included in this study. All patients had presented to hospital within four hours from the onset of symptoms and had received standard thrombolytic therapy consisting of 1.5 Megaunits streptokinase in 5 per cent dextrose administered intravenously over 60 minutes, subcutaneous heparin (5,000 units tid) and had subsequently been commenced on oral soluble aspirin (300mg/day), and oral metoprolol (100mg/day). The diagnosis of myocardial infarction was made on the basis of presenting history and electrocardiographic changes and thrombolysis was instituted prior to the receipt of the cardiac enzyme results. All the patients were well at the time of examination and, in particular, none had a history of an arrythmia which would have precluded adequate cardiac gating.

### 6E.2 Methods

Magnetic resonance imaging was carried out 5-7 days following the onset of chest pain using a low field system operating at 0.08 Tesla. All patients were first asked to remove all jewellery and watches, and were questioned about the presence of cardiac pacemakers, prosthetic heart valves or previous intra-cranial

disease.

A full explanation of the technique was given to all patients, and informed consent obtained prior to the examination.

Two different pulse sequences were used to measure myocardial infarct size namely an interleaved saturation recovery-inversion sequence to obtain a T1 map image, and a double spin-echo sequence to obtain T2 weighted images. A cardiac gating technique was employed, as previously described (Chapter 3B), to synchronise data acquisition 110ms after the upslope of the electrocardiographic R-wave (ie during end-systole), in both pulse sequences.

(a) Saturation recovery - inversion recovery pulse sequence

An interleaved saturation recovery - inversion recovery pulse sequence was employed using a TI = 200ms, and TE = 22ms from which a T1 map was calculated. The TR varied with the patient's heart rate. A 12mm slice thickness and separation was employed. Further details of the technique used and the method of analysis of the T1 images have already been given in Chapter 6D.2.

(b) Double spin-echo pulse sequence

Imaging Technique

Scout images were first performed in the coronal plane to visualise the long axis of the ventricles. Four slices were obtained using a

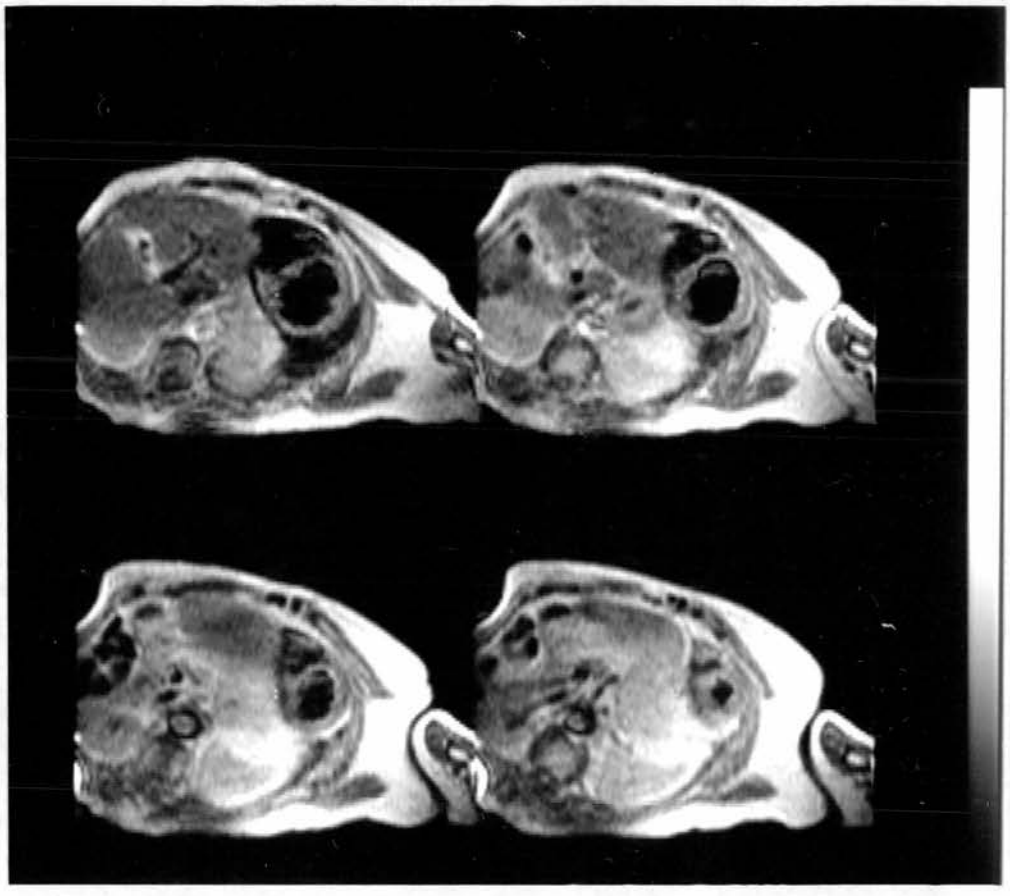

Figure 33. Typical example of a series of first-echo spin-echo images ( TE = 42ms; TR dependent on heart rate ) encompassing part of the left ventricle.

Figure 34. First-echo image demonstrating an area of increased signal intensity anteriorly due to acute infarction. An incidental finding of a pericardial effusion is noted posterolaterally.

16mm slice thickness and separation, to encompass the mediastinal structures. The images were obtained using a field of view of 384mm, a matrix size of 128 x 64, with no signal averaging, a short repetition time of 240ms, and a field echo time of 22ms. These images were used to prescribe short axis views of the ventricular chambers. Seven to eight slices of 12mm thickness and separation were normally acquired to obtain images from the cardiac apex to above the pulmonary outflow tract. A typical example of a series of first-echo images obtained is shown in Figure 33. Two slices with a 32ms time separation were obtained with each acquisition, which consisted of two averages of 64 phase encoding steps, and 128 frequency encoding steps resulting in a pixel size of 3 x 6mm. This data was interpolated to a 128 x 128 matrix (3 x3 mm) and smoothed on the final display monitor for image analysis. The double spin-echo sequence used echo delay times (TE) of 42 and 120ms for the first- and second- echo images respectively. The repetition time (TR) was determined by the patient's heart rate, but if this exceeded 95 bpm, data was only acquired every other heart beat.

Image Analysis

The first-echo image routinely provided good anatomical detail, with clear delineation of the endo-cardial border. Areas of acute myocardial infarction demonstrated increased signal intensity. Figure 34 shows a typical first-echo image in a patient with an acute anterior infarction. Only in a small number of patients was intracavitary signal present, particularly adjacent to areas of

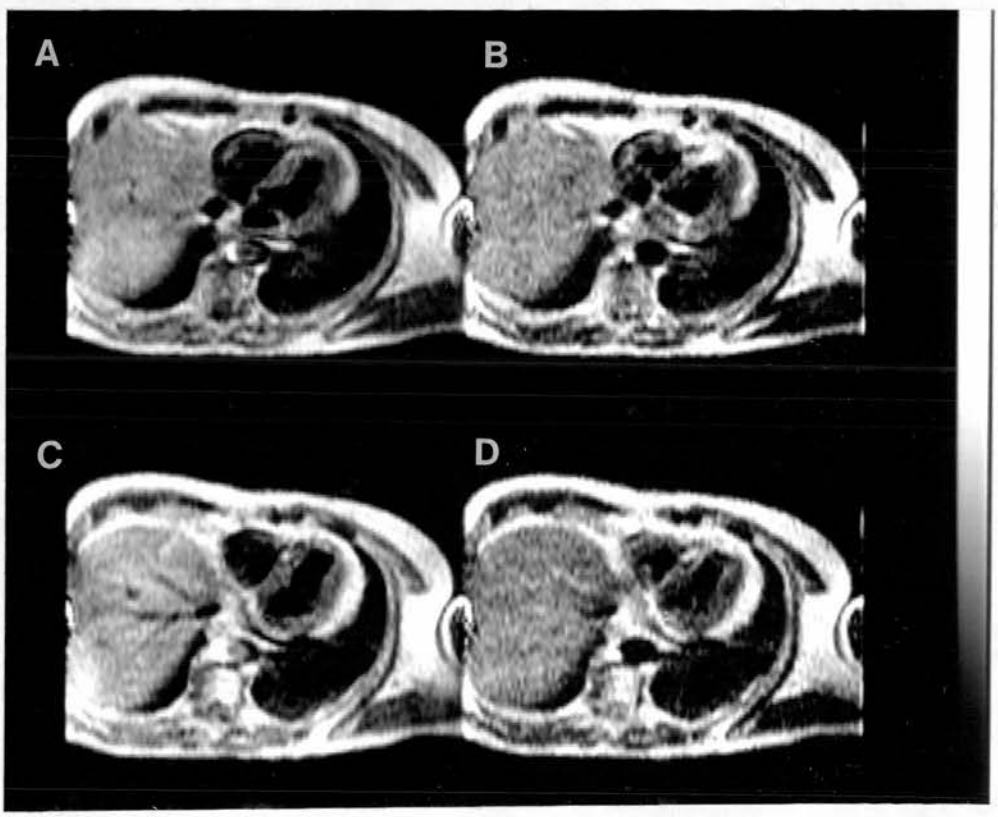


Figure 35. Two sections from a double spin-echo pulse sequence showing the first (a and c) and second-echo (b and d) images. The anterior myocardial infarct, represented by an area of increased signal intensity is more clearly demonstrated on the second echo images, although the resolution of these images is degraded by motion-induced loss of signal.

increased wall signal. These were assumed to represent altered blood flow at sites of regional left ventricular dysfunction. In most patients this did not interfere with delineation of the endocardial border, but in one patient the endocardial border could not be clearly identified and this patient was excluded.

Although the second echo image, showed better contrast definition between normal and infarcted myocardium, there was poorer definition of the myocardial border, due to motion-induced loss of signal (Figure 35) and altered intracavitary blood flow (Figure 36). Thus the first echo image was chosen to outline the left ventricular borders, using a computer-generated region of interest, controlled by an electronic "mouse".

From phantom studies (Chapter 3D) it is known that the T2 value of normal myocardium varied with heart rate. It was therefore necessary to calculate the mean T2 value and standard deviation of normal myocardium for each individual patient, by obtaining measurements from at least four irregular regions of interest, ($2cm^3$ or greater) obtained from different slices. The upper threshold for "normal" myocardium was then set by adding the mean plus two standard deviations. An irregular region of interest was then drawn around the left ventricle on all slices, and regions with a T2 value greater than this threshold were then generated by computer and their areas measured. The values obtained were then multiplied by the slice thickness to obtain the volume of infarcted myocardium for each slice. These values were then summed to obtain the total volume ($cm^3$) of infarcted myocardium.

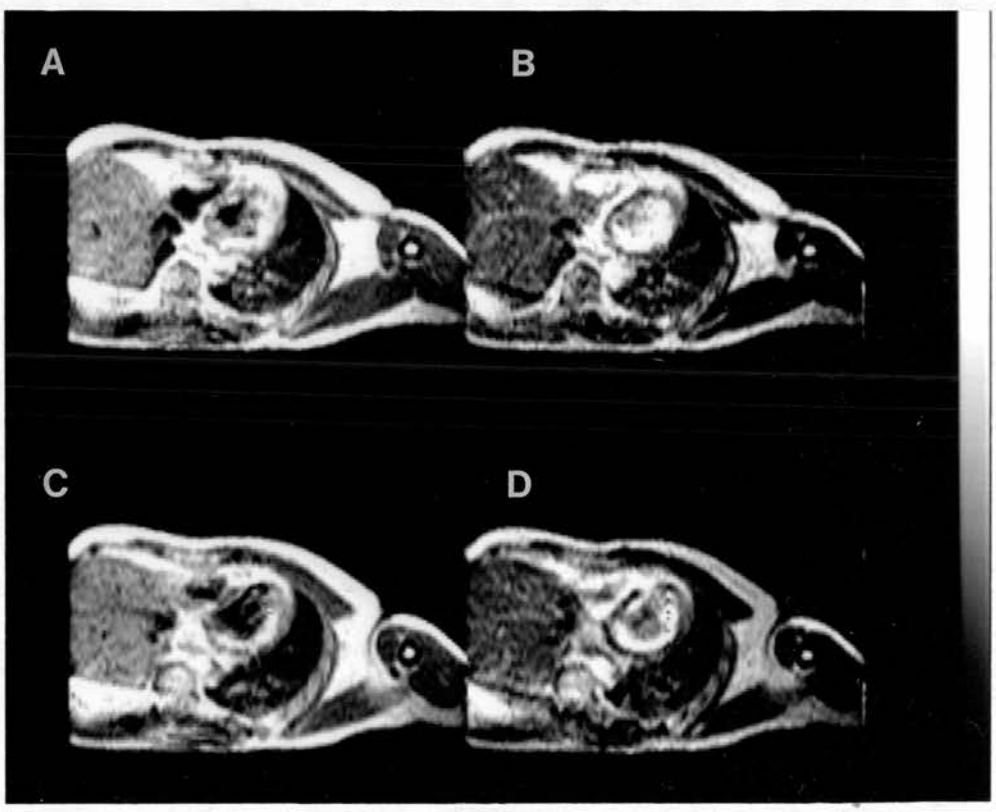


Figure 36. Two sections from a double spin-echo pulse sequence showing the first (a and c) and second-echo images (b and d). The acute anterior myocardial infarct is poorly defined on the second-echo images (particularly image b) due to signal from intracavitary blood.

TABLE 38

Comparison of Myocardial Infarct Size Measurement using Saturation Recovery-Inversion Recovery and Double Spin-Echo Pulse Sequences

| Patient | Myocardial Infarct Size ($cm^3$) | |
|---|---|---|
| | T1 | T2 |
| McE | 35.2 | 35.3 |
| CM | 46.2 | 54.0 |
| WM | 20.2 | 19.1 |
| SG | 12.8 | 19.9 |
| DD | 24.0 | 23.3 |
| TD | 27.5 | 31.8 |
| WMc | 26.6 | 22.1 |
| WB | 19.3 | 19.0 |
| SL | 52.3 | 49.6 |
| WB | 67.8 | 75.0 |

Due to partial volume effects it was impossible to differentiate areas of infarction at the extreme cardiac apex from increased T2 values due to pericardial fat. Thus the apical slice was discarded in all patients when the endocardial outline was not demonstrated.

### 6E.3 Statistical Analysis

In order to determine the agreement between myocardial infarct size measured using the two pulse sequences, a plot of the difference between values obtained, against their mean value (Bland & Altman 1986) was performed. This method of analysis is discussed in greater detail on page 291.

### 6E.4 Results

Table 38 shows the individual results for myocardial infarct size for both the T1 and T2 weighted images, for the 10 patients studied. The results were examined by two different statistical methods. Using a coefficient of correlation there was a highly significant agreement between results ($r = 0.97$; $p<0.0001$), Figure 37a. Figure 37b, shows a plot of the difference between measurements against the mean of the two measurements. The mean difference between measurements was $-1.7cm^3$, the standard deviation of the difference $4.5cm^3$, and the standard error of the difference was $1.4cm^3$. As the mean difference did not vary significantly from zero, and all values lay with the two standard deviation range, this indicated a good agreement between T1 and T2 measurements of infarct size.

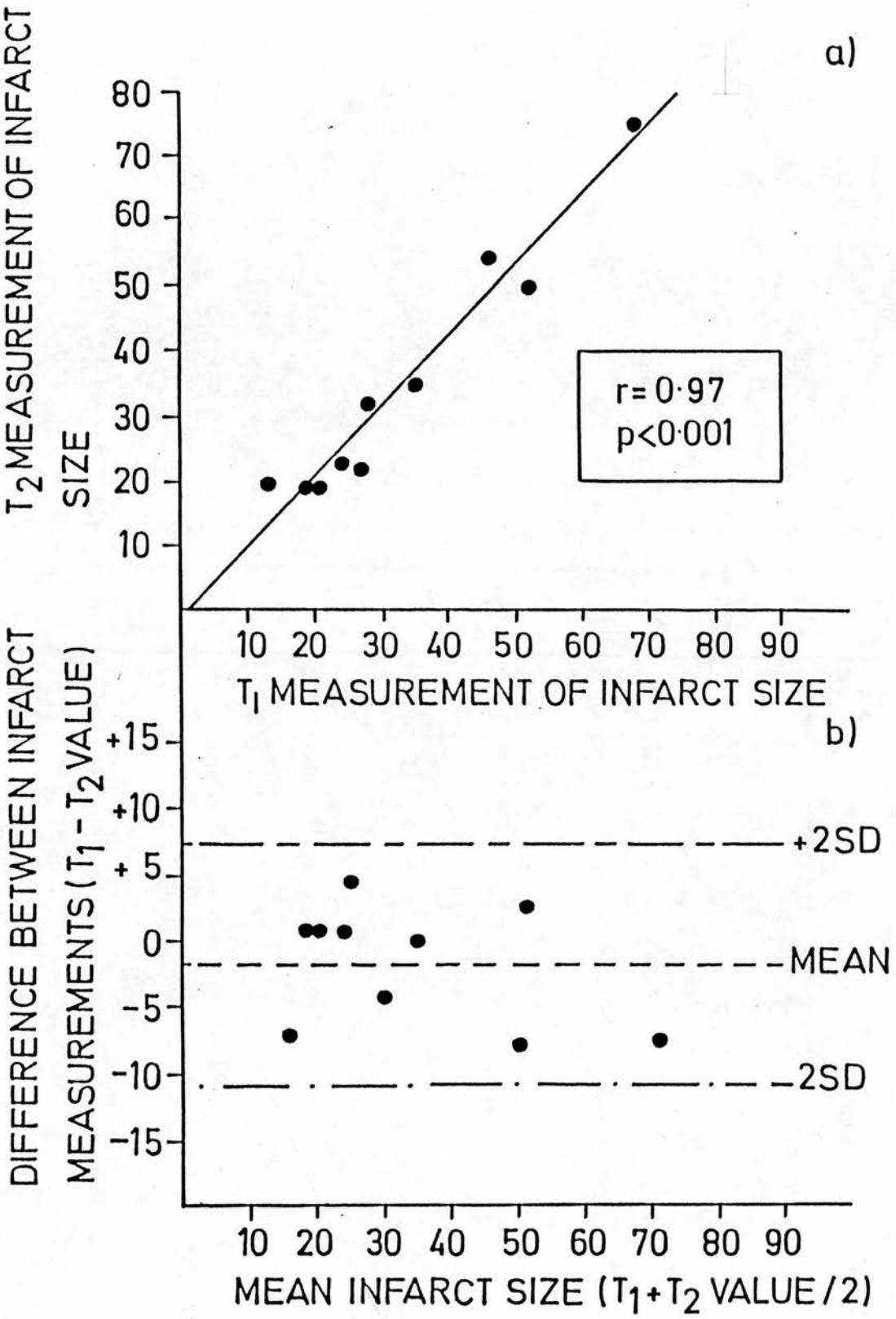


Figure 37. Comparison of T1 and T2 infarct size measurements using a) coefficient of correlation and b) plot of the difference between measurements against the mean of the two measurements.

## 6F CHANGES IN MYOCARDIAL INFARCT SIZE WITH TIME

### 6F.1 Patients

Twenty-four patients (22 male and 2 female) whose ages ranged from 41 to 74 years were included in this study. All patients had sustained their first uncomplicated myocardial infarction as diagnosed by typical presenting history and electrocardiographic changes. Twenty-one of the 24 patients received standard thrombolytic therapy, consisting of 1.5 Megaunits streptokinase in 5 per cent dextrose administered intravenously over 60 minutes, and were subsequently commenced on subcutaneous heparin (5,000 units tid), oral soluble aspirin (300mg/day) and oral metoprolol (100mg/day). Three patients did not receive thrombolytic therapy, either due to delayed admission to hospital or to pre-existing gastrointestinal ulceration. All patients were then randomly allocated to receive either placebo, captopril (12.5ms tid) or isosorbide dinitrate (20mg tid). This was continued for 4 weeks following the onset of chest pain, but if clear contra-indications developed, the treatment was reduced or discontinued.

Patients were only considered eligible for this part of the study, if there were no clear contra-indications to either captopril or isosorbide dinitrate, such as persistent hypotension or current use of large doses of diuretic, and if the patient was within 36 hours of the onset of symptoms suggestive of myocardial infarction. Of the 24 patients included in this study 7 received placebo, 12 captopril and 5 isosorbide dinitrate. All patients were well at

the time of examination, in particular none had a serious arrhythmia or evidence of acute pulmonary oedema. No contra-indications developed during the study period.

### 6F.2 Methods

Magnetic resonance imaging was carried out at 5-7 days and repeated at 6-8 weeks following the onset of acute symptoms, using a low field system operating at 0.08 Tesla. A double spin-echo pulse sequence was employed using echo delay times (TE) of 42 and 120ms for the first and second-echoes respectively. The repetition time (TR) varied according to the patient's heart rate. A 12mm slice thickness and separation was used and all images acquired using a cardiac gating technique to synchronise data acquisition with the downslope of the P wave ie during end-diastole. A full description of the technique and the method of image analysis used to determine myocardial infarct size has been discussed in detail in Chapter 6E.2.

### 6F.3 Results

One patient in each of the placebo, captopril and isosorbide dinitrate groups did not receive thrombolytic therapy. The mean time from onset of symptoms to the administration of thrombolysis for the remaining patients, varied from 225 mins (range 70-450 mins) for the placebo group, to 188 mins for both the captopril (range 80-420 mins) and isosorbide dinitrate (range 150-220 mins) groups. There was no significant difference in infarct sizes

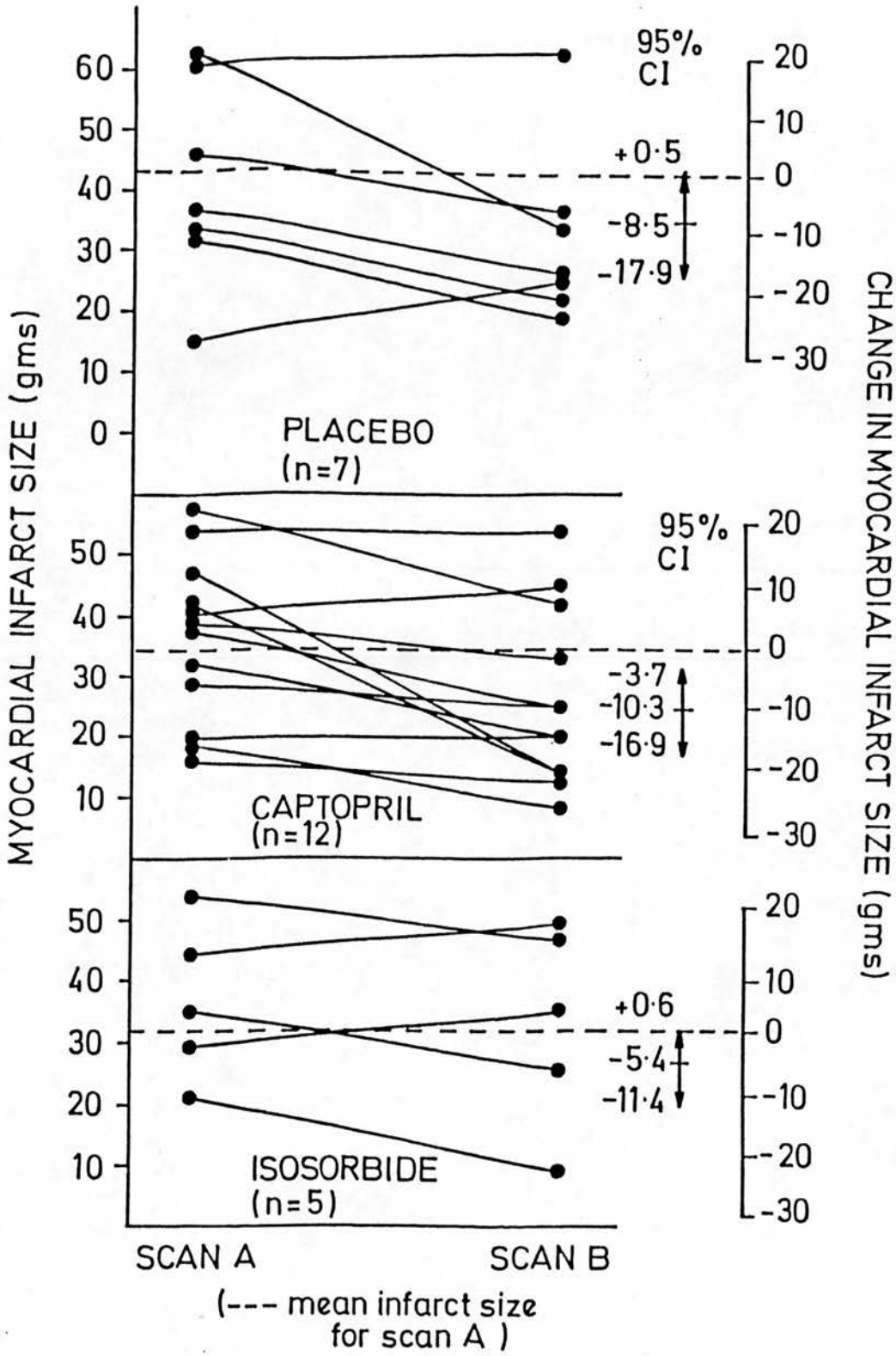


Figure 38. Changes in myocardial infarct size with time. Comparison of infarct size before (Scan A) and after treatment (Scan B) for the three groups.

between the three groups, prior to treatment with either placebo, captopril or isosorbide dinitrate. The mean infarct sizes and the standard deviations were as follows: placebo 42.9 $\pm$ 19.9 $cm^3$ (range 15.1 - 75.0$cm^3$); captopril 34.3 $\pm$ 15.2 $cm^3$ (range 8.3 - 58.1$cm^3$) and isosorbide dinitrate 31.9 $\pm$ 13.5 $cm^3$ (range 19.1 - 54.0$cm^3$).

Five of the 7 patients receiving placebo treatment, 9 of the 12 patients receiving captopril and 3 of the 5 patients receiving isosorbide dinitrate, showed a reduction in myocardial infarct size from the initial scan carried out at 5-7 days post infarction to the delayed scan at 6-8 weeks. Of the remaining patients - 2 of the placebo group, 1 of the captopril group and 2 of the isosorbide dinitrate group showed an increase in infarct size, while a further 2 patients receiving captopril showed no demonstrable change in infarct size.

Figure 38 shows the individual changes in infarct size, before and after treatment for the three patient groups, and the mean change and 95 per cent confidence intervals for the difference before and after treatment.

Following the 6 to 8 week convalescent period, the mean change in infarct size for the placebo group was -8.5$cm^3$, with the 95 per cent confidence interval extending from 0.5 to -17.9 $cm^3$. After treatment with oral captopril, the mean change was slightly, but not significantly greater, at -10.3$cm^3$ with a 95 per cent confidence interval of -3.7 to -16.9$cm^3$, while the mean change for the isosorbide dinitrate group was least at -5.4$cm^3$, with 95 per

cent confidence interval of 0.6 to -11.4$cm^3$.

## 6G EFFECT OF ORAL CAPTOPRIL AND ISOSORBIDE DINITRATE ON MYOCARDIAL INFARCT SIZE AND LEFT VENTRICULAR VOLUME

### 6G.1 Patients

Thirty-nine patients (34 male and 5 female) whose ages ranged from 41 to 77 years participated in this study. All patients had experienced their first myocardial infarction which was not complicated by either left ventricular failure or serious cardiac arrhythmias. All patients had received standard thrombolytic therapy (Chapter 6F.1) and had subsequently been randomly allocated to placebo therapy, oral captopril (12.5mg tid) or oral isosorbide dinitrate (20mg tid) for a four week period following hospital admission. Eleven patients were allocated to the placebo group, 17 to the captopril group and 11 to the isosorbide dinitrate group.

The contra-indications pertaining to the patient groups in Chapter 6F.1, were strictly adhered to in this study. Informed consent was obtained from all patients prior to entering the study.

### 6G.2 Methods

#### Imaging Technique

Magnetic resonance imaging was carried out at 6-8 weeks following the onset of chest pain, using a low field system operating at 0.08 Tesla. Patients with a cardiac pacemaker, metallic heart valve or previous intra-cranial surgery with insertion of ferromagnetic

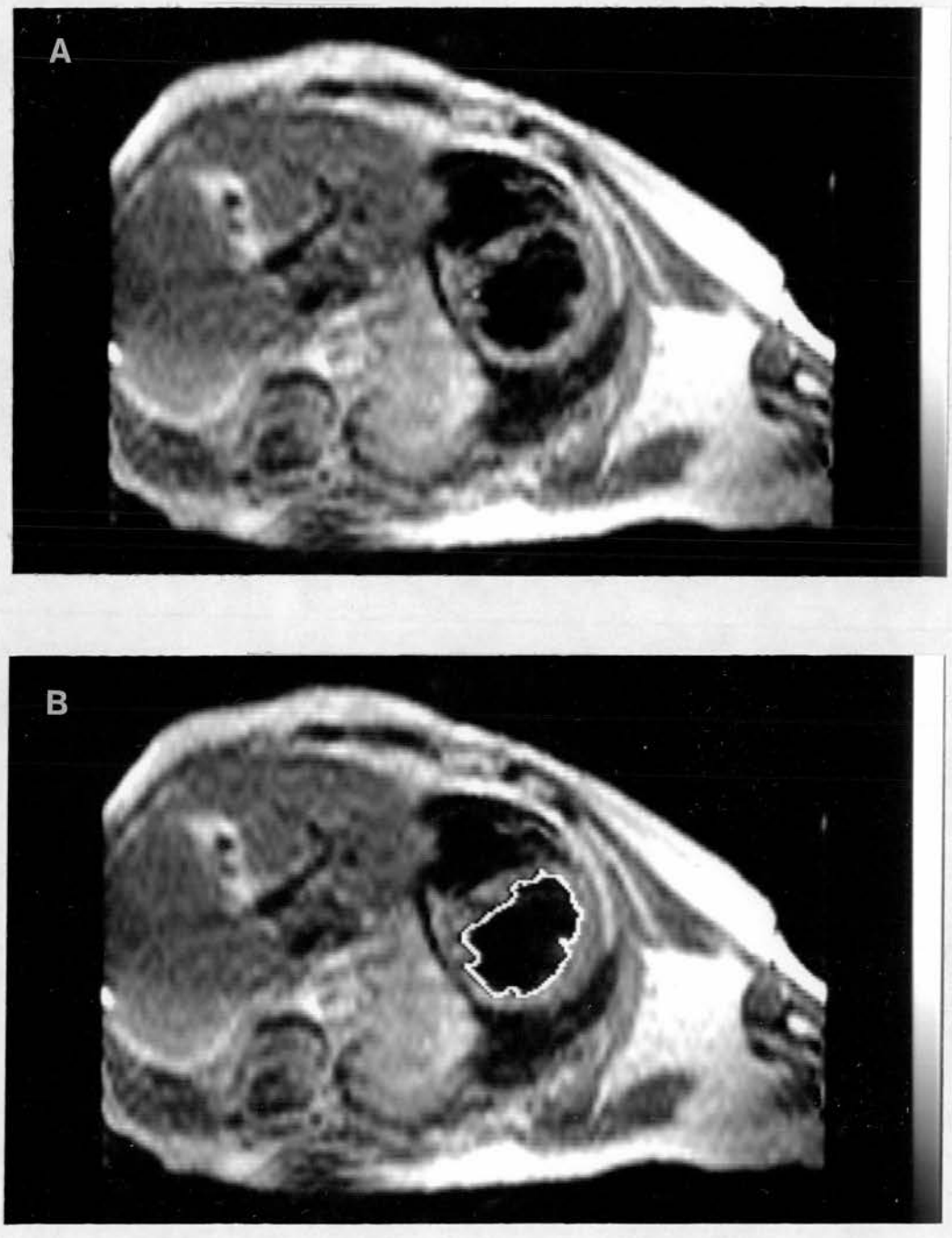


Figure 39. a) First-echo image showing satisfactory delineation of myocardium and blood pool.

b) Endocardial surface is outlined in white. The irregular region-of-interest is then measured to obtain the left ventricular chamber volume. Anterior and posterior papillary muscles are seen on the lateral left ventricular wall.

clips were excluded.

Ungated coronal scout images were initially performed to visualise the longitudinal axis of the ventricles, and from these short axis images were prescribed. A cardiac gating technique was employed, to synchronise data acquisition with end-diastole. The gating technique has previously been described in Chapter 2C.

A double spin-echo technique was employed using delay times of 42 and 120ms for the first and second-echoes respectively, with a variable repetition time depending on the R-R interval. Eight to ten slices of 12mm thickness and separation were acquired from below the cardiac apex to the level of the aortic arch. Four data acquisitions were used, each consisting of 2 slices with a 32ms time separation with each acquisition composed of two averages of 64 phase encoding steps and 128 frequency encoding steps, resulting in a pixel size of 3 x 6mm. This was interpolated to a 128 x 128 matrix (3 x 3mm) for analysis on the final display monitor.

Image Analysis

The method used to assess myocardial infarct size from the first-echo images has already been discussed in detail in Chapter 6E.2.

Good contrast, and satisfactory image resolution was routinely obtained in the first-echo image, allowing clear delineation between ventricular wall and the contained blood pool. To obtain the left ventricular volume an irregular region of interest

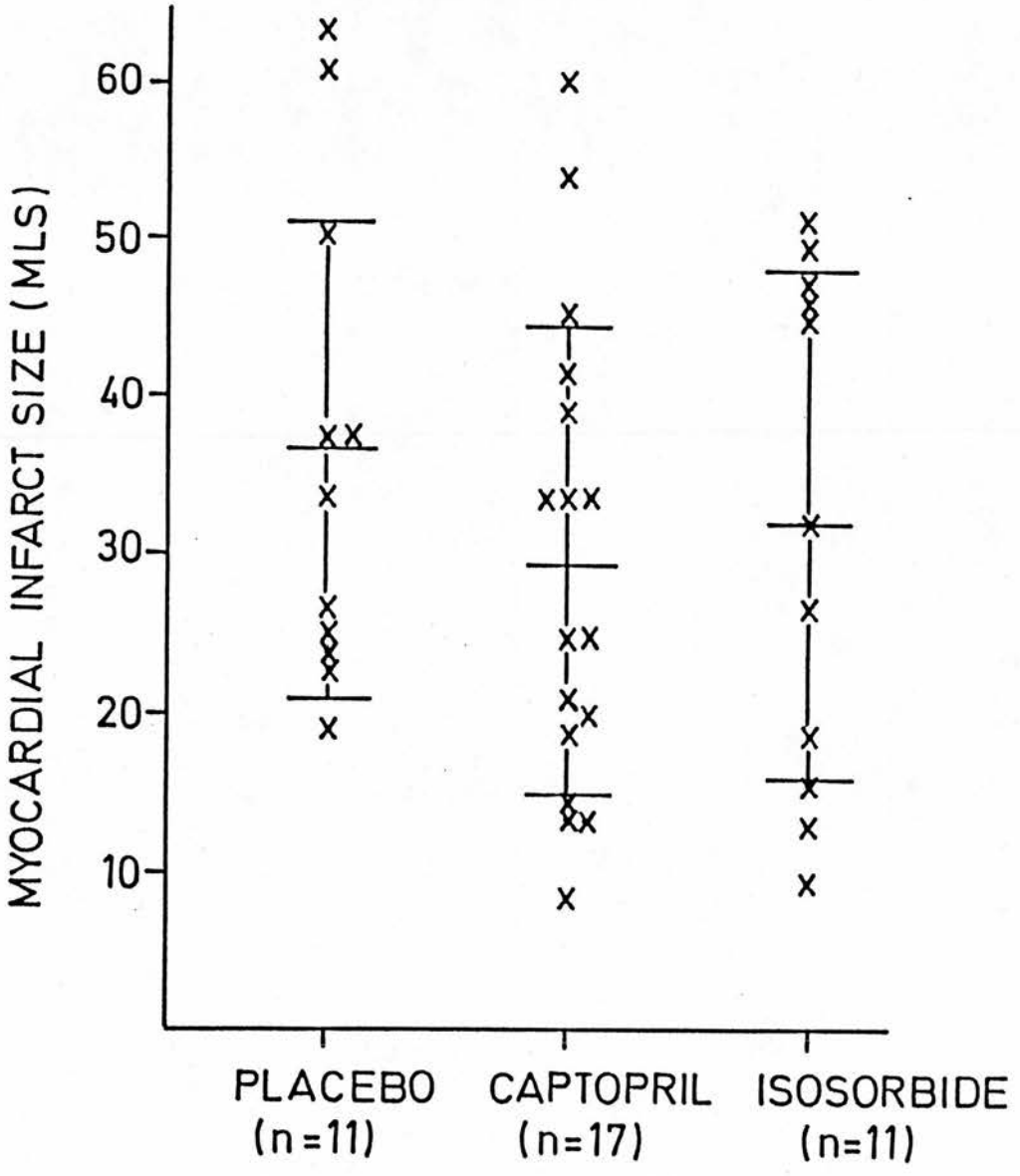


Figure 40. Range, mean and standard deviation of myocardial infarct size for the three treatment groups (placebo, captopril and isosorbide dinitrate) at 6-8 weeks post-infarction.

was drawn around the endo-cardial surface on all slices using image analysis software (Figure 39). The values obtained were then summed and multiplied by the slice thickness (12mm) to produce the total left ventricular volume.

Particular care was taken to accurately outline the ventricular chamber excluding the papillary muscles. Although the mitral valve was frequently not visualised on the spin-echo images, the difference in configuration between left atrial and left ventricular walls allowed the boundary of the left ventricle to be determined.

### 6G.3 Results

There was no significant difference between the three groups for the mean time between onset of chest pain and initiation of thrombolytic therapy. The mean time for the placebo group was 214 mins (range 70 - 450 mins) compared to 196 mins for the captopril group (range 65 - 420 mins) and 172 mins for the isosorbide dinitrate group (range 90 - 255 mins). The infarct sizes calculated from the T2 weighted spin-echo images showed a wide variation in all 3 treatment groups. Although the mean infarct size at 6-8 weeks for the placebo group was slightly greater at $36.5cm^3 \pm 15.5$ (range 19.2 - $63.7cm^3$) than the mean value for both the captopril group at $29.5 \pm 14.9\ cm^3$ (range 8.4 - $60.0cm^3$) and the isosorbide dinitrate group at $32.1 \pm 16.1\ cm^3$ (range 9.4 - $50.9cm^3$), there was no statistically significant difference. These

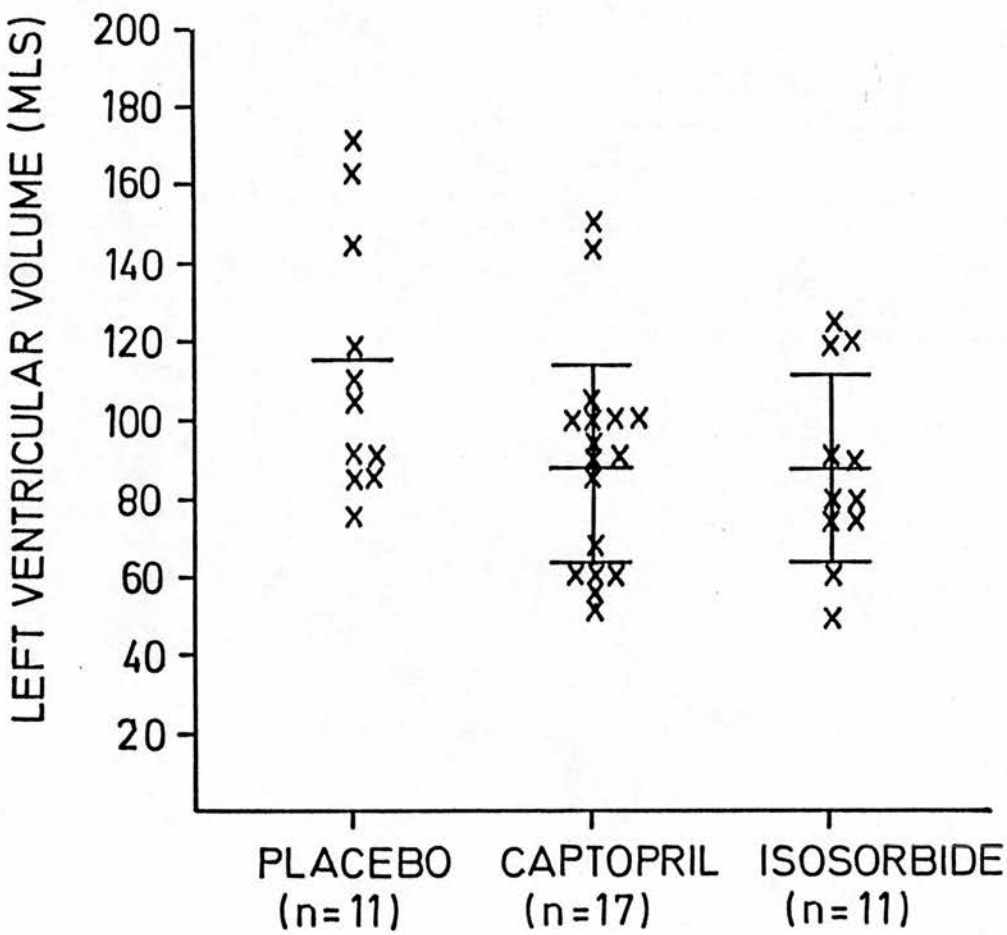


Figure 41. Mean, standard deviation and range of left ventricular volumes (mls) for the three treatment groups (placebo, captopril and isosorbide dinitrate) at 6-8 weeks post infarction.

results are expressed graphically in Figure 40.

A similarly wide spread of results was found for the left ventricular end-diastolic volumes, which are depicted in Figure 41. The left ventricular end-diastolic volumes for the captopril and isosorbide dinitrate groups were similar at 89.4 $\pm$ 27.5 $cm^3$ and 88.0 $\pm$ 24.1 $cm^3$ respectively. However, compared to the other two groups there was a slight increase in the left ventricular end-diastolic volumes for the placebo group, with a mean value of 110.0 $\pm$ 28.6 $cm^3$, but this did not reach statistical significance ($p>0.005$).

## 6H DISCUSSION

There is considerable interest in determining the size of myocardial infarction because of the prognostic value and the potential use for guiding therapy. However, despite its importance, routine clinical measurements of infarct size have not been available. In the past electrocardiographic techniques have been used to map the extent of infarction, but these are generally inaccurate and fail to demonstrate small non-transmural or posterior lesions. Currently 2-dimensional echocardiography is used mainly to determine areas of wall thinning, dyskinesis or akinesis, and to estimate ventricular chamber size, but it has major limitations in estimating infarct size and is considerably operator dependent. These techniques have been discussed in greater detail in Chapter 6A.

The two methods most frequently used are enzymatic and radionuclide estimation. In experimental studies on whole heart homogenates obtained from dogs following coronary artery ligation, the release of creatine kinase-MB into the blood correlates almost perfectly with the depletion of creatine kinase-MB from infarcted myocardium (Shell 1971, Shell 1973). Studies of acute myocardial infarction in man have demonstrated reasonable agreement between infarct size estimated by serum creatine kinase-MB and the left ventricular haemodynamics, prognosis and autopsy data. Although a number of workers have criticised the enzymatic models and were not able to reproduce results from experimental canine studies (Roe 1975, Roe 1977, Cairns 1978), there is now irrefutable data to support the

correlation between "peak" serum creatine kinase-MB values and histological infarct size in untreated patients. However with the advent of techniques designed to salvage ischaemic myocardium, doubt has again been cast on this relationship.

Reperfusion of ischaemic myocardium alters the shape of the serum creatine kinase-MB release curve. The rate of upstroke of the curve is more rapid and the peak values higher than would be expected without reperfusion (Schroder 1983, Ganz 1981, Blanke 1984, Vatner 1978).

Two different methods have been employed to assess myocardial infarct size using estimation of serum creatine kinase-MB release. Using the method described by Shell et al (1971) the myocardial infarct size assessed histologically and by enzyme release differed widely in unperfused and reperfused myocardial infarcts. This discrepancy can be accounted for by the different value of the model parameter $P_{CK}$ used in unperfused or reperfused infarcts ie the fraction of released creatine kinase-MB recovered in the plasma volume. This value equals 15 to 30 per cent in unperfused infarcts (Shell 1971, Roberts 1975) but is considered to be markedly increased in reperfused infarcts (Vatner 1978, Roberts 1983, Tamaki 1983, Blanke 1984, Roberts 1975). Using Shell's method, Tamaki et al found more creatine kinase-MB released into the plasma from recanalised infarcts than in unperfused infarcts. This was confirmed by other workers (Ganz 1981, Blanke 1984, Vatner 1978). The main difference was that at comparable degrees of left ventricular impairment, the cumulative amount of released creatine

kinase-MB was higher in the thrombolysis group than in the control group.

However the enzymatic estimation of infarct size developed by Witteveen et al (1975) is based on 100 per cent recovery of liberated enzymes and has been used in patients with acute myocardial infarction treated conventionally as well as with thrombolytic therapy. From animal studies Hermens (1982) demonstrated that, using this technique, any cytoplasmic enzyme released from irreversibly damaged myocardium was completely recovered in the plasma. Van der Laarse and colleagues (1988), using Witteveen's method of infarct size estimation, studied 266 patients treated either conventionally or with intracoronary thrombolysis and compared this with residual left ventricular function. Compared to conventional therapy, patients allocated to intracoronary thrombolysis had a 29 per cent smaller enzymatic infarct size ($p<0.001$), smaller left ventricular end-diastolic and end-systolic volume indexes by 10 per cent ($p<0.05$) and 20 per cent ($p<0.005$) respectively, and improved left ventricular ejection fraction ($55 \pm 1\%$ versus $49 \pm 1\%$; $p<0.001$). However although the size of infarction was limited by thrombolysis, there was no correlation between left ventricular chamber volume, or the ejection fraction and the amount of damaged myocardium.

Similar results were obtained in the ISAM study (1986) in which 1741 patients were randomly assigned to either a 60 minute intravenous infusion of 1.5m IU of streptokinase or placebo. Those treated with streptokinase demonstrated significant reduction in

creatine kinase-MB release compared to the placebo group ($p<0.02$) and angiograms obtained in 848 of these patients 3 to 4 weeks after infarction revealed a higher global ejection fraction (56.8 versus 53.9 per cent, $p<0.005$) and regional ejection fraction ($p<0.005$) in the streptokinase group. It was therefore concluded that streptokinase infusion early after the onset of infarction, limited the size of damage regardless of the location.

However it must be appreciated that many complex biological phenomena can affect creatine kinase-MB determinations. For example, in dogs the quantity of enzyme released was greater with patchy than with homogenous infarcts of similar size, presumably due to better haematogenous removal of enzyme from zones of patchy necrosis (Cairns 1978, Roe 1975, Swain 1980). In addition the appearance of creatine kinase-MB in serum also depends on cardiac lymphatic flow (Malberg 1972) and on the duration of exposure of creatine kinase-MB to lymph which is known to inactivate the enzyme (Robison 1978).

The only drugs prescribed to patients in this study were enteric coated aspirin and metoprolol, as drugs such as anaesthetics, sedatives and propranolol may change plasma enzyme kinetics by altering the rate of clearance from blood (Cairns 1977). It should also be remembered that other events such as direct current cardioversion, percutaneous transluminal coronary angioplasty and blunt chest trauma may also cause an early increase in creatine kinase-MB levels.

For these reasons, only patients who had not been treated with either thrombolytic therapy or coronary angioplasty were included in the study, comparing magnetic resonance imaging, pyrophosphate scanning and serum creatine kinase-MB release. Creatine kinase-MB release curves were only obtained in 11 of the 19 patients, but from this limited information, enzyme release correlated with estimation of infarct size by both imaging modalities.

As the peak release of creatine kinase-MB occurs within the first 24 hours when thrombolytic therapy has been instituted, compared to between 24 to 48 hours with conventional treatment, it is important that the timing of serum determinations be tailored to the clinical circumstances. Following thrombolytic therapy serum samples are required at 2 to 4, 12 and at 24 hours after the onset of symptoms to detect the early "peak" and total creatine kinase-MB release resulting from early washout. In an intensive care setting this frequent blood sampling can easily be achieved.

However, with the ever increasing therapeutic options, the potential alterations in serum creatine kinase-MB measurements cast doubt on the ability of this technique to give accurate measurements of infarct size.

Since the introduction of single photon emission computed tomography, pyrophosphate imaging has been considered a sensitive method for the diagnosis and measurement of acute myocardial infarction and is the only method in routine use, which provides direct data on infarct size. The use of single photon emission

computed tomography has allowed more accurate detection of posterior, inferior and small sub-endocardial infarcts particularly following the addition of blood pool overlay (Corbett 1984). This data has correlated well with the histological findings in animals (Stokely 1975), and with the analysis of serum creatine kinase-MB release (Jansen 1985) and residual left ventricular function in man (Van Der Laarse 1988).

Unfortunately there are certain limitations to pyrophosphate imaging. The delivery of the radionuclide to the centre of a large infarct may be incomplete due to alterations in the tissue perfusion. In 1976 Buja and co-workers showed from scintigraphy of infarcted canine myocardium that pyrophosphate uptake was confined to the macroscopically visible area of infarction and that the activity was most intense at the periphery of the lesion. The maximum concentration of pyrophosphate occurred in the outer peripheral zones of infarcts which exhibited variable degrees of residual blood flow. The average mean pyrophosphate uptake was 21.5 times normal in partially necrotic areas in the outer peripheries of the infarct, 24.5 times normal in areas of extensive to homogeneous necrosis in the outer peripheries, 7.8 times normal in the inner peripheries and only 1.7 times normal in the centre of the infarcts. This reflected the variable perfusion within the area of myocardial damage.

More uniform labelling of infarcted myocardium can be achieved with the use of antimyosin antibodies labelled with indium but the poorer imaging characteristics of indium compared to technetium

offset this advantage.

The technique described here attempts to overcome this problem by measuring the volume defined by pyrophosphate rather than quantifying the amount of isotope concentrated in the unevenly perfused tissue.

One of the potential criticisms of this technique is the value chosen for the 3-dimensional thresholding procedure. This has been examined in phantom studies by a number of workers, using a 99m-technetium filled balloon attached to the surface of a cone-shaped vial and suspended eccentrically in a water-filled cylinder to simulate normal anatomy. Imaging was repeated after the balloon was removed and the vial filled with 99m-technetium to simulate a left ventricular blood pool. From such studies a threshold value of 65 per cent has been shown to give optimal results and this has been confirmed by work in our laboratory. Use of a higher or lower threshold value would result in a corresponding decrease or increase in infarct volume.

A further source of error is the inability to accurately correct for photon attentuation in individual patients. Sources of error in this measurement include estimation of the distance between the heart and the gamma camera and the use of the linear attenuation coefficient of 99m-technetium photons in water as the physiological composition of the body. It should also be remembered that radionuclide imaging involves exposure to a significant radiation dose and is only useful for between five to seven days following

infarction.

Thus at the present time, tissue characterisation by any imaging modality remains problematical and a direct method of demonstrating myocardial infarction is required. A method such as magnetic resonance imaging is well suited to the measurement of myocardial infarct size, because variations in the proton relaxation parameters, T1 and T2 can be used to directly visualise myocardial pathology. The changes in relaxation times which have been attributed mostly to alterations in myocardial water content, cause an increase in signal intensity. Magnetic resonance imaging is already an established method for detecting both acute and chronic myocardial infarcts, and elevations of the relaxation parameters T1 and T2 have been demonstrated as early as 30 minutes following coronary occlusion (Tscholakoff 1986) and only gradually returned to normal after 3-6 months (Been 1988).

Results of several previous studies have shown that accurate quantitation of experimental infarct size is feasible by magnetic resonance imaging (Rokey 1986, Caputo 1987). Rokey et al used a calculated T2 image for the measurement of infarct size in an ex-vivo study on a canine model of 6 hours occlusion. They showed an excellent correlation between myocardial infarct size measured by magnetic resonance imaging and histochemical staining ($r = 0.98$, SEE = 1.86%). Caputo et al studying dogs in-vivo, also used a calculated T2 image to quantitate infarct size, 3 and 21 days after occlusion of the left anterior descending artery. The infarct mass measured by magnetic resonance imaging correlated significantly

with the pathological estimate (r = 0.94, SEE = 1.54gms) but interestingly the infarct mass at 3 and 21 days was not significantly different.

An overestimation of infarct size was noted by Buda et al (1985), who used a canine model with 2 to 4 hours of coronary occlusion followed by reperfusion. In their study imaging was performed on the excised heart only, and the infarct size measured by magnetic resonance compared better with hypoperfused myocardium as determined by autoradiography of the distribution of 99m-technetium microspheres, than pathological data. However, the correlations between the different techniques for infarct size evaluation was difficult to interpret because the regression line obtained was substantially influenced by three dogs without infarction.

In a recent report, Bouchard et al (1989) evaluated T2-weighted images for quantitation of the extent of myocardial injury 7 days after coronary occlusion in dogs. They compared in-vivo magnetic resonance images with anatomical data obtained from tissues stained with haematoxylin and eosin and with Gomori aldehyde fuchsin trichrome to verify the gross identification of the infarct borders. A significant relationship was obtained between in-vivo imaging and the pathological data (r = 0.88, p = <0.009), although magnetic resonance imaging generally overestimated the size of infarcts. Although it was thought that partial volume effects contributed to this finding, particularly where infarcts involved the apex, measurements of myocardial blood flow distribution demonstrated a significant relationship between magnetic resonance

estimates of infarct size and hypoperfused myocardium ($r = 0.92$, $p = 0.008$). Moreover, multiple regression analysis showed a better correlation between in-vivo magnetic resonance imaging and microsphere determined hypoperfused myocardium than the pathologically determined infarct size. This indicates that the increased signal was present in regions that were both reversibly and irreversibly damaged. This can be explained by the pathological events in progress.

Earlier studies of acute rejection following heterotopic cardiac transplantation (Adherne 1986) and myocardial involvement in systemic lupus erythematosus (Been 1988) have shown an increase in T1 values of myocardium. In both of these conditions cellular infiltration is a prominent histological feature. In acute myocardial infarction extensive neutrophil infiltration begins in infarcted and surrounding viable tissue at about 18 hours post occlusion. Routine microscopy of infarcted myocardium also shows diffuse swelling of cells and oedema of the interstitial spaces. These changes occur 6 to 7 hours after obstruction of the blood supply. Previous studies examining the protective effect of hyperosmotic mannitol in myocardial ischaemia and necrosis (Powell 1976) have shown the presence of oedema not only in infarcted myocardium but also in non-infarcted but ischaemic tissue. Thus, as cellular oedema and granulocyte infiltration occur in ischaemic but viable tissue and both give rise to increased signal intensity, this accounts for the apparently larger area of myocardial injury demonstrated by magnetic resonance imaging, compared to that defined pathologically.

The presence of reversible changes surrounding non-viable myocardial tissue is supported by this work. This study has shown a significant reduction in myocardial infarct size in 71 per cent of patients six weeks after onset of symptoms. Most of these patients (21 out of 24) had received intravenous thrombolytic therapy within 3 to 4 hours of infarction and then all had been randomly allocated to receive placebo, captopril or isosorbide dinitrate. As one would expect from traditional pathological teaching, the apparent myocardial size decreased with time in many patients, presumably secondary to resolution of the acute inflammatory changes. The reason for the slight increase in infarct size in 5 patients, and the lack of response in a further 2 patients is unknown. It is postulated that the presence of mural thrombus which is known to have increased signal intensity on spin-echo images, blood flow artefacts or alternatively extension of the infarct might account for these findings. In addition, the role of coronary artery reperfusion which is known to increase T1 values (Johnston 1985), and to increase cellular swelling (Kloner 1980) is unknown.

The measurement of myocardial infarct size by magnetic resonance imaging described here, correlated well with pyrophosphate scanning. However the mechanism of action of the two imaging modalities is quite different. Alteration in signal intensity in magnetic resonance imaging depends on the proportion of "free" to "bound" water molecules present. Radionuclide scanning depends on the absorption of 99m Tc-pyrophosphate with various forms of tissue calcium stores, and the uptake is not limited to necrotic cells.

Reversibly damaged border zone myocardium with mildly elevated calcium levels also shows significant pyrophosphate uptake.

The state of regional myocardial perfusion is the key factor in myocardial infarct detection by both modalities. Alteration in blood flow results in membrane damage, electrolyte shifts, elevation of both intra- and extra-cellular calcium levels, with or without mitochondrial calcium deposition and the influx of plasma proteins. This, in addition to increased capillary permeability, results in accumulation of tissue water. Thus, although the mechanism of action of magnetic resonance imaging and pyrophosphate scanning are different, the underlying pathological processes result in similar myocardial infarct volume determinations.

Previous investigators (Bouchard 1989) measured myocardial infarct size by first adjusting the width and level of the window so that no signal was obtained from normal tissue. The outer borders of the zone with increased signal intensity were then planimetered with a tracker ball. This method was considered too subjective particularly when patchy areas of necrosis were present and lead to the development of a thresholding technique. From both clinical and phantom studies it has been shown that the T1 and T2 values of normal myocardium vary with the repetition time. It was therefore essential to define a threshold level for normal tissue for each patient individually. Although identification of normal myocardium was carried out subjectively, allowing for the resolution of this system, the inter-observer variability of 10.1 per cent, for the threshold level of normal myocardium, would suggest that this is an

acceptable method.

In the past, comparison of two methods of measuring the same variable has relied heavily on correlation or regression coefficients and calculation of a p value. Both of these methods test the null hypothesis, which states that there is no association between two variables. However these methods are now considered inappropriate when dealing with measurements of the same variable by two different techniques (Bland 1986). Correlation coefficients measure the strength of a relation between two variables, but not the agreement between them. The magnitude of the correlation coefficient is strongly influenced by the range of values under study, and its "significance" is increased simply by increasing the number of subjects studied. Thus it does not provide information on the magnitude of any discrepancy between the two methods nor, whether the discrepancy is constant over a range of values. It is also important to be aware of systematic variations in the values over the range in question, and neither test provides such information. The method of analysis advocated by Bland and Altman (1986), and the use of confidence intervals, emphasises the clinical relevance by showing the extent to which the two methods studied give different results.

Both of these methods have been used in this study to examine the relationship between myocardial infarct size measured by magnetic resonance imaging and pyrophosphate scanning, although the latter technique provides the critical information. In this study the mean infarct size measured by magnetic resonance imaging and

pyrophosphate scanning differed by only 2.7cm3, indicating a good agreement over a wide range of values.

Some studies have suggested that the relaxation parameter T2, is better than T1 for the identification of infarcted tissue, but this may simply reflect the choice of imaging sequence used. For example in 1982, Brady employed a steady-state-free-precession technique but was unable to differentiate normal from damaged myocardium. As the resultant image is dependent not only on the radio-frequency pulse angle and proton density, but also on both the T1 and T2 relaxation times, it has been suggested that the relaxation times covaried in such a way as to produce no effect on the resultant image intensity of infarcted myocardium. In general the spin-echo pulse sequence tends to accentuate T2 differences between tissues, compared to other techniques, such as inversion recovery which emphasise the T1 differences.

The rationale for choosing a double spin-echo sequence was that the short echo time provided good anatomical definition of the myocardial borders, and reasonable contrast between normal and infarcted myocardium. The second echo time at 120ms, was performed after the shortest time interval allowed by the computer software, and provided increased T2 contrast difference but a poorer signal-to-noise ratio. The use of a longer repetition time, which allowed more complete relaxation, minimised the T1 effects which tended to decrease signal intensity. Thus it was occasionally necessary in cases of tachycardia to gate data acquisition from every second heart beat. One major problem arising from acquiring the second-

echo image at 120ms, compared to 42ms for the first-echo, was that imaging occurred slightly later in the cardiac cycle. This was unavoidable with the current computer software. The interleaved saturation recovery-inversion recovery pulse sequence employed in this study was particularly useful at determining changes in T1 values. The constant time for inversion in our technique coupled with a non-slice selective efficient inverting pulse (AFP), minimised the error in T1 caused by a variable R-R interval.

Both an interleaved saturation recovery-inversion recovery and a double spin-echo pulse sequence were performed in this study to measure infarct size, and thus directly compare results obtained for T1 and T2 images. The results indicated a good agreement between the two relaxation parameters, although spin-echo images provide better anatomical resolution.

Magnetic resonance imaging can indentify about 90 per cent (Fisher 1987) of infarcts using a T2-weighted spin-echo image. However, several pitfalls exist. Artificial variations in signal intensity of the myocardium may occur due to respiration or residual cardiac motion (Fisher 1987), slowly flowing blood in the ventricle may mimic subendocardial infarction and late echo images may be degraded by reduced signal-to-noise ratio. Thus attention has been drawn to substances which improve the detection and extent of infarction.

Certain substances by virtue of their paramagnetic properties, can modify the proton relaxation times T1 and T2 and thereby change the

image appearance. Although a paramagnetic contrast medium is not required to delineate between blood and myocardium, it has been used effectively to demonstrate myocardial perfusion (Peshock 1986). Such an agent, diethylenetriaminepentaacetic acid (Gd-DTPA), is delivered to an infarct in accordance with the extent of collateral circulation, neovascularisation and cellular damage, all of which result in reduced wash-out from the infarct zone (Tscholakoff 1986, McNamara 1986). By 10-15 minutes, Gd-DTPA has been removed from normal tissue but remains within the zone of injury, resulting in increased signal in T1-weighted images.

McNamara et al (1986) reported the potential use of Gd-DTPA for delineating perfusion defects in dogs. He showed that in dogs with reversible ischaemia (15 mins coronary artery occlusion, followed by reperfusion), no regional differences in signal intensity could be detected, but that in irreversible ischaemia (60 mins coronary artery occlusion followed by reperfusion) significant contrast enhancement was present. The situation is unfortunately less clear-cut in man. In 1989, De Roos showed that Gd-DTPA could improve visualisation of myocardial injury in both reperfused and non-perfused infarcts but could not distinguish between them. He studied 45 patients before and serially for 30 minutes after intravenous administration of Gd-DTPA. He found that there was a significant increase in signal intensity between reperfused/non-reperfused infarcted areas and normal myocardium up to 30 minutes after administration. Using Gd-DTPA as a marker for myocardial perfusion he identified four types of contrast enhancement within acutely occluded or reperfused myocardium: uniform, homogeneous

enhancement, predominantly subendocardial enhancement, inhomogeneous enhancement with dark areas within or adjacent to the enhancing area, secondary to haemorrhage, and a doughnut-shaped pattern of enhancement. However the overlap in enhancement patterns and similar maximal intensity ratios after Gd-DTPA administration for both reperfused and non-reperfused infarcts precluded a reliable differentiation.

The considerable discrepancy in findings between man and the experimental canine model, can been explained by the various pathological processes known to occur in humans. These include the presence of spasm, the previous development of collateral circulation and the occlusion of capillaries by white cells adherent to damaged endothelium. Such processes account for the variability and overlap in findings in the "reperfused" and "non-reperfused" infarcts.

Studies directed at salvaging ischaemic myocardium have concentrated almost exclusively on limiting tissue necrosis, but relatively little attention has been paid to potentially preventable early topographic changes which may occur within the infarcted zone, especially in large transmural infarcts. Previous work has shown that between 28 to 40 per cent of patients with an acute transmural infarct will undergo ventricular dilatation within the next six months (Jeremy 1989). In selected patients oral captopril has been shown to prevent post infarction ventricular dilatation (Sharpe 1988, Pfeffer 1988) and intravenous nitrate has improved left ventricular function (Judgate 1988). However it is

not known if these findings are applicable to patients treated with thrombolysis.

Magnetic resonance imaging is capable of accurately demonstrating ventricular anatomy. Our study showed that in the majority of patients receiving placebo following thrombolysis, there was no tendency to ventricular dilatation, and that vasodilator therapy produced no further benefit in terms of left ventricular chamber size, or indeed a further reduction in infarct size. Although the results were substantially influenced by the limited number of patients examined it is possible that vasodilator therapy is not an appropriate therapy for patients at low risk of ventricular dilatation ie with small infarcts, inferior territory necrosis and with patent infarct related coronary arteries.

In conclusion, magnetic resonance imaging offers a unique possibility to study infarct size and ventricular chamber morphology. This is of increasing importance with the advent of thrombolytic therapy and the use of B-blockade, vasodilators and angiotensin converting enzyme inhibitors. It is known that a discrepancy exists between survival following reperfusion and the residual left ventricular function (White 1987), and it has been suggested that the beneficial effects of thrombolysis may be more complex than a simple reduction in infarct size. Much work remains to be carried out in this area, but as experimental canine work does not equate with the more complex pathological processes seen in man, the setting up of mulit-centre trials will undoubtably be required.

## REFERENCES


Aber G M, Bayley T J, Bishop J M. Inter-relationships between Renal and Cardiac Function and Respiratory Gas Exchange in Obstructive Airways Disease. Clin Sci 1963; 25: 159-170.

Abraham A S, Hedworth-Whitty R B, Bishop J M. Effects of Acute Hypoxia and Hypervolaemia Singly and Together Upon the Pulmonary Circulation in Patients with Chronic Bronchitis. Clin Sci 1967; 33: 371-380.

Abraham A S, Kay J M, Cole R B, Pincock A C. Haemodynamic and Pathological Study of the Effects of Chronic Hypoxia and Subsequent Recovery of the Heart and Pulmonary Vasculature of the Rat. Cardiovasc Res 1971; 5: 95-102.

Acquatella H, Schiller N B, Sharpe D N, Chatterjee K. Lack of Correlation between Echocardiographic Pulmonary Valve Morphology and Simultaneous Pulmonary Arterial Pressure. Am J Cardiol 1979; 43: 946-950.

Adams D F, Hessel S J, Judy P F, Stein J A, Abrams H L. Computed Tomography of the Normal and Infarcted Myocardium. A J R 1976; 126: 786-791.

Adherne T, Tscholakoff D, Finkbeiner W, Sechtem U, Derugin N, Yee E, Higgins C B. Magnetic Resonance Imaging of Cardiac Transplants

: The Evaluation of Rejection of Cardiac Allografts with and without Immunosupression. Circulation 1986; 74: 145-156.

AIMS Trial Study Group. Effect of Intravenous APSAC on Mortality after Acute Myocardial Infection : Preliminary Report of a Placebo-Controlled Clinical Trial. Lancet 1988; i: 545-549.

Akins E W, Hill J A, Fitzsimmons J R, Pepine C J, Williams C M. Importance of Imaging Plane for Magnetic Resonance Imaging of the Normal Left Ventricle. Am J Cardiol 1985; 56: 366-372.

Alonso D R, Scheidt S, Post M, Killip T. Pathophysiology of Cardiogenic Shock. Quantification of Myocardial Necrosis, Clinical, Pathological, and Electrocardiographic Correlations. Circulation 1973; 48: 588-596.

Amparo E G, Higgins C B, Farmer D, Gamsu G, McNamara M. Gated MRI of Cardiac and Paracardiac Masses : Initial Experiment. A J R 1984; 143: 1151-1156.

Arcilla R A, Tsai P, Thilenius O, Ranniger K. Angiographic Method for Volume Estimation of Right and Left Ventricles. Chest 1971; 60: 446-454.

Ardito G, Lamberti L, Bigatti P, Prono G. Influence of a Constant Magnetic Field on Human Lymphocyte Culture. Bull Soc Ital Sper 1984; 60: 1341-1346.

Arvidsson H. Angiocardiographic Determination of Left Ventricular Volume. Acta Radiologica 1961; 56: 321-339.

Ashutosh K, Mead G, Dunsky M. Early Effects of Oxygen Administration and Prognosis in Chronic Obstructive Pulmonary Disease and Cor Pulmonale. Am Rev Respir Dis 1983; 127: 399-404.

Askanas A, Rajszys R, Sadowski Z, Stopczyk M. Measurement of Thickness of Left Ventricular Wall in Man Using the Ultrasound Technique. Pol Med J 1970; 9: 62-66.

Astorri E, Chizzola A, Visiola A, Anversa P, Olivetti G, Vitali-Mazza L. Right Ventricular Hypertrophy: A Cytometric Study on 55 Human Hearts. J Mol Cell Cardiol 1971; 2: 99-110.

Balcon R, Jewitt D E, Davies J P H, Oram S. A Controlled Trial of Propranolol in Acute Myocardial Infarction. Lancet 1966; 2: 917-920.

Banka V S, Chadda K D, Helfant R H. Limitations of Myocardial Revascularization in Restoration of Regional Contraction Abnormalities produced by Coronary Occlusion. Am J Cardiol 1974; 34: 164-170.

Been M, Kean D, Smith M A, Douglas R H B, Best J J K, Muir A L. Nuclear Magnetic Resonance in Hypertrophic Cardiomyopathy. Br Heart J 1985; 54: 48-52.

Been M, Smith M A, Ridgway J P, Brydon J W E, Douglas R H B, Kean D M, Best J J K, Muir A L. Characterisation of Acute Myocardial Infarction by Gated Magnetic Resonance Imaging. Lancet 1985; ii: 348-350.

Been M, Smith M A, Ridgway J P, Douglas R H B, De Bono D P, Best J J K, Muir A L. Serial Changes in the T1 Magnetic Relaxation Parameter after Myocardial Infarction in Man. Br Heart J 1988; 59: 1-8.

Been M, Thomson B J, Smith M A, Ridgway J P, Douglas R H B, Been M, Best J J K, Muir A L. Myocardial Involvement in Systemic Lupus Erythematosus Detected by Magnetic Resonance Imaging. Europ Heart J 1988; 9:1250-1256.

Beischer D E, Knepton J C Jr. Influence of Strong Magnetic Fields on the Electrocardiogram of Squirrel Monkeys (Saimiri sciureus). Aerospace Med 1964; 35: 939-944.

Bellossi A, de Certaines J, Bernard A M. Is There an Association between Myocardial Infarction and Geomagnetic Activity? Int J Biometeorol 1985; 29: 1-6.

Bellossi A, Toujas L. The Effect of a Static Uniform Magnetic Field on Mice. Radiat Environ Biophys 1982; 20: 153-157.

Berbel L N, Miro R E. Pulmonary Hypertension in the Pathogenesis of Cor Pulmonale. Cardiovasc Rev 1983; 4: 359-364.

Berger H J, Matthay R A, Loke J, Marshall R C, Gottschalk A, Zaret B L. Assessment of Cardiac Performance with Quantitative Radionuclide Angiocardiography : Right Ventricular Ejection Fraction with Reference to Findings in Chronic Obstructive Pulmonary Disease. Am J Cardiol 1978; 41: 897-905.

Berman E. Reproductive Effects. In: Biological Effects of Radiofrequency Radiation, Report EPA-600/8-83-026A. Bethesada, Md: US Environmental Protection Agency 1984.

Biernacki W, Flenley D C, Muir A L, MacNee W. The Effect of Pulmonary Hypertension and Right Ventricular Function in Patients with COPD. Chest 1988; 94: 1169-1175.

Bishop J M, Cross K W. Use of Other Physiological Variables to Predict Pulmonary Arterial Pressure in Patients with Chronic Respiratory Disease - A Multicentre Study. Eur Heart J 1981; 2: 509-517.

Bland J M, Altmann D G. Statistical Methods for Assessing Agreement between Two Methods of Clinical Measurement. The Lancet, February 8; 1986; 307-310.

Blanke H, Von Hardenberg D, Cohen M, Kaiser H, Karsch K R, Holt J, Smith H, Rentrop P. Patterns of Creatine Kinase Release during Acute Myocardial Infarction after Nonsurgical Reperfusion: Comparison with Conventional Treatment and Correlation with Infarct Size. J A C C 1984; 3: 675-680.

Bleifeld W, Mathey D, Hanrath P, Buss H, Effert S. Infarct Size Estimated from Serial Serum Creatine Phosphokinase in Relation to Left Ventricular Haemodynamics. Circulation 1977; 55: 303-311.

Bloch F, Hanson W W, Packard M E. Nuclear Induction. Physical Review 1946; 69: 127.

Bommer W, Weinert L, Neumann A, Neef J, Mason D T, DeMaria A. Determination of Right Atrial and Right Ventricular Size by Two-Dimensional Echocardiography. Circulation 1979; 60; 91-100.

Bonte F J, Parkey R W, Graham K D, Moore R T, Stokely E M. A New Method for Radionuclide Imaging of Myocardial Infarcts. Radiology 1974; 110: 473-474.

Bottomley P A, Edelstein W A. Power Deposition in Whole Body NMR Imaging. Med Phys 1981; 8: 510-512.

Bottomley P A, Reddington R W, Edelstein W A, Schenck J F. Estimating Radiofrequency Power Deposition in Body NMR Imaging. Magn Reson Med 1985; 2: 336-349.

Bouchard A, Reeves R C, Cranney G, Bishop S P, Pohost G M, Bischoff P. Assessment of Myocardial Infarct Size by Means of T2-weighted 1H Nuclear Magnetic Resonance Imaging. Am Heart J 1989; 117(2): 281-289.

Bove K E, Rowlands D T, Scott R C. Observations on the Assessment

of Cardiac Hypertrophy Utilising a Chamber Partition Technique. Circulation 1966; 33: 558-568.

Bowen W G, Branconi J M, Goldstein R A, Cain M E, Brodarick S M, Geltman E M, Jaffe A S, Ambos H D, Roberts R. A Randomized Prospective Study of the Effects of Intravenous Nitroglycerin in Patients During Myocardial Infarction. Circulation 1979; 60 (Suppl II. No 4): II-70.

Boyd K D, Thomas S J, Gold J and Boyd A D. A Prospective Study of Complications of Pulmonary Artery Catheterisation in 500 Consecutive Patients. Chest 1983; 84: 245-249.

Brady T J, Goldman M R, Pykett I L, Buonanno F S, Kistler J P, Newhouse J H, Burt C T, Hinshaw W S, Pohost G M. Proton Nuclear Magnetic Resonance Imaging of Regionally Ischemic Canine Hearts : Effect of Paramagnetic Proton Signal Enhancement. Radiology 1982; 144: 343-347.

Braunwald E. The Pathogenesis and Treatment of Shock in Myocardial Infarction. John Hopkins Med J 1967; 121: 421-429.

Buda A J, Aisen A M, Juni J E, Gallagher K P, Zotz R J. Detection and Sizing of Myocardial Ischaemia and Infarction by Nuclear Magnetic Resonance Imaging in the Canine Heart. Am Heart J 1985; 110: 1284-1290.

Budinger T F. Nuclear Magnetic Resonance (NMR) In Vivo Studies:

Known Thresholds for Health Effects. J Comput Assist Tomogr 1981; 5: 800-811.

Buja L M, Parkey R W, Stokley E M, Bonte F J, Willerson J T. Pathophysiology of Technetium-99m Stannous Pyrophosphate and Thallium-201 Scintigraphy of Acute Anterior Myocardial Infarcts in Dogs. J Clin Invest 1976; 57: 1508-1522.

Buja L M, Tofe A J, Kulkarni P V, Mukherjee A, Parkey R W, Francis M D, Bonte F J, Willerson J T. Sites and Mechanisms of Localization of Technetium-99m Phosphorus Radiopharmaceuticals in Acute Myocardial Infarcts and Other Tissues. J Clin Invest 1977; 60: 724-740.

Buonanno F S, Brady T J, Pykett I L, Burt C T, Vielma J, Newhoose P F J, Taveras J, Hinshaw W S, Goldman M R, Kistler J P, Pohost G M. NMR Clinical Results: Massachusetts General Hospital. In: Partain C L, James A E, Rollo F D, Price R R (Eds). NMR Imaging, Saunders, Philadelphia 1983, pp 207-230.

Burrows B, Strauss R H, Niden A H. Chronic Obstructive Lung Disease III. Interrelationships of Pulmonary Function Data. Am Rev Respir Dis 1965; 91: 861-868.

Bussman W D, Pasek D, Seidel W, Kaltenbach M. Reduction of CK and CK-MB Indexes of Infarct Size by Intravenous Nitroglycerin. Circulation 1981; 63: 615-622.

Bussman W D, Schofer H, Kurita A, Ganz W. Nitroglycerin in Acute Myocardial Infarction : X Effect of Small and Large Doses of Nitroglycerin on Sigma ST Segment Deviation - Experimental and Clincial Results. Clin Cardiol 1979; 2: 106-112.

Bydder G M, Goatcher A, Hughes J M B, Orr J S, Pennock J M, Steiner R E, Tripathi A. Effect of Oxygen Tension on Nuclear Magnetic Resonance Spin-lattice Relaxation Rate of Blood In-Vivo. J Physiol (Lond) 1982; 332: 46-47 (P).

Cairns J A, Holder D A, Tanser P, Missirlis E. Intravenous Hyaluronidase Therapy for Myocardial Infarction in Man : Double-blind Trial to Assess Infarct Size Limitation. Circulation 1982; 65: 764-771.

Cairns J A, Klassen GA. The Effect of Propranolol on Canine Myocardium CPK Distribution Space and Rate of Disappearance. Circulation 1977; 56: 284-288.

Cairns J A, Missirlis E, Fallen E L. Myocardial Infarction Size from Serial CPK : Variability of CPK Serum Entry Ratio with Size and Model of Infarction. Circulation 1978; 58: 1143-1153.

Caputo G R, Sechtem V, Tscholakoff D, Higgins C B. Measurement of Myocardial Infarct Size at Early and Late Time Intervals Using NMR Imaging. An Experimental Study in Dogs. Radiology 1987; 140: 237-243.

Carlsson E, Keene R J, Lee P, Goerke R J. Angiocardiographic Stroke-Volume Correlation of the Two Cardiac Ventricles in Man. Invest Radiol 1971; 6: 44-51.

Center for Devices and Radiological Health MR Product Reporting Program and Medical Device Report Program. Washington DC: U S Food & Drug Administration 1989.

Chapman C B, Baker O, Reynolds J, Bonte F J. Use of Biplane Cinefluorography for Measurement of Ventricular Volume. Circulation 1958; 18: 1105-1117.

Chandler A B, Chapman I, Erhardt L R, Roberts W C, Schwartz C J, Sinapius D, Spain D M, Sherry S, Nees P M, Simon T L. Coronary Thrombosis in Myocardial Infarction. Am J Cardiol 1974; 34: 823-832.

Chang S, Feigenbaum H. Subxiphoid Echocardiography. J Clin Ultrasound 1973; 1-14.

Chenevert T L, Brunberg J A, Pipe J G. Anisotropic Diffusion within Human White Matter : Demonstration with NMR Techniques In Vivo. Radiology 1990; 177: 401-405.

Chiche P, Baligadoo S J, Derrida J P. A Randomised Trial of Prolonged Nitroglycerin Infusion in Acute Myocardial Infarction. Circulation 1979; 60 (Suppl II): II-165. Abstract.

Cohen H A, Baird M G, Rouleau J R, Fuhrmann C F, Bailey I K, Summer W R, Strauss W, Pitt B. Thallium-201 Myocardial Imaging in Patients with Pulmonary Hypertension. Circulation 1976; 54: 790-795.

Corbett J R, Lewis S E, Wolfe C L, Jansen D E, Lewis M, Rellas J S, Parkey R W, Rude R E, Buja L M, Willerson J T. Measurement of Myocardial Infarct Size by Technetium Pyrophosphate Single-Photon Tomography. Am J Cardiol 1984; 54: 1231-1236.

Corbett J R, Lewis M, Willerson J T, Nicod P H, Huxley R L, Simon T, Rude R E, Henderson E, Parkey R, Rellas J S, Buja L M, Sokolov J J, Lewis S E. 99mTc-Pyrophosphate Imaging in Patients with Acute Myocardial Infarction : Comparison of Planar Images with Single-Photon Tomography with and without Blood Pool Overlay. Circulation 1984; 69: 1120-1128.

Corbett J R, Lewis M, Willerson J T, Huxley R, Simon T, Nicod P, Henderson E, Rude R E, Lewis S E. Technetium-99m Pyrophosphate Imaging in Acute Myocardial Infarction: Comparison of Planar Images with Superimposition Tomography (Abst). Circulation 1982; 66: Suppl II: II-273.

Cox J R, Roberts R, Ambus H D, Oliver C, Sobel B E. Relations between Enzymatically Estimated Myocardial Infarct Size and Early Ventricular Dysrhythmia. Circulation 1976; 53 (suppl 1): 150-155.

Cromie J B. Correlation of Anatomic Pulmonary Emphysema and Right

Ventricular Hypertrophy. Am Rev Respir Dis 1961; 84: 657-662.

Crooks L E, Barker B, Chang H, Feinberg D, Hoenninger J C, Watts J C, Arakawa M, Kaufman L, Sheldon P E, Botvinick E, Higgins C B. Magnetic Resonance Imaging Strategies for Heart Studies. Radiology 1984; 153: 459-465.

Cullen J H, Kaemmerlen J T, Daoud A, Katz H L. A Prospective Clinical-Pathologic Study of the Lungs and Heart in Chronic Obstructive Lung Disease. Am Rev Respir Dis 1970; 102: 190-204.

Damadian R. Apparatus and Method for Detecting Cancer in Tissue. US Patent No 3789832, Filed March 17, 1972.

Damadian R. Tumour Detection by Nuclear Magnetic Resonance. Science 1971; 171: 1151-1153.

Damadian R, Goldsmith M, Minkoff L. NMR in Cancer : XVI FONAR Image of the Live Human Body. Physiol Chem Phys 1977; 9: 97-100.

Damadian R, Goldsmith M, Minkoff L. NMR in Cancer : XX FONAR Scans of Patients with Cancer. Physiol Chem Phys 1978; 10: 285-287.

Davies L G, Goodwin J F, Steiner R E, Van Leuven B D. The Clinical and Radiological Assessment of the Pulmonary Arterial Pressure in Mitral Stenosis. Br Heart J 1953; 15: 393-400.

Davies M J, Woolf N, Robertson W P. Pathology of Acute Myocardial

Infarction with Particular Reference to Occlusive Coronary Thrombi. Br Heart J 1976; 38: 659-664.

Dehmer G J, Firth B G, Lewis S E, Willerson J T, Hillis L D. Direct Measurement of Cardiac Output by Gated Equilibrium Blood Pool Scintigraphy : Validation of Scintigraphic Volume Measurements by a Nongeometric Technique. Am J Cardiol 1981; 47: 1061-1067.

Dell'Italia L J, Starling M R, Walsh R A, Badke F R, Lasher J C, Blumhardt R. Validation of Attenuation - Corrected Equilibrium Radionuclide Angiographic Determinations of Right Ventricular Volume : Comparison with Cast - Validated Biplane Cineventriculography. Circulation 1985; 72(2); 317-326.

De Roos A, Van Rossum A C, Van der Wall E, Postema S, Doornbos J, Matheijssen N, Van Dijkman P R M, Visser F C, Van Voorthuisen A E. Reperfused and Non-reperfused Myocardial Infarction: Diagnostic Potential of Gd-DTPA-enhanced MR Imaging. Radiology 1989; 172: 717-720.

Dewhurst N G, Muir A L. Comparative Prognostic Value of Radionuclide Ventriculography at Rest and During Exercise in 100 Patients after First Myocardial Infarction. Br Heart J 1983; 49: 111-121.

De Wood M A, Spores J Notske R, Mouser, L T, Burroughs R, Golden M S, Lang H T. Prevalence of Total Coronary Occlusion During the Early Hours of Transmural Myocardial Infarction. N Engl J Med

1980; 303: 897-902.

Didier D, Higgins C B. Identification and Localization of Ventricular Septal Defects by Gated Magnetic Resonance Imaging. Am J Cardiol 1986; 57: 1363-1368.

Didier D, Higgins C B, Fisher M R, Osaki L, Silverman N H, Cheitlin M D. Gated Magnetic Resonance Imaging in Congenital Heart Disease: Experience in 72 Patients. Radiology 1986, 158: 227-236.

Dodge H T, Sandler H, Ballew D W, Lord J D Jr. The Use of Biplane Angiocardiography for Measurement of Left Ventricular Volume in Man. Am Heart J 1960; 60: 762-776.

Doherty J U, Whitman G J R, Robinson M D, Harken A H, Simson M B, Spear J F, Josephson M E. Changes in Cardiac Excitability and Vulnerability in NMR Fields. Invest Radiol 1985; 20: 129-135.

Dotter C T, Steinberg (Eds). Angiocardiography. New York: Harper and Brothers, 1953.

Duling B R, Berne R M. Longitudinal Gradients in Periarteriolar Oxygen Tension : A Possible Mechanism for the Participation of Oxygen in Local Regulation of Blood Flow. Circulat Res 1970; 27: 669-678.

Durand J, Leroy-Ladurie M, Ransom-Bitker B. Effects of Hypoxia and Hypercapnia on the Repartition of Pulmonary Blood Flow in Supine

Subjects. Prog Resp Res 1970; 5: 156-165.

Eaton L W, Bulkley B H. Expansion of Acute Myocardial Infarction : Its Relationship to Infarct Morphology in a Canine Model. Circulat Res 1981; 49: 80-88.

Edelstein W A, Hutchinson J M S, Johnson G and Redpath T W. Spin-warp NMR Imaging and Applications to Human-Whole Body Imaging. Phys Med Biol 1980; 25: 751-756.

Edelstein W A, Hutchinson J M S, Smith F W, Mallard J, Johnson G, Redpath T W. Human Whole-Body NMR Tomographic Imaging : Normal Sections. Br J Radiol 1981; 54: 149-151.

Ellis S G, Henschke C Im, Sandor T, Wynne J, Braunwald E, Kloner R A. Time Course of Functional and Biochemical Recovery of Myocardium Salvaged by Reperfusion. J A C C 1983; 1: 1047-1055.

EMI Ltd: Exhibit. Radiological Society of North America, Chicago, 1978.

Epstein S E, Braunwald E. Beta-Adrenergic Receptor Blocking Drugs : Mechanisms of Action and Clinical Applications. N Engl J Med 1966; 275: 1106-1112.

Epstein S E, Kent K M, Goldstein R E, Borer J S, Redwood D R. Reduction of Ischaemic Injury by Nitroglycerin During Acute Myocardial Infarction. N Engl J Med 1975; 292: 29-35.

Erlebacher J A, Weiss J L, Eaton L W, Kallman C, Weisfeldt M L, Bulkley B H. Late Effects of Acute Infarct Dilation on Heart Size : A Two Dimensional Echocardiographic Study. Am J Cardiol 1982; 49: 1120-1126.

Ertl G, Kloner R A, Alexander R W, Braunwald E. Limitation of Experimental Infarct Size by an Angiotension - Converting Enzyme Inhibitor. Circulation 1982; 65: 40-48.

Evans S J, Mills P, Dawson J. The End of the p Value? Br Heart J 1988; 60: 177-180.

Farmer D, Higgins C B, Yee E, Lipton M J, Wahr D, Ports T. Tissue Characterization by Magnetic Resonance Imaging in Hypertrophic Cardiomyopathy. Am J Cardiol 1985; 55: 230-232.

Feigenbaum H. Echocardiography. 2nd Ed. Philadelphia: Lea and Febiger, 1976: 255-266.

Feigenbaum H, Popp R L, Chip J N, Haine C L. Left Ventricular Wall Thickness Measured by Ultrasound. Arch Intern Med 1968; 121: 391-395.

Feigenbaum H, Popp R L, Wolfe S B, Troy B L, Pombo J F, Haine C L, Dodge H T. Ultrasound Measurements of the Left Ventricle. A Correlative Study with Angiocardiography. Arch Intern Med 1972; 129: 461-467.

Ferlinz J. Right Ventricular Function in Adult Cardiovascular Disease. Prog Cardiovasc Dis 1982; 25: 225-261.

Ferlinz J, Delvicario M, Gorlin R. Incidence of Right Ventricular Asynergy in Patients with Coronary Artery Disease. Am J Cardiol 1976; 38: 557-563.

Ferlinz J, Gorlin R, Cohn P F, Herman M V. Right Ventricular Performance in Patients with Coronary Artery Disease. Circulation 1975; 52: 608-615.

Fetter J, Aram G, Holmes D R Jr, Gray J E, Hayes D L. The Effects of Nuclear Magnetic Resonance Imagers on External and Implantable Pulse Generators. PACE 1984; 7: 720-727.

Fisher E A, DuBrow I W, Hastreiter A R. Right Ventricular Volume in Congenital Heart Disease. Am J Cardiol 1975; 36: 67-75.

Fisher M R, McNamara M T, Higgins C B. Acute Myocardial Infarction : MR Evaluation in 29 Patients. A J R 1987; 148: 247-251.

Fishman A P. Chronic Cor Pulmonale. Am Rev Respir Dis 1976; 114: 775-794.

Fishman A P. The Left Ventricle in "Chronic Bronchitis and Emphysema" (Editorial). N Eng J Med 1971; 285: 402-404.

Fishman A P, McClement J, Himmelstein A, Cournand A. Effects of

Acute Anoxia on the Circulation and Respiration in Patients with Chronic Pulmonary Disease Studied During the "Steady State". J Clin Invest 1952; 31: 770-781.

Flaherty J A, Hoskinson K. Emotional Distress During Magnetic Resonance Imaging. N Engl J Med 1989; 320: 467-468.

Flaherty J T, Becker L C, Weisfeldt M L. Results of a Prospective Randomised Clinical Trial of Intravenous Nitroglycerin in Acute Myocardial Infarction. Circulation 1980; 62 (Suppl III) III-82 Abstract.

Fletcher B D, Jacobstein M D, Nelson A D, Riemenschneider T A, Alfidi R J. Gated Magnetic Resonance Imaging of Congenital Cardiac Malformations. Radiology 1984; 150: 137-140.

Foale R, Nihoyannopoulos, McKenna W, Klienebenne A, Nadazdin A, Rowland E, Smith G. Echocardiographic Measurement of the Normal Adult Right Ventricle. Br Heart J 1986; 56: 33-44.

Foale R, Stefanini L, Rickards A, Somerville J. Left and Right Ventricular Morphology in Complex Congenital Heart Disease Defined by Two Dimensional Echocardiography. Am J Cardio 1982; 49: 93-99.

Foraker A G, Bedrossain C W M, Anderson A E Jr. Myocardial Dimensions and Proportions in Pulmonary Emyphysema. Arch Pathol 1970; 90: 344-347.

Fortuin N J, Hood W P, Sherman M E Jr, Craige E. Determination of Left Ventricular Volumes by Ultrasound. Circulation 1971; 44: 575-584.

Fowler N O, Daniels C, Scott R C, Faustino B S, Gueron M. The Electrocardiogram in Cor Pulmonale With and Without Emphysema. Am J Cardiol 1965; 16: 500-505.

Fowler N O, Westcott R N, Scott R C. The Q Wave in Precordial Electrocardiograms Overlying the Hypertrophied Right Ventricle : Intracavitary Leads. Circulation 1952; 5: 441-448.

Frahm J, Hasses A, Matthaei D. Rapid NMR Imaging of Dynamic Processes using the FLASH Technique. Magn Reson Med 1986; 3: 321-327.

Fulton R M, Hutchison E C, Jones A M. Ventricular Weight in Cardiac Hypertrophy. Br Heart J 1952; 14: 413-420.

Ganz W, Buchbinder N, Marcus H, Mondkar A, Maddahi J, Charuzi Y, O'Connor L, Shell W, Fishbein M C, Kass R, Miyamoto A, Swan H J C. Intracoronary Thrombolysis in Evolving Myocardial Infarction. Am Heart J 1981; 101: 4-13.

Ganz W, Geft I, Maddahi J, Berman D, Charuzi Y, Shah P K, Swan H J C. Non-surgical Reperfusion in Evolving Myocardial Infarction. J A C C 1983; 1: 1247-1253.

Geard C R, Osmack R S, Hall E J, Simon H E, Maudsley A A, Hilal S K. Magnetic Resonance and Ionizing Radiation: A Comparative Evaluation In Vitro of Oncogenic and Genotoxic Potential. Radiology 1984; 152: 199-202.

Geltman E M, Ehsani A A, Campbell M K, Schechtman K, Roberts R, Sobel B E. The Influence of Location and Extent of Myocardial Infarction on Long-term Dysrhythmia and Mortality. Circulation 1979; 60: 805-814.

Gentzler R D, Briselli M F, Gault J H. Angiographic Estimation of Right Ventricular Volume in Man. Circulation 1974; 50: 324-330.

George C R, Jacobs G, MacIntyre W J, Lorig R J, Go R T, Nose Y, Meaney T F. Magnetic Resonance Signal Intensity Patterns Obtained from Continuous and Pulsatile Flow Models. Radiology 1984; 151: 421-428.

Gerber K H, Higgins C G. Quantitation of Size of Myocardial Infarctions by Computerized Transmission Tomography. Comparison with Hot-spot and Cold-spot Radionuclide Scans. Invest Radiology 1983; 18: 238-244.

Ginks W R, Sybers H D, Maroko P R, Covell J W, Sobel B E, Ross J. Coronary Artery Reperfusion II. Reduction of Myocardial Infarct Size at One Week after Coronary Occlusion. J Clin Invest 1972; 51: 2717-2723.

The GISSI Study Group. Infarto Miocardico: L'esperienza del GISSI: Rilievi Preliminari. Presented at the 19th Corso di Aggiornamento. Milan, Italy, September 9-14, 1985.

Go R T, MacIntyre W J, Yeung H N, Kramer D M, Geisinger M, Chilcote W, George C, O'Donnell J K, Moodie D S, Meaney T F. Volume and Planar Gated Cardiac Magnetic Resonance Imaging: A Correlative Study of Normal Anatomy with Thallium-201 SPECT and Cadaver Sections. Radiology 1984; 150: 129-135.

Goerke R J, Carlsson E. Calculation of Right and Left Cardiac Ventricular Volumes: Method Using Standard Computer Equipment and Biplane Angiocardiograms. Invest Radiol 1967; 2: 360-367.

Goldberger E. Unipolar Lead Electrocardiography. 1947 H Kimpton, London.

Goodwin J F, Cleland W P, Hunter J D, Davies L G, Steiner R E. Mitral Valve Disease and Mitral Valvotomy. Br Med J 1955; 2: 573-585.

Graham T P, Jarmakani J M, Atwood G F, Canent R V. Right Ventricular Volume Determinations in Children : Normal Values and Observations with Volume or Pressure Overload. Circulation 1973; 47: 144-153.

Grande P, Hansen B F, Christiansen C, Naestoft J. Estimation of Acute Myocardial Infarct Size in Man by Serum CK-MB Measurements.

Circulation 1982; 65: 756-764.

Gray W R, Buja L M, Hagler H K, Parkey R W, Willerson J T. Computed Tomography for Localization and Sizing of Experimental Acute Myocardial Infarcts. Circulation 1978; 58: 497-504.

Gray W R, Parkey R W, Buja L M, Stokely E M, McAllister R E, Bonte F J, Willerson J T. Computed Tomography : In Vitro Evaluation of Myocardial Infarction. Radiology 1977; 122: 511-513.

Green K G, Chamberlain D A, Fulton R M, Hamer N A J, Oliver M F, Pentecost B L, Lewis J A, Tuson R. Reduction in Mortality after Myocardial Infarction with Long-term Beta-Adrenoceptor Blockade. Multicentre International Study : Supplementary Report. Br Med J 1977; 2: 419-421.

Gruppo Italiano per lo Studio della Streptochinasi nell'Infarto Miocardico (GISSI). Effectiveness of Intravenous Thrombolytic Treatment in Acute Myocardial Infarction. Lancet 1986; i: 397-402.

Gruppo Italiano per lo Studio della Streptochinasi nell'Infarto Miocardico (GISSI). Long-term Effects of Intravenous Thrombolysis in Acute Myocardial Infarction: Final Report of the GISSI Study. Lancet 1987; ii: 871-874.

Gulch R W, Lutz O. Influence of Strong Static Magnetic Fields on Heart Muscle Contraction. Phys Med Biol 1986; 31: 763-769.

Haneda T, Lee T, Ganz W. Metabolic Effects of Propranolol in the Ischaemic Myocardium Studied by Regional Sampling. Circulation 1973; 48 (Suppl IV): IV-174 Abstract.

Harnarayan C, Bennett M A, Pentecost B L, Brewer D B. Quantitative Study of Infarcted Myocardium in Cardiogenic Shock. Br Heart J 1970; 32: 728-732.

Harolds J A, Grove R B, Bowen R D, Powers T A. Right Ventricular Function as Assessed by Two Radionculide Techniques : Concise Communication. J Nucl Med 1981; 22: 113-115.

Harvey R M, Ferrer M I, Richards D W, Cournand A. Influence of Chronic Pulmonary Disease on the Heart and Circulation. Am J Med 1951; 10: 719-738.

Hasleton P S, Heath D, Brewer D B. Hypertensive Pulmonary Vascular Disease in States of Chronic Hypoxia. J Path Bact 1968; 95: 431-440.

Hawkes R C, Holland G N, Moore W S, Roebuck E J, Worthington B S. Nuclear Magnetic Resonance (NMR) Tomography of the Normal Heart. J Comput Assist Tomogr 1981; 5: 605-612.

Hayes D L, Holmes D R, Gray J E. The Effects of 1.5 Tesla Nuclear Magnetic Resonance Imaging Scanner on Implanted Permanent Pacemakers. J A C C 1987; 10: 782-786.

Heath D, Edwards C, Winson M, Smith P. Effects on the Right Ventricle, Pulmonary Vasculature, and Carotid Bodies of the Rat of Exposure to and Recovery from, Simulated High Alitude. Thorax 1973; 28: 24-28.

Heikkila J, Nieminen M S. Failure of Methylprednisolone to Protect Acutely Ischemic Myocardium : A Contrast with Subsequent Beta-Adrenergic Blockade in Man. Chest 1978; 73: 577-582.

Herfkens R J, Sievers R, Kaufman L, Sheldon P E, Ortendahl D A, Lipton M J, Crooks L E, Higgins C B. Nuclear Magnetic Resonance Imaging of the Infarcted Muscle : A Rat Model. Radiology 1983; 147: 761-764.

Hermens W T, Willems G M, Visser M P. Quantification of Circulating Proteins. Theory and Application Based on Analysis of Plasma Protein Levels. The Hague: Martins Nijhoff 1982.

Higgins C B. New Horizons in Cardiac Imaging. Radiology 1985; 156: 577-588.

Higgins C B, Byrd B F, McNamara M T, Lanzer P, Lipton M J, Botvinick E, Schiller N B, Crooks L E, Kaufman L. Magnetic Resonance Imaging of the Heart: A Review of the Experience in 172 Subjects. Radiology 1985; 155: 671-679.

Higgins C B, Byrd B F, Stark D, McNamara M, Lanzer P, Lipton M J, Schiller N B, Botvinick E, Chatterjee K. Magnetic Resonance

Imaging of Hypertrophic Cardiomyopathy. Am J Cardiol 1985; 55: 1121-1126.

Higgins C B, Herfkens R, Lipton M J, Sievers R, Sheldon P, Kaufman L, Crooks L E. Nuclear Magnetic Resonance Imaging of Acute Myocardial Infarction in Dogs: Alterations in Magnetic Relaxation Times. Am J Cardiol 1983; 52: 184-188.

Higgins C B, Lanzer P, Stark D, Botvinick E, Schiller N, Crooks L, Kaufman L, Lipton M J. Imaging by Nuclear Magnetic Resonance in Patients with Chronic Ischemic Heart Disease. Circulation 1984; 60: 523-531.

Hillis L D, Askenazi J, Braunwald E, Radvany P, Muller J E, Fishbein M C, Maroko P R. Use of Changes in the Epicardial QRS Complex to Assess Interventions which Modify the Extent of Myocardial Necrosis Following Coronary Artery Occlusion. Circulation 1976; 54: 591-598.

Hinshaw W S. Image Formation by NMR : The Sensitive Point Method. J App Phys 1976; 47: 3709.

Hinshaw W S. Spin Mapping : The Application of Moving Gradients to NMR. Phys Lett 1974; 48A: 87.

Hinshaw W S, Bottomley P A, Holland G N. Radiographic Thin-Section Image of the Human Wrist by Nuclear Magnetic Resonance. Nature 1977; 270: 722-723.

Hirata T, Wolfe S B, Popp R L, Helmen C H, Feigenbaum H. Estimation of Left Atrial Size Using Ultrasound. Am Heart J 1969; 78: 43-52.

Hirshfeld J W Jr, Borer J S, Goldstein R E, Barrett M J, Epstein S E. Reduction in Severity and Extent of Myocardial Infarction when Nitroglycerin and Methoxamine are Administered During Coronary Occlusion. Circulation 1974; 49: 291-297.

Hochman J S, Bulkley B H. Pathogenesis of Left Ventricular Aneurysms : An Experimental Study in the Rat Model. Am J Cardiol 1982; 50: 83-88.

Holman B L, Goldhaber S Z, Kirsch C M, Polak J F, Friedman B J, English R J, Wynne J. Measurement of Infarct Size Using Single Photon Emission Computed Tomography and Technetium-99m Pyrophosphate: A Description of the Method and Comparison with Patient Prognosis. Am J Cardiol 1982; 50: 503-511.

Holman B L, Tanaka T T, Lesch M. Evaluation of Radiopharmaceuticals for the Detection of Acute Myocardial Infarction in Man. Radiology 1976; 121: 427-430.

Holmes D R Jr, Hayes D L, Gray J E, Meredith J. The Effects of Magnetic Resonance Imaging on Implantable Pulse Generators. PACE 1986; 9: 360-370.

Hong C Z, Harmon D, Yu J. Static Magnetic Field Influence on Rat

Tail Nerve Function. Arch Phys Med Rehabil 1986; 67: 746-749.

Horn V, Mullins C B, Saffer S I, Jones D C, Freeborn W A, Knapp R S, Nixon J V. A Comparison of Mathematical Models for Estimating Right Ventricular Volumes in Animals and Man. Clin Cardiol 1979; 2: 341.

Horsfield K, Segel N, Bishop J M. The Pulmonary Circulation in Chronic Bronchitis at Rest and During Exercise Breathing Air and 80% Oxygen. Clin Sci 1968; 34: 473-483.

Hutchins G M, Bulkley B H. Infarct Expansion Versus Extension : Two Different Complications of Acute Myocardial Infarction. Am J Cardiol 1978; 41: 1127-1132.

ISAM Study Group. A Prospective Trial of Intravenous Streptokinase in Acute Myocardial Infarction (I S A M). Mortality, Morbidity and Infarct Size at 21 Days. N Eng J Med 1986; 314: 1465-1471.

ISIS-2 (Second International Study of Infarct Survival) Collaborative Group. Randomised Trial of Intravenous Streptokinase, Oral Aspirin, Both, or Neither Among 17,187 Cases of Suspected Acute Myocardial Infarction: ISIS-2. Lancet 1988: 2: 349-360.

Jacobstein M D, Fletcher B D, Goldstein S, Riemenschneider T A. Evaluation of Atrioventricular Septal Defect by Magnetic Resonance Imaging. Am J Cardiol 1985; 55: 1158-1161.

Jansen D E, Corbett J R, Wolfe C L, Lewis S E, Gabliani G, Filipchuk N, Radish G, Parkey R W, Buja L M, Jaffe A S, Rude R, Sobel B E, Willerson J T. Quantification of Myocardial Infarction: A Comparison of Single Photon-Emission Computed Tomography with Pyrophosphate to Serial Plasma MB-Creatine Kinase Measurements. Nucl Cardiol 1985; 72: 327-333.

Jaszczak R J, Chang L T, Stein N A, Moore F E. Whole-Body Single-Photon Emission Computed Tomography Using Dual, Large-Field-of-View Scintillation Cameras. Phys Med Biol 1979; 24: 1123-1143.

Jaszczak R J, Coleman R E, Whitehead F R. Physcial Factors Affecting Quantitative Measurements Using Camera-Based Single Photon Emission Computed Tomography. IEEE Trans Nucl Sci 1981; NS-28: 69-80.

Jehensen P, Duboc D, Lavergne T, Guize L, Guerin F, Degeorges M, Syrota A. Changes in Human Cardiac Rhythm Induced by a 2-T Static Magnetic Field. Radiology 1988; 166: 227-230.

Jeremy R W, Allnan K C, Bantovitch G, Harris P J. Patterns of Left Ventricular Dilatation During the Six Months after Myocardial Infarction. J A C C 1989; 13: 304-310.

Johnston D L, Brady T J, Ratner A V, Rosen B R, Nowell J B, Pohost G M, Okada R D. Assessment of Myocardial Ischemia with Proton Magnetic Resonance : Effects of a Three Hour Coronary Occlusion With and Without Reperfusion. Circulation 1985; 71: 595-601.

Jugdutt B I, Becker L C, Hutchins G M, Bulkley B H, Reid P R, Kallman C H. Effect of Intravenous Nitroglycerin on Collateral Blood Flow and Infarct Size in the Conscious Dog. Circulation 1981; 63: 17-28.

Karmen A, Wroblewski F, La Due J S. Transaminase Activity in Human Blood. J Clin Invest 1955; 34: 126-133.

Kaufman L, Crooks L E, Sheldon P, Hricak H, Herfkens R, Bank W. The Potential Impact of Nuclear Magnetic Resonance Imaging on Cardiovascular Diagnosis. Circulation 1983; 67: 251-257.

Kaul S, Wisner G L, Brady T J, Johnston D L, Weyman A E, Okada R D, Dinsmore R E. Measurement of Normal Left Heart Dimensions using Optimally Orientated MR Images. A J R 1986; 146: 75-79.

Kawakami Y, Kishi F, Yamamoto H, Miyamoto K. Relation of Oxygen Delivery, Mixed Venous Oxygenation, and Pulmonary Hemodynamics to Prognosis in Chronic Obstructive Pulmonary Disease. N Engl J Med 1983; 308: 1045-1049.

Khaja F U, Alam M, Goldstein S, Anbe D T, Marks D S. Diagnostic Value of Visualization of the Right Ventricle using Thallium-201 Myocardial Imaging. Circulation 1979; 59: 182-188.

Khaja F U, Parker J O. Right and Left Ventricular Performance in Chronic Obstructive Lung Disease. Am Heart J 1971; 82: 319-327.

Kilburn K H, Asmundsson T, Britt R C, Cardon R. Effects of Breathing 10 per cent Carbon Dioxide on the Pulmonary Circulation of Human Subjects. Circulation 1969; 39: 639-653.

Kloner R A, Braunwald E, Maroko P R. Long-term Preservation of Ischaemic Myocardium in the Dog by Hyaluronidase. Circulation 1978; 58: 220-226.

Kloner R A, Rude R E, Carlson N, Maroko P R, De Boer L W V, Braunwald E. Ultrastructural Evidence of Micro-Vascular Damage and Myocardial Cell Injury after Coronary Artery Occlusion : Which Comes First? Circulation 1980; 62: 945-952.

Knox E G, Armstrong E, Lancashire R. Heart Attacks and Geomagnetic Activity. Nature 1975; 281.

Kountz W B, Alexander H L, Prinzmetal M. The Heart in Emphysema. Am Heart J 1936; 11: 163.

Lamb D. Heart Weight and Assessment of Ventricular Hypertrophy. In Recent Advances in Clinical Pathology, Series 6, SC Dykes ed, Churchill Livingstone, London 1973; 133-148.

Lanzer P, Botvinick E H, Schiller N B, Crooks L E, Arakawa M, Kaufman L, Davis P L, Herfkens R, Lipton M J, Higgins C B. Cardiac Imaging Using Gated Magnetic Resonance. Radiology 1984; 150: 121-127.

Lauterbur P C. Image Formation by Induced Local Interactions : Examples Employing Nuclear Magnetic Resonance. Nature 1973; 242: 190-191.

LeBihan D. Diffusion/Perfusion MR Imaging of the Brain : From Structure to Function. Radiology 1990; 177: 328-329.

Lerski R A, Straughan K and Orr J S. Calibration of Proton Density Measurements in Nuclear Magnetic Resonance Imaging. Phys Med Biol 1984; 29: 271-276.

Lewis M H, Willerson J T, Lewis S E, Bonte F J, Parkey R W, Stokely E M. Attenuation Compensation on Single-Photon Emission Tomography: A Comparative Evaluation. J Nucl Med 1982; 23: 1121-1127.

Lewis S E, Corbett J R, Morgan C, Izquierdo C, Huxley R, Nicod P, Devous M D, Buja L M, Willerson J T. Single Photon Emission Tomographic Sizing of Experimental Myocardial Infarction: A Comparison of Infarct-Avid and Perfusion Markers (Abstr). J Nucl Med 1982; 23: p24.

Lewis S E, Devous M D, Corbett J R, Izquierdo C, Nicod P, Wolfe C L, Parkey R W, Buja L M, Willerson J T. Measurement of Infarct Size in Acute Canine Myocardial Infarction by Single-Photon Emission Computed Tomography with Technetium-99m Pyrophosphate. Am J Cardiol 1984; 54: 193-199.

Lieberman J M, Alfidi R J, Nelson A D, Botti R E, Moir T W, Haaga J R, Kopiwoda S, Miraldi F D, Cohen A M, Butler H E, Nara A, Hellerstein H K. Gated Magnetic Resonance Imaging of the Normal and Diseased Heart. Radiology 1984; 152: 465-470.

Liang C S, Gavras H, Black J, Sherman L G, Hood W B. Renin-Angiotension System Inhibition in Acute Myocardial Infarction in Dogs : Effects on Systemic Haemodynamics, Myocardial Blood Flow, Segmental Myocardial Function and Infarct Size. Circulation 1982; 66: 1249-1255.

Longmore D B, Klipstein R H, Underwood S R, Firmin D N, Hounsfield G N, Watanabe M, Bland C, Fox K, Poole-Wilson P A, Rees R S O, Denison D, McNeilly A M, Burman E D. Dimensional Accuracy of Magnetic Resonance in Studies of the Heart. Lancet 1985; 1: 1360-1362.

McAlpine H M, Findlay I N, Gillan G, Henderson E, Wilson J T, Dargie H J. Neuroendocrine Mechanisms in Acute Myocardial Infarction. Br Heart J 1986; 55: 503-504.

McKusick K A, Bingham J B, Pohost G M, Strauss H W. The Gated First Pass Radionuclide Angiogram : A Method for Measurement of Right Ventricular Ejection Fraction (Abstr). Circulation 1978; 58, Suppl ii: 11-30.

McNamara M T, Higgins C B, Schechtmann N, Botvinick E, Lipton M J,

Chatterjee K, Amparo E G. Detection and Characterization of Acute Myocardial Infarction in Man with the Use of Gated Magnetic Resonance. Circulation 1985; 71: 717-724.

McNamara M T, Tscholakoff D, Revel D, Soulen R, Schechtmann N, Botvinick E, Higgins C B. Differentiation of Reversible and Irreversible Myocardial Injury by MR Imaging with and without Gadolinium-DTPA. Radiology 1986; 158: 765-769.

MacNee W, Prince E, Flenley D C, Muir A L. The Effects of Pulmonary Hypertension on Right Ventricular Performance. Prog Respir Res 1984; 20: 108-116.

MacNee W, Wathen C G, Flenley D C, Muir AL. The Effects of Controlled Oxygen Therapy on Ventricular Function in Patients with Stable and Decompensated Cor Pulmonale. Am Rev Respir Dis 1988; 137: 1289-1295.

MacNee W, Xue Q F, Hannan W J, Flenley D C, Adie C J, Muir A L. Assessment by Radionuclide Angiography of Right and Left Ventricular Function in Chronic Bronchitis and Emphysema. Thorax 1983; 38: 494-500.

Maddahi J, Berman D S, Matsuoka D T, Waxman A D, Stankus K E, Forrester J S, Swan H J C. A New Technique for Assessing Right Ventricular Ejection Fraction using Rapid Multiple-Gated Equilibrium Cardiac Blood Pool Scintigraphy. Circulation 1979; 60: 581-589.

Mallard J. Royal Society Meeting of Nuclear Magnetic Resonance Intact Biological Systems 1979. McNamara M T, Tscholakoff D, Revel D, Soulen R, Schechtmann N, Botvinick E, Higgins C B. Differentiation of Reversible and Irreversible Myocardial Injury by MR Imaging with and without Gadolinium-DTPA. Radiology 1986; 158: 765-769.

MacNee W, Prince E, Flenley D C, Muir A L. The Effects of Pulmonary Hypertension on Right Ventricular Performance. Prog Respir Res 1984; 20: 108-116.

MacNee W, Wathen C G, Flenley D C, Muir AL. The Effects of Controlled Oxygen Therapy on Ventricular Function in Patients with Stable and Decompensated Cor Pulmonale. Am Rev Respir Dis 1988; 137: 1289-1295.

MacNee W, Xue Q F, Hannan W J, Flenley D C, Adie C J, Muir A L. Assessment by Radionuclide Angiography of Right and Left Ventricular Function in Chronic Bronchitis and Emphysema. Thorax 1983; 38: 494-500.

Maddahi J, Berman D S, Matsuoka D T, Waxman A D, Stankus K E, Forrester J S, Swan H J C. A New Technique for Assessing Right Ventricular Ejection Fraction using Rapid Multiple-Gated Equilibrium Cardiac Blood Pool Scintigraphy. Circulation 1979; 60: 581-589.

Mallard J. Royal Society Meeting of Nuclear Magnetic Resonance

Intact Biological Systems 1979.

Malmberg P. Time Course of Enzyme Escape Via Heart Lymph Following Myocardial Infarction in the Dog. Scan J Clin Lab Invest 1972; 30: 405-409.

Mansfield P, Maudsley A A, Baines T. Fast Scan Proton Density Imaging by NMR. J Phys E: Sci Instrum 1976; 9: 271-278.

Mansfield P, Pykett I L. Biological and Medical Imaging by NMR Imaging. J Magn Reson 1978; 29: 355-373.

Markiewicz W, Sechtem U, Higgins C B. Evaluation of the Right Ventricle by Magnetic Resonance Imaging. Am Heart J 1987; 113: 8-15.

Maroko P R, Kjekshus J K, Sobel B E, Watanabe T, Covell J W, Ross J, Braunwald E. Factors Influencing Infarct Size Following Experimental Coronary Artery Occlusions. Circulation 1971; 43: 67-82.

Maroko P R, Libby P, Bloor C M, Sobel B E, Braunwald E. Reduction by Hyaluronidase of Myocardial Necrosis Following Coronary Artery Occlusion. Circulation 1972; 46: 430-437.

Maroko P R, Libby P, Covell J W, Sobel B E, Ross J R, Braunwald E. Precordial S-T Segment Elevation Mapping : An Atraumatic Method for Assessing Alterations in the Extent of Myocardial Ischemic Injury.

Am J Cardiol 1972; 29: 223-230.

Maroko P R, Libby P, Ginks W R, Bloor C M, Shell W E, Sobel B E, Ross J. Coronary Artery Reperfusion I. Early Effects on Local Myocardial Function and the Extent of Myocardial Necrosis. J Clin Invest 1972; 51: 2710-2716.

Martins De Oliveira J, Carballo R, Zimmerman H A. Intravenous Injection of Hyaluronidase in Acute Myocardial Infarction : Preliminary Report of Clinical and Experimental Observations. Am Heart J 1959; 57: 712-722.

Mason D T, De Maria A N, Berman D S. Principles of Non-invasive Cardiac Imaging. In: Echocardiography and Nuclear Cardiology. New York : Le Jacq 1980: 39.

Massie B, Kramer B. Radionuclide Determination of Left Ventricular Volume : Comparison of Counts-Based and Geometric Methods (Abstr). Am J Cardiol 1981; 47: 454.

Mathey G, Bleifeld W, Buss H, Hanrath P. Creatine Kinase Release in Acute Myocardial Infarction : Correlation with Clinical, Electrocardiographic, and Pathological Findings. Br Heart J 1975; 37: 1161-1168.

Mathey D, Kuck K H, Remmecke J, Tilsner V, Bleifeld W. Transluminal Recanalization of Coronary Artery Thrombosis : A Preliminary Report of its Application in Cardiogenic Shock. Eur

Heart J 1980; 1 : 207.

Matsukubo H, Matsuura T, Endo N, Asayama J, Watanabe T, Furukawa K, Kunishige H, Katsume H, Ijichi H. Echocardiographic Measurement of Right Ventricular Wall Thickness. A New Application of Subxiphoid Echocardiography. Circulation 1977; 56: 278-284.

Maudsley A A. Multiple Line Scanning Spin Density Imaging. J Mag Res 1980; 41: 112.

Medical Research Council Working Party. Long Term Domiciliary Oxygen Therapy in Chronic Hypoxic Cor Pulmonale Complicating Chronic Bronchitis and Emphysema. Lancet 1981; 1: 681-686.

Michelson N. Bilateral Ventricular Hypertrophy Due to Chronic Pulmonary Disease. Dis Chest 1960; 38: 435-446.

Mitchell R S, Stanford R E, Silvers G W, Dart G. The Right Ventricle in Chronic Airways Obstruction: A Clinicopathologic Study. Am Rev Resp Dis 1976; 114: 147-154.

Miura M, Thomas R, Ganz W, Sokol T, Shell W E, Toshimitsu T, Kwan A C, Singh B N. The Effect of Delay in Propranolol Administration on Reduction of Myocardial Infarct Size after Experimental Coronary Artery Occlusion in Dogs. Circulation 1979; 59: 1148-1157.

Mogelvang J, Stubgaard M, Thomsen C, Henriksen O. Evaluation of Right Ventricular Volumes Measured by Magnetic Resonance Imaging.

Eur Heart J 1988; 9: 529-533.

Morrison D A, Henry R, Goldman S. Preliminary Study of the Effects of Low Flow Oxygen on Oxygen Delivery and Right Ventricular Function in Chronic Lung Disease. Am Rev Respir Dis 1986; 133: 390-395.

Motley H L, Cournand A, Werko L, Himmelstein A, Dresdale D. The Influence of Short Periods of Induced Acute Anoxia Upon Pulmonary Artery Pressures in Man. Am J Physiol 1947; 150: 315-320.

Mounsey J P D, Ritzmann L W, Selverstone N J. Cardiographic Studies in Severe Pulmonary Emphysema. Br Heart J 1952; 14: 442-450.

Mueller H S, Ayres S M, Religa A, Evans R G. Propranolol in the Treatment of Acute Myocardial Infarction : Effect on Myocardial Oxygenation and Hemodynamics. Circulation 1974; 49: 1078-1087.

Muir A L, Hannah W J, Brash H M, Baldwa V, Miller H C, Ogilvie B. The Assessment of Left Ventricular Ejection Fraction in Patients with Ischaemic Heart Disease by Contrast Ventriculography and Nuclear Angiography. Clin Sci Mol Med 1977; 53: 55-61.

Muir A L, Hannah W J, Sapru R P, Boardman A K, Wraith P K, Brash H M. The Effects of Isoprenaline, Atropine and Dobutamine on Ventricular Volume Curves obtained by Radionuclide Ventriculography. Clin Sci 1980; 58: 357-364.

Muller J E, Maroko P R, Braunwald E. Evaluation of Precordial Electrocardiographic Mapping as a Means of Assessing Changes in Myocardial Ischemic Injury. Circulation 1975; 52: 16-27.

Murphy M L, Adamson J, Hutcheson F. Left Ventricular Hypertrophy in Patients with Chronic Bronchitis and Emphysema. Ann Intern Med 1974; 81: 307-313.

Murray R G, Peshock R M, Parkey R W, Bonte F J, Willerson J T, Blomqvist C G. ST Isopotential Precordial Surface Maps in Patients with Acute Myocardial Infarction. J Electrocardiol 1979; 12: 55-64.

Myers G B. QRS-T Patterns in Multiple Precordial Leads that may be mistaken for Myocardial Infarction. II. Right Ventricular Hypertrophy and Dilatation. Circulation 1950; 1: 8650-877.

Myers G B, Klein H A, Stofer B E. The Electrocardiographic Diagnosis of Right Ventricular Hypertrophy. Amer Heart J 1948; 35: 1-40.

National Radiological Protection Board. Revised Guidlines on Acceptable Limits of Exposure During Nuclear Magnetic Resonance Imaging. Br J Radiol 1983; 56: 974-977.

Neuhaus K L, Tebbe U, Sauer G, Kreuzer H, Kostering H. High Dose Intravenous Streptokinase in Acute Myocardial Infarction. Clin Cardiol 1983; 6: 426-434.

Nocturnal Oxygen Therapy Trial Group. Continuous or Nocturnal Oxygen Therapy in Hypoxemic Chronic Obstructive Lung Disease. Ann Intern Med 1980; 93: 391-398.

Norris R M, Caughey D E, Scott P J. Trial of Propranolol in Acute Myocardial Infarction. Br Med J 1968; 2: 398-400.

Norwegian Multicenter Study Group. Timolol - Induced Reduction in Mortality and Reinfarction in Patients Surviving Acute Myocardial Infarction. N Engl J Med 1981; 304: 801-807.

O'Donnell J K, Go R T, Bolt-Silverman C, Feiglin D H I, Salcedo E E, MacIntyre W J. Cardiac Amyloidosis : Comparison of MR Imaging and Echocardiography. Radiology 1984; 153(P): 261 (Abstract).

Office of Health Economics. Preventing Bronchitis. London; Office of Health Economics, 1977.

Olvey S K, Reduto L A, Stevens P M, Deaton W J, Miller R R. First Pass Radionuclide Assessment of Right and Left Ventricular Ejection Fraction in Chronic Pulmonary Disease: Effect of Oxygen Upon Exercise Response. Chest 1980; 78: 4-9.

Ong L, Coromilas J, Padmanabhan V, Robbins M, Reiser P, Morrison J. Ventricular Volumes by Gated Equilibrium Radionuclide Angiography (Abstr). Clin Res 1980; 28: 617A.

Page D L, Caulfield J B, Kaster J A, DeSanctis R W, Sanders C A.

Myocardial Changes Associated with Cardiogenic Shock. N Engl J Med 1971; 285: 133-137.

Parkey R W, Bonte F J, Meyer S L, Atkins J M, Curry G L, Stokely E M, Willerson J T. A New Method for Radionuclide Imaging of Acute Myocardial Infarction in Humans. Circulation 1974; 50: 540-546.

Pavlicek W, Geisinger M, Castle L, Borkowski G P, Meaney T F, Bream B L, Gallagher J H. The Effects of Nuclear Magnetic Resonance on Patients with Cardiac Pacemakers. Radiology 1983; 147: 149-153.

Peshock R M, Malloy C R, Buja L M, Nunnally R L, Parkey R W, Willerson J T. Magnetic Resonance Imaging of Acute Myocardial Infarction : Gadolinium Diethylenetriamine Pentaacetic Acid as a Marker for Reperfusion. Circulation 1986; 74: 1434-1440.

Peter T, Heng M K, Singh B H, Ambler P, Nisbet H, Elliot R, Norris R M. Failure of High Doses of Propranolol to Reduce Experimental Myocardial Ischemic Damage. Circulation 1978; 57: 534-540.

Peter T, Norris R M, Clark E D, Heng M K, Singh B N, Williams B, Howell D R, Ambler D K. Reduction of Enzyme Levels by Propranolol after Acute Myocardial Infarction. Circulation 1978; 57: 1091-1095.

Pettigrew R I, Eisner R L, Ziffner J. Dynamic Cardiac MRI Using Dual Spin Echoes. Dynamic Cardiovasc Imaging 1988; 1: 214.

Pfeffer J M, Pfeffer M A, Braunwald E. Influence of Chronic Captropril Therapy on the Infarcted Left Ventricle of the Rat. Circulation Res 1985; 57: 84-95.

Pflugfelder P W, Wisenberg G, Prato F S, Carroll E S, Turner K L. Early Detection of Canine Myocardial Infarction by Magnetic Resonance Imaging In Vivo. Circulation 1985; 71: 587-594.

Philips S J, Kongtahworn C, Zeff R H, Benson M, Iannone L, Brown T, Gordon D F. Emergency Coronary Artery Revascularization : A Possible Therapy for Acute Myocardial Infarction. Circulation 1979; 60: 241-246.

Pierce W S, Carter D R, McGavran M H, Waldhausen J A. Modification of Myocardial Infarct Volume : An Experimental Study in the Dog. Arch Surg 1973; 107: 682-687.

Pizer S M, Todd-Pokropek A E. Improvement of Scintigrams by Computer Processing. Semin Nucl Med 1978; 8: 125-146.

Pohost G M, Goldman M R, Pykett I L, Brady T J, Foale R A, Buonanno F S, Dunsmore R E, Miller S W, Weyman A E, Kistler J P, Hinshaw W S. Gated NMR Imaging in Canine Myocardial Infarction. Circulation 1982; 66 (suppl II): II-39.

Poliner L R, Buja L M, Parkey R W, Stokely E M, Stone M J, Harris R, Saffer S W, Templeton G H, Bonte F J, Willerson J T. Comparison of Different Non-invasive Methods of Infarct Sizing During

Experimental Myocardial Infarction. J Nucl Med 1977; 18: 517-523.

Pombo J F, Troy B L, Russell R O. Left Ventricular Volumes and Ejection Fraction by Echocardiography. Circulation 1971; 43: 480-490.

Popp R L, Wolfe S B, Hirata T, Feigenbaum H. Estimation of Right and Left Ventricular Size by Ultrasound. A Study of the Echoes from the Interventricular Septum. Am J Cardiol 1969; 24: 523-530.

Powell W J Jr, Di Bona D R, Flores J, Leaf A. The Protective Effect of Hyperosmotic Mannitol in Myocardial Ischaemia and Necrosis. Circulation 1976; 54: 603-615.

Purcell E M, Torrey H C, Pound R V. Resonance Absorption by Nuclear Magnetic Moments in a Solid. Physical Review 1946; 60: 37.

Quirk M E, Letendre A J, Ciottone R A, Lingley J F. Anxiety in Patients Undergoing MR Imaging. Radiology 1989; 170: 463-466.

Rasmussen M M, Reimer K A, Kloner R A, Jennings R B. Infarct Size Reduction by Propranolol before and after Coronary Ligation in Dogs. Circulation 1977; 56: 794-798.

Ratner A V, Barrett L V, Gang D L. Alterations of the Proton Nuclear Magnetic Resonance Spin-Lattice Relaxation Time (T1) In Rejecting Cardiac Allografts. J A C C 1984; 3: 538 (Abstract).

Ratner A V, Okada R D, Thompson R D, Goldman M D, Pohost G M. Characterisation of Myocardium Using Proton NMR Relaxation Times. Proc Scientific Prog Soc MR Med, New York, August 1983, p 291 (Abstract).

Redpath TW. Calibration of the Aberdeen NMR Imager for Proton Spin-lattice Relaxation Time Measurements In-vivo. Phys Med Biol 1982; 27: 1057-1065.

Reduto L A, Berger H J, Cohen L S, Gottschalk A, Zaret B L. Sequential Radionuclide Assessment of Left and Right Ventricular Performance after Acute Myocardial Infarction. Ann Int Med 1978; 89: 441-447.

Reedy T, Chapman C B. Measurement of Right Ventricular Volume by Cineangiofluorography. Am Heart J; 1963: 66(2): 221-225.

Register General of Scotland. Annual Report, Edinburgh, HM Stationery Office, Edinburgh, 1982.

Rehr R B, Malloy C R, Filipchuk N G, Peshock R M. Left Ventricular Volumes Measured by MR Imaging. Radiology 1985; 156: 717-719.

Reimer K A, Lowe J E, Rasmussen M M, Jennings R B. The Wavefront Phenomenon of Ischemic Cell Death. 1. Myocardial Infarct Size vs Duration of Coronary Occlusion in Dogs. Circulation 1977; 56: 786-794.

Reiner L, Mazzoleni A, Rodriguez F L, Freudenthal R R. The Weight of the Human Heart. Arch Pathol 1959; 68: 58-73.

Renzetti A D, McClement J H, Litt B D. The Veterans Administration Cooperative Study of Pulmonary Function III. Mortality in Relation to Respiratory Function in Chronic Obstructive Lung Disease. Am J Med 1966; 41: 115-129.

Ridolfi R L, Hutchins G M. The Relationship Between Coronary Artery Lesions and Myocardial Infarcts : Ulceration in Atherosclerotic Plaques Precipitating Coronary Thrombosis. Am Heart J 1977; 93: 469-486.

Roberts R, Henry P D, Sobel B E. An Improved Basis for Enzymatic Estimation of Infarct Size. Circulation 1975; 52: 743-754.

Roberts R, Ishikawa Y. Enzymatic Estimation of Infarct Size During Reperfusion. Circulation 1983; 68: (suppl 1): 83-89.

Robison A K, Garlick P B, Humphrey S M, Shillingford J P. The Effect of Drugs on Enzyme Release from the Hypoxic Myocardium. Eur J Cardiol 1978; 7: 421-436.

Roe C R. Validity of Estimating Myocardial Infarct Size from Serial Measurements of Enzyme Activity in Serum. Clin Chem 1977; 23: 1807-1812.

Roe C R, Cobb F R, Starmer C F. The Relationship between Enzymatic

and Histologic Estimates of the Extent of Myocardial Infarction in Conscious Dogs with Permanent Coronary Occlusion. Circulation 1977; 55: 438-449.

Roe C R, Starmer C F. A Sensitivity Analysis of Enzymatic Estimation of Infarct Size. Circulation 1975: 52; 1-5.

Rokey R, Verani M S, Bolli R, Ruo L C, Ford J J, Wendt R E, Schneiders N J, Bryan R N, Roberts R. Myocardial Infarct Size Quantification by MR Imaging Early after Coronary Artery Occlusion in Dogs. Radiology 1986; 158: 771-774.

Ross J Jr, Franklin D. Analysis of Regional Myocardial Function, Dimensions and Wall Thickness in the Characterisation of Myocardial Ischaemia and Infarction. Circulation 1976; 53: Suppl I: 88-92.

Sandler H, Dodge H T. The Use of Single Plane Angiocardiograms for the Calculation of Left Ventricular Volume in Man. Am Heart J 1968; 75: 325-334.

Saunders R D, Orr J S. Biologic Effects of NMR. In Partain C L, James A E, Rollo F D, Price R R eds. Nuclear Magnetic Resonance Imaging. Philadelphia: Saunders, 1983; 383-396.

Schaefer D J. Safety aspects of magnetic resonance imaging. In Wehrli F W, Shaw D, Kneeland B J eds. Biomedical Magnetic Resonance Imaging : Principles, Methodology and Applications. New York : VCH, 1988: 553-578.

Schaefer S, Peshock R M, Malloy C R, Katz, Parkey R W, Willerson J T. Nuclear Magnetic Resonance Imaging in Marfan's Syndrome. J A C C 1987; 9: 70-74.

Schaper J, Schaper W. Reperfusion of Ischemic Myocardium Ultrastructural and Histochemical Aspects. J A C C 1983; 1: 1037-1046.

Schrijen F, Uffholtz H, Polu J M, Poincelot F. Pulmonary and Systemic Haemodynamic Evolution in Chronic Bronchitis. Am Rev Resp Dis 1978; 117: 25-31.

Schroder R, Biamino G, v Leitner E R, Linderer T, Bruggemann T, Heitz J, Vohringer H F, Wegscheider K. Intravenous Short-term Infusion of Streptokinsase in Acute Myocardial Infarction. Circulation 1983; 67: 536-548.

Scott R W, Garvin C G. Cor Pulmonale: Observations in 50 Autopsy Cases. Am Heart J 1941; 22: 56-63.

Sharpe N, Murphy J, Smith H, Hannan S. Treatment of Patients with Symptomless Left Ventricular Dysfunction after Myocardial Infarction. Lancet 1988; 1: 255-259.

Shell W E, Kjekshus J K, Sobel B E. Quantitative Assessment of the Extent of Myocardial Infarction in the Conscious Dog by Means of Analysis of Serial Changes in Creatine Phosphokinase Activity. J Clin Invest 1971; 50: 2614-2625.

Shell W E, Lavelle J F, Covell J W, Sobel B E. Early Estimation of Myocardial Damage in Conscious Dogs and Patients with Evolving Acute Myocardial Infarction. J Clin Invest 1973; 52: 2579-2590.

Shellock F G. MR Imaging of Metallic Implants and Materials: a Compilation of the Literature. A J R 1988; 151: 811-814.

Shellock F G, Crues J V. Corneal Temperature Changes Induced by High Field-Strength MR Imaging with a Head Coil. Radiology 1987; 167: 809-811.

Shellock F G, Rothman B, Sarti D. Heating of the Scrotum by High Field-Strength MR Imaging. A J R 1990; 154: 1229-1232.

Simoons M L, Serruys P W, Van den Brand M, Res J, Verheugt F W A, Krauss X H, Remme W J, Bar F, de Zwaan C, Van der Laarse A, Vermeer F, Lubsen J. Early Thrombolysis in Acute Myocardial Infarction: Limitation of Infarct Size and Improved Survival. J A C C 1986; 7: 717-728.

Sjogren A L, Hytonen I, Frick M H. Ultrasonic Measurements of Left Ventricular Wall Thickness. Chest 1970; 57: 37-40.

Slutsky R, Bhargava V, Dittrich H, Costello D. Comparison of Single-plane and Biplane Contrast Analyses of Right Ventricular Function and Size. Am Heart J 1982; 104: 100-104.

Slutsky R, Hooper W, Gerber K, Battler A, Froelicher V, Ashburn W,

Karliner J. Assessment of Right Ventricular Function at Rest and During Exercise in Patients with Coronary Heart Disease : A New Approach Using Equilibrium Radionuclide Angiography. Am J Cardiol 1980; 45: 63-71.

Slutsky R, Karliner J, Ricci D, Kaiser R, Pfisterer M, Gordon D, Peterson K, Ashburn W. Left Ventricular Volumes by Gated Equilibrium Radionuclide Angiography : A New Method. Circulation 1979; 60: 556-564.

Smith E R, Redwood D R, McCarron W E, Epstein S E. Coronary Artery Occlusion in the Conscious Dog : Effects of Alterations in Arterial Pressure Produced by Nitroglycerin, Hemorrhage, and Alpha-Adrenergic Agonists on the Degree of Myocardial Ischemia. Circulation 1973; 47: 51-57.

Smith M A, Ridgway J P, Brydon J W E, Been M, Douglas R H B, Kean D M, Muir A L, Best J J K. ECG Gated Tl Images of the Heart. Phys Med Biol 1986; 3: 771-778.

Snow P J D. Effect of Propranolol in Myocardial Infarction. Lancet 1965; 2: 551-553.

Sobel B E, Bresnahan G F, Shell W E, Yoder R D. Estimation of Infarct Size in Man and its Relation to Prognosis. Circulation 1972; 46: 640-648.

Sokolow M, Lyon T P. The Ventricular Complex in Right Ventricular

Hypertrophy as obtained by Unipolar Precordial and Limb Leads. Amer Heart J 1949; 38: 273-294.

Soulen R L, Stark D D, Higgins C B. Magnetic Resonance Imaging of Constrictive Pericardial Disease. Am J Cardiol 1985; 55: 480-484.

Spain D M, Handler B J. Chronic Cor Pulmonale. Arch Intern Med 1946; 77: 37-65.

Spann J F, Sherry S, Carabello B A, Denenberg B S, Mann R H, McCann W D, Gault J H, Gentzler R D, Belber A D, Maurer A H, Cooper E M. Coronary Thrombolysis by Intra-venous Streptokinase in Acute Myocardial Infarction : Acute and Follow-up Studies. Am J Cardiol 1984; 53: 655-661.

Spatt S D, Grayzel D M. Cor Pulmonale : Observations on Forty-two Autopsied Patients. Am J Med 1948; 5: 252.

Stark D D, Higgins C B, Lanzer P, Lipton M J, Schiller N, Crooks L E, Botvinick E B, Kaufman L. Magnetic Resonance Imaging of the Pericardium: Normal and Pathological Findings. Radiology 1984; 150: 469-474.

Starling M R, Crawford M H, Sorensen S G, O'Rourke R A. A New Two-Dimensional Echocardiographic Technique for Evaluating Right Ventricular Size and Performance in Patients with Obstructive Lung Disease. Circulation 1982; 66: 612-620.

Stratemeier E J, Thompson R, Brady T J, Miller S W, Saini S, Wismer G L, Okada R D, Dinsmore R E. Ejection Fraction Determination by MR Imaging : Comparison with Left Ventricular Angiography. Radiology 1986; 158: 775-777.

Steiner R E. The Hammersmith Clinical Experience with Nuclear Magnetic Resonance. Clin Radiol 1983; 34: 13-23.

Steiner R E. Nuclear Magnetic Resonance Imaging of the Heart and Mediastinum. Br Heart Bull 1984; 40: 191-193.

Steiner R E, Bydder G M, Selwyn A, Deanfield J, Longmore D B, Klipstein R H, Firmin D. Nuclear Magnetic Resonance Imaging of the Heart. Current Status and Future Prospects. Br Heart J 1983; 50: 202-208.

Stokely E M, Buja L M, Lewis S E, Parkey R W, Bonte F J, Harris R A, Willerson J T. Measurement of Acute Myocardial Infarcts in Dogs with 99m Tc-stannous Pyrophosphate Scintigrams. J Nucl Med 1975; 17: 1-5.

Strauss H W, Zaret B L, Hurley P J, Natarajan T K, Pitt B. A Scintiphotographic Method for Measuring Left Ventricular Ejection Fraction in Man without Cardiac Catheterisation. Am J Cardiol 1971; 28: 575-580.

Suzuki J I, Sakamoto T, Takenaka K, Kawakubo K, Amano K, Takahashi H, Hasegawa I, Shiota T, Hada Y, Sugimoto T, Nishikawa J I.

Assessment of the Thickness of the Right Ventricular Free Wall by Magnetic Resonance Imaging in Patients with Hypertrophic Cardiomyopathy. Br Heart J 1988; 60: 440-445.

Swain J L, Cobb F R, McHale P A, Coe C R. Nonlinear Relationship between Creatine Kinase Estimates and Histologic Extent of Infarction in Conscious Dogs : Effects of Regional Myocardial Blood Flow. Circulation 1980; 62: 1239-1247.

Tamaki S, Murakami T, Kadota K, Kambara H, Yui Y, Nakajima H, Suziki, Y Nohara R, Takatsu Y, Kawai C, Tamaki N, Mukai T, Torizuka K. Effects of Coronary Artery Reperfusion on Relation Between Creatine Kinase-MB Release and Infarct Size Estimated by Myocardial Emission Tomography with Thallium-201 in Man. J A C C 1983; 2: 1031-1038.

Thomas A J. Right Ventricular Hypertrophy in the Pneumoconiosis of Coalminers. Br Heart J 1951; 13: 1-9.

Thompson P L, Fletcher E E, Katavatis V. Enzymatic Indices of Myocardial Necrosis : Influence on Short- and Long-term Prognosis after Myocardial Infarction. Circulation 1979; 59 113-119.

Thurlbeck W M, Henderson J A, Fraser R G, Bates D V. Chronic Obstructive Lung Disease: A Comparison Between Clinical, Roentgenologic, Functional and Morphological Criteria in Chronic Bronchitis, Emphysema, Asthma and Bronchiectasis. Medicine 1970; 49: 81-145.

Thurlbeck W M, Simon G. Radiographic Appearance of the Chest in Emphysema. A J R 1978; 130: 429-440.

Tillett W S, Sherry S. Effect in Patients of Streptococcal Fibrinolysis (Streptokinase) and Streptococcal Desoxyribonuclease on Fibrinous, Purulent and Sanginous Pleural Effusions. J Clin Invest 1949; 28: 173-190.

Timms R M, Khaja F U, Williams G W, and the Nocturnal Oxygen Therapy Trial Group. Haemodynamic Response to Oxygen Therapy in Chronic Obstructive Pulmonary Disease. Ann Intern Med 1985; 102: 29-36.

Tscholakoff D, Aherne T, Yee E S, Derugin N, Higgins C B. Cardiac Transplantations in Dogs: Evaluation with MR. Radiology 1985; 157: 697-702.

Tscholakoff D, Higgins C B, Sechtem U, Caputo G, Derugin N. MRI of Reperfused Myocardial Infarct in Dogs. A J R 1986: 146: 925-930.

Tscholakoff D, Higgins C B, Sechtem U, McNamara M T. Occlusive and Reperfused Myocardial Infarcts : Effects of Gd-DTPA on ECG-gated MR Imaging. Radiology 1986; 160: 515-519.

Twieg D, Lewis S, Harper J, Curry G C, Mullins C B, Nixon J V. Assessment of Right Ventricular Function in Chronic Severe Pulmonary Hypertension by Multiple Gated First Pass Radionuclide Angiography (Abstr). Circulation 1979; 60: Suppl ii: 11-148.

Underwood S R, Gill C R W, Firmin D N, Klipstein R H, Mohiaddin R H, Rees R S O, Longmore D B. Left Ventricular Volume Measured Rapidly by Oblique Magnetic Resonance Imaging. Br Heart J 1988; 60: 188-195.

Van der Laarse A, Kerkhof P L M, Vermeer K, Serruys P W, Hermens W T, Verheugt F W A, Bar F W, Krauss H, Van der Wall E E, Simoons M L. Relation between Infarct Size and Left Ventricular Performance Assessed in Patients with First Acute Myocardial Infarction Randomized to Intracoronary Thrombolytic Therapy or to Conventional Treatment. Am J Cardiol 1988; 61: 1-7.

Van der Laarse A, Vermeer F, Hermens W T, Willems G H, de Neef K, Simoons M L, Serruys P W, Res J, Verheugt F W A, Krauss X H, Bar F, de Zwaan C, Lubsen J. Effects of early Intracoronary Streptokinase on Infarct Size Estimation from Cumulative Enzyme Release and on Enzyme Release Rate : A Randomized Trial of 533 Patients with Acute Myocardial Infarction. Am Heart J 1986; 112: 672-681.

Vatner S F, Baig H, Manders T, Maroko P R. Effects of Coronary Artery Reperfusion on Myocardial Infarct Size Calculated from Creatine Kinase. J Clin Invest 1978; 61: 1048-1056.

Veno S, Harada K, Shiokawa K. The Embryonic Development of Frogs Under Strong DC Magnetic Fields. IEEE Trans Magn 1984; MAG-20: 1663-1665.

Von Schulthess G K, Higashino S M, Higgins S S, Didier D, Fisher M

R, Higgins C B. Coarctation of the Aorta: MR Imaging. Radiology 1986; 158: 469-474.

Waagstein F, Hjalmarson A C. Effect of Cardioselective Beta-blockers on Heart Function and Chest Pain in Acute Myocardial Infarction. Acta Med Scand (Suppl) 1975; 587: 210-204.

Walker I C, Helm R A, Scott R C. Right Ventricular Hypertrophy. 1. Correlation of Isolated Right Ventricular Hypertrophy at Autopsy with the Electrocardiographic Findings. Circulation 1955; 11: 215-227.

Watanabe T, Katsume H, Matsukubo H, Furukawa K, Ijichi H. Estimation of Right Ventricular Volume with Two Dimensional Echocardiography. Am J Cardiol 1982; 49: 1946-1953.

Weitzenblum E, Hirth C, Ducolone A, Mirhom R, Rasaholinjanahary J, Ehrhart M. Prognostic Value of Pulmonary Artery Pressure in Chronic Obstructive Pulmonary Disease. Thorax 1981; 36: 752-758.

Weitzenblum E, Loiseau A, Hirth C, Mirhom R, Rasaholinjanahary J. Course of Pulmonary Haemodynamics in Patients with Chronic Pulmonary Haemodynmics in Patients with Chronic Obstructive Pulmonary Disease. Chest 1979; 75: 656-662.

Weitzenblum E, Zielinski E, Bishop J M. The Diagnosis of Cor Pulmonale by Non-invasive Methods : A Challenge for Pulmonologists and Cardiologists. Bull Eur Physiopathol Respir 1983; 19: 423-426.

Wesbey G E, Higgins C B, Lanzer P, Botvinick E, Lipton M J. Imaging and Characterization of Acute Myocardial Infarction In Vivo by Gated Nuclear Magnetic Resonance. Circulation 1984; 69:125-130.

Wesbey G E, Higgins C B, McNamara M T, Engelstad B L, Lipton M J, Sievers R, Ehman R L, Lovin J, Brash R C. Effect of Gadolinium-DTPA on the Magnetic Relaxation Times of Normal and Infarcted Myocardium. Radiology 1984; 153: 165-169.

Wescott R N, Fowler N O, Scott R C, Hauenstein V D, McGuire J. Anoxia and Pulmonary Vascular Resistance. J Clin Invest 1951; 30: 957-970.

White H D, Norris R M, Brown M A, Takayama M, Maslowski A, Bass N M, Ormiston J A, Whitlock T. Effects of Intravenous Streptokinase on Left Ventricular Function and Early Survival after Myocardial Infarction. New Eng J Med 1987; 317: 855-858.

Wilhelmsson C, Vedin J A, Wilhelmsen L, Tibblin G, Werko L. Reduction of Sudden Deaths after Myocardial Infarction by Treatment with Alprenolol. Lancet 1974; 2: 1157-1160.

Williams E S, Kaplan J I, Thatcher F, Zimmerman G, Knoebel S B. Prolongation of Proton Spin Lattice Relaxation Times in Regionally Ischemic Tissue From Dog Hearts. J Nucl Med 1980; 21: 449-453.

Wilson F N, Johnston F D, Rosenbaum F F, Erlanger H, Kossmann C E, Hecht H, Cotrim N, de Oliveira R M, Scarsi R, Barker P S. The

Precordial Electrocardiogram. Amer Heart J 1944; 27: 19-85.

Withers H R, Mason K A, Davis C A. MR Effect on Murine Spermatogenesis. Radiology 1985; 156: 741-742.

Witteveen S A G J, Hemker H C, Hollaar L, Hermens W Th. Quantification of Infarct Size in Man by Means of Plasma Enzyme Levels. Br Heart J 1975; 37: 795-803.

Wolff S, Crooks L E, Brown P, Howard R, Painter R B. Tests for DNA and Chromosomal Damage Induced by Nuclear Magnetic Resonance Imaging. Radiology 1980; 136: 707-710.

Wolff S, James T L, Young G B, Margulis A R, Bodycote J, Afzal V. Magnetic Resonance Imaging: Absence of In Vitro Cytogenetic Damage. Radiology 1985; 155: 163-165.

World Health Organisation. Chronic Cor Pulmonale. A Report of the Expert Committee. Circulation 1963; 27: 594-615.

Wynne J, Green L H, Mann T, Levin D, Grossman W. Estimation of Left Ventricular Volumes in Man from Biplane Cineangiograms Filmed in Oblique Positions. Am J Cardiol 1978; 41: 726-732.

Young I R, Burl M, Bydder G M. Comparative Efficiency of Different Pulse Sequences in MR Imaging. J Comp Asst Tomogr 1986; 10: 271-286.

Yusuf R, Ramsdale D, Peto R, Furse L, Bennett D, Bray C, Sleight P. Early Intravenous Atenolol in Suspected Acute Myocardial Infarction : Preliminary Report of a Randomised Trial. Lancet 1980; 2: 273-276.

Zimmerman H A, Ryan J M. Cor Pulmonale. Dis Chest 1951; 20: 286-289.

# APPENDIX 1

TABLE 5

Variation in measured T1 value with heart rate and slice angulation for a calibrated T1 value of 118ms

| Heart rate bpm | Degree of Angulation from transverse plane | | | |
|---|---|---|---|---|
| | $0^{o}$ | $10^{o}$ | $20^{o}$ | $30^{o}$ |
| 55 | 94 | 95 | 98 | 97 |
| 60 | 94 | 97 | 98 | 97 |
| 65 | 95 | 96 | 98 | 98 |
| 70 | 95 | 95 | 99 | 97 |
| 75 | 94 | 96 | 98 | 98 |
| 80 | 94 | 96 | 98 | 97 |
| 85 | 94 | 96 | 97 | 98 |
| 90 | 93 | 97 | 98 | 99 |
| 95 | 94 | 97 | 95 | 98 |

TABLE 6

Variation in measured T1 value with heart rate and slice angulation for a calibrated T1 value of 240ms

| Heart rate bpm | Degree of Angulation from transverse plane | | | |
|---|---|---|---|---|
| | $0^{o}$ | $10^{o}$ | $20^{o}$ | $30^{o}$ |
| 55 | 197 | 199 | 201 | 202 |
| 60 | 195 | 197 | 203 | 202 |
| 65 | 195 | 199 | 203 | 202 |
| 70 | 193 | 195 | 202 | 205 |
| 75 | 190 | 193 | 200 | 202 |
| 80 | 190 | 192 | 199 | 200 |
| 85 | 189 | 190 | 198 | 200 |
| 90 | 187 | 191 | 196 | 199 |
| 95 | 188 | 190 | 194 | 197 |

TABLE 7

Variation in measured T1 value with heart rate and slice angulation for a calibrated T1 value of 333ms

| Heart rate bpm | Degree of Angulation from transverse plane | | | |
|---|---|---|---|---|
| | $0^{o}$ | $10^{o}$ | $20^{o}$ | $30^{o}$ |
| 55 | 277 | 281 | 284 | 283 |
| 60 | 270 | 279 | 285 | 282 |
| 65 | 267 | 274 | 283 | 281 |
| 70 | 266 | 269 | 280 | 282 |
| 75 | 260 | 266 | 276 | 279 |
| 80 | 257 | 265 | 270 | 277 |
| 85 | 254 | 263 | 268 | 276 |
| 90 | 254 | 260 | 266 | 272 |
| 95 | 251 | 257 | 260 | 267 |

TABLE 8

Variation in measured T1 value with heart rate and slice angulation for a calibrated T1 value of 444ms

| Heart rate bpm | Degree of Angulation from transverse plane | | | |
|---|---|---|---|---|
| | $0^{o}$ | $10^{o}$ | $20^{o}$ | $30^{o}$ |
| 55 | 362 | 368 | 360 | 362 |
| 60 | 351 | 365 | 367 | 358 |
| 65 | 347 | 359 | 366 | 361 |
| 70 | 339 | 349 | 359 | 358 |
| 75 | 331 | 339 | 350 | 353 |
| 80 | 323 | 331 | 346 | 349 |
| 85 | 319 | 329 | 338 | 347 |
| 90 | 310 | 321 | 332 | 343 |
| 95 | 313 | 322 | 326 | 336 |

TABLE 9

Variation in measured T1 value with heart rate and slice angulation for a calibrated T1 value of 500ms

| Heart rate bpm | Degree of Angulation from transverse plane | | | |
|---|---|---|---|---|
| | $0^{o}$ | $10^{o}$ | $20^{o}$ | $30^{o}$ |
| 55 | 408 | 414 | 405 | 404 |
| 60 | 392 | 407 | 412 | 407 |
| 65 | 389 | 406 | 412 | 402 |
| 70 | 373 | 393 | 404 | 402 |
| 75 | 366 | 379 | 395 | 392 |
| 80 | 359 | 369 | 385 | 391 |
| 85 | 354 | 360 | 380 | 385 |
| 90 | 350 | 361 | 370 | 374 |
| 95 | 345 | 355 | 360 | 377 |

TABLE 10

Variation in measured T1 value with heart rate and slice angulation for a calibrated T1 value of 991ms

| Heart rate bpm | Degree of Angulation from transverse plane | | | |
|---|---|---|---|---|
| | $0^{o}$ | $10^{o}$ | $20^{o}$ | $30^{o}$ |
| 55 | 896 | 931 | 868 | 863 |
| 60 | 790 | 939 | 883 | 843 |
| 65 | 787 | 887 | 845 | 867 |
| 70 | 756 | 830 | 853 | 818 |
| 75 | 674 | 764 | 806 | 773 |
| 80 | 645 | 726 | 749 | 746 |
| 85 | 626 | 737 | 701 | 771 |
| 90 | 580 | 680 | 674 | 734 |
| 95 | 616 | 652 | 664 | 709 |

# APPENDIX 2

Table 13

Individual T1 Values for Right and Left Ventricular Wall and Chamber Contents for Patients with Chronic Obstructive Pulmonary Disease

T1 Values

| Patients | Ventricular Wall | | Heart Rate | Chamber | |
|---|---|---|---|---|---|
| | RV | LV | | RV | LV |
| MMcA | 306.3 | 350.5 | 75 | 572.7 | 496.1 |
| TH | 304.5 | 327.5 | 53 | 593.6 | 522.0 |
| RW | 319.6 | 349.3 | 90 | 519.9 | 595.5 |
| WH | 270.4 | 318.8 | 80 | 629.4 | 714.6 |
| RH | 344.4 | 370.1 | 70 | 546.9 | 554.6 |
| AE | 356.8 | 339.3 | 96 | 502.6 | 487.5 |
| MD | 329.6 | 366.7 | 55 | 501.7 | 517.5 |
| RC | 251.2 | 326.2 | 83 | 575.0 | 475.8 |
| WF | 290.6 | 328.1 | 70 | 551.0 | 541.5 |
| TW | 327.9 | 398.8 | 100 | 631.5 | 560.9 |
| JW | 295.3 | 306.5 | 60 | 518.1 | 499.9 |
| AM | 341.3 | 349.9 | 45 | 510.7 | 488.5 |
| RS | 307.4 | 298.7 | 75 | 539.8 | 657.5 |
| SD | 370.0 | 331.4 | 72 | 910.4 | 759.6 |
| MA | 308.8 | 320.9 | 65 | 695.1 | 673.6 |
| JB | 262.4 | 304.9 | 100 | 499.2 | 498.9 |
| Mean $\pm$SD | 311.7 $\pm$33.3 | 336.7 $\pm$26.6 | 62 $\pm$31.7 | 581.1 $\pm$104.0 | 565.3 $\pm$89.2 |

Table 14

Individual Tl Values for Right and Left Ventricular Wall and Chamber Contents for Patients with Ischaemic Heart Disease

Tl Values

| Patients | Ventricular Wall | | Heart Rate | Chamber | |
|---|---|---|---|---|---|
| | RV | LV | | RV | LV |
| BI | 319.7 | 336.4 | 74 | 546.2 | 574.0 |
| GM | 373.1 | 376.2 | 60 | 621.1 | 618.1 |
| EC | 342.5 | 355.0 | 55 | 612.8 | 532.9 |
| MW | 279.3 | 409.6 | 92 | 563.4 | 673.9 |
| JH | 275.2 | 282.2 | 75 | 333.4 | 401.3 |
| WS | 291.8 | 287.7 | 82 | 298.2 | 343.6 |
| SC | 348.7 | 353.2 | 66 | 548.5 | 413.6 |
| MMcM | 348.0 | 325.4 | 70 | 737.9 | 630.4 |
| FF | 329.3 | 415.8 | 85 | 547.8 | 639.1 |
| DO | 284.5 | 304.9 | 100 | 550.8 | 478.7 |
| JG | 309.2 | 301.1 | 74 | 488.1 | 483.7 |
| JB | 279.0 | 303.2 | 90 | 430.4 | 464.3 |
| TN | 300.8 | 277.3 | 100 | 433.1 | 429.2 |
| JD | 423.2 | 406.2 | 60 | 832.4 | 753.5 |
| HW | 317.0 | 340.0 | 88 | 741.8 | 544.4 |
| MS | 286.0 | 292.1 | 95 | 391.5 | 427.5 |
| MC | 319.2 | 341.6 | 70 | 706.3 | 703.5 |
| ECu | 330.2 | 338.5 | 75 | 498.6 | 529.9 |
| KG | 355.9 | 359.3 | 58 | 566.3 | 552.5 |
| Mean ±SD | 321.7 ±38.0 | 337.2 ±53.6 | 77 ±14.2 | 549.9 ±140.6 | 536.5 ±112.3 |

Table 15

Individual T1 Values for Right and Left Ventricular Wall and Chamber Contents for Age-Matched Control Group

| Patients | T1 Values | | | | |
|---|---|---|---|---|---|
| | Ventricular Wall | | Heart Rate | Chamber | |
| | RV | LV | | RV | LV |
| JMcD | 314.6 | 352.1 | 65 | 802.0 | 796.3 |
| ML | 319.2 | 297.3 | 82 | 478.6 | 454.1 |
| IC | 305.1 | 329.2 | 76 | 877.7 | 836.3 |
| HC | 297.9 | 324.9 | 80 | 775.6 | 608.7 |
| MS | 304.4 | 332.1 | 79 | 752.1 | 654.3 |
| Mean ±SD | 308.2 ±8.5 | 327.1 ±19.7 | 76.4 ±6.7 | 737.2 ±152.1 | 669.9 ±153.5 |

Table 16

Individual T1 Values for Right and Left Ventricular Wall and Chamber Contents for Normal Young Volunteer Group

T1 Values

| Patients | Ventricular Wall | | Heart Rate | Chamber | |
|---|---|---|---|---|---|
| | RV | LV | | RV | LV |
| LT | 320.3 | 339.8 | 89 | 935.6 | 845.1 |
| JPR | 301.3 | 310.9 | 77 | 587.2 | 556.7 |
| WMcN | 333.7 | 314.1 | 70 | 814.7 | 721.3 |
| CS | 304.9 | 307.1 | 79 | 746.1 | 599.6 |
| Mean ±SD | 315.1 ±14.9 | 318.0 ±14.8 | 78.8 ±7.8 | 770.9 ±145.4 | 680.7 ±129.9 |

TABLE 17

Right and Left Ventricular "Free" Wall and Chamber Volumes Obtained at End-Systole in Patients with Chronic Obstructive Pulmonary Disease

| Patient | Age | Chamber Volume ($cm^3$) | | Ventricular Wall Volume ($cm^3$) | |
|---|---|---|---|---|---|
| | | RV | LV | RV | LV |
| MMcA | 82 | 49.9 | 32.3 | 69.0 | 133.1 |
| TH | 70 | 56.5 | 81.1 | 69.0 | 164.2 |
| RW | 73 | 45.3 | 17.1 | 70.4 | 157.8 |
| RH | 64 | 56.8 | 79.4 | 40.8 | 169.4 |
| WH | 69 | 48.3 | 42.6 | 96.0 | 102.6 |
| AE | 66 | 16.3 | 67.4 | 11.8 | 101.4 |
| MD | 62 | 24.6 | 42.4 | 46.2 | 104.6 |
| RC | 73 | 41.4 | 35.5 | 41.8 | 152.2 |
| WF | 75 | 54.6 | 56.5 | 76.0 | 154.7 |
| TW | 70 | 18.7 | 115.8 | 44.5 | 115.8 |
| JW | 74 | 22.1 | 40.6 | 27.7 | 169.8 |
| AM | 64 | 87.4 | 57.8 | 73.6 | 120.3 |
| RS | 76 | 29.1 | 24.6 | 38.1 | 143.8 |
| SD | 58 | 40.6 | 37.4 | 84.2 | 132.0 |
| MA | 46 | 28.8 | 8.8 | 60.6 | 135.2 |
| MB | 63 | 56.2 | 53.4 | 60.5 | 136.9 |
| Mean ±SD | 68 | 42.3 ±19.1 | 49.5 ±26.9 | 56.9 ±22.2 | 137.1 ±23.3 |

TABLE 18

Right and Left Ventricular "Free" Wall and Chamber Volumes Obtained at End-Systole in Patients with Ischaemic Heart Disease

| Patient | Age | Chamber Volume ($cm^3$) | | Ventricular Wall Volume ($cm^3$) | |
|---|---|---|---|---|---|
| | | RV | LV | RV | LV |
| BI | 33 | 20.7 | 137.8 | 23.5 | 205.8 |
| GM | 71 | 24.9 | 78.2 | 21.1 | 137.0 |
| EC | 65 | 18.9 | 71.5 | 29.2 | 147.8 |
| MW | 44 | 33.4 | 105.3 | 23.4 | 125.6 |
| JH | 60 | 17.1 | 88.3 | 23.4 | 206.8 |
| WS | 60 | 22.5 | 148.6 | 24.7 | 238.4 |
| SC | 44 | 48.1 | 139.2 | 33.3 | 111.5 |
| MMcM | 63 | 45.7 | 93.6 | 39.4 | 173.0 |
| FF | 81 | 11.2 | 93.8 | 19.0 | 130.0 |
| DO | 41 | 8.6 | 71.7 | 32.2 | 174.6 |
| JG | 67 | 35.7 | 71.5 | 25.4 | 132.4 |
| Mean $\pm$SD | 58 | 26.1 $\pm$13.1 | 100.1 $\pm$29.1 | 26.8 $\pm$6.1 | 171.6 $\pm$38.3 |

TABLE 19

Right and Left Ventricular "Free" Wall and Chamber Volumes Obtained at End-Systole in Age-Matched Controls

| Patient | Age | Chamber Volume ($cm^3$) | | Ventricular Wall Vol ($cm^3$) | |
|---|---|---|---|---|---|
| | | RV | LV | RV | LV |
| JMcD | 77 | 40.9 | 61.1 | 31.7 | 161.4 |
| ML | 67 | 16.5 | 60.3 | 9.1 | 186.6 |
| IC | 79 | 30.4 | 32.6 | 31.2 | 155.4 |
| HC | 70 | 12.8 | 46.1 | 10.0 | 182.2 |
| MS | 63 | 18.3 | 20.3 | 21.9 | 129.9 |
| Mean | 71 | 23.8 | 44.1 | 20.8 | 163.0 |
| $\pm$SD | | +11.6 | $\pm$17.7 | +11.0 | $\pm$22.9 |

TABLE 20

Right and Left Ventricular "Free" Wall and Chamber Volumes

Obtained in Young Normal Volunteers

| Patient | Age | Chamber Volume ($cm^3$) | | Ventricular Wall Volume ($cm^3$) | |
|---|---|---|---|---|---|
| | | RV | LV | RV | LV |
| LT | 34 | 12.4 | 31.8 | 20.7 | 116.2 |
| JPR | 30 | 15.6 | 30.4 | 23.5 | 132.5 |
| WMc | 37 | 20.3 | 28.6 | 34.1 | 180.2 |
| CS | 35 | 21.4 | 31.4 | 35.6 | 151.2 |
| Mean | 34 | 17.4 | 30.6 | 28.5 | 145.0 |
| $\pm$SD | | $\pm$4.2 | $\pm$1.4 | $\pm$7.5 | $\pm$27.5 |